Thermodynamics and Dynamics of Molecular Fluids with Classical Density Functional Theory

Antoine Carof

UNIVERSITÉ DE LORRAINE

École doctorale C2MP

Thermodynamique et dynamique des fluides moléculaires par la théorie de la fonctionnelle de la densité classique

Thermodynamics and Dynamics of Molecular Fluids with Classical Density Functional Theory

Habilitation à diriger des recherches de l'Université de Lorraine (Chimie-Physique)

Soutenue le 5 décembre 2025

Antoine Carof

Composition du jury :

Présidente :	Hong Xu	Professeure, Université de Lorraine
Rapporteur.e.s :	Hélène Berthoumieux	Chargée de recherche, HDR, PSL University
	Guillaume Jeanmairet	Chargé de recherche, HDR, Sorbonne Université
	Martin Oettel	Professeur, Universität Tübingen
Examinateur :	Guillaume Galliero	Professeur, Université de Pau et des Pays de l'Adour
Marraine scientifique :	Francesca Ingrosso	Professeure, Université de Lorraine

Laboratoire de Physique et Chimie Théoriques - LPCT - UMR CNRS 7019

Remerciements

Je remercie chaleureusement l'ensemble de mon jury d'avoir accepté de me lire et de m'écouter pour défendre cette HDR. Tout d'abord Hélène, Guillaume J. et Martin qui ont accepté de rapporter mon manuscrit, et avec qui j'espère continuer à avoir de nombreuses discussions scientifiques dans les prochaines années. Je remercie aussi Hong pour sa relecture attentive du manuscrit et pour la présidence du jury, ainsi que Guillaume G. pour sa participation et pour notre future collaboration. Enfin, je tiens à remercier tout particulièrement Francesca qui m'a accueilli et accompagné depuis mon arrivée à Nancy en 2019. J'ai pu profiter de ses grandes compétences scientifiques, mais surtout de ses qualités humaines. Merci !

Ces travaux ont été réalisés au LPCT. Je tiens à remercier les différentes directions du laboratoire (Xavier, Dragi, François, Jean-Christophe, Chiara) pour leur soutien et leur bienveillance, ainsi que l'équipe administrative (Séverine, Charlotte et Véronique) qui est d'une efficacité redoutable ! Je remercie l'ensemble du laboratoire, et en particulier Claude qui a relancé mon intérêt pour la dynamique microscopique. Je souhaite remercier fortement Dominika, ma sœur jumelle scientifique. On va pouvoir réaliser tous nos projets dans les prochaines années ! En dehors du labo, je veux remercier les trois acteurs clés qui m'ont permis de lancer le projet sur le CO_2: Daniel et Luc qui m'ont formé à la DFT classique et qui ont partagé tout leur code de simulation, et bien sûr Mohamed, un premier doctorant idéal. Mon second projet concerne la dynamique dans les électrolytes, et je remercie Pierre pour m'avoir fait découvrir la SDFT et Benjamin, pour son suivi attentioné depuis plus de 10 ans et pour les discussions scientifiques. J'espère un jour pouvoir élucider enfin mon projet de thèse...

En tant que maître de conférences, j'exerce une double mission : recherche et enseignement. Je remercie mes collègues de la Fac de Pharma : dans le pôle informatique (Alexandrine, Sophie, Sébastien) ou dans la filière industrie (Sabrina, Maia, Coumba). J'ai beaucoup appris pour mon métier d'enseignant, et je découvre tous les jours le monde de la pharmacie.

Sur le plan personnel, je voudrais dire merci aux "copains du RU" (Damien C., Damien M., Erwan, Gwendal, Romain), qui m'ont permis de m'acclimater à la vie à Nancy et à rendre plus facile cette double vie entre Nancy et Paris.

A ma famille, mes ami.e.s et celui que j'aime

Contents

List of Figures

List of Tables

Avant-propos

Ever since my early years of studying chemistry, I have been drawn to two different aspects of the molecular theory. Initially, I was fascinated by the visual aspect of imagining how molecules interact at a microscopic level — how they bounce off each other, rotate and exchange atoms or electrons. Secondly, I became intellectually interested in understanding how thermodynamics and transport properties emerge from chaotic molecular-level mechanisms. Although I was initially lured by the graphical representation of reaction mechanisms in organic chemistry, I quickly realised that my experimental skills were limited—as the existing models of these reactions. I therefore shifted my focus towards the physical chemistry and the chemical physics of fluids, where reactions are rare, but other molecular motions (rotation and translation) and collective fluctuations play the main role.

Aside from my personal interests, fluids are ubiquitous in many natural environments and technologies. Modern questions related to molecular fluids cover topics such as energy storage and generation, improving synthesis processes, carbon capture, cleaning and decontaminating industrial products, and the role of solvents in biological systems. In terms of classification, I organise for myself fluids according to their molecular properties, from the simplest to the most complex. Starting with simple fluids consisting of atomic particles, the following features can be considered/added: (i) dipole and other electrostatic moments, (ii) shape, (iii) hydrogen bonding/associativity, (iv) internal flexibility, and (v) reactivity. However, when the molecules of the fluid become long (polymer), bi- or tri-dimensional (membrane, nanoparticle), or messy (biomolecule), we usually leave the realm of the physical chemistry of fluids to enter that of soft matter — an area that I haven't explored in my work.

I completed my PhD under the supervision of B. Rotenberg (PHENIX, Paris, 2012-2015). My research here aimed to determine which molecular motions control the nuclear magnetic resonance (NMR) relaxation of aqueous atomic ions at infinite dilution. I explored several hypotheses (*e.g.*, rotation of water molecules in the first solvation shell, rotation of the shell itself, or translation of the ion), but none of them were successful. (I passed my PhD nevertheless, as we at least managed to correctly reproduce the NMR relaxation time using a combination of molecular and quantum simulations.) I then moved to London to temporarily leave the world of the molecular motions and learn about the (nether)world of semi-classical molec-

ular simulations and their applications to charge transfer in organic crystals and proteins (group of J. Blumberger, UCL, London, 2015-2018). I returned to Paris in 2018 (with R. Vuilleumier, PASTEUR, Paris, 2018-2019) to join a project about the development of the molten carbonate electrolyser cells. Using ab-initio and classical simulations, I determined the solvation structure and dynamics of different solvated species within the molten carbonate, as well as the transport and structure of the bulk molten carbonate at different temperatures and compositions.

I joined the Université de Lorraine in September 2019 to work at the Laboratoire de Physique et Chimie Théoriques (LPCT) for the scientific part and at the Faculté de Pharmacie (College of Pharmacy) on the teaching side. I will develop in this manuscript the work I have done on both these aspects. At LPCT, I was warmly welcomed within the group of F. Ingrosso and the team "Liquid-state, interfaces, solvation". My scientific work focused on the properties of molecular fluids, the main project involved developing a molecular density functional theory to study the solvation within the supercritical CO_2. I also contributed to other projects investigating the dynamical properties at the molecular scale. These projects included modelling of spectroscopic properties under confinement with F. Ingrosso, studying of the displacement of chiral liquids under a rotating electric field with C. Millot, and developing theory for the dielectric properties in dipolar electrolytes with P. Illien and B. Rotenberg.

My future research projects will strengthen the work conducted previously. I will continue to focus on the modelling of molecular fluids, aiming to develop density-based theories that can efficiently model the thermodynamic and dynamical properties. These theories will then be applied to more complex fluids, such as molten salts, deep eutectic solvents, and confined fluids. In this manuscript, I present my ideas for technical developments: firstly, improving and extending the classical DFT approach to study supercritical CO_2 at different temperatures, different pressures and with a cosolvent; and secondly, developing a molecular dynamics DFT approach to investigate the solvation dynamics of electrolytes.

Chapter 1 of the manuscript will summarise my previous work up to my arrival in Nancy. Chapter 2 will present my current and future work on the molecular DFT for supercritical CO_2. Chapter 3will focus on the dynamic aspect, exploring the development of a stochastic DFT for modelling molecular fluids. Chapter 4 will conclude the manuscript by covering the other collaborative projects. Annex A will review my scientific output (published papers, conferences, supervised students), while annex B will present all the non-scientific aspects of my work, including my teaching, collective and administrative duties.

In conclusion, I would like to clarify the purpose of this manuscript. Of course, it is my thesis for obtaining the Habilitation à Diriger des Recherches, the ultimate qualification in the French academic system. While writing it, I also took the opportunity to document some unpublished works and to force myself to grasp difficult concepts that were still unclear to me (*e.g.*, classical DFT). I compiled a patchwork of grant proposals, published and unpublished results, and human resource reports, attempting to organise them coherently. In the future, I hope to use this manuscript as a preparation for future publications, as a textbook for my own understanding, and as a roadmap for my future research. In terms of notation, I indicate the supervised or co-supervised students in bold, and I present the published articles to which I contribute as [AC1], in accordance with the numbering in section I. I have also chosen to present the bibliography with the author and date stated explicitly, as this makes it easier for the reader to identify the cited paper (*e.g.*, [Chandler, 1993]). Now that everything is in place, let us begin.

CHAPTER 1

Previous Works

Since the beginning of my thesis in 2012, I have focused my research on two areas: i) the dynamic and thermodynamic processes in the condensed phase, and ii) the development of innovative theoretical and numerical methods to study these processes. My research journey has unfolded as follows:

- M2 internship with B. Rotenberg and V. Marry on the dynamics of ions in clay sheets,
- Thesis with B. Rotenberg on NMR relaxation of ions in aqueous solution,
- Post-doc with J. Blumberger on charge transport in organic materials,
- Post-doc with R. Vuilleumier and F.X. Coudert on solvation in molten carbonates,
- Lecturer at the Laboratory of Theoretical Physics and Chemistry (LPCT, UMR 7019).

This research journey enabled me to specialise in density theories for molecular liquids.

I PhD: Modelling NMR relaxometry in condensed phase

The measurement of NMR relaxation times (called relaxometry) allows extracting information on microscopic dynamics in complex systems. [Redfield, 1957] The relaxometry of atomic ions, for example, provides access to transport properties in multiscale materials such as clays or polymers. [Korb, 2018] The interpretations of these experiments generally rely on overly simplistic models of microscopic dynamics, considering, for example, only Brownian motions for the translation and rotation of molecules. [Chubak et al., 2023] My PhD project was therefore to develop a new simulation method to calculate the NMR relaxation times of atomic ions and to propose a more realistic interpretation of the relaxation mechanism. We chose to restrict ourselves to quadrupolar ions (*i.e.*, with a spin $I \geq 1$) in water at infinite dilution. For these ions, linear response theory [Redfield, 1957] allows writing the NMR relaxation time as

$$\frac{1}{T_1} = A\,(1+\gamma_\infty)^2 \int_0^\infty \mathrm{d}t\; C_{\mathrm{EFG}}(t) \tag{1.1}$$

where A is a numerical prefactor dependent on the nucleus under consideration, the Sternheimer factor γ_∞ describes the response of the electronic cloud of the considered ion in the presence of the solvent [Sternheimer, 1950], and $C_{\mathrm{EFG}}(t)$ is the correlation function of the electric field gradient (EFG), which arises from the solvent fluctuations around the ion. The calculation of relaxation times presents the dual challenge of accurately describing the interactions between the nucleus and the electronic cloud (γ_∞) and sampling the molecular fluctuations around these nuclei ($C_{\mathrm{EFG}}(t)$).

During this project, I developed an original method combining precise quantum calculations to determine γ_∞ and classical molecular dynamics trajectories to calculate $C_{\mathrm{EFG}}(t)$. The factor γ_∞ is defined by the hypothesis of a linear relationship between the EFG from the ion's electronic cloud V^{cloud} and the EFG from the solvent V^{solv}, $V^{\mathrm{cloud}} = (1+\gamma_\infty)V^{\mathrm{solv}}$. [Sternheimer, 1950] We validated this hypothesis by comparing the EFG calculated using an ab-initio method (V^{AI}) and the EFG from the point charge distribution of water molecules from a classical force field (denoted V^{PIM}). Figure 1.1(a) confirms the linear relationship between these two EFG and allows calculating γ_∞. Figure 1.1(b) shows the evolution of $C_{\mathrm{EFG}}(t)$, which decays in two successive modes, plus a third oscillating mode for lithium. The inset represents the integral of the correlation function $\int_0^\infty \mathrm{d}t C_{\mathrm{EFG}}(t)$, from which the relaxation time is calculated (equation 1.1).

With these results, I was able to quantitatively reproduce the NMR relaxation times for alkali, alkaline earth, and chloride ions in water at infinite dilution. Table 1.1 summarises the theoretical values obtained during my thesis alongside the experimental values found in the literature. I also adapted this method for sodium ions diffusing in a silicate matrix and for aqueous solutions at finite concentrations. Finally, I proposed original analyses of molecular movements to understand which microscopic modes control NMR relaxation. By exploiting the modularity of the simulations, I was able to test the importance of the first solvation sphere, the mass of water molecules, or the charge of the ion. This highlighted the invalidity of the models usually employed to describe the experiments (based on a stochastic reorientation of water) and emphasised the essential role of collective density fluctuations in the ion's solvation sphere. This work resulted in three articles. [AC3][AC4][AC6]

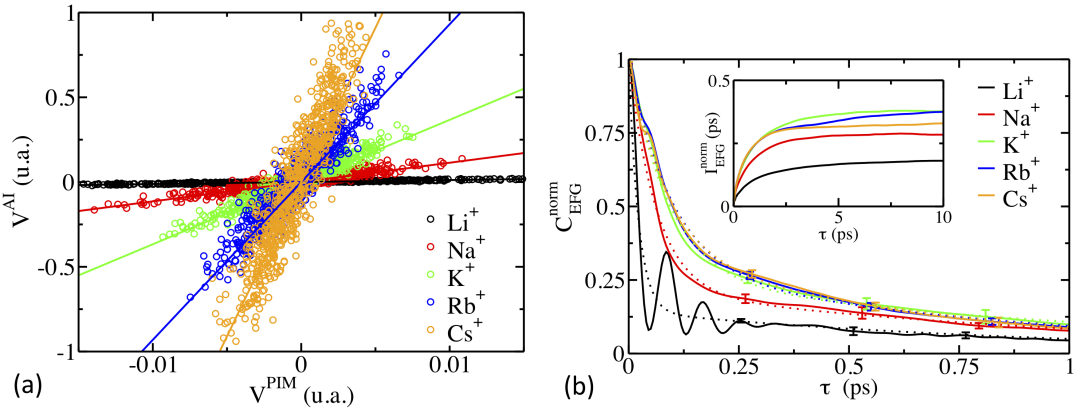

Figure 1.1 – Main results of my thesis. Figure (a) represents the EFG obtained by an ab-initio calculation V^{AI} as a function of the EFG obtained by the force field V^{PIM}. For each ion, 100 configurations containing one ion and 63 water molecules were used. The continuous line represents the best linear fit, allowing the calculation of γ_∞. Figure (b) represents the normalised autocorrelation function of the EFG $C^{\mathrm{norm}}_{\mathrm{EFG}}(t) = C_{\mathrm{EFG}}(t)/C_{\mathrm{EFG}}(0)$. For each ion, 500 ps of molecular simulations containing one ion and 215 water molecules were used. The inset figure represents $\int_0^\tau \mathrm{d}t C^{\mathrm{norm}}_{\mathrm{EFG}}(t)$.

Ions	$^{7}Li^{+}$	$^{23}Na^{+}$	$^{39}K^{+}$	$^{87}Rb^{+}$	$^{133}Cs^{+}$	$^{25}Mg^{2+}$	$^{35}Cl^{-}$
$\left(\frac{1}{T_1}\right)_{\mathrm{sim}}$ (s^{-1})	0.032	6.7	15	370	0.055	1.8	40
$\left(\frac{1}{T_1}\right)_{\mathrm{exp}}$ (s^{-1})	0.03	17	18-26	370-420	0.075	4.16	28-42

Table 1.1 – Comparison of NMR relaxation times obtained by simulations $\left(\frac{1}{T_1}\right)_{\mathrm{sim}}$ and by experiments $\left(\frac{1}{T_1}\right)_{\mathrm{exp}}$. The good quantitative agreement highlights the validity of our modelling.

This project allowed me to study the collective fluctuations of water around ions, to link these fluctuations to the experimentally measured T_1, and to develop an original simulation method for calculating these T_1. I was particularly interested in the dynamics of the solvent around a solute, especially when described in terms of solvent density. [Perng and Ladanyi, 1998] This project continued after my thesis: I supervised I. Chubak, a post-doc working with B. Rotenberg in 2022 and 2023. Building on the method I had developed during my thesis, he extended it to new ions in water and to alternative classical force fields. [AC16] [Chubak et al., 2023]. This work recently led us to collaborate with P. Illien in an attempt to model NMR relaxation using stochastic density functional theory (SDFT), [Dean, 1996] which led us to build SDFT for electrolytes (see the chapter 3). [AC22]

II Post-doctorate 1: charge transfer in organic materials

After completing my thesis, I joined J. Blumberger's group to participate in a very different project: modelling charge transport in organic crystals. These organic crystals are electrical conductors and flexible materials, making them interesting for photovoltaic technologies. [Coropceanu et al., 2007] However, their use is limited by their low electrical mobility. This weakness stems from the coupling between charge dynamics and molecular fluctuations (phonons), but no theory had qualitatively modelled this coupling in 2015 (neither hopping transport theories nor band transport theories). [Troisi, 2011, Oberhofer et al., 2017] The goal of J. Blumberger's group was therefore to use molecular simulations to improve our understanding the charge transport mechanism in these materials with the ultimate goal of proposing new, more efficient organic crystals. Molecular simulations were, however, faced with the three challenges of describing electronic dynamics in excited states (where transport occurs), coupling this dynamics with molecular fluctuations (the coupling), and modelling sufficiently large systems (100 nm) and for a sufficiently long time (10 ps).

We have therefore developed a new molecular simulation method, called Fragment-Orbital Based Surface Hopping (FOB-SH). This method is based on an original combination of non-adiabatic molecular dynamics (*i.e.*, integrating excited states [Tully, 2012, Crespo-Otero and Barbatti, 2018]) with calculations of energies, forces, and non-adiabatic couplings using classical force fields (much less costly than ab-initio methods). This enables the propagation of electrical dynamics coupled to molecular fluctuations at a low numerical cost. I played a key role in the theoretical and numerical development of this new method, from its conception to the implementation of the main ingredients in the CP2K simulation code. [AC7][AC9][AC11] I then participated in its validation by comparing it with numerous experimental results. [AC12] Figure 1.2 (right) shows the excellent agreement between our simulations and experiments, a result that had previously been unattainable for any theory.

We then used this method to elucidate the transport mechanism, demonstrating that it involves an alternation of localised charge phases and brief yet extensive delocalisation. [AC10] The duration of these localisation/delocalisation phases and the size of the charge during delocalisation depend on both temperature and coupling strength. Figure 1.2 (right, A-B) illustrates the trajectory and the extension of a charge at two temperatures. The higher the temperature, the more significant the molecular fluctuations, and the more localised and less mobile the charge will be. During this project, I had the opportunity to supervise **S. Giannini**, who was a PhD student with J. Blumberger (2017-2020), on a daily basis. I continued to work with J. Blumberger's group for a few years. Thanks to the FOB-SH method, we were able to test new organic crystals, propose rules for designing more efficient organic crystals, and study exciton transport in organic crystals. [AC14][AC17]

In addition to my work on developing and applying FOB-SH, I was involved in a project to determine the rate of electron transport in proteins. This project was a collaboration between experimentalists (in biology and physics) and J. Blumberger's group for simulations. Using the standard charge transport hopping simulation method, [Blumberger, 2015] we were able to provide a microscopic interpretation of the experiments carried out by our collaborators and determine, for the first time, the electron transfer speed within a multi-heme protein. [AC8][AC13] This project corresponded to the thesis of **X. Jiang** (2015-2019), whom I helped to supervise in the early stages of the project.

The research themes that interest me now are quite different from the work of my first

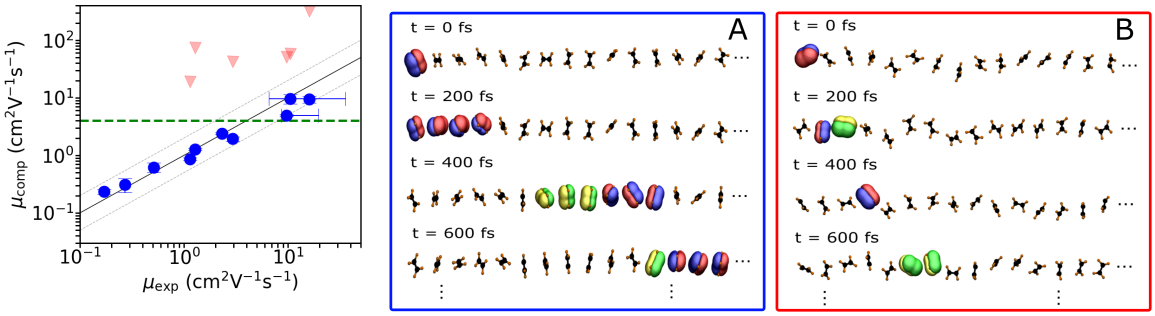

Figure 1.2 – Left figure: comparison between experimental electrical mobilities μ_{exp} and those obtained by simulation μ_{comp}. The points represent the results of the FOB-SH method for 10 different organic crystals, the red triangles represent the results of a band theory, and the green dashed line is the limit of the predictions of hopping theories. Right figure: snapshots taken at different times during two FOB-SH trajectories in an ethylene chain with an electronic coupling of 120 meV at 50 K (A) and 1000 K (B). Increasing the temperature decreases the size of the charge and its mobility.

postdoctoral position. I learnt however some key concepts about mixed classical/quantum simulations that could be useful in future projects on photochemistry and the solvation of excited states, for example. I also developed advanced scientific programming skills in both Fortran 2003 and Python. I also had the opportunity to supervise several PhD and Master's students. This postdoctoral position was therefore an essential step in my training as a researcher.

III Post-doctorate 2: solvation in molten carbonate

I then decided to undertake a second postdoctoral position focusing on the thermodynamics of solvation in complex liquids—the molten carbonates. This project was funded by the ANR MCEC (Molten Carbonate Electrolyser Cell, principal investigator: M. Cassir), and I was supervised by R. Vuilleumier and F.-X. Coudert in the Chemistry Department of ENS Paris. The ANR MCEC project aimed to develop of a new type of molten carbonate electrolyser (MCEC) for the valorization of CO_2 captured in industrial installations. [Chery et al., 2016, Chery, 2015] My role in the project was to provide microscopic information on the structure and solvation dynamics of the different carbon oxides that appear during the operation of an electrolyser. I learnt new dynamic simulation techniques (ab-initio molecular, thermodynamic integration) and adapted them to reactive liquids, such as molten carbonates. Thanks to these techniques, I was able to characterise the structure and dynamics of the different species dissolved in molten carbonate (CO, CO_2, O^{2-}, $C_2O_4^{2-}$) that play a major role during the operation of an MCEC electrolyser. In particular, I demonstrated that CO_2 reacted with the carbonate ion CO_3^{2-} to form a transient species, pyrocarbonate $C_2O_5^{2-}$. This species has a very short lifespan (a few hundred femtoseconds), yet it is present 25% of the time, which affects the dynamics and solubility of CO_2. We also showed the stability of the oxalate species $C_2O_4^{2-}$, the CO species, and characterised the quasi-rigid nature of the (O^{2-}, $4Li^+$) complex. Figure 1.3 illustrates the solvation of pyrocarbonate and oxalate species in molten carbonate. These results are essential for understanding the operation of an MCEC, particularly the charging and discharging processes that occur at the interface between the electrode and the molten carbonate. [AC15]

As part of this ANR project, I also collaborated with experimentalists from the CEMHTI laboratory (UPR 3079, Univ. Orléans). Together, we studied the structural and dynamic properties of two molten carbonates (Li_2CO_3-Na_2CO_3 and Li_2CO_3-K_2CO_3) at several concentrations. We compared NMR experiments (spectrum and calculation of diffusion coefficient) and electrical conductivity with molecular simulation results. [AC18]

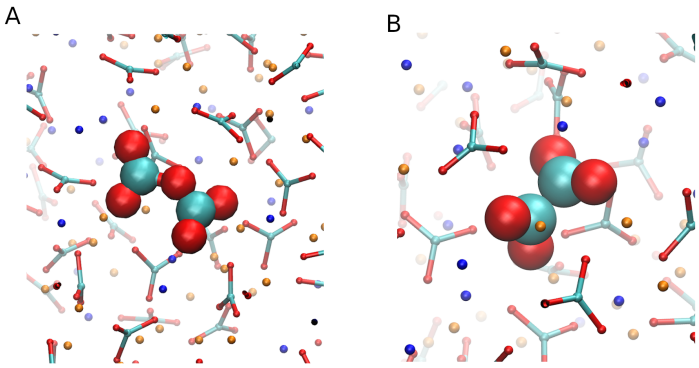

Figure 1.3 – Snapshots of two carbon oxides solvated in molten carbonate: (A): pyrocarbonate $C_2O_5^{2-}$ and (B): oxalate $C_2O_4^{2-}$.

This postdoctoral position enabled me to acquire new theoretical and numerical skills, for example in ab-initio molecular dynamics and thermodynamic integration. It also reinforced my strong interest in studying solvation in complex liquids, particularly in relation to developing ecological technologies.

CHAPTER 2

Classical Density Functional Theory for Supercritical CO_2

Contents

I joined the LPCT in Nancy in 2019 with the project to develop a new method for determining the solvation properties of supercritical CO_2 ($scCO_2$). The team in Nancy (F. Ingrosso, M. Ruiz-López, A. Lambert) already had significant expertise in understanding the specific molecular interactions between the CO_2 and the solute using MD simulations and DFT calculations. [Altarsha et al., 2012b, Azofra et al., 2013, San-Fabián et al., 2014, Ingrosso et al., 2016, Ingrosso and Ruiz-López, 2017, Ingrosso and Ruiz-López, 2018] Recognizing the limitations of these methods in terms of efficiency, I wanted to implement classical density functional theory (cDFT), a fast and accurate molecular simulation method. I was of course inspired by the recent project of D. Borgis, L. Belloni, G. Jeanmairet, M. Levesque and their collaborators, who designed a powerful cDFT for water under ambient conditions, the so-called MDFT (molecular DFT). [Jeanmairet et al., 2013b, Ding et al., 2017] They notably included the molecular nature of the solvent by integrating the rotational degrees of freedom into the solvent density $\rho(\boldsymbol{r}, \boldsymbol{\omega})$, where $\boldsymbol{\omega}$ describes the 3 Euler angles of the considered solvent molecule.

To carry out this project, I first requested funding from the "molecular chemistry and molecular physics" (CPM) department in 2020 to purchase a computing computer. In April 2021, I submitted a request for thesis funding to both the CPM department and the C2MP doctoral school with F. Ingrosso. We recruited **M. Houssein Mohamed** for a thesis (October 2021/September 2024). In collaboration with D. Borgis and L. Belloni, we successfully developed a first cDFT approach for $scCO_2$ in the near-critical region. [Houssein Mohamed, 2024, Houssein Mohamed et al., 2025] We assessed the accuracy of our cDFT approach by comparing its results with those of standard molecular simulations. This was particularly the work of two M2 interns **G. Szczepan** (February 23 - July 23) and **C. Cao** (February 25 - July

25). The next step in this research project is now to build a cDFT that covers the entire supercritical regime (and not just a single condition). This work is the subject of the ANR JCJC BAC2MOL grant obtained in July 2024, which also includes potential applications for studying $scCO_2$ in confinement, in collaboration with G. Galliero.

In this chapter, I will first provide an overview of $scCO_2$ as a solvent and review the state of the art for modelling of solvation properties in $scCO_2$. Secondly, I will describe what classical DFT is in theory —and in practice. The third section will summarise the PhD project of M. Houssein Mohamed and its recent continuation. In the final section, I will present the BAC2MOL project and my ideas for developing a powerful and flexible cDFT approach to studying $scCO_2$ as a solvent.

I The supercritical CO_2, a powerful green solvent.

I.A Industrial and ecological contexts for the use of $scCO_2$

The $scCO_2$ is a valuable eco-friendly solvent with very interesting properties for various industrial applications. [Anastas and Eghbali, 2010] It is non-toxic to humans and the environment, and non-flammable, making it a powerful "greener" alternative to the traditional organic solvents. It can be brought into the supercritical state under mild conditions. Its phase diagram is presented in figure 2.1, where the critical point is located at $P_c = 73.8$ bar, $T_c = 304$ K and $\rho_c = 468$ kg.m^{-3}. In this supercritical state, physical and chemical properties gradually change from liquid-like to gas-like, in a way that can be easily controlled by small pressure adjustments. The ability to fine-tune the density changes in the supercritical CO_2 can be used to modify its dissolving power, [Liu et al., 2010] *e.g.* for instance through the retrograde condensation process. [Johnston et al., 1987, Tai et al., 2000] On the other hand, the gas-like behaviour ensures a better mass transport (and lower viscosity) than in the liquid phase. Under confinement, the supercritical fluid can produce a Casimir effect: the confinement of the walls suppresses the long-range fluctuations, resulting in a pressure difference between the confined fluid and the bulk fluid and in a thermodynamic attractive force between the walls. [Dantchev and Dietrich, 2023, Schurtenberger and Heuberger, 2012] These properties provide a wide range of applications, especially in the chemical industry. The supercritical CO_2 is used for example as a selective solvent, specifically solvating certain molecules of interest. It is used to extract target molecules from natural substances (*e.g.*, to produce decaffeinated coffee), [Reverchon, 1997, Zosel, 1978] to impregnate polymers with medical applications, [Coutinho et al., 2021, Weinstein et al., 2010] to perform supercritical fluid chromatography, [Lesellier and West, 2015, Molineau et al., 2021] or to separate racemic mixtures. [Johnston et al., 1987, Tai et al., 2000] On the other hand, the properties of supercritical CO_2 are also used for the synthesis of nanoparticles (*e.g.*, drug carriers) via the micronisation processes (supercritical anti-solvent, expansion of supercritical solution, [Türk, 2009] and particles from gas-saturated solutions. [Rossmann et al., 2012, Sampaio de Sousa et al., 2007, Türk, 2009]

Moreover, $scCO_2$ is also at the heart of carbon capture and utilisation technologies (CCU), which are emerging as a promising strategy to reduce CO_2 emissions from industrial processes and fight against global warming. [Agency, 2022] For example, the CO_2 fluid can be stored in a geological reservoir to prevent its release into the atmosphere. In such a reservoir, the CO_2 fluid is present both as a pure fluid or in a mixture — and often in its supercritical state. From acting as a green solvent to long-term storage, the $scCO_2$ plays a key role in advancing

technologies that mitigate the global warming and promote environmental sustainability.

The development and optimization of these various applications requires a detailed understanding of the properties of the CO_2 fluid interacting with a multiscale environment (*e.g.*, a solute, an interface, a cosolvent, or a confinement). Such understanding is challenging due to the multiple length and timescales involved, the various thermodynamic conditions and the different properties of interest (thermodynamics, structure, transport). Molecular modelling approaches seem to be the perfect tool for this task: by specifying the microscopic structure and interactions, they could compute different CO_2 fluid properties at different scales and for different thermodynamic conditions. However, a suitable molecular modelling must provide accurate CO_2 properties in an cost-effective way. As we will discuss in the following section I.B, there is currently no existing molecular modelling method that satisfies all the criteria of accuracy, efficiency, and versatility.

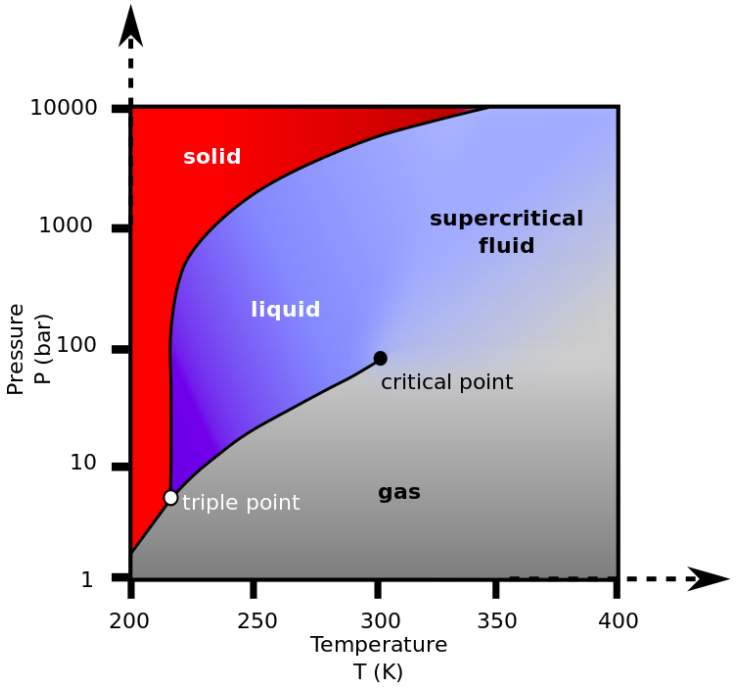

Figure 2.1 – CO_2 pressure-temperature phase diagram

I.B State of the art of the modellings of CO_2

In this section, we will review the current modellings of CO_2 fluid used in industry, chemical engineering research and physical chemistry research, and highlight their limitations and the need for a new theory.

I.B.1 Thermodynamics and empirical methods

Equation of state. In the chemical industry, the thermodynamic properties of the CO_2 fluid are routinely determined using cubic equations of state (cubic equation of state). [Huang et al., 1985, Span and Wagner, 1996, Vega, 2018] These equations consist of analytical expressions that allow to quickly calculate the thermodynamic properties – speed is an essential feature for industrial applications (*e.g.*, to investigate fluid transport with pressure and temperature gradients). [Zhao et al., 2017] These equations rely on 5 to 10 empirical parameters that must

be determined for each mixture. [Le Guennec et al., 2016] While they accurately reproduce the thermodynamic properties of the bulk fluid, their macroscopic nature fails to capture the properties of the CO_2 fluid at a the microscopic level. They cannot model the CO_2 interactions with nanoconfinements or with complex solutes.

Parametric solubility approaches. In the case of solvation in CO_2 fluid, specific parametric approaches have been developed: to determine the solubility (i) the equation of state approach, [Colussi et al., 2006, Garlapati and Madras, 2009] where the solubility is obtained from an equation of state of a mixture of two fluids (the CO_2 and the solute/cosolvent); (ii) the density-based approach, which relates the solubility directly to the solvent density with a semi-empirically derived equation (different functional forms exist in the literature); [Bartle et al., 1991, Chrastil, 1982, Kumar and Johnston, 1988, Mendez-Santiago and Teja, 2012, Tabernero, 2011] and (iii) the solvation models, generally with two parameters (interaction energy and molecular volume). [Cheng et al., 2003, Iwai et al., 1992, Shin et al., 2001] Overall, all these parametrized methods can correctly reproduce the solubility for a wide range of pressures and temperatures with a relative error (10%, thanks to the fitting procedure). However, they lack flexibility for any system modification as they must be re-parametrized again for each solute and each new system (*e.g.*, the presence of an interface or a cosolvent).

I.B.2 Molecular simulations

Unlike the empirical/thermodynamic approaches, molecular simulations consider an atomic-level description of the CO_2 fluid and its environment. These microscopic models generate N-body trajectories from which the microscopic and macroscopic properties are calculated. These trajectories are obtained via the equations of motion (molecular dynamics simulation, MD) or via an efficient stochastic sampling (Monte-Carlo simulation, MC). [Frenkel and Smit, 2002] These models are widely used in the scientific literature to study the CO_2 fluids, [Stubbs, 2016] with different levels of approximation, ranging from simple point-charge force-fields [Harris and Yung, 1995, Potoff and Siepmann, 2001, Su and Maroncelli, 2006] to the on-the-fly ab-initio dynamics. [Mi et al., 2019, Saharay and Balasubramanian, 2004] They facilitate the study of the CO_2 fluid properties in many situations: bulk, [Mi et al., 2019, Saharay and Balasubramanian, 2004] solvation, [Noroozi et al., 2016, Noroozi and Paluch, 2017, Reddy and Saharay, 2019, Su and Maroncelli, 2006] mixtures, [Idrissi et al., 2010, Potoff and Siepmann, 2001] and confinement. [Fuentes-Azcatl and Domínguez, 2019, Rébiscoul et al., 2019] In particular, they can accurately calculate the solvation free energies (on the order of a few kJ/mol) [Noroozi et al., 2016, Noroozi and Paluch, 2017, Stubbs et al., 2005, Su and Maroncelli, 2006] or provide precise details on the local structure and dynamics of the solvation (*e.g.*, spectroscopic data). [Foltran et al., 2011, Kajiya and Saitow, 2013] They help to clarify several key concepts related to the solvation in supercritical CO_2, such as the effect of the local density augmentation, [Idrissi et al., 2010, Su and Maroncelli, 2006, Yoon et al., 2017] of large density inhomogeneity, and CO_2-philicity, a particular interaction between CO_2 and certain chemical functions (*e.g.*, carbonyl group). [Altarsha et al., 2012a, Azofra et al., 2013, Ingrosso and Ruiz-López, 2018, San-Fabián et al., 2014]

They have numerous advantages: they are accurate; they naturally include the microscopic scale and anisotropic interactions, and can easily be adapted to different complex systems and thermodynamic conditions. Their main limitation remains the computational cost. While the cost is moderate to study the microscopic structure of one specific system (few CPU.hours), it is ten times higher to compute thermodynamic properties, where specific simulation tech-

niques are required (Widom insertion, thermodynamic integration, etc.) [Frenkel and Smit, 2002] This cost prohibits the use of molecular simulations to model the CO_2 fluid properties in several multi-scale environments and under multiple thermodynamic conditions.

I.C The solvation properties

In terms of modelling, the objective of my current and future projects is specific: the calculation of the solvation properties, *e.g.* the solvation free energy, the solvent density and the partial molar volume. I am not considering the calculation of the solubility for now, as this would also require determining also the free energy of the corresponding solid formed by the solute molecules.

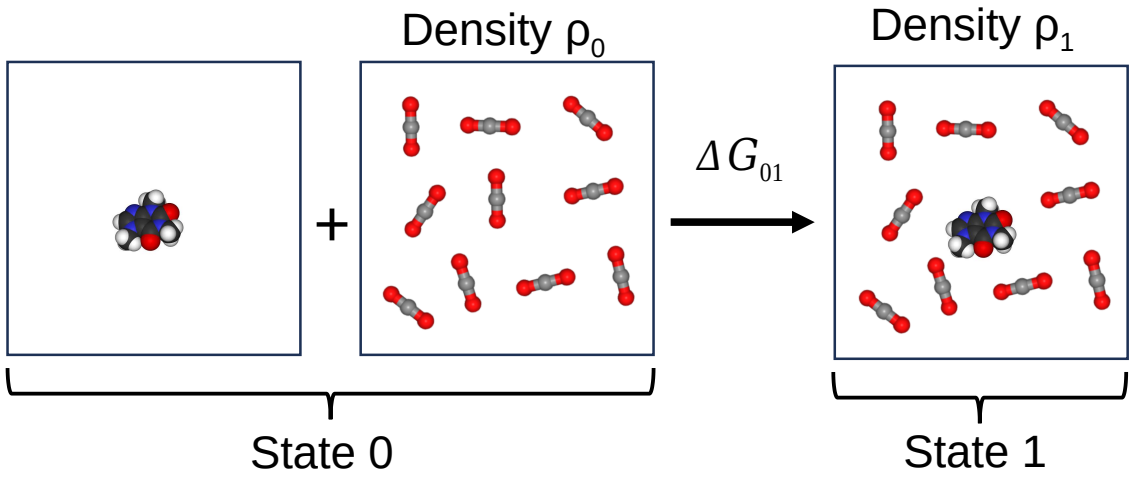

Figure 2.2 – Diagram of the thermodynamic process studied in this work: the initial state 0 corresponds to a solute molecule in a vacuum (here a caffeine molecule) and pure $scCO_2$, the final state 1 corresponds to a solute molecule in solution in $scCO_2$.

The solvation free energy corresponds to the energy required to transfer a particle (an atom, a molecule, an interface or a confinement) from a vacuum to the molecular fluid of $scCO_2$. Inserting a particle into $scCO_2$ activates a potential V_{ext} that describes the interaction between the inserted particle and the $scCO_2$ molecules. The Hamiltonian of the solvated system is given

$$H_1 = H_0 + V_{\text{ext}} \ , \tag{2.1}$$

with H_0 the sum of the Hamiltonians of the bulk $scCO_2$ and of the particle in vacuum. Figure 2.2 illustrates the process. We aim to calculate,

$$\Delta G_{01} = G_1 - G_0 \ , \tag{2.2}$$

where G_0 and G_1 are the Gibbs free energies of the non-interacting and solvated systems, respectively. Similarly, we will denote the molecular densities of the solvent ρ_0 and ρ_1 for state 0

(without solute) and state 1 (in the presence of the solute). I will now explain what the classical DFT is and how we will use it to calculate the solvation properties.

II Classical DFT for molecular fluids

II.A Statistical physics of molecular fluid

II.A.1 Hamiltonian and partition function

The classical DFT of molecular fluids focus on fluids formed with nonspherical particles (molecules) and without quantum effects. I will also restrict myself to system in 3 dimensions. The Hamiltonian that characterises this type of system is the sum of a kinetic energy term and a potential energy term representing the interactions between the constituents of the fluid. [Hansen and McDonald, 2013] For a molecular fluid, it reads

$$H = \sum_{i=1}^{N} \frac{1}{2} \left(\frac{\mathbf{p}_i^2}{m_i} + \mathbf{L}_i \cdot \mathbf{I}_i^{-1} \mathbf{L}_i \right) + U\left(\boldsymbol{r}^N, \boldsymbol{\omega}^N\right) \ , \tag{2.3}$$

where N is the number of molecules, $\mathbf{p}_i$ and m_i are the momentum vector and mass of molecule i, $\mathbf{L}_i$ and $\mathbf{I}_i$ are the angular momentum and moment of inertia of molecule i, U is the potential energy, $\boldsymbol{r}^N$ stands for the positions of the centres of mass of the N molecules, and $\boldsymbol{\omega}^N$ stands for the orientations of the N molecules, defined by three Euler angles in the laboratory frame, $\boldsymbol{\omega}_i \equiv (\theta, \phi, \psi)$. In presence of an external field, we will note $U = U_0 + V_{\text{ext}}$, where U_0 is the interaction energy between the molecules. We define the partition function denoted as Q,

$$Q(N, V, T) = \mathrm{Tr}_{\text{tot}} \exp\left(-\beta H\right) \ , \tag{2.4}$$

with the trace

$$\mathrm{Tr}_{\text{tot}} = \frac{1}{h^{6N} N!} \int \mathrm{d}\boldsymbol{r}^N \int \mathrm{d}\mathbf{p}^N \int \mathrm{d}\boldsymbol{\omega}^N \int \mathrm{d}\mathbf{L}^N \ , \tag{2.5}$$

where $\beta = \frac{1}{k_B T}$, k_B is the Boltzmann constant, and h is the Planck constant. For a classical fluid, the kinetic degrees of freedom $\mathbf{p}^N$ and $\mathbf{L}^N$ can be integrated out directly, resulting in a partition function of the form:

$$Q(N, V, T) = \frac{1}{N!} \frac{Q_{\text{rot}}}{\prod_i^N \lambda_i^3} Z(N, V, T) \ , \tag{2.6}$$

where Q_{rot} is the molecular kinetic partition function, which depends solely on the temperature and of the moments of inertia of the molecules in the system and λ is the de Broglie wavelength, $\lambda_i = \sqrt{h^2/(2\pi k_B T m_i)}$. [McQuarrie, 2000] The configuration integral Z reads

$$Z(N, V, T) = \mathrm{Tr} \exp\left(-\beta U(\boldsymbol{r}^N, \boldsymbol{\omega}^N)\right) \ , \tag{2.7}$$

with the configurational trace

$$\mathrm{Tr} = \int \mathrm{d}\boldsymbol{r}^N \int \mathrm{d}\boldsymbol{\omega}^N \ . \tag{2.8}$$

It is not possible to calculate this integral analytically for a realistic potential energy with a large number of molecules.

II.A.2 Pair correlation function

The pair correlation function is central in the statistical physics of liquids, particularly in systems that interact via a pair potential. [Hansen and McDonald, 2013] It enables physical properties to be determined without having to calculate the configuration integral (equation 2.7), which is a computationally challenging process. Let us start by presenting the n-particle density function,

$$\rho^{(n)}(\boldsymbol{r}_1, \boldsymbol{\omega}_1, ..., \boldsymbol{r}_n, \boldsymbol{\omega}_n) = \frac{N!}{(N-n)!} \frac{\int \exp\left(-\beta U(\boldsymbol{r}^N, \boldsymbol{\omega}^N)\right) \mathrm{d}\boldsymbol{r}^{N-n} \mathrm{d}\boldsymbol{\omega}^{N-n}}{Z} \ . \tag{2.9}$$

In particular, the equilibrium 1-body density is $\rho^{(1)} = \frac{N}{V}$ and the equilibrium N-body density is $\rho^{(N)} = \exp\left(-\beta U(\boldsymbol{r}^N, \boldsymbol{\omega}^N)\right)/Z$. We define the n-particle correlation functions,

$$g^{(n)}(\boldsymbol{r}_1, \boldsymbol{\omega}_1, ..., \boldsymbol{r}_n, \boldsymbol{\omega}_n) = \frac{\rho^{(n)}(\boldsymbol{r}_1, \boldsymbol{\omega}_1, ..., \boldsymbol{r}_n, \boldsymbol{\omega}_n)}{\prod_{i=1,N} \rho^{(1)}(\boldsymbol{r}_i, \boldsymbol{\omega}_i)} = \frac{\rho^{(n)}(\boldsymbol{r}_1, \boldsymbol{\omega}_1, ..., \boldsymbol{r}_n, \boldsymbol{\omega}_n)}{\rho_0^n} \ . \tag{2.10}$$

The pair correlation function $g \equiv g^{(2)}$ is the most important one. It depends on the distance $r = r_{12}$ between the two molecules and their orientations $\boldsymbol{\omega}_1$ and $\boldsymbol{\omega}_2$. It characterises the structure of the fluid and can be used to calculate various thermodynamic properties. We also define the direct correlation function c *via* the Ornstein-Zernike relation, [Ornstein and Zernike, 1917]

$$h(\boldsymbol{r}_{12}, \boldsymbol{\omega}_1, \boldsymbol{\omega}_2) = c(\boldsymbol{r}_{12}, \boldsymbol{\omega}_1, \boldsymbol{\omega}_2) + \frac{\rho_0}{8\pi^2} \int \int c(\boldsymbol{r}_{32}, \boldsymbol{\omega}_3, \boldsymbol{\omega}_2) h(\boldsymbol{r}_{13}, \boldsymbol{\omega}_3, \boldsymbol{\omega}_1) d\boldsymbol{r}_3 \mathrm{d}\boldsymbol{\omega}_3. \tag{2.11}$$

The direct correlation function plays a central role in classical DFT. Before discussing this theory, I will explain how translational and rotational invariance shape the correlation functions.

II.A.3 Rotational invariants

We will consider systems that are both translationally and rotationally invariant, which implicates a specific structure for the correlation functions. For instance, the translational invariance implies, for any fields A and B, that,

$$C_{AB}(\boldsymbol{r}_1, \boldsymbol{r}_2) = \langle A(\boldsymbol{r}_1) B(\boldsymbol{r}_2) \rangle = \langle A(\boldsymbol{r}_1 - \boldsymbol{r}_2) B(0) \rangle \ . \tag{2.12}$$

It also means that the proper "basis functions" to describe the spatial part are $\exp(\mathrm{i}\boldsymbol{k}\cdot\boldsymbol{r})$ and that the correlation function could be expressed in Fourier space as,

$$C_{AB}(\boldsymbol{r}_1,\boldsymbol{r}_2)=\frac{1}{(2\pi)^3}\int \mathrm{d}\boldsymbol{k}\exp\left(\mathrm{i}\boldsymbol{k}\cdot(\boldsymbol{r}_1-\boldsymbol{r}_2)\right)\tilde{C}_{AB}(\boldsymbol{k})\ , \tag{2.13}$$

where $\tilde{C}_{AB}(\boldsymbol{k})$ is (not exactly) the Fourier transform of $C_{AB}(\boldsymbol{r}_1,\boldsymbol{r}_2)$. With the same idea, Blum and Torruella proposed in 1972 using the correct "basis functions" to describe the angular part of the correlations in a system with rotational invariance. [Blum, 1972, Blum and Torruella, 1972] They termed these functions the rotational invariants and denoted them as $\Phi^{mnl}_{\mu\nu}$. Using Blum's notation, any correlation function f can be expanded onto this basis as

$$\begin{aligned} f(\boldsymbol{r}_{12},\boldsymbol{\omega}_1,\boldsymbol{\omega}_2) &= f(r_{12},\boldsymbol{\omega}_1,\boldsymbol{\omega}_2,\hat{r}_{12}) \\ &= \sum_{m,n,l,\mu,\nu} f^{mnl}_{\mu\nu}(r_{12})\Phi^{mnl}_{\mu\nu}(\boldsymbol{\omega}_1,\boldsymbol{\omega}_2,\hat{r}_{12}) \end{aligned} \tag{2.14}$$

with r_{12} the distance between the centres of mass of molecules 1 and 2, $\hat{r}_{12}$ the orientation of the vector between the centres of mass, and where $f^{mnl}_{\mu\nu}(r_{12})$ plays the role of the "Fourier transform" (where the integers m,n,l,μ, and ν plays the same role as $\boldsymbol{k}$), but now with respect to the rotational invariant basis. The rotational invariants $\Phi^{mnl}_{\mu\nu}$ are defined by

$$\Phi^{mnl}_{\mu\nu}(\boldsymbol{\omega}_1,\boldsymbol{\omega}_2,\hat{r}_{12})=\sqrt{(2m+1)(2n+1)}\sum_{\mu',\nu',\lambda'}\begin{pmatrix} m & n & l \\ \mu' & \nu' & \lambda' \end{pmatrix} R^m_{\mu'\mu}(\boldsymbol{\omega}_1)R^n_{\nu'\nu}(\boldsymbol{\omega}_2)R^l_{\lambda'0}(\hat{r}_{12}). \tag{2.15}$$

The coefficients $\begin{pmatrix} m & n & l \\ \mu' & \nu' & \lambda' \end{pmatrix}$ are the Wigner 3-j symbols and $R^m_{\mu'\mu}(\boldsymbol{\omega})$ are the generalized Wigner spherical harmonics,

$$R^m_{\mu'\mu}(\boldsymbol{\omega})=R^m_{\mu'\mu}(\phi,\beta,\psi)=\exp(-i\mu'\phi)r^m_{\mu'\mu}(\beta)\exp(-i\mu\psi)\ , \tag{2.16}$$

with $r^m_{\mu'\mu}$ the generalized Legendre polynomials. [Messiah, 1962] The expression 2.14 generalizes to all the functions studied in this work. We denote $\Theta=(\boldsymbol{\omega}_1,\boldsymbol{\omega}_2,\hat{r}_{12})$ the five angles characterizing the relative orientations of two molecules, with $\boldsymbol{\omega}_i$ the three Euler angles of molecule i and $\hat{r}_{12}$, two angles defining the local frame.

II.B Principles of the cDFT

The classical density functional theory (classical DFT) is a powerful theory for determining the 1-body density of a fluid in the presence of an external potential. [Mermin, 1965,Evans, 1979,Löwen, 2002,Wu, 2006,Evans et al., 2016,Hansen and McDonald, 2013] By providing exact reformulation of the statistical mechanics of fluids, it enables one to escape the N-body integrals. It relies instead on minimising of a functional of 1-body the density, which is much more efficient numerically. Similar to the famous electronic DFT, classical DFT suffers from the same major problem: while the reformulation is exact, the exact functional remains definitely unknown, and approximate functionals must be developed.

II.B.1 Fundamental theorem

I will propose here an alternative derivation of the cDFT theorem, based on the Levy-Lieb search idea and the recent work of Jeanmairet et Giner. [Levy, 1979,Lieb, 1983,Jeanmairet and Giner, 2025] I find this approach more intuitive and grounded in physics than the original *ad absurdum* derivation [Mermin, 1965,Evans, 1979]. I will derive it in the canonical ensemble and then I will discuss how to extend it to the grand canonical ensemble.

We consider the N-body probabilities $f^{(N)}$, such that $\mathrm{Tr} f^{(N)} = 1$, and define the following functional,

$$F_G\left[f^{(N)}\right] = -k_B T \,\mathrm{Tr}\left(f^{(N)} \ln\left(\frac{\exp(-\beta U)}{f^{(N)}}\right)\right) = -k_B T \left\langle \ln\left(\frac{\exp(-\beta U)}{f^{(N)}}\right)\right\rangle_{f^{(N)}} , \tag{2.17}$$

where we introduce the notation $\langle A\rangle_{f^{(N)}} = \mathrm{Tr}(f^{(N)}A)$. We note that $F_G\left[f^{(N)} = \rho^{(N)}\right] = -k_B T \ln Z = F$, where $\rho^{(N)} = \exp(-\beta U)/Z$ is the equilibrium N-body probability and F the free energy. By invoking the Jensen's inequality, we obtain

$$F_G[f] \geq -k_B T \ln\left\langle \frac{\exp(-\beta U)}{f^{(N)}}\right\rangle_{f^{(N)}} = -k_B T \ln Z = F \, . \tag{2.18}$$

This demonstrates that the Helmholtz free energy can be obtained by minimising the N-body probabilities,

$$F = \min_{f^{(N)}} F_G\left[f^{(N)}\right] \, . \tag{2.19}$$

We now consider the case of interest in classical DFT: a fluid under the influence of an external potential, *i.e.* $U = U_0 + V_{\mathrm{ext}}$, where U_0 the interaction energy of the bulk fluid and V_{ext} is an external potential of the form,

$$V_{\mathrm{ext}} = \int \mathrm{d}\boldsymbol{r} \int \mathrm{d}\boldsymbol{\omega} v_{\mathrm{ext}}(\boldsymbol{r},\boldsymbol{\omega})\rho(\boldsymbol{r},\boldsymbol{\omega}) \, , \tag{2.20}$$

where ρ is the 1-body density. The F_G functional now reads

$$F_G\left[f^{(N)}\right] = -k_B T \left\langle \ln\left(\frac{\exp(-\beta U_0)}{f^{(N)}}\right)\right\rangle_{f^{(N)}} + \int \mathrm{d}\boldsymbol{r} \int \mathrm{d}\boldsymbol{\omega} v_{\mathrm{ext}}(\boldsymbol{r},\boldsymbol{\omega}) \left\langle \rho(\boldsymbol{r},\boldsymbol{\omega})\right\rangle_{f^{(N)}} \, . \tag{2.21}$$

We can proceed with the Levy-Lieb constrained search in two steps: [Levy, 1979, Lieb, 1983, Jeanmairet and Giner, 2025] (i) we fix the 1-body density ρ and minimise over all the N-body

probabilities that give ρ (*i.e.*, $\langle\rho\rangle_{f^{(N)}} = \rho$, (ii) we minimise over all the 1-body densities. The Helmholtz free energy is given as

$$\begin{aligned} F &= \min_{\rho}\left[\min_{f^{(N)}\to\rho}\left(-k_BT\left\langle\ln\left(\frac{\exp(-\beta U_0)}{f^{(N)}}\right)\right\rangle_{f^{(N)}}\right)+\int \mathrm{d}\boldsymbol{r}\int \mathrm{d}\boldsymbol{\omega} v_{\mathrm{ext}}(\boldsymbol{r},\boldsymbol{\omega})\rho(\boldsymbol{r},\boldsymbol{\omega})\right] \\ &= \min_{\rho}\left[\mathcal{F}\left[\rho\right]+\int \mathrm{d}\boldsymbol{r}\int \mathrm{d}\boldsymbol{\omega} v_{\mathrm{ext}}(\boldsymbol{r},\boldsymbol{\omega})\rho(\boldsymbol{r},\boldsymbol{\omega})\right], \end{aligned} \tag{2.22}$$

where define the intrinsic functional

$$\mathcal{F}\left[\rho\right] = \min_{f^{(N)}\to\rho}\left(-k_BT\left\langle\ln\left(\frac{\exp(-\beta U_0)}{f^{(N)}}\right)\right\rangle_{f^{(N)}}\right). \tag{2.23}$$

The power of cDFT is that the intrinsic functional $\mathcal{F}\left[\rho\right]$ does not depend on the external potential v_{ext}, but only on the fluid interactions. If we would know this functional, we would be able to determine the free energy and equilibrium 1-body density for any external potential, just by following the minimisation procedure.

The intrinsic functional $\mathcal{F}[\rho]$ can be written as the sum of two parts: the ideal gas functional $\mathcal{F}_{id}$ and the excess part $\mathcal{F}_{\mathrm{exc}}$ that includes the interaction between the particles

$$\mathcal{F}[\rho] = \mathcal{F}_{\mathrm{id}}[\rho] + \mathcal{F}_{\mathrm{exc}}[\rho]. \tag{2.24}$$

The ideal part (*i.e.*, the case without interaction) corresponds to the entropy and is written as

$$\mathcal{F}_{\mathrm{id}}[\rho] = k_BT\int \mathrm{d}\boldsymbol{r}\mathrm{d}\boldsymbol{\omega}\rho(\boldsymbol{r},\boldsymbol{\omega})\left(\ln\left(\lambda^3\rho(\boldsymbol{r},\boldsymbol{\omega})\right)-1\right). \tag{2.25}$$

II.B.2 Extension to the grand canonical ensemble

The standard proof of the classical DFT theorem is based on the grand canonical formulation and demonstrates that there is a one-to-one correspondence between the equilibrium density and the external potential $\rho_1 \Leftrightarrow v_{\mathrm{ext}}$. On the other hand, Lutsko recently demonstrated that in the case of the canonical ensemble, the equilibrium density corresponds to a family of external potentials that are defined up to an additive constant. [Lutsko, 2022] The Levy-lieb approach in the grand canonical ensemble appears feasible, albeit impractical in terms of notation. The trace will be written as

$$Tr_{GC} = \sum_{N=0}^{\infty}\exp(\mu N)\int \mathrm{d}\boldsymbol{r}^N\mathrm{d}\boldsymbol{\omega}^N, \tag{2.26}$$

and the initial function to express the grand potential will be

$$\Omega_G\left[\{f\}\right] = -k_B T \sum_{N=0}^{\infty} \int \mathrm{d}\boldsymbol{r}^N \mathrm{d}\boldsymbol{\omega}^N f^{(N)} \ln\left(\frac{\exp(-\beta U + \beta\mu)}{f^{(N)}}\right) \tag{2.27}$$

where $\{f\} = f^{(1)}, f^{(2)}, f^{(2)}, ...$ is a family of j-body probabilities. To continue, I should understand how to apply the Jensen's inequality and in which set of probabilities function the minimisation akin to equation 2.19 should be performed. For the remainder of this manuscript, I will assume the standard classical DFT theorem and express the grand potential as

$$\Omega = \min_{\rho} \Omega_{v_{\mathrm{ext}}}\left[\rho\right] \ , \tag{2.28}$$

with the grand potential functional

$$\Omega_{v_{\mathrm{ext}}}\left[\rho\right] = \mathcal{F}[\rho] - \mu \int \mathrm{d}\boldsymbol{r} \int \mathrm{d}\boldsymbol{\omega} \rho(\boldsymbol{r},\omega) + \int \mathrm{d}\boldsymbol{r} \int \mathrm{d}\boldsymbol{\omega} v_{\mathrm{ext}}(\boldsymbol{r},\boldsymbol{\omega}) \rho(\boldsymbol{r},\boldsymbol{\omega}) \tag{2.29}$$

where $\mathcal{F}$ is the intrinsic functional that does not depend on the external potential v_{ext}.

II.B.3 Expression of the direct correlation functionals

We define the 1- and 2-body direct correlation functionals,

$$c^{(1)}(\boldsymbol{r},\boldsymbol{\omega};\rho) = -\frac{\delta\beta\mathcal{F}_{\mathrm{exc}}}{\delta\rho(\boldsymbol{r},\boldsymbol{\omega})}[\rho] \tag{2.30}$$

$$c^{(2)}(\boldsymbol{r},\boldsymbol{\omega},\boldsymbol{r}',\boldsymbol{\omega}';\rho) = \frac{\delta c^{(1)}(\boldsymbol{r},\boldsymbol{\omega};\rho)}{\delta\rho(\boldsymbol{r}',\boldsymbol{\omega}')} = -\frac{\delta^2\beta\mathcal{F}_{\mathrm{exc}}}{\delta\rho(\boldsymbol{r}',\boldsymbol{\omega}')\delta\rho(\boldsymbol{r},\boldsymbol{\omega})} \tag{2.31}$$

$$= c^{(2)}(\boldsymbol{r}',\boldsymbol{\omega}',\boldsymbol{r},\boldsymbol{\omega};\rho) \tag{2.32}$$

They are functions of the particle positions and orientations, as well as functionals of the 1-body density. The 2-body direct correlation functional is related to the (2-body) direct correlation function, which is defined through the Ornstein-Zernike equation 2.11, $c(\boldsymbol{r},\boldsymbol{\omega},\boldsymbol{r}',\boldsymbol{\omega}') \equiv c^{(2)}(\boldsymbol{r},\boldsymbol{\omega},\boldsymbol{r}',\boldsymbol{\omega}';\rho_0)$. Combining equations 2.25 and 2.30, the minimisation 2.28 takes the form

$$\lambda^3\rho_1(\boldsymbol{r},\boldsymbol{\omega}) = \exp\left(-\beta\mu - \beta v_{\mathrm{ext}}(\boldsymbol{r},\boldsymbol{\omega}) + c^{(1)}(\boldsymbol{r},\boldsymbol{\omega})\right) \tag{2.33}$$

where $c^{(1)}(\boldsymbol{r},\boldsymbol{\omega}) = c^{(1)}(\boldsymbol{r},\boldsymbol{\omega};\rho_1)$ is a one-body effective potential that takes into account the contribution of interactions between particles. For $g(\boldsymbol{r},\boldsymbol{\omega}) = \frac{\rho_1(\boldsymbol{r},\boldsymbol{\omega})}{\rho_0}$, the previous relation becomes

$$g(\boldsymbol{r},\boldsymbol{\omega}) = \exp\left(-\beta v_{\mathrm{ext}}(\boldsymbol{r},\boldsymbol{\omega}) + c^{(1)}(\boldsymbol{r},\boldsymbol{\omega}) - c^{(1)}(\rho_0)\right) \ , \tag{2.34}$$

where $c^{(1)}(\rho_0)$ is the excess chemical potential of the bulk system. It is defined by

$$c^{(1)}(\rho_0) = -\frac{\delta\beta\mathcal{F}_{\text{exc}}}{\delta\rho(\boldsymbol{r},\boldsymbol{\omega})}[\rho] = -\beta\mu + \beta\mu_{id}(\rho_0) \ , \tag{2.35}$$

where $\mu_{id}(\rho_0) = k_B T \ln \lambda^3 \rho_0$ is the chemical potential of the ideal gas. For the case of the ideal gas (no inter-particle interactions) $c^{(1)} = 0$, we recover the Boltzmann relation of the ideal fluid in the presence of an external potential $v_{\text{ext}}(\boldsymbol{r},\boldsymbol{\omega})$.

II.B.4 Application to the solvation

For the bulk, the grand potential functional is written as

$$\Omega_{v_{\text{ext}}=0}[\rho_0] = \mathcal{F}[\rho_0] - \mu \int \mathrm{d}\boldsymbol{r}\mathrm{d}\boldsymbol{\omega}\rho_0(\boldsymbol{r},\boldsymbol{\omega}) \ , \tag{2.36}$$

while the grand potential of a system subjected to an external potential, with the same chemical potential and the same temperature, is

$$\Omega_{v_{\text{ext}}}[\rho] = \mathcal{F}[\rho] - \mu \int \mathrm{d}\boldsymbol{r}\mathrm{d}\boldsymbol{\omega}\rho(\boldsymbol{r},\boldsymbol{\omega}) + \int \mathrm{d}\boldsymbol{r}\mathrm{d}\boldsymbol{\omega}\rho(\boldsymbol{r},\boldsymbol{\omega})v_{\text{ext}}(\boldsymbol{r},\boldsymbol{\omega}) \tag{2.37}$$

The difference between these functionals gives

$$\begin{aligned}
\Delta\Omega[\rho] &= \Omega_{v_{\text{ext}}}[\rho] - \Omega_{v_{\text{ext}}=0}[\rho_0] \\
&= \mathcal{F}[\rho] - \mathcal{F}[\rho_0] + \int \mathrm{d}\boldsymbol{r}\mathrm{d}\boldsymbol{\omega}\rho(\boldsymbol{r},\boldsymbol{\omega})v_{\text{ext}}(\boldsymbol{r},\boldsymbol{\omega}) - \int \mathrm{d}\boldsymbol{r}\mathrm{d}\boldsymbol{\omega}\mu\Delta\rho(\boldsymbol{r},\boldsymbol{\omega}) &(2.38)\\
&= (\mathcal{F}_{\text{id}}[\rho] - \mathcal{F}_{\text{id}}[\rho_b]) + (\mathcal{F}_{\text{exc}}[\rho] - \mathcal{F}_{\text{exc}}[\rho_b]) + F_{\text{ext}}[\rho] \ . &(2.39)
\end{aligned}$$

The difference between the excess free energy can be obtained a thermodynamic integration between the reference state (with density ρ_0) and the density ρ. Using the relations 2.30 and 2.32, this gives

$$\begin{aligned}
(\mathcal{F}_{\text{exc}}[\rho] - \mathcal{F}_{\text{exc}}[\rho_0]) &= k_B T \int_0^1 \mathrm{d}\lambda \int \mathrm{d}\boldsymbol{r}\mathrm{d}\boldsymbol{\omega}\Delta\rho(\boldsymbol{r},\omega)c^{(1)}(\boldsymbol{r},\boldsymbol{\omega};\rho_\lambda) &(2.40)\\
&= k_B T \int \mathrm{d}\boldsymbol{r}\mathrm{d}\boldsymbol{\omega} \int \mathrm{d}\boldsymbol{r}'\mathrm{d}\boldsymbol{\omega}'\Delta\rho(\boldsymbol{r},\omega)\mathcal{C}(\boldsymbol{r},\boldsymbol{\omega},\boldsymbol{r}',\boldsymbol{\omega}')\Delta\rho(\boldsymbol{r}',\omega') \\
&\quad - k_B T \int \mathrm{d}\boldsymbol{r}\mathrm{d}\boldsymbol{\omega}\Delta\rho(\boldsymbol{r},\boldsymbol{\omega})c^{(1)}(\rho_0) &(2.41)
\end{aligned}$$

where

$$\mathcal{C}(\boldsymbol{r},\boldsymbol{\omega},\boldsymbol{r}',\boldsymbol{\omega}') = \int_0^1 d\alpha(\alpha-1)c^{(2)}(\boldsymbol{r},\boldsymbol{\omega},\boldsymbol{r}',\boldsymbol{\omega}';\rho_\alpha) \tag{2.42}$$

and $\Delta\rho = \rho - \rho_0$. Using equation 2.35, the solvation free energy can be re-organised as the sum of three terms,

$$\Delta\Omega[\rho] = \Delta\Omega_{\rm id}[\rho] + \Delta\Omega_{\rm exc}[\rho] + F_{\rm ext}[\rho] \tag{2.43}$$

with $\Delta\Omega_{\rm id}[\rho]$, $\Delta\Omega_{\rm exc}[\rho]$ and $F_{\rm ext}[\rho]$ the ideal, excess, and external solvation functionals. The ideal and external solvation functionals are explicitly known,

$$\Delta\Omega_{\rm id}[\rho] = k_BT \int \Big[\rho(\boldsymbol{r},\boldsymbol{\omega}) \ln\Big(\frac{\rho(\boldsymbol{r},\boldsymbol{\omega})}{\rho_0}\Big) - \rho(\boldsymbol{r},\boldsymbol{\omega}) + \rho_0\Big] \mathrm{d}\boldsymbol{r}\mathrm{d}\boldsymbol{\omega} \ , \tag{2.44}$$

$$F_{\rm ext}[\rho] = \int \rho(\boldsymbol{r},\boldsymbol{\omega}) v_{\rm ext}(\boldsymbol{r},\boldsymbol{\omega}) \mathrm{d}\boldsymbol{r}\mathrm{d}\boldsymbol{\omega}. \tag{2.45}$$

while the excess solvation functional reads

$$\Delta\Omega_{\rm exc}[\rho] = k_BT \int \mathrm{d}\boldsymbol{r}\mathrm{d}\boldsymbol{\omega}\Delta\rho(\boldsymbol{r},\omega)\mathcal{C}(\boldsymbol{r},\boldsymbol{r}',\boldsymbol{\omega},\boldsymbol{\omega}')\Delta\rho(\boldsymbol{r}',\omega') \ . \tag{2.46}$$

I mention that (i) the 1-body term $-k_BT \int \mathrm{d}\boldsymbol{r}\mathrm{d}\boldsymbol{\omega}\Delta\rho(\boldsymbol{r},\boldsymbol{\omega})c^{(1)}(\rho_0)$ was absorbed in the definition of $\Delta\Omega_{\rm id}$ and not in $\Delta\Omega_{\rm exc}$, and, therefore, (ii) $\Delta\Omega_{\rm exc} \neq \mathcal{F}_{\rm exc}[\rho] - \mathcal{F}_{\rm exc}[\rho_b]$, hence the difference in notation. I will now discuss the different approximations that have been proposed in the literature for modelling the unknown part of the functional $\Delta\Omega[\rho]$— the excess functionals $\mathcal{F}_{\rm exc}[\rho]$ or $\Delta\Omega_{\rm exc}[\rho]$.

II.C Construction of the excess functional

In this section, I will review different strategies for developing the excess functionals, either directly ($\mathcal{F}_{\rm exc}$) or in their solvation expressions ($\Delta\Omega_{\rm exc}[\rho]$, equation 2.46). As most of the theories were developed for spherical particles, I will use the notation $\mathbf{x}$ for the spatial degrees of freedom, representing either position $\mathbf{x} \equiv \boldsymbol{r}$ only, or position and orientation, $\mathbf{x} \equiv \boldsymbol{r},\boldsymbol{\omega}$.

II.C.1 Fundamental measure theory

The development of the statistical physics of fluids is often based on the hard sphere model, which captures the essence of the microscopic structure and thermodynamics of real fluids. Within the cDFT framework, the development of the excess functional known as FMT (fundamental measure theory) has been tremendously successful in accurately reproducing the properties of hard sphere fluids in the presence of an external potential. [Rosenfeld, 1989, Roth, 2010] For a hard sphere fluid, the FMT functional is given by

$$\mathcal{F}_{\rm exc}[\rho] = \int \mathrm{d}\mathbf{x}\Phi\left(\{\hat{\rho}_\alpha(\mathbf{x})\}\right) \tag{2.47}$$

where $\hat{\rho}_\alpha(\mathbf{x})$ denotes the weighted densities of the 1-body density with a weight function w_α, $\hat{\rho}_\alpha(\mathbf{x}) = \int \mathrm{d}\mathbf{x}' w_\alpha(\mathbf{x},\mathbf{x}')\rho(\mathbf{x}')$. The weight functions $\{w_\alpha\}$ are based on the geometric characteristics of the overlap between hard spheres. [Rosenfeld, 1989, Roth, 2010] The function Ψ

is related to the bulk free energy of the hard sphere fluid, for which different expressions have been developed. [Roth et al., 2002, Hansen-Goos and Roth, 2006] Extending the FMT to non-spherical hard bodies is an active area of research. [Hansen-Goos and Mecke, 2009, Hansen-Goos and Mecke, 2010, Marechal et al., 2011, Roth et al., 2012, Wittmann et al., 2015, Wittmann et al., 2016, Wittmann et al., 2017]

II.C.2 Perturbation-base functionals

Exact perturbation We consider that the pair interaction between the solvent particles can be divided into two terms, $v = v_0 + v_w$, where v_w usually represents the weak, attractive interactions while v_0 represents the the strong repulsion between the particles. We define the intermediate potentials $v_\lambda = v_0 + \lambda v_w$, for $0 < \lambda < 1$. After performing a thermodynamic integration along the path $\lambda = 0 \to 1$, the excess free energy functional can be expressed exactly as [Hansen and McDonald, 2013]

$$\mathcal{F}_{\text{exc}}[\rho] = \mathcal{F}^0_{\text{exc}}[\rho] + \mathcal{F}_{\text{MF}}[\rho] + \mathcal{F}_{\text{corr}}[\rho] \ , \tag{2.48}$$

where $\mathcal{F}^0_{\text{MF}}[\rho]$ is the excess function for a fluid with pair potential v_0, $\mathcal{F}_{\text{MF}}[\rho]$ is the mean-field term which depends quadratically on ρ,

$$\mathcal{F}_{\text{MF}}[\rho] = \frac{1}{2} \int \mathrm{d}\mathbf{x} \int \mathbf{x}' \rho(\mathbf{x}) v_w(\mathbf{x}, \mathbf{x}') \rho(\mathbf{x}') \ , \tag{2.49}$$

and where $\mathcal{F}_{\text{corr}}[\rho]$ is called the correlation functional and reads

$$\mathcal{F}_{\text{corr}}[\rho] = \frac{1}{2} \int \mathrm{d}\lambda \int \mathrm{d}\mathbf{x} \int \mathbf{x}' \rho(\mathbf{x}) w(\mathbf{x}, \mathbf{x}') \rho(\mathbf{x}') \left(g^{(2)}_\lambda(\boldsymbol{r}, \mathbf{x}, \boldsymbol{\omega}') - 1 \right) \ . \tag{2.50}$$

This term depends on all the 2-point pair distribution functions $g^{(2)}_\lambda$ associated with the intermediate potentials v_λ. This exact perturbation scheme cannot be used directly, both the reference functional $\mathcal{F}^0_{\text{exc}}[\rho]$ and the correlation functional $\mathcal{F}_{\text{corr}}[\rho]$ must be approximated.

Standard mean-field approximation The standard mean-field approach assumes that $\mathcal{F}_{\text{corr}}[\rho] = 0$. The accuracy of this approach therefore depends on the approximation used for the reference term and on the relative smallness of the potential v_w. In the literature, the most common strategy is to employ the FMT functional for the reference term, which model the short-range repulsion, while the van der Waals and electrostatic interactions are taken into account in the mean-field functional $\mathcal{F}_{\text{MF}}$. [Archer et al., 2017] In the case of supercritical CO$_2$, this strategy was recently followed by Budkov et al. to study the solvation properties. [Kalikin et al., 2021a, Kalikin et al., 2020, Kalikin et al., 2021b] They obtained the qualitative evolution of the solvation free energy for different pressures and temperatures. They focused in particular on molecules of pharmaceutical interest (aspirin, ibuprofen, carbamazepine). However, the spherical approximation in FMT neglects anisotropic interactions between CO$_2$ and the solute, which prevents the important specific interactions from being accurately described.

Baker-Henderson functional The standard mean-field approximation is equivalent to write that $g_\lambda^{(2)} \approx 1$ in the expression of the correlation functional. 2.50 The correlation term could be approximated more accurately by assuming instead that $g_\lambda^{(2)} \approx g_1^{(2)}$. This gives the Baker-Henderson excess functional, $\mathcal{F}_{\text{exc}} = \mathcal{F}_{\text{exc}}^0 + \mathcal{F}_{\text{MF}} + \mathcal{F}_{\text{corr}}^{\text{BH}}$, where

$$\mathcal{F}_{\text{corr}}^{\text{BH}}[\rho] = \frac{1}{2}\int \mathrm{d}\mathbf{x} \int \mathbf{x}'\rho(\mathbf{x})v_w(\mathbf{x},\mathbf{x}')\rho(\mathbf{x}')\left(g^{(2)}(\mathbf{x},\mathbf{x}')-1\right) \ . \tag{2.51}$$

This method is relative expansive, since it requires to determine the 2-point correlation $g^{(2)}$ for each density during the minimisation process. [Tschopp et al., 2020]

II.D Thermodynamics-based functionals

Local density approximation The local density approximation (LDA) assumes that each small volume element $\mathrm{d}\mathbf{x}$ is in equilibrium with a given density $\rho(\boldsymbol{r})$. The excess free energy is therefore given by

$$\mathcal{F}_{\text{exc}}[\rho] = \int \mathrm{d}\mathbf{x} a(\rho(\mathbf{x})) \ , \tag{2.52}$$

where $\Psi(\rho)$ is the Helmholtz free energy density of the bulk fluid. [Duque et al., 2004] This is a significant approximation as it neglects all non-local contributions to the free energy, *e.g.*, the surface tension between regions with density differences.

Density gradient functional In order to include some interfacial effects, the LDA can be extended to include a gradient term. This yields the functional of the density gradient theory (DFT): [Duque et al., 2004]

$$\mathcal{F}_{\text{exc}}[\rho] = \int \mathrm{d}\mathbf{x} \left(a(\rho(\mathbf{x})) + \frac{\gamma}{2}|\nabla\rho(\mathbf{x})|^2\right) \ , \tag{2.53}$$

where γ is related to the surface tension of the fluid. This approach is still based on macroscopic thermodynamics concepts, and neglects the microscopic interactions between the solvent particles. In practice, the Helmholtz free energy and the surface tension can be derived using equations of state.

Statistical associated fluid theories One such family of equation of state are the statistical associated fluid theories (SAFT). The SAFT were designed to include a microscopic information, in contrast with the standard cubic equation of state. [Vega, 2018] They have primarily been developed by the chemical engineering community. They are based on stat-mech theory; the molecular interactions are the sum of three contributions: the hard sphere potential for the short-range interactions, the perturbation theory for the long-range interactions (*e.g.*, electrostatic), and Wertheim's perturbation method for the other associative interactions. [Chapman et al., 1989, Wertheim, 1984] Near the critical point, the SAFT have been combined with the renormalisation group approach to include the critical divergence and non mean-field properties. [Llovell and Vega, 2006, Llovell and Vega, 2007] SAFT have also been used to investigate

mesoscale interfacial properties (*e.g.* surface tension or structure in mesoconfinement). [Klink and Gross, 2014, Klink et al., 2015, Malheiro et al., 2014b, Malheiro et al., 2014a, Bernet et al., 2020, Miqueu and Grégoire, 2020, Dufour-Décieux et al., 2025] The SAFT family is of a powerful and versatile framework for studying the properties of CO_2 fluids at macro- and mesoscales. [Dias et al., 2006, Llovell and Vega, 2015, da Silva et al., 2018, Tang and Gross, 2010] But, like the cubic equation of state, the SAFT equations require several parameters to be fitted for CO_2 fluid and its mixtures, which limits their transferability to the study of real CO_2-based processes. In addition, the SAFT do not account for the anisotropy of the interactions at the molecular scale. This key feature is essential for modelling the CO_2 fluid close to a microscopic environment, such as nanoconfinements or complex solutes.

Exact weighted density approximation The LDA formulation 2.52 becomes valid for coarse-grained densities, where the microscopic fluctuations are averaged out. This idea led to the weighted density approximation, in which the excess functional is [Nordholm et al., 1980,Curtin and Ashcroft, 1985, Tarazona, 1985b, Tarazona, 1985a]

$$\mathcal{F}_{\mathrm{exc}}[\rho] = \int \mathrm{d}\mathbf{x}\rho\Psi(\bar{\rho}(\mathbf{x})) \; . \tag{2.54}$$

The coarse-grained density $\bar{\rho}$ is obtained from a convolution product with a weight function w,

$$\bar{\rho}(\mathbf{x}) = \int \mathrm{d}\mathbf{x}' w(\mathbf{x},\mathbf{x}')\rho(\mathbf{x}') \; . \tag{2.55}$$

The form of the weight function could be chosen empirically, *e.g.* a Gaussian weight could be used with a screening length parameter. [Borgis et al., 2020] It could also be determined more accurately by ensuring that the functional derivatives of $\mathcal{F}_{\mathrm{exc}}[\rho]$ (*i.e.* the direct correlation functions) are equal to those of the homogeneous bulk fluid at different densities. [Tarazona, 1985b] This requirement gives rise to a series of complicated equations, which are particularly difficult to solve if the pair potential contains an attractive interaction.

II.E Homogeneous reference fluid and bridge corrections

In a dense fluid, we can assume that the solvent correlations close to the solute are similar to those in the bulk (*i.e.*, without interference from the solute). This idea lies at the heart of the Gaussian field theory developed by Chandler and collaborators, [Chandler, 1993, Sergievskyi et al., 2017] in particular for studying hydrophobicity. [Lum et al., 1999] In the cDFT framework, this means that the 2-point correlations of the bulk, c, should play a central role. With this in mind, the exact excess solvation free energy (equation 2.46) can be reformulated exactly as follows:

$$\Delta\Omega_{\mathrm{exc}}[\rho] = \Delta\Omega_{\mathrm{HRF}}[\rho] + \Delta\Omega_{\mathrm{bridge}}[\rho] \; , \tag{2.56}$$

where $\Delta\Omega_{\mathrm{HRF}}[\rho]$ is the free energy induced by the bulk correlation, at the quadratic level. It reads

$$\Delta\Omega_{\mathrm{HRF}}[\rho] = -\frac{k_B T}{2} \int \mathrm{d}\mathbf{x} \int \mathbf{x}' \Delta\rho(\mathbf{x}) c(\mathbf{x}, \mathbf{x}') \Delta\rho(\mathbf{x}'), \tag{2.57}$$

where $\Delta\rho = \rho - \rho_0$, which measures the excess density around the solute. The bridge functional $\Delta\Omega_{\mathrm{bridge}}[\rho] = \Delta\Omega_{\mathrm{exc}}[\rho] - \Delta\Omega_{\mathrm{HRF}}[\rho]$ contains all the effects of the solute on the solvent correlations. After minimisation, the equilibrium density in presence of a solute is

$$\rho_1(\mathbf{x}) = \rho_0 \exp\left(-\beta v_{\mathrm{ext}}(\mathbf{x}) + \int \mathbf{x}' c(\mathbf{x}, \mathbf{x}') \Delta\rho(\mathbf{x}') + b_1(\mathbf{x})\right) , \tag{2.58}$$

where b_1 is the bridge function

$$b_1(\mathbf{x}) = \frac{\delta \Delta\Omega_{\mathrm{bridge}}}{\delta\rho(\mathbf{x})}[\rho_1] , \tag{2.59}$$

In this approach, the excess functional requires two inputs: the bulk direct correlation function c and on the bridge functional $\Delta\Omega_{\mathrm{bridge}}[\rho]$.

II.E.1 Calculating the bulk correlation

The determination of accurate bulk correlations c is paramount for the success of this strategy. I will discuss two methods to calculate them.

Integral equations The integral equations are a set of liquid-state theories developed for calculating the structural and thermodynamic properties of bulk fluids. [Hansen and McDonald, 2013] Taking as inputs the pair potential v and the thermodynamic conditions, they output the thermodynamic properties and various correlation functions, such as the pair distribution g and the direct correlation c. In practice, they rely on combination of the Ornstein-Zernike equation 2.11; the equilibrium pair distribution (obtained from equation 2.58),

$$g = \exp\left(-\beta v_{\mathrm{ext}} + g - 1 - c + b_0\right) , \tag{2.60}$$

where b is the bridge function for the bulk fluid, $b(\mathbf{x}) = \frac{\delta \Delta\Omega_{\mathrm{bridge}}}{\delta\rho(\mathbf{x})}[\rho_0]$; and a closure equation relating the bridge function to either the pair distribution function $b[g]$ or to the pair potential $b[v]$. Numerous closure relations have been developed, achieving some successes in specific systems (*e.g.*, hard sphere fluids, electrolytes). [Hansen and McDonald, 2013] For instance, the hypernetted chain approximation (HNC) involves neglecting the bridge term, $b = 0$, and can accurately predict the structural properties of simple liquids. [Lado et al., 1983, Fries and Patey, 1985, Anta et al., 1995] In the presence of a solute with a potential v_{ext}, we note that using the c from HNC into the HRF functional (equation 2.57) and disregarding the bridge functional ($\delta\Delta\Omega_{\mathrm{bridge}} = 0$) results in a classical DFT that is identical to the HNC integral equations for a for a binary solute/solvent mixture. [Hansen and McDonald, 2013]

MD simulations Alternatively, the direct correlations can be calculated rigorously using molecular dynamics simulations. The Ornstein-Zernike equation 2.11 can be inverted using the pair distribution functions obtained from the MD simulations to determine the exact c. [Ramirez et al., 2002, Puibasset and Belloni, 2012, Belloni, 2017] While this approach can provide c and $\Delta\Omega_{\mathrm{HRF}}$, it is however severely limited by the computational cost of calculating the direct correlation functions, since such correlations must be calculated for each temperature, and long MD simulations are required.

II.E.2 Calculating the bridge functional

Homogeneous reference fluid The second term in the excess functional 2.56 is the bridge functional. For a simple liquid, this term should be viewed as a correction, since the most important contributions of the interactions are accounted for in the $\Delta\Omega_{\mathrm{HRF}}[\rho] = 0$. The simplest approximation is to neglect this, $\Delta\Omega_{\mathrm{bridge}}[\rho] = 0$ and is called HRF (for homogeneous reference fluid). [Hansen and McDonald, 2013] This amounts to writing the excess functional as

$$\Delta\Omega_{\mathrm{exc}}^{\mathrm{HRF}} = \Delta\Omega_{\mathrm{HRF}}. \tag{2.61}$$

This HRF approximation, combined with the c calculated from Md simulations, lies at the heart of the molecular density functional theory (MDFT), developed by D. Borgis, L. Belloni, M. Levesque, and G. Jeanmairet to investigate the solvation in water at ambient conditions. [Zhao et al., 2011c, Jeanmairet et al., 2013b, Jeanmairet et al., 2016, Ding et al., 2017] MDFT has successfully reproduced the structure and thermodynamics of the hydration of simple solutes, interfaces and biomolecules. [Levesque et al., 2012, Jeanmairet et al., 2014, Jeanmairet et al., 2019, Luukkonen et al., 2020, Borgis et al., 2021] This approach is however not fully accurate in the case of water, as the hydrogen bond tetrahedral network cannot be captured with a quadratic term as in equation 2.57. [Jeanmairet et al., 2013a, Jeanmairet et al., 2015, Borgis et al., 2020] The HRF approximation also fails to correctly determine the solvation free energy of macroscopic solutes. Consider for instance a hard sphere with a volume V_{sol}, the HRF approximation predicts that the solvation free energy is $\Delta G = -P_{\mathrm{HRF}} V_{\mathrm{sol}}$, where

$$P_{\mathrm{HRF}} = \frac{1}{2}\tilde{c}(k=0) k_B T \rho_0 \,. \tag{2.62}$$

In fact, the exact solvation free energy for the macroscopic hard sphere is $\Delta G = -PV_{\mathrm{sol}}$, with P the fluid pressure. The difference between P and P_{HRF} could be dramatic for certain liquids, *e.g.*, for water. The developers of MDFT proposed accounting for this HRF failure by adding an a posteriori correction to the free energy $\Delta G = -(P - P_{\mathrm{HRF}})V_{\mathrm{sol}}$. [Jeanmairet et al., 2015, Sergiievskyi et al., 2014, Sergiievskyi et al., 2015] The volume V_{sol} remains however ambiguous for a real solute, and this a posteriori correction will not correct the fluid density around the solute.

Hard sphere bridge The bridge functional can also be approximated using the FMT excess functional ($\Delta\Omega_{\mathrm{exc}}^{\mathrm{FMT}}$, equation 2.47). [Rosenfeld and Ashcroft, 1979, Rosenfeld, 1993, Kahl et al., 1996, Zhao et al., 2011b, Zhao et al., 2011a, Liu et al., 2013a, Liu et al., 2013b, Li et al., 2020]. The idea is to use only the FMT functional to account for the bridge contribution,

$$\Delta\Omega_{\rm exc}^{\rm HSB} = \Delta\Omega_{\rm HRF} + \underbrace{\Delta\Omega_{\rm exc}^{\rm FMT} - \Delta\Omega_{\rm HRF}^{\rm FMT}}_{\Delta\Omega_{\rm bridge}^{\rm FMT}} \tag{2.63}$$

where the functionals $\Delta\Omega^{\rm FMT}$ and $\Delta\Omega_{\rm HRF}^{\rm FMT}$ are

$$\Delta\Omega_{\rm exc}^{\rm FMT}[\rho] = \mathcal{F}_{\rm exc}^{\rm FMT}[\rho] - \mathcal{F}_{\rm exc}^{\rm FMT}[\rho_0] \tag{2.64}$$

$$\Delta\Omega_{\rm HNC}^{\rm FMT}[\rho] = -\frac{\delta\Delta\Omega_{\rm exc}^{\rm FMT}}{\delta\rho} + \frac{1}{2}\int {\rm d}\mathbf{x}{\rm d}\mathbf{x}'\Delta\rho(\mathbf{x})c^{\rm HS}(\mathbf{x},\mathbf{x}')\Delta\rho(\boldsymbol{r}') \tag{2.65}$$

with $c^{\rm HS}$ the direct correlation function for a hard sphere fluid of radius $R_{\rm sd}$. We can set this radius by imposing that it allows us to reproduce the correct pressure of the pure solvent or the correct solvation free energy for hard-sphere solutes with various radius. [Borgis et al., 2020]

WDA-like bridge Since the microscopic interactions between the solvent molecules are captured with the functional $\Delta\Omega_{\rm HRF}$, the bridge functional can be considered at a coarse-grained level, based on macroscopic considerations. For instance, it could have a local density form (equation 2.52),

$$\Delta\Omega_{\rm bridge}^{\rm LDA}[\rho] = \int {\rm d}\mathbf{x} f_{\rm bridge}(\rho(\mathbf{x}))\ , \tag{2.66}$$

where $f_{\rm bridge}(\rho)$ is the bridge free energy, per molecule, for the bulk fluid, defined by

$$f_{\rm bridge}(\rho) = f(\rho) - k_BT\left(x\ln(x) - x + 1\right) + P_{\rm HRF}(1-x)^2\ , \tag{2.67}$$

where $x = \rho/\rho_0$, and where f is the total free energy of the bulk fluid at density ρ, from which we remove the HRF contribution. Unfortunately, with this bridge term, the MDFT functional $\Delta\Omega$ (equation 2.39) cannot be minimised because the functional $\Delta\Omega_{\rm bridge}^{\rm LDA}$ diverges. [Evans, 1979] To overcome this limitation, the bridge functional can be made dependent on the coarse-grained density, [Borgis et al., 2020, Borgis et al., 2021]

$$\Delta\Omega_{\rm bridge}^{\rm WDA}[\rho] = \int d\mathbf{x}\, f_{\rm bridge}(\bar{\rho}(\mathbf{x}))\ , \tag{2.68}$$

where $\hat{\rho}(\boldsymbol{r})$ is given in equation 2.55. This strategy was recently employed in MDFT, with an empirical Gaussian weight,

$$\hat{\rho}(\boldsymbol{r}) = \int {\rm d}\boldsymbol{r}'\boldsymbol{\omega}'\rho(\boldsymbol{r}',\boldsymbol{\omega}')\frac{1}{\sqrt{2\pi\sigma_g^2}^3}\exp\left(-\frac{|\boldsymbol{r}-\boldsymbol{r}'|}{2\sigma_g^2}\right)\ , \tag{2.69}$$

where σ_g is the coarse-graining length. The functional bridge $\Delta\Omega_{\rm bridge}^{\rm WDA}[\rho]$ depends on this length σ_g and on the free energy of the bulk, $f_{\rm bridge}$. We will discuss in section III.D how to construct this bridge for $scCO_2$.

Inhomogeneous reference fluid Bui and Cox recently proposed to include the large scale fluctuations of the solvent using an ingenious scheme, inspired by the hydrophobicity theory of Lum, Chandler, and Weeks. [Bui and Cox, 2024,Lum et al., 1999] Instead of directly performing the thermodynamic integration from the reference bulk fluid (ρ_0) to the fluid in presence of the solute (ρ_1) (as in equation 2.41), they integrate first from the reference ρ_0 and an inhomogeneous coarse-grained density ($\bar{\rho}$), and then from the coarse-grained density to ρ_1. The coarse-grained density models the large-scale fluctuations of the solvent, such as the surface tension, and is typically described by an excess functional in a macroscopic form, as in equation 2.53. The coarse-grained density is coupled with the density ρ_1, which enables the latter to overcome the quadratic free energy (equation 2.57) and to reach a vapour density in the vicinity of the solute. [Ten Wolde and Chandler, 2002]

II.F Machine-learned functionals

The rise of the machine learning technologies provides a new opportunity for the development of accurate excess functionals. [Wu and Gu, 2023,Simon and Oettel, 2024] The general idea is based on the thermodynamic integral formulation of the excess functional, which reads

$$\mathcal{F}_{\text{exc}} = -\int_0^1 \mathrm{d}\lambda \int \mathrm{d}\mathbf{x}\rho(\mathbf{x})c_\lambda^{(1)}(\mathbf{x}) \ , \tag{2.70}$$

and to learn the functional relationship between $c^{(1)}$ and ρ_λ. [Shang-Chun and Oettel, 2019,Sammüller et al., 2023] In practice, the learning dataset is created from numerous molecular simulations of the fluid subjected to various external potentials. From each simulation, the density ρ_λ and the correlation function $c_\lambda^{(1)}$ are extracted, and a neural network is used to interpolate the relationship between them. This method was initially developed for 1D systems, but it is a rapidly expanding field of research, with recent developments towards anisotropic particles, [Simon and Oettel, 2024, Simon et al., 2025, Yang et al., 2025] and ionic liquids. [Bui and Cox, 2025]

This machine learning approach will likely enable us to construct highly accurate excess functionals for a given fluid. However, an important question remains: how transferable are these machine-learned functionals to an external potential v_{ext} that differs significantly from the potentials in the original dataset? In particular, we could question its effectiveness in the presence of a large solute/interface, where solvent fluctuations explore a larger part of the phase diagram and phase transitions could occur near the solute/the interface. [Ten Wolde and Chandler, 2002, Huang and Chandler, 2000] A recent work of Evans *et al.* [Robitschko et al., 2025] shows that learning the functionals only in a region of the supercritical phase diagram is sufficient to predict the coexistence curve and the interfacial profile in the subcritical domain. This is encouraging for the future development of a machine-learned functional for supercritical CO_2.

I will now review M. Houssein Mohamed's PhD project on constructing an MDFT functional for the supercritical CO_2.

III Previous work: M. Houssein Mohamed's PhD project.

M. Houssein Mohamed's PhD project focused on the development of a MDFT functional for $scCO_2$ in the near-critical region. In collaboration with D. Borgis and L. Belloni, we

determined the two terms of the excess functional: $\Delta\Omega_{\mathrm{HRF}}$ and the bridge functional $\Delta\Omega_{\mathrm{bridge}}$. The HRF functional (equation 2.57) depends on the direct correlation functions of the bulk fluid. We explored two methods of calculating the direct correlation functions (i) MD simulations and (ii) the HNC integral equation. We also tested different bridge functionals: no bridge (HRF), a WDA-like bridge (HRF+WDA, equation 2.68) and a hard sphere bridge (HRF+HBS, equation 2.63

III.A CO_2 modelling and thermodynamic conditions

We studied the CO_2 fluid at four densities under supercritical conditions ($0.4\ \rho_c$, $0.7\ \rho_c$, $0.8\ \rho_c$, and $2\ \rho_c$) at $T = 1.05\ T_c$, where ρ_c and T_c are the critical density and temperature of the CO_2 model, respectively. Among the force fields proposed in the literature for CO_2 [Harris and Yung, 1995, Potoff and Siepmann, 2001, Zhang and Duan, 2005, Cygan et al., 2012], we opted for the rigid version of the EPM2 model by Harris and Yung, [Harris and Yung, 1995]. This model reproduces the phase diagram of CO_2 in the supercritical region using a simple description of molecular interactions. It describes CO_2 as a linear molecule with fixed C-O distances, $d_{\mathrm{CO}} = 1.149$ Å and O-C-O angle. Intermolecular interactions are obtained as the sum of Lennard-Jones and Coulomb potentials. The critical point coordinates for this force field are: $T_c = 313.4$ K, $\rho_c = 453$ kg/m^3, and $P_c = 76.5$ bar. [Harris and Yung, 1995]

We calculated the direct correlation functions from the MD simulations and the HNC integral equation. The MD simulations were performed with the LAMMPS software, and the numerical details can be found in the reference [AC23]). The HNC calculations were performed in collaboration with L. Belloni, using one of his in-house codes. [Puibasset and Belloni, 2012, Belloni, 2017] The iterative resolution of equation 2.11 with the HNC closure relation (equation 2.60 with b =0) is a standard technique, although it is computationally expansive for anisotropic interactions. [Patey, 1977, Lado, 1982, Fries and Cosnard, 1987, Fries and Cosnard, 1987, Anta et al., 1995, Lado et al., 1995] L. Belloni recently proposed a powerful algorithm to accelerate the iterative resolution of anisotropic HNC for water. [Belloni and Chikina, 2014]

III.B Structure and thermodynamics of scCO_2

We first evaluated the ability of HNC to reproduce the thermodynamic properties and the local structure in the supercritical region. The EPM2 force field was designed specifically to accurately reproduce the experimental liquid-vapour coexistence curve [Harris and Yung, 1995]. A comparison of the experimental and MD curves is presented in Figure 2.3. On the other hand, HNC theory does not predict a coexistence curve, since there is no valid physical solution to the HNC equation over a range of pressures and temperatures. [Belloni, 1993, Rull et al., 1996] This forbidden HNC region has been added for comparison, although its boundary is more or less identified with the spinodal line. [Belloni, 1993, Rull et al., 1996] Since $T_c(\mathrm{HNC}) > T > T_c$, the HNC approach does not account for a small part of the isotherm relative to density, near the true critical point.

We then compared the local structure predicted by MD and HNC. Instead of considering the site-to-site distribution functions, we examined the pair distribution functions $g(r, \Theta)$ for four different orientations between CO_2 molecules: parallel, perpendicular (in the same plane), aligned, and cross. Figure 2.4 shows the pair distribution functions calculated by MD and by HNC for the three densities for which HNC admits solutions and for the four orientations (shown in the insets). We observe good agreement between the HNC and MD pair

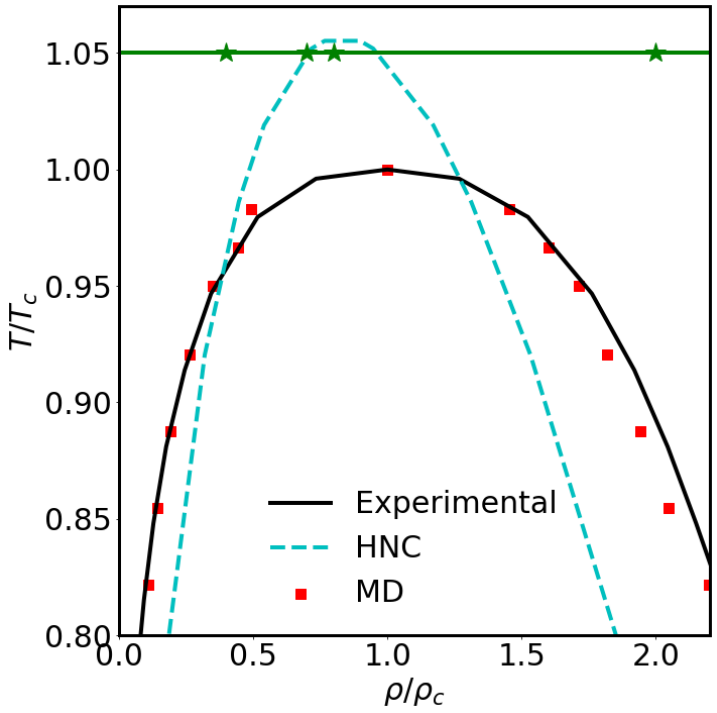

Figure 2.3 – Phase diagram of $scCO_2$ obtained with MD (EPMF force field) and HNC. Liquid-vapour coexistence curve obtained from experiments, MD simulations, and HNC calculations. For HNC, the dashed line indicates the limit of existence of HNC solutions (and not a physical transition line). The horizontal line and the star symbols indicate the isotherm and the four densities studied in M. Houssein Mohamed's project.

distribution functions at short range, as they coincide for all densities and orientations. The pair distribution functions for these four orientations reveal a strong microscopic organisation of the $scCO_2$ fluid: the first peak of the pair distribution is around 4 Å and is highest for the perpendicular (in-plane) orientation ($g \sim 6$, see figure 2.4(b)), slightly lower for the transverse orientation ($g \sim 2$, see figure 2.5(d)), and significantly lower for the other two orientations (parallel and aligned, $g \sim 6$, see figure 2.5(a) and (c)). This demonstrates that two neighbouring CO_2 molecules preferentially arrange themselves in the perpendicular (in-plane) orientation, a configuration that minimises the quadrupole-quadrupole interaction.

III.C Calculation of the $\Delta\Omega_{\mathrm{HRF}}$ Term

Determining the functional $\Delta\Omega$ requires calculating the direct correlation functions c using HNC or MD.

Numerical calculations of the MD correlation functions The MD-based c function can be obtained by inverting the Ornstein-Zernike equation 2.11 using the pair distributions g as inputs. However, the MD simulation data are only available for a limited range of distances r, *i.e.*, $r < L_{\mathrm{box}}/2$, and the long-range tail of the pair distribution functions cannot be calculated. This prevents an accurate inversion of the Ornstein-Zernike equation 2.11. This problem can be circumvented by using the available MD data at short distances ($r < r_{\mathrm{max}}$) and neglecting b at longer distances ($r > r_{\mathrm{max}}$), thus defining a new mixed closure:

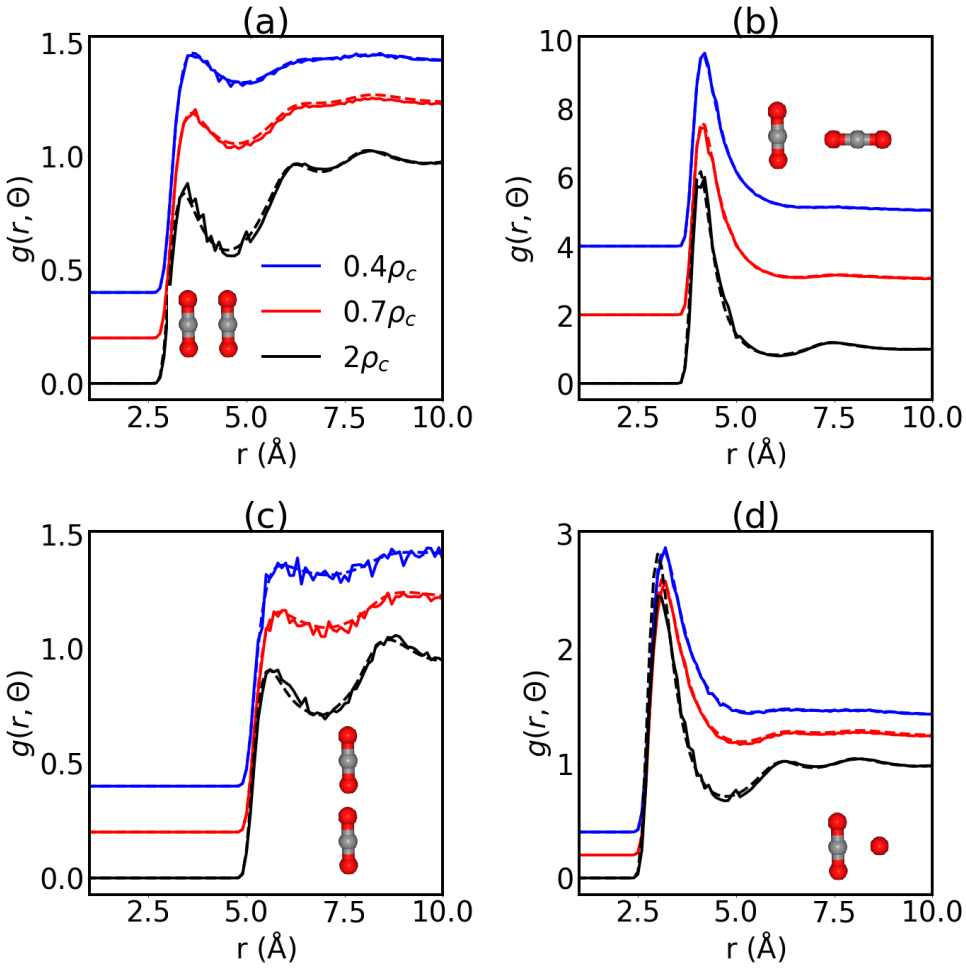

Figure 2.4 – Pair distribution functions $g(r,\Theta)$ for four characteristic orientations Θ, displayed as insets. The MD results are indicated by solid lines and the HNC results by dashed lines. The results are presented for three densities for which HNC solutions exist (0.4, 0.7, and 2 ρ_c). No results are presented for $0.8\ \rho_c$, as the MD pair distribution functions do not differ from those at $0.7\ \rho_c$ and the HNC calculation fails. The functions are shifted upwards for easier comparison.

$$g^{\alpha}(r) = g^{\alpha}(r)(\mathrm{MD}), \quad r \leq r_{\max} \tag{2.71}$$

$$= \left\langle \exp\left[-\beta v(r,\Theta) + \sum_{\alpha'} \gamma_{\alpha'}(r)\Phi_{\alpha'}(\Theta)\right] \Phi^{*}_{\alpha}(\Theta) \right\rangle, \quad r > r_{\max} \tag{2.72}$$

where v is the interaction potential between CO_2 molecules, γ is the indirect correlation function, $\gamma = h - c$, Φ_α are the rotational invariants, and $r_{\max} < L_{\mathrm{box}}/2$. The iterative solution with respect to $\gamma(r > r_{\max})$ is similar to that of HNC. The absence of a discontinuity in the functions $g^{\alpha}(r)$ at $r_{\max}$ will a posteriori confirm the validity of this mixed closure approach.

Comparison of Direct Correlation Functions c MD and HNC Figure 2.5 shows the direct correlation functions for the three densities for which HNC admits a solution and for the four mutual CO_2/CO_2 orientations described previously for the pair distribution functions. Figures 2.5(a)-(d) show the direct correlation functions $c(r,\Theta)$ in real space, while Figures 2.5(e)-(h) show their Fourier transforms $\tilde{c}(k,\Theta)$).

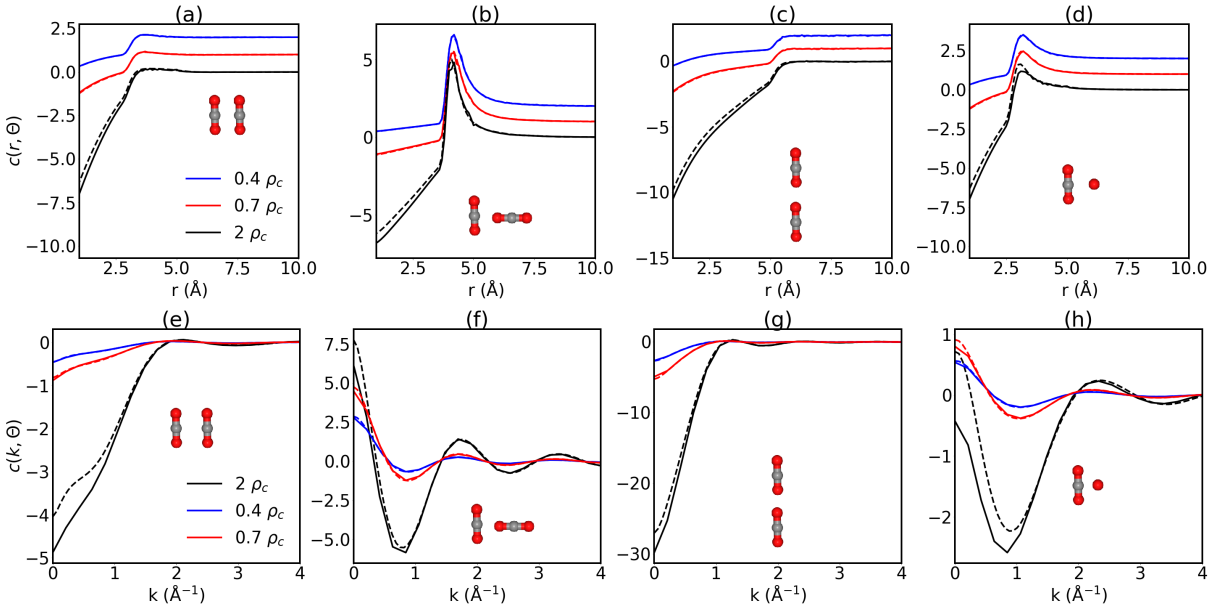

Figure 2.5 – Direct correlation function $c(r, \Theta)$ for four characteristic orientations Θ indicated in the insets. As in Figure 2.4, the MD results are indicated by solid lines and the HNC results by dashed lines. The results for three densities are represented (0.4, 0.7, and 2 ρ_c), with an upward shift (for graphs a, b, c, and d).

In direct space, all direct correlation functions behave similarly. There is an increase from negative values to 0 below 4 Å, an abrupt change in slope between 3 and 5 Å, a peak around 4-5 Å and a decrease to zero for higher distances. The highest peak is observed for the perpendicular orientation (2.5(b)), a smaller peak for the transverse orientation (2.5(d)), and an almost invisible peak for the other two orientations (parallel and aligned, (a) and (c)). The different densities only impact the initial values of the direct correlation functions; otherwise, a trend similar to that of the pair distribution functions is observed (Figure 2.4). In Fourier space (Figure 2.5(e)-(h)), the direct correlation functions differ mainly in the case of perpendicular and crossed orientations compared to parallel and aligned orientations. First, the initial values $\tilde{c}(k = 0, \Theta)$ are positive for perpendicular and crossed orientations, while they are negative for parallel and aligned orientations. Furthermore, the perpendicular and crossed orientations exhibit pronounced oscillations, related to the peaks in direct space, whereas the direct correlation functions in Fourier space for the parallel and aligned orientations are smoother.

If we now compare the HNC and MD direct correlation functions, we notice that they overlap perfectly for all distances at densities 0.4 ρ_c and 0.7 ρ_c. For the density 2 ρ_c, they only overlap beyond 4 Å (*i.e.*, beyond the slope change). Below 4 Å, the HNC direct correlation functions evolve slightly above the MD direct correlation functions, although the difference is small. In Fourier space, the HNC and MD direct correlation functions are completely identical for 0.4 ρ_c and 0.7 ρ_c. For 2 ρ_c, the HNC and MD direct correlation functions are similar above 1.5 Å^{-1}, while the HNC direct correlation functions evolve slightly above the MD direct correlation functions below 1.5 Å^{-1}. Notably, at 2 ρ_c, the direct correlation functions calculated using HNC differ from the MD results at both short and long distances (below 4 Å) and at long distance (below 1.5 Å^{-1}). The intermediate structure is well reproduced by HNC in the liquid region. For lower densities, the HNC and MD direct correlation functions are similar for all distances.

III.D Calculation of the $\Delta\Omega_{\text{bridge}}$ Term

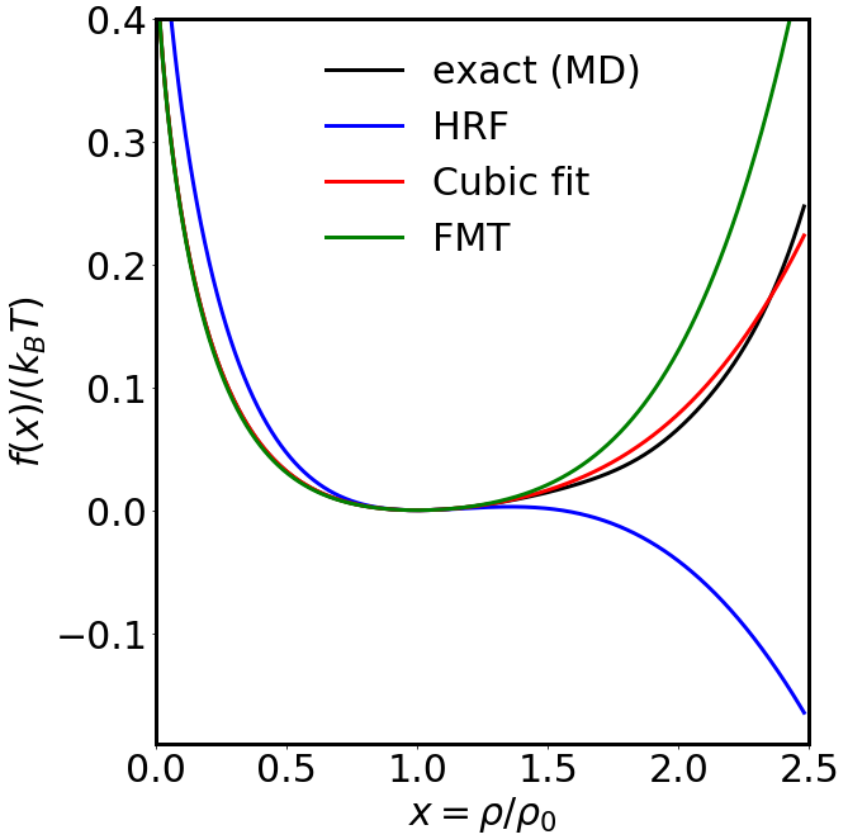

Figure 2.6 – Construction of the WDA bridge from the homogeneous fluid equation of state. Total free energy per molecule of the bulk fluid calculated with 4 methods: exact results from MD (black), HRF approximation (blue), cubic fit of the homogeneous bridge (red), FMT bulk functional (green). See the text for details.

We will now present the construction of the second term, $\Delta\Omega_{\text{bridge}}$, but only for the condition $\rho_0 = 0.8\ \rho_c$ and $T = 1.05\ T_c$. We implemented two strategies: the WDA-like approach (equation 2.68) and the HBS approach (equation 2.63). The WDA-like approach requires the determination of the homogeneous bridge 2.67. We assumed this bridge to have the simple form $f_{\text{bridge}}(x) = a_3 \Delta x^3$, where a_3 is a parameter to be determined, and $\Delta x = x - 1$. To do so, we performed a series of bulk MD calculations at different densities along the isotherm $T = 1.05\ T_c$, from. This enabled us to calculate the exact (MD-based) bulk free energy, and the exact homogeneous bridge (equation 2.67). We then fitted the exact bridge to the cubic approximation ($a_3 \Delta x^3$) and found $a_3 = 0.119$. Figure 2.6 shows the bulk free energy obtained from the MD simulations, the cubic fit, and the HRF approximation. The fitted bridge $f_{\text{bridge}}(x) = a_3 \Delta x^3$ perfectly reproduces the exact bulk free energy, whereas the HRF approximation ($f_{\text{bridge}}(x) = 0$) dramatically fails at high densities. The second parameter of the WDA-like bridge is the screening length of the Gaussian weight, σ_g. We determined this parameter by calculating the solvation free energy of a range of hard-sphere solutes with various radius σ. The best correspondence between MD and MDFT results was obtained for $\sigma_g = 1.45$ Å.

We similarly determined the hard sphere HBS bridge functional (equation 2.63) by fitting the hard-sphere radius R_{sd} to reproduce the bulk free energy. We found $R_{\text{sd}} = 1.78$ Å and

the FMT bulk free energy is presented in figure 2.6. The bulk FMT reproduces the MD results very well for densities $\rho < 1.5\rho_c$, but overestimates them beyond this point.

In summary, we have identified all the necessary ingredients for implementing different variants of the MDFT functional: the direct correlation functions c calculated from MD or MD, and the bridge functionals with the HRF, WDA-like, and HBS formulations. It remains to be seen how these MDFT The performance of these MDFT variants in reproducing the solvation properties remains to be seen.

III.E Comparison of MD and MDFT

We then compared the predictions of the various MDFT functionals with the MD results. We focused on the density $0.8\ \rho_c$ and the temperature $T = 1.05\ T_c$. We used two sets of solutes: LJ solutes with different radius/interaction energies, and small molecular solutes. The molecular solutes were modelled using the OPLS-AA force field, [Jorgensen et al., 1996] except for water, for which we used SPCE. [Berendsen et al., 1987] For each solute, we determined the pair distribution functions between the solute and the solvent, as well as the solvation free energy. The MD solvation free energies were calculated using Bennett's method by M. Houssein Mohamed, and were recently recalculated using thermodynamic integration by **C. Cao**, a Master 2 intern (February 25-July 25). Please refer to M. Houssein Mohamed's manuscript for the numerical details of both the MD simulations and MDFT calculations. [Houssein Mohamed, 2024]

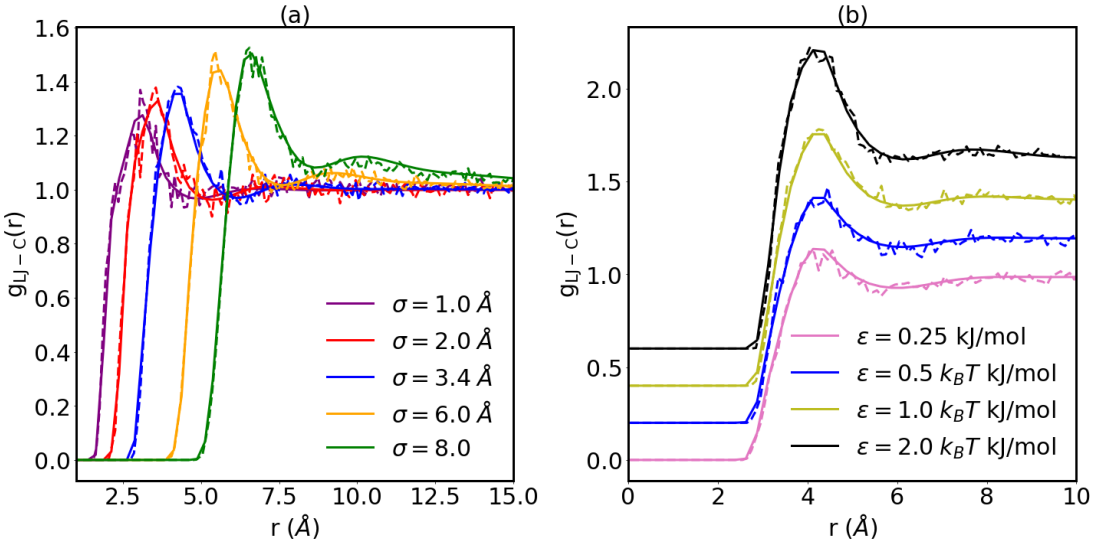

Figure 2.7 – Comparison of the solvation structure of $scCO_2$ around a spherical solute obtained by MD and MDFT: pair distribution function between the LJ solute and the C atom of the CO_2 solvent molecules obtained using two methods: predictions from MDFT (solid line) and calculations from MD (dashed lines). We studied two sets of LJ solutes: (a) with different radius σ and a fixed interaction energy $\varepsilon = 1.$ kJ/mol, and (b) with a fixed radius $\sigma = 3.4$ Å and various interaction energies.

Solvation of spherical solutes Figure 2.7 shows the radial distribution functions between the different LJ solutes and the C atom of the CO_2 molecule, $g_{\mathrm{LJ-C}}(r)$. We observe a perfect overlap between the predictions of MDFT and the results of the MD simulations, for all the solute radius and all the interaction energies investigated. We then considered the solvation free energies,

which are presented in figure 2.8 for 4 different methods: MD simulations and MDFT with 3 different bridge functionals: HRF (equation 2.61), HRF+HBS (equation 2.63) and HRF+WDA-like (equation 2.68). We observe again a perfect agreement between the solvation free energies and the MDFT calculations, except for the smallest interaction energy ($\varepsilon = 0.25$ kJ/mol) and the larger solutes ($\sigma > 7$ Å). For these solutes, the predictions of the HRF approximation are higher than the MD calculations and the difference is increasing with respect to the solute size. Conversely, MDFT with a bridge (HRF+HBS and HRF+WDA-like) predict almost the same solvation energy and in close agreement with the MD calculations.

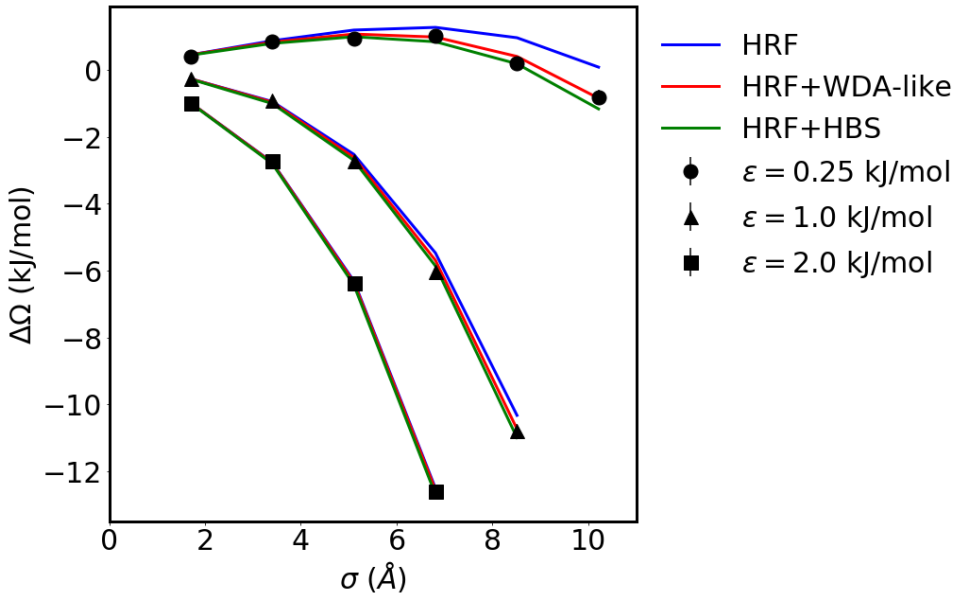

Figure 2.8 – Comparison of the solvation free energies of spherical solute in $scCO_2$ obtained by MD and MDFT. The MD results are indicated with different symbols according to the interaction energy. The MDFT predictions was performed with 3 different versions: HRF (blue line), HRF+WDA-like (red line), and HRF+HBS (green line).

Solvation of molecular solutes We focused next on small molecular solutes to evaluate the performance of MDFT in the presence of a nonspherical solute. Figure 2.9 presents the pair distribution functions between the CO_2 solute and the water solute and the CO_2 solvent, calculated using MDFT and MD. Using a solvent molecule as solute means simply that $v_{\text{ext}} = v$, this could be a severe test for a classical DFT approach. Figure 2.9 shows perfect overlaps between MD results and MDFT predictions for the CO_2 and the water solutes, albeit the MD results are noisier for the water.

The solvation free energy predictions for a range of molecular solutes are presented in figure 2.10. I updated M. Houssein Mohamed's previous MD results with those of C. Cao, which differ by less than 1%. For the MDFT results, we considered a functional without a bridge (HRF), and two with a bridge (WDA and HBS). We also plotted the prediction of the ideal solvent, which simply involves neglecting the excess solvation free energy ($\Delta\Omega_{\text{exc}} = 0$). Figure 2.10 shows that the three MDFT variants reproduce well the MD calculations over a wide range of solvation free energy (-12 to -1 kJ/mol). The only discrepancies occur for the toluene and isopropanol, and we are still investigating why. Moreover, the three MDFT variants produce identical results, indicating that the bridge contribution is negligible for the solutes considered here. Finally, the solvation free energies of the ideal solvents differ by few kJ/mol from the

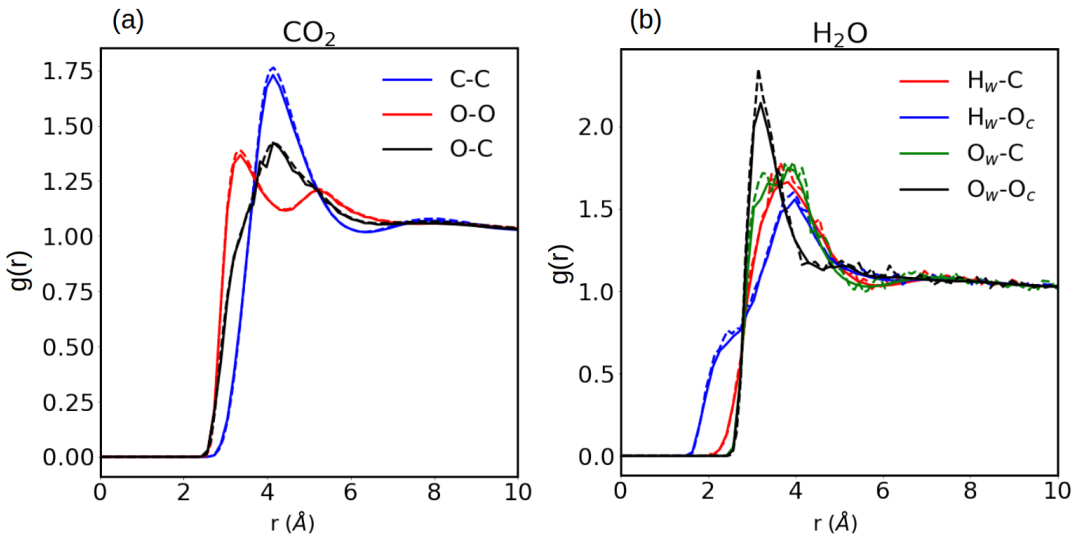

Figure 2.9 – Comparison of the solvation structures around two molecular solutes: (a) CO_2 and (b) water. All the site-site pair distribution functions are shown, with the MDFT predictions indicated by solid lines and the MD calculations by dashed lines.

correct results. These results demonstrate the ability of the MDFT approach to reproduce both the solvation free energy and the structure of molecular solutes.

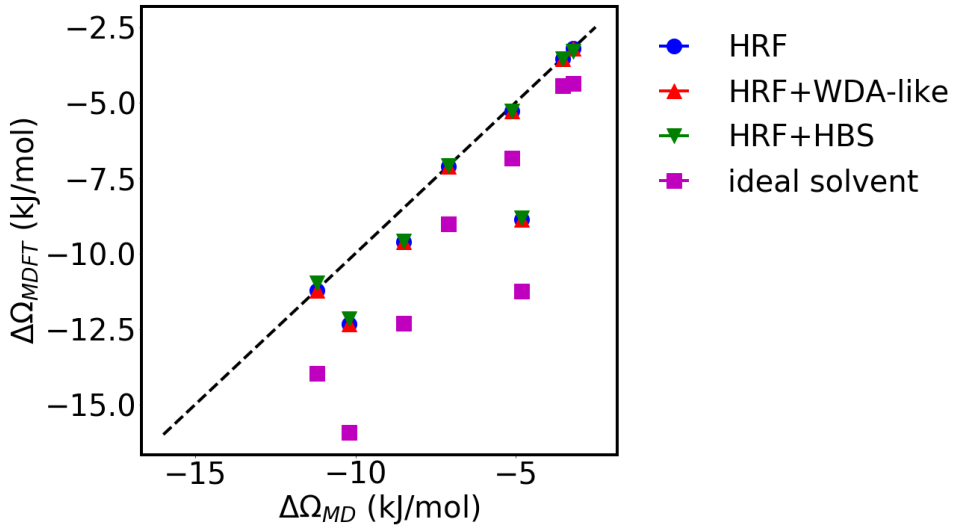

Figure 2.10 – Correlation between the solvation energies (SFE) calculated by MD and MDFT for the following molecular solutes: ethylene glycol, toluene, benzene, ethanol, methanol, isopropanol, water, ethane, ordered according to the MD solvation free energy. The MDFT predictions were obtained using different approximations of the bridge functions (HRF, HRF+WDA-like and HRF+HBS), while the ideal results correspond to cDFT without the excess functional ($\Delta\Omega_{\text{exc}} = 0$). The dashed line corresponds to the identity function.

Chemical potential of CO_2 at different densities So far, we have only considered the density $\rho_0 = 0.8\ \rho_c$ to determine the solvation properties using MDFT. We then evaluated the ability of MDFT to predict the solvation properties at the other densities (0.4 ρ_c, 0.7 ρ_c, and 2.0 ρ_c). We focused only on the solvation free energy of CO_2 in CO_2 (*i.e.*, the chemical potential) and we

compared three methods: MD calculations, MDFT predictions with the HRF approximation and HNC predictions. As discussed in subsection II.E.1, the HNC is equivalent to using the HRF functional (equation 2.61) in combination with the direct correlation functions c^{HNC} obtained with the HNC integral equations (presented as dashed lines in figure 2.5). The MD calculations were performed using Widom's insertion technique. [Widom, 1963]

The results for the solvation free energies of CO_2 in supercritical CO_2 for the four densities, obtained using the three methods are indicated in table 2.1. At low densities ($< \rho_c$), the solvation free energies obtained using the three methods are remarkably similar. This demonstrates the strength of integral equations: to obtain the same results, HNC requires 100,000 times fewer numerical resources than MD simulations. It is interesting to note that the HNC method is equivalent to the HRF method for densities 0.4 and 0.7 ρ_c. This confirms the similarity of the direct correlation functions calculated by MD or HNC, which was discussed previously in section III.C. At the density of 2.0 ρ_c, the MD solvation free energy differs by more than 2.0 kJ/mol from the HRF results. The HRF approximation is known to fail in dense liquids as it overestimates the pressure (section II.E.2). In the future, we will consider adding a hard sphere or WDA-like bridge functional. This approach has been shown to be effective for large LJ solutes (figure 2.8). Its application at a the density 2.0 ρ_c is underway.

Table 2.1 – Solvation free energies ΔG_{sol} (in kJ/mol) of a CO_2 molecule in supercritical CO_2 at $T = 1.05\ T_c$ for four density values, calculated with three methods: MD, HRF, and HNC. Details are provided in the text.

ρ_0	0.4 ρ_c	0.7 ρ_c	0.8 ρ_c	2 ρ_c
MD	-1.83	-2.91	-3.21	-3.79
HRF	-1.83	-2.88	-3.16	-0.918
HNC	-1.83	-2.87	-	-1.50

Computational cost differences MDFT provides an accurate reproduction of MD results for both Lennard-Jones and molecular solutes, in terms of both solvation structures and solvation free energies. However, an MDFT calculation takes just a few tens of seconds on a laptop, whereas a typical Bennett calculation or thermodynamic integration takes 100 hours on computing clusters with several CPU cores running in parallel. In terms of computational cost (measured in CPU hours), MDFT is 200,000 times cheaper than MD— and with the same level of accuracy!

III.F Conclusion of M. Houssein Mohamed's project.

M. Houssein Mohamed's project was a real success. We constructed the first MDFT functionals for the supercritical CO_2 and we demonstrated their ability to accurately reproduce the solvation properties of molecular solutes. The MDFT functionals required to determine the direct correlation functions c, which were calculated for four densities in the supercritical region and using two methods: MD simulations and HNC calculations. Extracting the c from MD simulations is technically challenging, as it requires inverting the molecular Ornstein-Zernike equation in combination with a mixed closure equation. We also compared the structures, thermodynamics and correlation functions obtained using MD and HNC. HNC fails to reproduce to reproduce the phase diagram of $scCO_2$, but correctly obtains the short-range structure for all orientations, as well as the smooth transition from an unstructured gaseous fluid to a more

liquid-like fluid at higher densities. We also determined the parameters of two bridge functionals at the condition $\rho_0 = 0.8\ \rho_c$ and $T = 1.05\ T_c$: the WDA-like bridge functional, based on a cubic fit of the homogeneous solvent functional, and the HBS bridge functional, which uses the highly accurate FMT for hard sphere fluids. We then presented solvation free energy results for molecular solutes. The MDFT results are in very good agreement with those of MD, except for toluene and isopropanol. Moreover, at the density $\rho_0 = 0.8\ \rho_c$, the HRF approximation seems sufficient. We finally considered the CO_2 chemical potential for the three other densities $\rho_0 = 0.4, 0.7$ and $2\ \rho_c$. We compared the results obtained from MD, from HNC and from HRF. For low densities ($< \rho_c$), the excess chemical potentials of MD are perfectly reproduced with both HNC and HRF methods, unlike at $2.0\ \rho_c$, where they do not provide satisfactory results. These successes and this limitation encourage us to develop a more general excess functional that would be valid across the entire supercritical region.

IV Present development: the BAC2MOL project

To generalise the MDFT functional at different thermodynamic conditions, I designed the BAC2MOL project, which was awarded an ANR grant for junior researcher in 2024. This is a collaborative project, which involves a local team at the LPCT (F. Ingrosso, D. Lesnicki) and G. Galliero (Laboratory of complex fluids and their reservoirs, Université de Pau et des Pays de l'Adour). The grant enabled me to recently recruit a new PhD student, **O. Tannous**, who joined the LPCT in October 2025. The BAC2MOL project aims to develop a generalised MDFT functional capable of handling various temperatures and pressures. This new MDFT functional will be used to study the properties of CO_2 in the presence of complex solutes and molecular confinement. This will pave the way for more realistic industrial applications, for which MDFT would need to be extended to account for solvent mixtures.

I will present my ideas for developing new functionals for supercritical CO_2 at various pressures and temperatures, and in complex environments. The focus will be on the accuracy and transferability of these functionals to complex solvation processes. I will then discuss the potential applications, including the various envisaged applications, which include the solvation of complex solutes and the nanoscale confinement of CO_2 fluids.

IV.A Development of P,T functional for the scCO$_2$

To develop the generalised MDFT, I envision to test different strategies that have already been proposed in the existing literature. Some of these strategies only require implementation work, while others require more challenging development.

Integral equations The results of M. Houssein Mohamed's project discussed in section I demonstrated that combining the direct correlation functions c obtained with HNC, and the HRF approximation (*i.e.*, no bridge functional) produced already accurate results at low densities. We note this combination corresponds in fact to the HNC approximation for a binary solute/solvent mixture. [Hansen and McDonald, 2013] HNC is very efficient, as it only requires the force fields of the solute and the solvent as input. It can therefore determine the solvation properties across the entire phase diagram, without the need to perform MD calculations to parametrise it. However, we have also shown that HNC fails to converge in the near-critical region [Belloni, 1993, Rull et al., 1996] and cannot predict the correct solvation energy at high densities (see

subsection III.E). I think it would be nevertheless interesting to compare the generalised MDFT with HNC as a baseline strategy, and I plan to implement this method in the MDFT code.

Mean-field approach The mean-field strategy discussed in subsection II.C.2 is also valid at any pressure and temperature. If the mean-field approach fails for complex liquids such as water, it would be worth testing it for CO_2. The reference functional could be one of the existing FMT for spherical solvent particles, [Rosenfeld, 1989, Roth et al., 2002, Roth, 2010, Hansen-Goos and Roth, 2006] or for nonspherical particles. [Hansen-Goos and Mecke, 2009, Hansen-Goos and Mecke, 2010, Marechal et al., 2011, Roth et al., 2012, Wittmann et al., 2015, Wittmann et al., 2016, Wittmann et al., 2017] The MDFT code can already deal with the rotational invariants framework discussed in subsection II.A.3 and should be able to accommodate the implementation of the mean-field functional (equation 2.49) in terms of rotational invariants. This would be the second step towards the generalised MDFT.

Weighted density approximation The mean-field functional will however fails to correctly predict the phase diagram of the bulk supercritical CO_2. I plan to add a correction functional in the form of a WDA-like functional (equation 2.68), where some parameters will need to be adjusted in order to reproduce the equation of state of the underlying solvent force fields (*e.g.*, EPM2). Another option would be to use an accurate experimental equation of state to parametrise the correction functional, [Huang et al., 1985, Span and Wagner, 1996] with the risk to have some inconsistencies. The exact WDA (equation 2.54 could also be considered. [Tarazona, 1985b] L. Belloni and D. Borgis have already started developing a WDA functional for CO_2, using as inputs the direct correlation functions c at various densities. (I do not contribute to this work, I merely supply them with MD trajectories.) While this strategy appears extremely promising in terms of accuracy, constructing the functional at a given temperature requires many MD calculations, which contradicts the objective of creating a transferable MDFT functional across the phase diagram. The exact WDA could still provide a rigorous framework for combining the microscopic direct correlations c obtained from mean-field or HNC, with a macroscopic equation of state.

Renormalization of integral equations. Another challenge rises in the near-critical region, where industrial applications often occur (*i.e.*, T between T_c and $1.2\ T_c$, P between P_c and $2\ P_c$). When approaching the critical point, the mean-field theories cannot capture the long-range divergence of the correlations and the algebraic power-law of the equations of state. [Wilson, 1971] This difficulty can be overcome by using a group-renormalisation approach, an iterative procedure that averages out the short-range fluctuations while refining the long-range ones. [White and Zhang, 1993, White and Zhang, 1995] This strategy has already been used for SAFT, [Bymaster et al., 2008, Forte et al., 2011, Reatto and Parola, 1996] in which G. Galliero has an interesting expertise.

Machine-learned functional Finally, as I mentioned earlier, machine-learning based functionals are developing rapidly. [Simon and Oettel, 2024, Simon et al., 2025, Yang et al., 2025, Bui and Cox, 2025, Robitschko et al., 2025, Wu and Gu, 2023, Simon and Oettel, 2024, Shang-Chun and Oettel, 2019, Sammüller et al., 2023] I think that would be a highly efficient route for the development of a generalised MDFT, particularly given the transferability of machine-learned functions across the phase diagram. [Robitschko et al., 2025] I would however highlight two limitations: (i) The machine-learned functional depends on the force fields used to construct

the learning set. These functionals may therefore be difficult to tune if we want to ensure that they correctly reproduce the equations of state. (ii) Supercritical CO_2 is often mixed with a co-solvent, both in industrial processes or in geological reservoirs. How transferable would these machine-learned functionals be at different cosolvent concentrations?

IV.B Application to technology-oriented processes: solvation and confinement

Application to solvation. Supercritical CO_2 is a powerful solvent, used in several industrial processes for the extraction of natural substances or the synthesis of nanoparticles or polymer matrices (see the discussion in section I). Equipped with the generalised MDFT, we will calculate the solvation properties of multiple solutes at any temperature and pressure. We will follow a gradual approach, by first applying this strategy to simple solutes and comparing the results with MD simulations (*e.g.*, 3D-density and solvation free energy). We plan to start with small molecules (noble gas, methane, water), before moving on to larger molecules, for which a large amount of numerical and experimental data is available, such as naphthalene or anthracene. [Bartle et al., 1991, Stubbs et al., 2005, Su and Maroncelli, 2006] We will next target more challenging and valuable molecules with chemical groups that specifically interact with CO_2 (carbonyl groups: acetone, aspirin or fluorine atom: [Dardin et al., 1998, Shimoyama et al., 2008] fluorene or perfluoro-n-hexane). Finally, we will focus on molecules that have significant applications in food processing or in the pharmaceutical industry (*e.g.*, caffeine, ibuprofen, paracetamol, statin). [Champeau et al., 2016, Dujarric et al., 2022, Hojjati et al., 2007, Sampaio de Sousa et al., 2007] Our objective is to demonstrate the ability of MDFT to obtain the same results as MD in these complex solvation processes at different temperatures and pressures, but with a negligible computational cost.

Application to confinement. The CO_2 fluid is also present in porous materials, such as geologic reservoirs and zeolites. [Fuentes-Azcatl and Domínguez, 2019,Oulebsir et al., 2018,Rébiscoul et al., 2019] If the pore size is nanometric, the macroscopic equations of state will fail to model the strong interactions between CO_2 molecules and the solid interfaces. [Bernet et al., 2020,Malheiro et al., 2014a,Miqueu and Grégoire, 2020] The new MDFT will enable the determination of the CO_2 3D-density and the absorption free energy. We will first test this strategy on simple systems, such as CO_2 confined between two flat walls of uncharged atoms (*e.g.*, Lennard-Jones walls). We will then compare the 3D-density and thermodynamics with MD results, as a function of the pressure, the temperature and the distance between the walls. We will then consider more complex pore geometries and more realistic interfaces (*e.g.*, graphene or mineral walls). In a second step, we will focus on the critical Casimir effect. [Dantchev and Dietrich, 2023, Schurtenberger and Heuberger, 2012] Thanks to the renormalisation strategy that we will develop, [Reatto and Parola, 1996, White, 1992, White and Zhang, 1995] we expect that the new MDFT to capture this effect. This result will pave the way to study interesting phenomena, such as self-assembly under supercritical conditions. [Wolde and Frenkel, 1997]

V Conclusion

In this chapter, I present my research project on the development of a molecular density functional theory (MDFT) for studying the solvation properties of supercritical CO_2. Supercritical CO_2s a promising solvent for developing ecological industrial processes, as it can replace

toxic organic solvents and be used to store CO_2 emissions. While there are efficient models of supercritical CO_2, macroscopic models disregard the molecular interactions between a solute and the CO_2, while microscopic simulations are accurate but costly. On the other hand, classical density functional theory (classical DFT) provides an efficient framework for accurately capturing molecular interactions and determining the solvation free energy and structure at minimal cost.

I discussed the various forms of classical DFT found in the literature, paying particular attention to molecular DFT. I then reviewed M. Houssein Mohamed's PhD project, in which we implemented various MDFT strategies and demonstrated their ability to accurately reproduce the solvation properties of small solutes. However, the MDFT strategy is limited to one thermodynamic condition. This is why I designed the BAC2MOL project: a collaborative initiative aimed at generalising MDFT across the phase diagram of supercritical CO_2. Long-term extensions would involve including cosolvents in order to model the realistic applications of CO_2 in geological reservoirs or industrial processes.

CHAPTER 3

Stochastic Density Functional Theory for Molecules and Electrolytes

The second part of my research project focuses on the dynamical properties of molecular fluids at the microscopic scale. Specifically, I am interested in the "solvation" dynamics, *i.e.* in all the molecular processes related to the collective motion of "solvent molecules" around a central "solute molecule", as well as how these processes affect the self-dynamics of the solute (translation, rotation, and conformational change). This topic has been central to some of my previous works. For instance, during my Ph.D. project, I examined how the collective fluctuations of water molecules surrounding quadrupolar ions drive the NMR relaxation. For my Master 2 project, I investigated how a pulled particle drags an added mass with it. Finally, my second postdoctoral fellowship focuses on the dynamics of carbon oxides solvated in molten carbonates.

In 2023, I resumed studying of the microscopic dynamics of molecular fluids through various different collaborative projects. The main project builds upon my Ph.D. research and is conducted in collaboration with my former supervisor B. Rotenberg (PHENIX, Paris). His team calculated the NMR relaxation rates for electrolytes at finite concentrations. [Chubak et al., 2021, Wolf et al., 2025] I joined the project to try to explain how the NMR rate evolves with respect to the ionic concentration, the temperature, the viscosity, etc. Such an understanding requires modelling the electrostatic fluctuations experienced by a central ion, which would also provide insight into other interesting properties, such as rotational and translational electronic frictions. In parallel, I worked with C. Millot (LPCT, Nancy) on the enantiomeric separation driven by an external field. Here, we attempted to rationalise how a polarised field could create two opposing currents in an enantiomeric mixture. [Clemens et al., 2015] This effect is directly related to the coupling between the translational and rotational motions at the microscopic scale.

In the future, I intend to extend the analysis to the microscopic dynamics of other experimental properties and of more complex fluids. The ultrafast spectroscopic experiments can measure the solvent relaxation after an excitation, providing information on energy transfer

and molecular dynamics at the microscopic scale. [Song et al., 1996, Banerjee and Bagchi, 2019, Maroncelli and Fleming, 1988, Jimenez et al., 1994, Geissler and Chandler, 2000, Roy et al., 2015] The team in Nancy (F. Ingrosso, M. Pastore at the LPCT) has a strong expertise in the molecular simulations of the excited solvation dynamics. [Prampolini et al., 2019, Cerezo et al., 2023] In terms of systems, I would also like to work with molten salts and deep eutectic solvents. These fluids play a key role in various innovative technologies due to their solvation properties. [Hansen et al., 2021, Wang et al., 2025, Sheridan et al., 2018]

This chapter will focus on my current projects and future plans for extending SDFT to molecular fluids. First, I will present the specific observables that I intend to calculate, alongside a review of the relevant literature. The second section will review the fundamental principles of SDFT, as well as a recent development towards non-Gaussian fluctuations in mean-field treatment (reference [AC25]). The third section will present SDFT for electrolyte with an implicit solvent. I will present in particular a novel functional formulation of SDFT for electrolytes in an implicit solvent. The fourth section will discuss the recent development toward a SDFT for electrolytes with an explicit dipolar solvent (reference [AC22]). Section 6 will present new work on how to incorporate the size of the particles (solute and solvent) into SDFT. The final section will apply these different extensions of SDFT to determine the NMR relaxation rate for quadrupolar ions in an electrolyte at different concentrations. In the conclusion, I will highlight other extensions to SDFT that enable this theory to model the dynamic properties of fluids at the molecular scale.

I Modelling the solvation dynamics

I.A Role of the solvent density fluctuations

In this chapter, I will focus on the calculation of dynamic solvation properties. I will consider a spherical tracer particle with position $\boldsymbol{R}$ solvated in a solvent with molecular density $\rho(\boldsymbol{r}, \boldsymbol{\omega})$. I am interested in a given solvation observable, A, which depends linearly on the solvent density ρ,

$$A(t) = \int \mathrm{d}\boldsymbol{r}\mathrm{d}\boldsymbol{\omega} a(\boldsymbol{r}, \boldsymbol{\omega})\rho(\boldsymbol{r} + \boldsymbol{R}(t), \boldsymbol{\omega}, t) \ , \tag{3.1}$$

where a is the local contribution of the solvent molecules in position $\boldsymbol{r}$ and orientation $\boldsymbol{\omega}$ (in the tracer frame) to the observable A. The observable A could represent the force, the electrostatic potential, the electrostatic field or the electrostatic field gradient (EFG) experienced by the tracer particle. The observable A could be related to a macroscopic property, such as the friction coefficient, [Hansen and McDonald, 2013] the frequency shift during an ultrafast spectroscopy [Song et al., 1996, Banerjee and Bagchi, 2019, Maroncelli and Fleming, 1988, Jimenez et al., 1994, Geissler and Chandler, 2000, Roy et al., 2015] or the NMR relaxation rate. [Abragam, 1983] The link between A and the macroscopic measurement often relies on the linear response theory, [Zwanzig, 2001] which involves the time autocorrelation of A,

$$C_A(t) = \langle A(t)A(0)\rangle = \int \mathrm{d}\boldsymbol{r}\mathrm{d}\boldsymbol{\omega} \int \mathrm{d}\boldsymbol{r}'\mathrm{d}\boldsymbol{\omega}' a(\boldsymbol{r}, \boldsymbol{\omega})a(\boldsymbol{r}', \boldsymbol{\omega}')C(\boldsymbol{r}, \boldsymbol{\omega}, t, \boldsymbol{r}', \boldsymbol{\omega}', 0) \ , \tag{3.2}$$

where we introduce the 2-point density correlations

$$C(\boldsymbol{r},\boldsymbol{\omega},t,\boldsymbol{r}',\boldsymbol{\omega}',t') = \langle \rho(\boldsymbol{r}+\boldsymbol{R}(t),\boldsymbol{\omega},t)\rho(\boldsymbol{r}'+\boldsymbol{R}(t'),\boldsymbol{\omega}',t')\rangle \ . \tag{3.3}$$

This quantity is central to the study of solvation dynamics. It is however very difficult to obtain, as it depends on the dynamics of both the solute and the solvent. For the purposes of this work, I will restrict my analysis to the case of a fixed tracer,

$$C(\boldsymbol{r},\boldsymbol{\omega},t,\boldsymbol{r}',\boldsymbol{\omega}',t') = \langle \rho(\boldsymbol{r},\boldsymbol{\omega},t)\rho(\boldsymbol{r}',\boldsymbol{\omega}',t')\rangle_1 \ , \tag{3.4}$$

where the 1 index denotes that the average is obtained for a solvent subjected to the effect of the tracer, which acts as an external potential v_{ext}. The C is still difficult to determine, particularly because the system (now the solvent) is no longer translationally invariant. In my current work, I also restrict myself to observables for which the local contribution is independent of the local orientation of the solvent and takes the form

$$a(\boldsymbol{r}) = a^{lm}(r)Y_{lm}(\theta,\phi) \ , \tag{3.5}$$

where Y_{lm} is the spherical harmonic of degree lm and θ,ϕ are the polar and azimuthal angles of $\boldsymbol{r}$. This is a typical form for electrostatic properties. A can now be written as

$$A(t) = \int \mathrm{d}\boldsymbol{r} a(\boldsymbol{r})\bar{\rho}(\boldsymbol{r},t) = \int_\sigma^\infty \mathrm{d}r r^2 a^{lm}(r)\bar{\rho}^{lm}(r,t) \ , \tag{3.6}$$

where $\bar{\rho}(\boldsymbol{r},t) = \int \mathrm{d}\boldsymbol{\omega}\rho(\boldsymbol{r},\boldsymbol{\omega},t)$ and I expand the solvent density in terms of spherical harmonics,

$$\bar{\rho}(\boldsymbol{r},t) = \sum_{l=0}^{\infty}\sum_{m=-m}^{l} \bar{\rho}^{lm}(r,t)Y_{lm}(\theta,\phi) \ . \tag{3.7}$$

The time autocorrelation function can now be written as

$$C_A(t) = \int_\sigma^\infty \mathrm{d}r \int_\sigma^\infty \mathrm{d}r' a^{lm}(r)a^{lm}(r')C^{lm}(r,r',t,0) \ , \tag{3.8}$$

where the density correlation function read

$$C^{lm}(r,t,r',t') = \left\langle \bar{\rho}^{lm}(r,t)\bar{\rho}^{lm}(r',t')\right\rangle_1 \ . \tag{3.9}$$

Alternatively, the property A could have also been written in Fourier space as

$$A(t) = \frac{1}{(2\pi)^3}\int \mathrm{d}\boldsymbol{k}\tilde{a}(\boldsymbol{k})\tilde{\bar{\rho}}(\boldsymbol{k},t) = \frac{1}{(2\pi)^3}\int \mathrm{d}k k^2 \tilde{a}^{lm}(k)\tilde{\bar{\rho}}^{lm}(k,t)\ , \tag{3.10}$$

where I introduced the spatial Fourier transforms of a and $\bar{\rho}$ as well as the Hankel-Fourier transforms of a^{lm} and $\bar{\rho}^{lm}$. Using this formulation, the autocorrelation function is

$$C_A(t) = \int \mathrm{d}\boldsymbol{k}\int \mathrm{d}\boldsymbol{k}'\tilde{a}(\boldsymbol{k})\tilde{a}(\boldsymbol{k}')\tilde{C}(\boldsymbol{k},t,\boldsymbol{k}',t')\ , \tag{3.11}$$

$$= \int \mathrm{d}k\int \mathrm{d}k' k^2 k'^2 \tilde{a}^{lm}(k)\tilde{a}^{lm}(k')\tilde{C}^{lm}(k,t,k',t')\ , \tag{3.12}$$

where

$$\tilde{C}(\boldsymbol{k},t,\boldsymbol{k}',t') = \langle\tilde{\bar{\rho}}(\boldsymbol{k},t)\tilde{\bar{\rho}}(\boldsymbol{k}',t')\rangle_1 \tag{3.13}$$

$$\tilde{C}^{lm}(k,t,k',t') = \left\langle\tilde{\bar{\rho}}^{lm}(k,t)\tilde{\bar{\rho}}^{lm}(k',t')\right\rangle_1\ . \tag{3.14}$$

Modelling the solvation dynamics is therefore equivalent to modelling of these density fluctuations, C^{lm}.

I.B State-of-the-art

Most of the theories developed in the literature to model solvation dynamics rely on the so-called uniform approximation,

$$C(\boldsymbol{r},t,\boldsymbol{r}',t') \approx C_u(\boldsymbol{r},t,\boldsymbol{r}',t') = \langle\rho(\boldsymbol{r},t)\rho(\boldsymbol{r}',t')\rangle_0\ , \tag{3.15}$$

where I dropped the bar notation, and the index 0 indicates that the average is taken in the absence of the solute ($v_{\mathrm{ext}} = 0$). In this approximation, the density correlation is translationally invariant and the correlation of A reads

$$C_A(t) = \int \mathrm{d}\boldsymbol{k}|a(\boldsymbol{k})|^2\tilde{C}_u(\boldsymbol{k},t)\ , \tag{3.16}$$

where $\tilde{C}_u(\boldsymbol{k},t) = \tilde{C}_u(\boldsymbol{k},-\boldsymbol{k},t,0)/\delta(\boldsymbol{k}+\boldsymbol{k}')$. The quantity $|a(\boldsymbol{k})|^2$ is sometimes called the vertex and plays the role to select the k-mode of the solvent fluctuations that contribute to the correlation of A. However, this approximation neglects the impact of the solute on the solvent dynamics. Even in the case of a hard-sphere solute that simply excludes the solvent density from its core, Chandler and his collaborators have demonstrated that the solute affects the solvent modes. [Song et al., 1996, Song and Chandler, 1998].

Much of the existing literature ignores the effect of the excluded volume of the solute. On the other hand, there exists a wealth of powerful theories that can accurately model the bulk density correlations $C_u(\boldsymbol{r},t,\boldsymbol{r}',t')$. Bagchi and his collaborators developed an effective

dynamical density functional theory (DDFT) for the dipolar density $\rho_S(\boldsymbol{r}, \hat{\boldsymbol{u}}, t)$ of a dielectric solvent, where $\hat{\boldsymbol{u}}$ is the unit vector indicating the orientation of the molecular dipole. [Bagchi, 1989, Bagchi and Jana, 2010] Their theory is based on the equilibrium and the homogeneous correlation functions of the solvent. They combined spectroscopic experimental data with integral equations to obtain these correlations and analyse various properties of a dielectric solvent: solvation dynamics, [Chandra and Bagchi, 1989b, Bagchi and Chandra, 1992, Roy and Bagchi, 1993, Nandi et al., 1995] rotational diffusion, [Chandra and Bagchi, 1989a, Chandra and Bagchi, 1990, Bagchi, 2001] or translational diffusion. [Bagchi and Chandra, 1988, Chandra and Bagchi, 1988, Vijayadamodar et al., 1989] They also extended their theory to the case of electrolytes by coupling the dipolar density with the ionic densities. [Biswas and Bagchi, 1997, Bagchi and Biswas, 1998, Bagchi, 1998, Chandra and Bagchi, 2000, Dufrêche et al., 2002, Banerjee and Bagchi, 2019] Their DDFT is however heuristic and mixes different levels of approximation. The DDFT approach was also employed in combination with the atomic densities $\rho_i(\boldsymbol{r}, t)$, where i denotes one of the atomic species of the system. This approach extends the reference interaction site model to the dynamical domain for dipolar fluid, [Chong and Hirata, 1998b, Chong and Hirata, 1998a, Chong and Hirata, 1999, Chong and Hirata, 1998c, Nishiyama et al., 2009] or for water [Yamaguchi and Hirata, 2002, Yamaguchi et al., 2002, Yamaguchi et al., 2003, Yamaguchi et al., 2004, Kobryn et al., 2005] It was employed to study the diffusion in supercritical solvent, [Egorov et al., 2002, Egorov, 2003] In the context of colloidal studies, DDFT was given a more formal derivation and has recently been extended to nonspherical particles. [te Vrugt et al., 2020, Rex et al., 2007, Grelet et al., 2008, Archer, 2009, Wittkowski and Löwen, 2011, Durán-Olivencia et al., 2016]

Overall, these different approaches suffer from the same two major approximations: (i) they neglect the effect of the solute size and (ii) they neglect the coupling between the solute dynamics and the solvent dynamics. To properly address the solvation dynamics, we therefore require a theory capable of describing fluctuations, nonequilibrium responses, 3-point correlation functions. To this end, I will explore the potential of the stochastic density functional theory (SDFT), a powerful and rigorous approach for modelling the dynamics at a microscopic scale. [Dean, 1996, Illien, 2025] I will first review this theory for the simple case of spherical particles.

II Principles of stochastic density functional theory

Let us start with the simple SDFT for identical particles that interact via a pair interaction . [Dean, 1996] I will first present the derivation of the core SDFT equation—the Dean-Kawasaki equation—and then discuss recent results on the non-Gaussian fluctuations of the density field in the mean-field limit. The Dean-Kawasaki equation is a stochastic equation for the microscopic density, unlike DDFT or other coarse-grained theories which focus on some average densities. [te Vrugt et al., 2020] SDFT is thus the appropriate framework for unusual correlation functions, such as 2-point correlations in the presence of an external field or in a moving frame, or 3-point correlations. An excellent review on SDFT was recently put forward by P. Illien. [Illien, 2025]

II.A Dean-Kawasaki equation

We consider a system of N particles interacting with a pair potential v and embedded in an implicit solvent and with a bare diffusion coefficient D. Their dynamics is given by a set

of N coupled overdamped Langevin equations obeyed by the positions $\boldsymbol{r}_i$ of the particles:

$$\frac{\mathrm{d}}{\mathrm{d}t}\boldsymbol{r}_i(t) = -\frac{D}{k_B T}\sum_{j=1,j\neq i}^{N}\nabla v(\boldsymbol{r}_i(t)-\boldsymbol{r}_j(t)) + \sqrt{2D}\boldsymbol{\eta}_i(t) \tag{3.17}$$

$$= -\frac{D}{k_B T}\int \mathrm{d}\boldsymbol{r}'\rho(\boldsymbol{r}')\nabla v(\boldsymbol{r}_i(t)-\boldsymbol{r}') + \sqrt{2D}\boldsymbol{\eta}_i(t) \tag{3.18}$$

with k_B the Boltzmann constant, T the temperature, $\boldsymbol{\eta}_i(t)$ a unit Gaussian white noise vector with statistics,

$$\langle \eta_i^\alpha(t)\rangle = 0, \tag{3.19}$$

$$\left\langle \eta_i^\alpha(t)\eta_j^\beta(t')\right\rangle = \delta_{ij}\delta_{\alpha\beta}\delta(t-t')\ . \tag{3.20}$$

η_i^α are the Cartesian components of the noise $\boldsymbol{\eta}_i(t)$. In equation 3.18, we introduce the microscopic density,

$$\rho(\boldsymbol{r},t) = \sum_{i=1}^{N}\delta(\boldsymbol{r}-\boldsymbol{r}_i(t))\ . \tag{3.21}$$

SDFT consists of an exact recasting of the N overdamped Langevin equations that provides the dynamical evolution of $\rho(\boldsymbol{r},t)$ *via* the so-called Dean-Kawasaki equation [Dean, 1996]

$$\frac{\partial}{\partial t}\rho(\boldsymbol{r},t) = D\nabla^2\rho(\boldsymbol{r},t) + \nabla\cdot\left[\boldsymbol{\xi}(\boldsymbol{r},t)\sqrt{2D\rho(\boldsymbol{r},t)}\right] + \frac{D}{k_B T}\nabla\cdot\left[\rho(\boldsymbol{r},t)\int \mathrm{d}\boldsymbol{r}'\rho(\boldsymbol{r}',t)\nabla v(\boldsymbol{r}-\boldsymbol{r}')\right]\ , \tag{3.22}$$

where $\boldsymbol{\xi}(\boldsymbol{r},t)$ is a unit Gaussian white noise vector fields with statistics,

$$\langle \xi^\alpha(\boldsymbol{r},t)\rangle = 0, \tag{3.23}$$

$$\left\langle \xi^\alpha(\boldsymbol{r},t)\xi^\beta(\boldsymbol{r}',t')\right\rangle = \delta_{\alpha\beta}\delta(t-t')\delta(\boldsymbol{r}-\boldsymbol{r}')\ . \tag{3.24}$$

The Dean-Kawasaki equation is a stochastic equation for a stochastic variable, the microscopic density $\rho(\boldsymbol{r},t)$. Due to its multiplicative noise ($\nabla\cdot\left[\boldsymbol{\xi}(\boldsymbol{r},t)\sqrt{2D\rho(\boldsymbol{r},t)}\right]$), it cannot be solved exactly, except in the case without interactions ($v=0$) or in the mean-field limit (see the next subsection II.C). There exists other formulations of the Dean-Kawasaki equation. I do like the one that introduces a kind of microscopic free energy. [Dean, 1996] It reads

$$\frac{\partial}{\partial t}\rho(\boldsymbol{r},t) = \nabla\cdot\left[\boldsymbol{\xi}(\boldsymbol{r},t)\sqrt{2D\rho(\boldsymbol{r},t)}\right] + \frac{D}{k_BT}\nabla\cdot\left[\rho(\boldsymbol{r},t)\nabla\frac{\delta\mathcal{F}[\rho]}{\delta\rho(\boldsymbol{r},t)}\right] \ , \tag{3.25}$$

with the functional of the microscopic free energy

$$\mathcal{F}[\rho] = k_BT\int \mathrm{d}\boldsymbol{r}\rho(\boldsymbol{r})\ln\rho(\boldsymbol{r}) + \frac{1}{2}\int\mathrm{d}\boldsymbol{r}\int\mathrm{d}\boldsymbol{r}'\rho(\boldsymbol{r})v(\boldsymbol{r}-\boldsymbol{r}')\rho(\boldsymbol{r}') \ . \tag{3.26}$$

The latter functional also appears in the equilibrium probability of the microscopic density,

$$\mathcal{P}_{\mathrm{eq}}[\rho] \sim \exp(-\beta\mathcal{F}[\rho]) \ . \tag{3.27}$$

II.B Path integral formulation

Another expression relies on the path integral formulation of stochastic dynamics. This formulation is based on the initial works of Martin-Siggia-Rose [Martin et al., 1973] and Janssen [Janssen, 1976], and is now used by Mallick and co-workers to study fluctuating hydrodynamics [Krapivsky et al., 2014, Krapivsky et al., 2015, Mallick et al., 2022, Dandekar et al., 2023, Dandekar et al., 2024]. I will detail here how to obtain this formulation. First, using the fact that $\boldsymbol{\xi}$ is a Gaussian noise with probability $\mathcal{P}[\boldsymbol{\xi}] = \exp(-\int_0^T \mathrm{d}t\int\mathrm{d}\boldsymbol{r}|\boldsymbol{\xi}(\boldsymbol{r},t)|^2$ (where T is the typical observation time of the trajectory), the probability of observing a time-dependent microscopic density given the initial configuration $\rho(\boldsymbol{r},t=0)$ can be written as

$$\begin{aligned}\mathcal{P}[\rho|\rho(\boldsymbol{r},t=0)] = \int\mathcal{D}\boldsymbol{\xi}\delta\Bigg[\frac{\partial}{\partial t}\rho(\boldsymbol{r},t) - D\nabla^2\rho(\boldsymbol{r},t) - \nabla\cdot\left[\boldsymbol{\xi}(\boldsymbol{r},t)\sqrt{2D\rho(\boldsymbol{r},t)}\right] \\ -\frac{D}{k_BT}\nabla\cdot\left[\rho(\boldsymbol{r},t)\int\mathrm{d}\boldsymbol{r}'\rho(\boldsymbol{r}',t)\nabla v(\boldsymbol{r}-\boldsymbol{r}')\right]\Bigg]\exp\left(-\int_0^T\mathrm{d}t\int\mathrm{d}\boldsymbol{r}|\boldsymbol{\xi}(\boldsymbol{r},t)|^2\right) \ .\end{aligned} \tag{3.28}$$

We then employ the Fourier-like expression of the Dirac functional,

$$\delta[G] = \int\mathcal{D}\hat{\rho}\exp\left(-\int_0^T\mathrm{d}t\int\mathrm{d}\boldsymbol{r}G(\boldsymbol{r},t)\hat{\rho}(\boldsymbol{r},t)\right) \ , \tag{3.29}$$

which gives

$$\begin{aligned}\mathcal{P}[\rho|\rho(\boldsymbol{r},t=0)] = \int\mathcal{D}\boldsymbol{\xi}\int\mathcal{D}\hat{\rho}\exp\Bigg(-\int_0^T\mathrm{d}t\int\mathrm{d}\boldsymbol{r}\hat{\rho}\Bigg(\frac{\partial}{\partial t}\rho(\boldsymbol{r},t) - D\nabla^2\rho(\boldsymbol{r},t) \\ -\nabla\cdot\left[\boldsymbol{\xi}(\boldsymbol{r},t)\sqrt{2D\rho(\boldsymbol{r},t)}\right] - \frac{D}{k_BT}\nabla\cdot\left[\rho(\boldsymbol{r},t)\int\mathrm{d}\boldsymbol{r}'\rho(\boldsymbol{r}',t)\nabla v(\boldsymbol{r}-\boldsymbol{r}')\right]\Bigg)\Bigg) \\ \times\exp\left(-\int_0^T\mathrm{d}t\int\mathrm{d}\boldsymbol{r}|\boldsymbol{\xi}(\boldsymbol{r},t)|^2\right) \ .\end{aligned} \tag{3.30}$$

After doing an integration by parts on the noise multiplicative terms $\hat{\rho}\nabla\cdot\left[\boldsymbol{\xi}(\boldsymbol{r},t)\sqrt{2D\rho(\boldsymbol{r},t)}\right] \rightarrow -\nabla\hat{\rho}\cdot\left[\boldsymbol{\xi}(\boldsymbol{r},t)\sqrt{2D\rho(\boldsymbol{r},t)}\right]$, we can perform a Gaussian integration over the noise and obtain

$$\mathcal{P}[\rho|\rho(t=0)] = \int \mathcal{D}\hat{\rho}\exp\left(-\mathcal{S}_{\rho_0}[\rho,\hat{\rho}]\right) \tag{3.31}$$

with the action

$$\begin{aligned}\mathcal{S}_{\rho_0}[\rho,\hat{\rho}] &= \int_0^T \mathrm{d}t \int \mathrm{d}\boldsymbol{r}\left(\hat{\rho}\frac{\partial}{\partial t}\rho - D\hat{\rho}\nabla^2\rho - \hat{\rho}\frac{D}{k_BT}\nabla\cdot\left[\rho(\boldsymbol{r},t)\int \mathrm{d}\boldsymbol{r}'\rho(\boldsymbol{r}',t)\nabla v(\boldsymbol{r}-\boldsymbol{r}')\right]\right. \\ &\quad \left. - D\rho|\nabla\hat{\rho}|^2\right) \qquad (3.32)\\ &= \int_0^T \mathrm{d}t \int \mathrm{d}\boldsymbol{r}\left(\hat{\rho}\frac{\partial}{\partial t}\rho + D\nabla(\hat{\rho})\cdot\nabla\rho + \frac{D}{k_BT}\rho\nabla(\hat{\rho})\cdot\left[\rho(\boldsymbol{r},t)\int \mathrm{d}\boldsymbol{r}'\rho(\boldsymbol{r}',t)\nabla v(\boldsymbol{r}-\boldsymbol{r}')\right]\right. \\ &\quad \left. - D\rho|\nabla\hat{\rho}|^2\right), \qquad (3.33)\end{aligned}$$

where the last term $-D\rho|\nabla\hat{\rho}|^2$ originates directly from the Gaussian integration of the noise. The second line is obtained by performing integrations by parts of the form $(\nabla\hat{\rho}) \rightarrow -\hat{\rho}\nabla$, and is identical to equation 4 in reference [AC25]. The action can also be expressed in terms of the microscopic free energy (equation 3.26),

$$\begin{aligned}\mathcal{S}_{\rho_0}[\rho,\hat{\rho}] &= \hat{\rho}\frac{\partial}{\partial t}\rho - \hat{\rho}\frac{D}{k_BT}\nabla\cdot\left[\rho(\boldsymbol{r},t)\nabla\frac{\delta F[\rho]}{\delta\rho(\boldsymbol{r},t)}\right] - D\rho|\nabla\hat{\rho}|^2 \qquad (3.34)\\ &= \hat{\rho}\left(\frac{\partial}{\partial t}\rho - \frac{D}{k_BT}\nabla\cdot\left[\rho(\boldsymbol{r},t)\nabla\frac{\delta F'[\rho]}{\delta\rho(\boldsymbol{r},t)}\right]\right), \qquad (3.35)\end{aligned}$$

where

$$F'[\rho] = F[\rho] - k_BT\int \mathrm{d}\boldsymbol{r}\rho(\boldsymbol{r})\hat{\rho}(\boldsymbol{r}), \tag{3.36}$$

corresponds to a microscopic free energy (equation 3.26) in presence of an external field $-k_BT\hat{\rho}$. Finally, we obtain the probability to observe a time-dependent microscopic density by averaging over all initial condition and find

$$\mathcal{P}[\rho] = \int \mathcal{D}\hat{\rho}\exp\left(-\mathcal{S}[\rho,\hat{\rho}]\right) \tag{3.37}$$

with the generalized action,

$$\mathcal{S}[\rho,\hat{\rho}] = \mathcal{S}_{\rho_0}[\rho,\hat{\rho}] - \ln\mathcal{P}_0[\rho(\boldsymbol{r},t=0)], \tag{3.38}$$

where $\mathcal{P}_0[\rho(\boldsymbol{r},t=0)]$ is the initial distribution of the density.

Cumulant generative functional. In order to calculate the correlation functions, we will use the successive derivatives of the cumulant generating functional,

$$\mu[\lambda] = \ln \left\langle \exp\left[\int_0^T \mathrm{d}t \int \mathrm{d}\boldsymbol{r}\lambda(\boldsymbol{r},t)\rho(\boldsymbol{r},t)\right]\right\rangle \tag{3.39}$$

$$= \ln\left(\frac{\int \mathcal{D}\rho \int \mathcal{D}\hat{\rho} \exp\left(-\mathcal{S}[\rho,\hat{\rho}] + \int_0^T \mathrm{d}t \int \mathrm{d}\boldsymbol{r}\lambda(\boldsymbol{r},t)\rho(\boldsymbol{r},t)\right)}{\int \mathcal{D}\rho \int \mathcal{D}\hat{\rho} \exp\left(-\mathcal{S}[\rho,\hat{\rho}]\right)}\right) \tag{3.40}$$

$$= \ln\left(\frac{\int \mathcal{D}\rho \int \mathcal{D}\hat{\rho} \exp\left(-\mathcal{S}_\lambda[\rho,\hat{\rho}]\right)}{\int \mathcal{D}\rho \int \mathcal{D}\hat{\rho} \exp\left(-\mathcal{S}[\rho,\hat{\rho}]\right)}\right) , \tag{3.41}$$

where we define the tilted action

$$\mathcal{S}_\lambda[\rho,\hat{\rho}] = \mathcal{S}[\rho,\hat{\rho}] + \int_0^T \int \mathrm{d}\boldsymbol{r}\lambda(\boldsymbol{r},t)\rho(\boldsymbol{r},t) \ . \tag{3.42}$$

For instance, the average density and the connected 2-point correlation functions can be computed as

$$\langle\rho(\boldsymbol{r},t)\rangle = \frac{\delta\mu[\lambda]}{\delta\lambda(\boldsymbol{r},t)}|_{\lambda=0} \ , \tag{3.43}$$

$$\langle\delta\rho(\boldsymbol{r},t)\delta\rho(\boldsymbol{r}',t')\rangle = \frac{\delta^2\mu[\lambda]}{\delta\lambda(\boldsymbol{r},t)\delta\lambda(\boldsymbol{r}',t')}|_{\lambda=0} \tag{3.44}$$

$$= \frac{\delta\left\langle\rho(\boldsymbol{r},t)\right\rangle_\lambda}{\delta\lambda(\boldsymbol{r}',t')}|_{\lambda=0} \ , \tag{3.45}$$

where $\delta\rho(\boldsymbol{r},t) = \rho(\boldsymbol{r},t) - \langle\rho(\boldsymbol{r},t)\rangle$ and $\langle\cdot\rangle$ indicates on average with the tilted action. Similar expressions can be found for the n-point connected correlation functions.

II.C Mean-field limit and non-Gaussian fluctuations

I will now present how we used the path integral formulation to determine the n-point correlation functions in the mean-field. This work was carried out in collaboration with P. Illien (as the PI) and L. Le Bon (M2 intern), and has recently been published in the reference [AC25] .

Mean-field approximation To determine the correlations explicitly , we will consider the following joint limit: $\rho_0 \to \infty$ and $\rho_0 v = \mathcal{O}(1)$. The action in equation 3.32 can be written as $\mathcal{S}_{\rho_0}[\rho,\hat{\rho}] = \rho_0\mathcal{S}_{\rho_0}[\rho/\rho_0,\hat{\rho}]$, where $\mathcal{S}_{\rho_0}[\rho/\rho_0,\hat{\rho}] = \mathcal{O}(1)$. In this joint limit, we can apply the saddle-point approximation, which means that the average with the tilted action $\mathcal{S}_\lambda$ is dominated by the most probable path — the path which minimises the action. We denote this path (q,p), and it satisfies the minimisation conditions,

$$\frac{\delta \mathcal{S}_\lambda[\rho,\hat{\rho}]}{\delta \hat{\rho}(\boldsymbol{r},t)}|_{q,p} = 0 \ , \tag{3.46}$$

$$\frac{\delta \mathcal{S}_\lambda[\rho,\hat{\rho}]}{\delta \rho(\boldsymbol{r},t)}|_{q,p} = 0 \ . \tag{3.47}$$

This gives the following equations

$$\frac{\partial}{\partial t} q = \frac{D}{k_B T} \nabla \cdot \left[q(\boldsymbol{r},t) \nabla \frac{\delta \mathcal{F}[q]}{\delta q(\boldsymbol{r},t)} \right] - 2D \nabla \cdot (q \nabla p) \ , \tag{3.48}$$

$$\frac{\partial}{\partial t} p = -\frac{D}{k_B T} \frac{\delta}{\delta q} \nabla \cdot \left[q(\boldsymbol{r},t) \nabla \frac{\delta \mathcal{F}'[q]}{\delta q(\boldsymbol{r},t)} \right] - \lambda \ , \tag{3.49}$$

where I explicitly write down these equations in terms of the microscopic free energy (equation 3.26) to propose an alternative formulation as the one written in the reference [AC25]. The equation for q is similar to the full Dean-Kawasaki equation 3.25, but where the multiplicative noise term is no more a stochastic variable, $\boldsymbol{\xi}(\boldsymbol{r},t)\sqrt{2D\rho(\boldsymbol{r},t)} \to -2Dq\nabla p$.We also note that the dynamics of p is given by an "anti-diffusion" equation.

Calculation of the correlation functions Equations 3.48 and 3.49 cannot be solved, except for the case without interactions (see for instance the supplementary information C of the reference [AC25]). We propose instead to focus on the correlations. We assume that q and p can be expanded into power of λ, $q(\boldsymbol{r},t) = \sum_i q_n(\boldsymbol{r},t)\lambda(\boldsymbol{r},t)^n$ (and likewise for p). We obtain the following equations at order 0

$$\frac{\partial}{\partial t} q_0 = D\nabla^2 q_0 - 2D\nabla \cdot (q_0 \nabla p_0) + \frac{D}{k_B T} \nabla \cdot \left(q_0 \left(\int \mathrm{d}\boldsymbol{r}' q_0(\boldsymbol{r}') \nabla v(\boldsymbol{r}-\boldsymbol{r}') \right) \right) \ , \tag{3.50}$$

$$\begin{aligned} \frac{\partial}{\partial t} p_0 = &-D\nabla^2 p_0 - D|\nabla p_0|^2 + \frac{D}{k_B T} (\nabla p_0) \cdot \left(\int \mathrm{d}\boldsymbol{r}' q_0(\boldsymbol{r}') \nabla v(\boldsymbol{r}-\boldsymbol{r}') \right) \\ &- \frac{D}{k_B T} \left(\int \mathrm{d}\boldsymbol{r}' q_0(\boldsymbol{r}') \nabla p_0(\boldsymbol{r}') \cdot \nabla v(\boldsymbol{r}-\boldsymbol{r}') \right) \ , \end{aligned} \tag{3.51}$$

which corresponds to the mean-field equations 3.48 and 3.49 with $\lambda = 0$. In the following, we will assume that we are considering the case of fluctuations around a uniform state, *i.e.* $q_0(\boldsymbol{r},t) = \rho_0$ and $p_0(\boldsymbol{r},t) = 0$. This allows us to express the order 1 as

$$\frac{\partial}{\partial t} q_1 - D\nabla^2 q_1 - \frac{D}{k_B T} \rho_0 \int \mathrm{d}\boldsymbol{r}' q_1(\boldsymbol{r}') \nabla^2 v(\boldsymbol{r}-\boldsymbol{r}') + 2D\rho_0 \nabla^2 p_1 = 0 \ , \tag{3.52}$$

$$\frac{\partial}{\partial t} p_1 + D\nabla^2 p_1 + \frac{D}{k_B T} \rho_0 \int \mathrm{d}\boldsymbol{r}' p_1(\boldsymbol{r}') \nabla^2 v(\boldsymbol{r}-\boldsymbol{r}') = -\lambda \ . \tag{3.53}$$

The right-hand side consists of a linear operator acting on the vector (q_1, p_1), while the left-hand side contains the source term $-\lambda$. After performing space and time Fourier transforms, the equation for p_1 gives $\tilde{p}_1(\boldsymbol{k},\omega) = \tilde{\lambda} / \left[\mathrm{i}\omega + Dk^2 + \frac{D}{k_B T} \rho_0 k^2 \tilde{v}(\boldsymbol{k}) \right]$ and

$$q_1(\boldsymbol{k},\omega) = \frac{2D\rho_0 k^2}{-\mathrm{i}\omega + Dk^2 + \frac{D}{k_BT}\rho_0 k^2 \tilde{v}(\boldsymbol{k})}\tilde{p}_1 = \frac{2D\rho_0 k^2 \tilde{\lambda}}{\omega^2 + \left(Dk^2 + \frac{D}{k_BT}\rho_0 k^2 \tilde{v}(\boldsymbol{k})\right)^2} \,. \tag{3.54}$$

After a derivation over λ, one find the 2-point connected correlations:

$$\langle \delta\tilde{\rho}(\boldsymbol{k},\omega)\delta\tilde{\rho}(\boldsymbol{k}',\omega')\rangle = \frac{2D\rho_0 k^2}{\omega^2 + \left(Dk^2 + \frac{D}{k_BT}\rho_0 k^2 \tilde{v}(\boldsymbol{k})\right)^2}\delta(\boldsymbol{k}+\boldsymbol{k}')\delta(\omega+\omega') \,. \tag{3.55}$$

We can apply the same strategy for the 3-point connected correlations. The mean-field equations at order 3 read

$$\begin{aligned}\frac{\partial}{\partial t}q_2 - D\nabla^2 q_2 - \frac{D}{k_BT}\rho_0 \int \mathrm{d}\boldsymbol{r}' q_2(\boldsymbol{r}')\nabla^2 v(\boldsymbol{r}-\boldsymbol{r}') + 2D\rho_0\nabla^2 p_2 &= -2D\nabla\cdot(q_1\nabla p_1) \\ &+\frac{D}{k_BT}\nabla\left(q_1\left(\int \mathrm{d}\boldsymbol{r}' q_1(\boldsymbol{r}')\nabla V(\boldsymbol{r}'-\boldsymbol{r}')\right)\right) \,, \qquad (3.56) \\ \frac{\partial}{\partial t}p_2 + D\nabla^2 p_2 + \frac{D}{k_BT}\rho_0 \int \mathrm{d}\boldsymbol{r}' p_2(\boldsymbol{r}')\nabla^2 v(\boldsymbol{r}-\boldsymbol{r}') &= -D|\nabla p_1|^2 \\ &+\frac{D}{k_BT}(\nabla p_1)\cdot\left(\int \mathrm{d}\boldsymbol{r}' q_1(\boldsymbol{r}')\nabla V(\boldsymbol{r}'-\boldsymbol{r}')\right) \\ &-\frac{D}{k_BT}\left(\int \mathrm{d}\boldsymbol{r}' q_1(\boldsymbol{r}')\nabla p_1(\boldsymbol{r}')\cdot\nabla V(\boldsymbol{r}'-\boldsymbol{r}')\right) \,. \qquad (3.57)\end{aligned}$$

We observe that the left-hand side consists of the same operator as in the equations of order 1, but applied to (q_2, p_2). The right-hand side no longer contains the term λ any more, but rather products of q_1 and p_1, which are known from the resolution of the first order equations. More generally, we will have equations of order n of the form

$$\frac{\partial}{\partial t}q_n - D\nabla^2 q_n - \frac{D}{k_BT}\rho_0 \int \mathrm{d}\boldsymbol{r}' q_n(\boldsymbol{r}')\nabla^2 v(\boldsymbol{r}-\boldsymbol{r}') + 2D\rho_0\nabla^2 p_n = Q_n \,, \tag{3.58}$$

$$\frac{\partial}{\partial t}p_n + D\nabla^2 p_n + \frac{D}{k_BT}\rho_0 \int \mathrm{d}\boldsymbol{r}' p_n(\boldsymbol{r}')\nabla^2 v(\boldsymbol{r}-\boldsymbol{r}') = P_n \,, \tag{3.59}$$

where Q_n and P_n are known functions of q_i and p_i for $i < n$. These equations can be formally solved as,

$$\tilde{p}_n(\boldsymbol{k},\omega) = -\frac{\tilde{P}_n}{\mathrm{i}\omega + Dk^2 + \frac{D}{k_BT}\rho_0 k^2 \tilde{v}(\boldsymbol{k})} \text{ and} \tag{3.60}$$

$$\tilde{q}_n(\boldsymbol{k},\omega) = \frac{\tilde{Q}_n}{-\mathrm{i}\omega + Dk^2 + \frac{D}{k_BT}\rho_0 k^2 \tilde{v}(\boldsymbol{k})} + \frac{2D\rho_0 k^2 \tilde{P}_n}{\omega^2 + \left(Dk^2 + \frac{D}{k_BT}\rho_0 k^2 \tilde{v}(\boldsymbol{k})\right)^2} \,. \tag{3.61}$$

The resolution for $n = 3$ and $n = 4$ is presented in the reference [AC25] — thanks to L. Le Bon! I would like to conclude this discussion by highlighting an important limitation for me: the joint mean-field limit ($\rho_0 \to \infty$ and $\rho_0 v = \mathcal{O}(1)$) is questionable from a physical point of view. Which pair interactions evolve as $1/\rho_0$? Nevertheless, this approach provides a robust route to determine the high-order correlations.

II.D Possible extension of SDFT

SDFT was originally developed to address the dynamics of colloids and other particles that are much larger than the solvent molecules. [Dean, 1996, Illien, 2025] The mass/size difference entails a timescale separation between the colloids and the solvent dynamics, enabling the modelling of the colloids dynamics with the overdamped Langevin equations or, equivalently, with SDFT. Furthermore, SDFT particles are often spherical and without internal degree of freedoms. In order to apply SDFT to molecular fluids of interest, we must adapt the theory to include numerous physical effects at the microscopic length and time scales. Below is a list of features that I consider essential for properly modelling a molecular fluid:

1. **Size of the particles**. In practical applications, SDFT neglects the short-range repulsive interactions (*i.e.*, the particles size). [Illien, 2025] To model solvation dynamics, it seems essential to incorporate these repulsive interactions — at least, to take into account the steric effect of the solute on the solvent dynamics. [Song et al., 1996, Song and Chandler, 1998]
2. **Nonspherical particles**. SDFT has mainly been applied to spherical particles (*e.g.*, colloids) with radial pair interactions. However, to accurately model rotational dynamics or rotation/translation couplings, it will be necessary to write a SDFT for the molecular density $\rho(\boldsymbol{r}, \boldsymbol{\omega}, t)$. We recently proposed a SDFT for a dipolar solvent [AC25], a raising subject in the literature. [Cugliandolo et al., 2015]
3. **Associativity**. Water (and other complex fluids) forms hydrogen bonds, which are strong and directional interactions, in-between of nonbonding and bonding interactions. Such hydrogen bonds can be formally treated as an orientation-dependent pair interaction, as in the force fields developed for water (*e.g.* SPCE, TIP3P, etc.). However, I envisage that modelling hydrogen bonds specifically using the patchy particle formalism, [Simon and Oettel, 2024] for example, will help to take them into account within the SDFT framework.
4. **Inertial effects**. SDFT is primary employed within the framework of the overdamped Langevin equation. [Dean, 1996] An accurate description of the dynamics at the picosecond scale will require inertial effects such as ballistic motion or momentum conservation. There is existing extensions of SDFT to consider the phase space density $f(\boldsymbol{r}, \boldsymbol{v})$. [Das and Yoshimori, 2013,Nakamura and Yoshimori, 2009] For instance, it could be interesting to use SDFT to explain the solvent structure in presence of a pulled particles, [Lesnicki et al., 2020, Lesnicki and Vuilleumier, 2017, Lesnicki et al., 2021, Poncet et al., 2021] [AC5] In combination with the work on the molecular SDFT, I intend to develop a SDFT for the phase density of position, orientation, translational velocity, and angular velocity $f(\boldsymbol{r}, \boldsymbol{\omega}, \boldsymbol{v}, \dot{\boldsymbol{\omega}}, t)$. This inertial SDFT will more naturally accounts for collisions between molecules.
5. **Non-Markovian dynamics**. The standard SDFT is based on the (overdamped) Langevin equation, which assumes that all translational and rotational motions are Markovian (*i.e.*, memoryless). However, microscopic dynamics are often non-Markovian. For example,

the rotational dynamics of water occurs through "jumps" [Laage and Hynes, 2006], while the diffusion of small solutes in dense liquids can be described as a hopping process between cages. [Polimeno and Moro, 1994, Bier et al., 2008, Acharya et al., 2015, Dokko et al., 2018] I will seek to integrate these non-Markovian effects by proposing a SDFT with memory, starting from the generalised Langevin equations, [Zwanzig, 2001] which reads

$$m_i \frac{\mathrm{d}}{\mathrm{d}t} \boldsymbol{v}_i(t) = -\int K(t-u)\boldsymbol{v}_i(u)\mathrm{d}u + \boldsymbol{\eta}_i(t) \tag{3.62}$$

where m_i is the mass of the particle i and K is called the memory kernel, which takes into account the non-Markovian effects on the molecular dynamics. I intend here to derive a SDFT with this kind of formalism. In practical application, the calculation of this memory can rely on the algorithms developed during my M2 internship [AC1][AC2].

6. **Intramolecular degrees of freedom**. "Large" molecules (those with more than 4 atoms) exhibit various intramolecular motions: bending, stretching, dihedral rotation. These motions can couple with the rotational or translational dynamics of the molecule, especially the dihedral rotation, which can affect its interaction with the surrounding molecules. Including the intramolecular dynamics will be essential when studying large solutes or complex solvents, such as the deep eutectic solvents.

I have just started exploring the first two features on this list, namely the size of the particles and their non-sphericity in collaboration with P. Illien and B. Rotenberg. Addressing all these aspects will necessarily be a collaborative work, to which I hope to provide some decisive contributions. I will next review SDFT for an electrolytes in an implicit solvent.

III SDFT for electrolytes in implicit solvent

Electrolyte solutions are ubiquitous in our world, appearing in many industrial applications and biological or geological systems. Current hot topics related to electrolytes include the development of the blue energy technology [Rastgar et al., 2023], the modelling of the electric double-layer [Jeanmairet et al., 2022] or of the solvation shell of biomolecules, [Laage et al., 2017] and the characterization the long-range correlations. [Smith et al., 2016, Elliott et al., 2024, Rondepierre et al., 2025] When the ionic concentration increases (and the solvent one decreases), the electrolytes reach a regime called water-in-salt, [Goloviznina et al., 2024, Feng et al., 2025, Nguyen et al., 2025] then the ionic liquid regime where no solvent is present.

Due to their importance, there exists a rich variety of theoretical methods to determine the equilibrium properties of electrolytes. [Hansen and McDonald, 2013, Kjellander, 2020b] In particular, I am interested in the density-based approaches, such as the classical DFT, [Härtel, 2025, Bültmann and Härtel, 2022, Gillespie et al., 2002, Piron and Blenski, 2019] or the field theories. [Gao et al., 2023, Di Caprio et al., 1998, Maggs and Everaers, 2006, Levy et al., 2012, Adar et al., 2018, Budkov, 2020, Berthoumieux and Maggs, 2015, Berthoumieux, 2018, Berthoumieux and Paillusson, 2019, Vatin et al., 2021, Hedley et al., 2023, Becker et al., 2025] My project is however focused on the modelling of the dynamics of the electrolytes surrounding a given solute. This will involve to calculate complex correlation functions, such as 3-point correlations or 2-point correlations in presence of an external field. SDFT is the perfect tool to model these

complex correlations. For instance, SDFT has already been used to calculate the conductivity of electrolytes [Démery and Dean, 2016, Bernard et al., 2023], the frequency-dependent conductivity, [Bonneau et al., 2023, Bonneau et al., 2024, Bonneau et al., 2025], or the conductivity at high ionic concentration [Avni et al., 2022b, Avni et al., 2022a, Berthoumieux et al., 2024]. As SDFT is powerful framework tailored to model the fluctuations, it has also be employed to investigate the nonequilibrium Casimir effect in driven electrolytes. [Dean and Podgornik, 2014, Lu et al., 2015, Dean et al., 2016, Mahdisoltani and Golestanian, 2021b, Mahdisoltani and Golestanian, 2021a, Du et al., 2025a, Du et al., 2025b]

Before applying SDFT to determine charge correlations and the NMR relaxation rate, this section will review SDFT for electrolytes with an implicit solvent. [Démery and Dean, 2016] First, I will review the Dean-Kawasaki equations for cation and anion densities, followed by the standard linearisation scheme. In the final subsection, I will derive the path integral formulation of SDFT for electrolytes for the first time, which could be used in future work for NMR modelling. As an exercise, I will also derive the mean-field equations satisfied by the most probable path, although I am unsure whether the mean-field limit is relevant to the study of electrolytes.

III.A Dean-Kawasaki equations for electrolytes

In the following, we consider a symmetric binary electrolyte consisting of N cations and N anions, with respective charges $\pm ze$. We denote their overall densities $C_I = N/V$, where V is the volume of the system. Their respective mobilities will be denoted by $\mu^{\pm}$, and their bare diffusion coefficients by $D^{\pm}$ (we assume that the fluctuation-dissipation relation holds, in such a way that $D^{\pm} = \mu^{\pm} k_{\mathrm{B}} T$). We assume for simplicity that $\mu^+ = \mu^- \equiv \mu_I$ (*i.e.* $D^+ = D^- \equiv D_I$). The ion dynamics is described by the set of $2N$ coupled overdamped Langevin equations obeyed by the positions $\boldsymbol{r}_i^{\pm}$ of the ions:

$$\frac{\mathrm{d}}{\mathrm{d}t}\boldsymbol{r}_i^{\pm}(t) = \pm\frac{D_I}{k_B T} ze[-\nabla\varphi(\boldsymbol{r}_i^{\pm}(t))] + \sqrt{2D_I}\boldsymbol{\eta}_i^{\pm}(t), \tag{3.63}$$

where $\boldsymbol{\eta}_i^{\pm}(t)$ are unit white noises with correlations:

$$\langle \eta_i^{\alpha\pm}(t)\rangle = 0, \tag{3.64}$$

$$\langle \eta_i^{\alpha\pm}(t)\eta_j^{\beta\pm}(t')\rangle = \delta_{ij}\delta_{\alpha\beta}\delta_{\pm}\delta(t-t'), \tag{3.65}$$

with α and β denote Cartesian coordinates, and where φ is the electrostatic potential. The latter is a solution of the Poisson equation:

$$-\nabla^2\varphi(\boldsymbol{r},t) = \frac{ze}{\varepsilon_w}\left[\rho^+(\boldsymbol{r},t) - \rho^-(\boldsymbol{r},t)\right] \ , \tag{3.66}$$

where $\varepsilon_0\varepsilon_w$ is the static dielectric permittivity of water with ε_w. the relative permittivity We define the microscopic densities of cations and anions,

$$\rho^+(\boldsymbol{r},t) = \sum_{\alpha=1}^{N}\delta(\boldsymbol{r}-\boldsymbol{r}_\alpha^+(t)), \tag{3.67}$$

$$\rho^-(\boldsymbol{r},t) = \sum_{\alpha=1}^{N}\delta(\boldsymbol{r}-\boldsymbol{r}_\alpha^-(t)). \tag{3.68}$$

The solution of the Poisson equation reads

$$\varphi(\boldsymbol{r},t) = \int \mathrm{d}\boldsymbol{r}'\, \mathcal{G}(\boldsymbol{r}-\boldsymbol{r}')ze\left[\rho^+(\boldsymbol{r},t) - \rho^-(\boldsymbol{r},t)\right], \tag{3.69}$$

where $\mathcal{G}(\boldsymbol{r}) = 1/(4\pi\varepsilon_0\varepsilon_w r)$ is the Green function associated with Poisson equation. Applying Dean's strategy, we can obtain the Dean-Kawasaki equations for the cationic and anionic densities [Dean, 1996, Démery and Dean, 2016]

$$\frac{\partial}{\partial t}\rho^+ = D_I\nabla^2\rho^+ + \frac{D_I}{k_BT}ze\nabla\cdot(\rho^+\nabla\varphi) + \nabla\cdot(\sqrt{2D_I\rho^+}\boldsymbol{\xi}^+(\boldsymbol{r},t)), \tag{3.70}$$

$$\frac{\partial}{\partial t}\rho^- = D_I\nabla^2\rho^- - \frac{D_I}{k_BT}ze\nabla\cdot(\rho^-\nabla\varphi) + \nabla\cdot(\sqrt{2D_I\rho^-}\boldsymbol{\xi}^-(\boldsymbol{r},t)), \tag{3.71}$$

where $\xi^\pm$ are two uncorrelated unit Gaussian white noise vector fields with statistics,

$$\left\langle \xi^{\alpha\pm}(\boldsymbol{r},t)\right\rangle = 0, \tag{3.72}$$

$$\left\langle \xi^{\alpha\pm}(\boldsymbol{r},t)\xi^{\beta\pm}(\boldsymbol{r}',t')\right\rangle = \delta_{\alpha\beta}\delta(t-t')\delta(\boldsymbol{r}-\boldsymbol{r}')\delta_\pm\,. \tag{3.73}$$

Following [Mahdisoltani and Golestanian, 2021a], using the charge density ($\rho_I = ze(\rho^+ - \rho^-)$) and the number density ($\mathcal{C} = \rho^+ + \rho^-$) as variables, we obtain the following equations

$$\frac{\partial}{\partial t}\rho_I = D_I\nabla^2\rho_I + \frac{D_I}{k_BT}(ze)^2\nabla\cdot(\mathcal{C}\nabla\varphi) + \nabla\cdot\boldsymbol{\Xi}_{\rho_I}, \tag{3.74}$$

$$\frac{\partial}{\partial t}\mathcal{C} = D_I\nabla^2\mathcal{C} + \frac{D_I}{k_BT}\nabla\cdot(\rho_I\nabla\varphi) + \nabla\cdot\boldsymbol{\Xi}_{\mathcal{C}}, \tag{3.75}$$

where $\boldsymbol{\Xi}_{\mathcal{C}}(\boldsymbol{r},t)$ and $\boldsymbol{\Xi}_{\rho_I}(\boldsymbol{r},t)$ are unit Gaussian white noise vector fields with correlations

$$\left\langle \Xi^\alpha_{\rho_I}(\boldsymbol{r},t)\right\rangle = \langle\Xi^\alpha_{\mathcal{C}}(\boldsymbol{r},t)\rangle = 0, \tag{3.76}$$

$$\left\langle \Xi^\alpha_{\rho_I}(\boldsymbol{r},t)\Xi^\beta_{\rho_I}(\boldsymbol{r}',t')\right\rangle = (ze)^2 2D_I\mathcal{C}\,\delta_{\alpha\beta}\delta(t-t')\delta(\boldsymbol{r}-\boldsymbol{r}')\,, \tag{3.77}$$

$$\left\langle \Xi^\alpha_{\mathcal{C}}(\boldsymbol{r},t)\Xi^\beta_{\mathcal{C}}(\boldsymbol{r}',t')\right\rangle = 2D_I\mathcal{C}\,\delta_{\alpha\beta}\delta(t-t')\delta(\boldsymbol{r}-\boldsymbol{r}')\,, \tag{3.78}$$

$$\left\langle \Xi^\alpha_{\mathcal{C}}(\boldsymbol{r},t)\Xi^\beta_{\rho_I}(\boldsymbol{r}',t')\right\rangle = 2D_I\rho_I\,\delta_{\alpha\beta}\delta(t-t')\delta(\boldsymbol{r}-\boldsymbol{r}')\,, \tag{3.79}$$

$$\left\langle \Xi^\alpha_{\rho_I}(\boldsymbol{r},t)\Xi^\beta_{\mathcal{C}}(\boldsymbol{r}',t')\right\rangle = -2D_I\rho_I\,\delta_{\alpha\beta}\delta(t-t')\delta(\boldsymbol{r}-\boldsymbol{r}')\,. \tag{3.80}$$

III.B Linearisation

We linearise the set of equations 3.74-3.75 by assuming that the fluctuations of ρ^+ and ρ^- around their homogeneous values are small: $\rho^\pm = C_I + \delta\rho^\pm$ with $\delta\rho^\pm \ll C_I$. $\rho_I = \rho^+ - \rho^-$ is of linear order in the perturbation, while the number density is written as $\mathcal{C} = 2C_I + c$, which $c = \delta\rho^+ + \delta\rho^- = \mathcal{O}(\delta\rho^1)$. The linearised evolution equation for ρ_I and c read:

$$\frac{\partial}{\partial t}\rho_I(\boldsymbol{r},t) = D_I\nabla^2\rho_I - D_I\kappa_{\text{imp}}^2\rho_I + (ze)\sqrt{4D_IC_I}\Xi_{\rho_I}(\boldsymbol{r},t), \tag{3.81}$$

$$\frac{\partial}{\partial t}c(\boldsymbol{r},t) = D_I\nabla^2 c + \sqrt{4D_IC_I}\Xi_c(\boldsymbol{r},t), \tag{3.82}$$

where we define the Debye length κ_{imp}^{-1} through $\kappa_{\text{imp}}^2 = 2C_Iz^2e^2/(\varepsilon_0\varepsilon_w k_{\text{B}}T)$. The noises Ξ_{ρ_I} and Ξ_c are uncorrelated, have zero average, and have correlations:

$$\langle\Xi_{\rho_I/c}(\boldsymbol{r},t)\Xi_{\rho_I/c}(\boldsymbol{r}',t')\rangle = -\nabla^2\delta(\boldsymbol{r}-\boldsymbol{r}')\delta(t-t')\delta_{\rho_I/c}\,. \tag{3.83}$$

Equations 3.81 and 3.82 are uncoupled and can be solved directly with space and time Fourier transforms. It gives for ρ_I,

$$\tilde{\rho}_I(\boldsymbol{k},\omega) = \frac{(ze)\sqrt{4D_IC_I}\tilde{\Xi}_{\rho_I}}{-\mathrm{i}\omega + D_Ik^2 + D_I\kappa_{\text{imp}}^2}\,. \tag{3.84}$$

The correlation of the Fourier-transformed noises is derived in the annex I.A. It reads

$$\left\langle\tilde{\Xi}_{\rho_I}(\boldsymbol{k},\omega)\tilde{\Xi}_{\rho_I}(\boldsymbol{k}',\omega')\right\rangle = (2\pi)^4k^2\delta(\boldsymbol{k}+\boldsymbol{k}')\delta(\omega+\omega')\,, \tag{3.85}$$

and the 2-point correlation function is

$$\langle\tilde{\rho}_I(\boldsymbol{k},\omega)\tilde{\rho}_I(\boldsymbol{k}',\omega')\rangle = \frac{4(2\pi)^4D_IC_I(ze)^2k^2}{\omega^2 + D_I^2\left(k^2+\kappa_{\text{imp}}^2\right)^2}\delta(\boldsymbol{k}+\boldsymbol{k}')\delta(\omega+\omega') \tag{3.86}$$

$$= \frac{2(2\pi)^4D_I\varepsilon_0\varepsilon_w k_BT\kappa_{\text{imp}}^2k^2}{\omega^2 + D_I^2\left(k^2+\kappa_{\text{imp}}^2\right)^2}\delta(\boldsymbol{k}+\boldsymbol{k}')\delta(\omega+\omega')\,. \tag{3.87}$$

In time domain, it reads,

$$C_I(\boldsymbol{k},t,\boldsymbol{k}',t') = \langle\tilde{\rho}_I(\boldsymbol{k},t)\tilde{\rho}_I(\boldsymbol{k}',t')\rangle \tag{3.88}$$

$$= \frac{2(2\pi)^3C_I(ze)^2k^2}{k^2+\kappa_{\text{imp}}^2}\exp\left(-D_I\left(k^2+\kappa_{\text{imp}}^2\right)|t-t'|\right)\delta(\boldsymbol{k}+\boldsymbol{k}')\,, \tag{3.89}$$

$$= \frac{(2\pi)^3D_I\varepsilon_0\varepsilon_w k_BT\kappa_{\text{imp}}^2k^2}{k^2+\kappa_{\text{imp}}^2}\exp\left(-D_I\left(k^2+\kappa_{\text{imp}}^2\right)|t-t'|\right)\delta(\boldsymbol{k}+\boldsymbol{k}')\,. \tag{3.90}$$

This correlation may enter in the calculation of the autocorrelation of A in the uniform approximation shown in equation 3.16.

III.C Mean-field approximation for electrolytes

Here, I will present new result: the path integral formulation and mean-field approximation of SDFT for electrolytes with an implicit solvent. In the literature, Farhadi and Limmer proposed (very) recently a path integral formulation for the electrolyte dynamics in presence of an external field. [Farhadi and Limmer, 2025] They did not however construct the Martin-Siggia-Rose action and did not consider the mean-field limits. In the following, I will derive this action using the same route as before in subsection II.B. First, we express the probability to observe a given microscopic joint densities of anions and cations,

$$\begin{aligned}\mathcal{P}[\rho^+,\rho^-|(t=0)] = \int \mathcal{D}\boldsymbol{\xi}^+\mathcal{D}\boldsymbol{\xi}^- \\ \times \delta\left[\frac{\partial}{\partial t}\rho^+ - D_I\nabla^2\rho^+ - \frac{D_I}{k_BT}(ze)\nabla\cdot(\rho^+\nabla\varphi) - \nabla\cdot(\sqrt{2D_I\rho^+}\boldsymbol{\xi}^+)\right] \\ \times \delta\left[\frac{\partial}{\partial t}\rho^- - D_I\nabla^2\rho^- + \frac{D_I}{k_BT}(ze)\nabla\cdot(\rho^-\nabla\varphi) - \nabla\cdot(\sqrt{2D_I\rho^-}\boldsymbol{\xi}^-)\right] \\ \times \exp\left(-\int_0^T\int \mathrm{d}\boldsymbol{r}|\boldsymbol{\xi}^+|^2\right)\exp\left(-\int_0^T\int \mathrm{d}\boldsymbol{r}|\boldsymbol{\xi}^-|^2\right) \ . \end{aligned} \tag{3.91}$$

After inserting the Fourier-like expression of the Dirac functional and integrating over the Gaussian noises, we obtain the probability

$$\mathcal{P}[\rho^+,\rho^-|(t=0)] = \int \mathcal{D}\hat{\rho}^+\mathcal{D}\hat{\rho}^- \exp\left(-\mathcal{S}_{\rho_0}[\rho^+,\rho^-,\hat{\rho}^+,\hat{\rho}^-]\right) \tag{3.92}$$

with the action,

$$\begin{aligned}\mathcal{S}_{\rho_0}[\rho^+,\rho^-,\hat{\rho}^+,\hat{\rho}^-] = \int_0^T\int \mathrm{d}\boldsymbol{r}\Bigg[\hat{\rho}^+\left(\frac{\partial}{\partial t}\rho^+ - D_I\nabla^2\rho^+ - \frac{D_I}{k_BT}(ze)\nabla\cdot(\rho^+\nabla\varphi)\right) - D\rho^+|\nabla\hat{\rho}^+|^2 \\ + \hat{\rho}^-\left(\frac{\partial}{\partial t}\rho^- - D_I\nabla^2\rho^- + \frac{D_I}{k_BT}(ze)\nabla\cdot(\rho^-\nabla\varphi)\right) - D\rho^-|\nabla\hat{\rho}^-|^2\Bigg] \ . \end{aligned} \tag{3.93}$$

After integrating over the initial conditions, one obtains the generalized action

$$\mathcal{S} = \mathcal{S}_{\rho_0}[\rho^+,\rho^-,\hat{\rho}^+,\hat{\rho}^-] - \ln\mathcal{P}_0\left[\rho^+(\boldsymbol{r},t=0),\rho^-(\boldsymbol{r},t=0)\right] \ , \tag{3.94}$$

where is the joint initial distribution of the densities. We then define the tilted action,

$$\mathcal{S}_{\lambda^+,\lambda^-} = \mathcal{S} + \int_0^T\int \mathrm{d}\boldsymbol{r}\left(\lambda^+(\boldsymbol{r},t)\rho^+(\boldsymbol{r},t) + \lambda^-(\boldsymbol{r},t)\rho^-(\boldsymbol{r},t)\right) \ . \tag{3.95}$$

In the joint limit of large densities ($C_I \to \infty$) and small pair potentials ($C_I v = \mathcal{O}(1)$), we can apply the saddle-point approximations. We denote q^+, q^-, p^+, p^- the path which minimises the action, it satisfies the conditions:

$$\frac{\delta \mathcal{S}_{\lambda^+,\lambda^-}[\rho^+,\rho^-,\hat{\rho}^+,\hat{\rho}^-]}{\delta \rho^+(\boldsymbol{r},t)}|_{q^+,q^-,p^+,p^-} = \frac{\delta \mathcal{S}_{\lambda^+,\lambda^-}[\rho^+,\rho^-,\hat{\rho}^+,\hat{\rho}^-]}{\delta \hat{\rho}^+(\boldsymbol{r},t)}|_{q^+,q^-,p^+,p^-} = 0 \,, \tag{3.96}$$

$$\frac{\delta \mathcal{S}_{\lambda^+,\lambda^-}[\rho^+,\rho^-,\hat{\rho}^+,\hat{\rho}^-]}{\delta \rho^-(\boldsymbol{r},t)}|_{q^+,q^-,p^+,p^-} = \frac{\delta \mathcal{S}_{\lambda^+,\lambda^-}[\rho^+,\rho^-,\hat{\rho}^+,\hat{\rho}^-]}{\delta \hat{\rho}^-(\boldsymbol{r},t)}|_{q^+,q^-,p^+,p^-} = 0 \,. \tag{3.97}$$

These conditions explicitly read

$$\frac{\partial}{\partial t} q^+ = D_I \nabla^2 q^+ - \frac{D_I}{k_B T}(ze)\nabla \cdot (q^+ \nabla \varphi) - 2D \nabla \cdot (q^+ \nabla p^+) \,, \tag{3.98}$$

$$\begin{aligned} \frac{\partial}{\partial t} p^+ = & -D_I \nabla^2 p^+ - D_I |\nabla p^+|^2 \\ & + \frac{D_I}{k_B T}(ze)\left[\nabla p^+ \cdot \nabla \varphi + ze \int \mathrm{d}\boldsymbol{r}' \left(\nabla p^+(\boldsymbol{r}') q^+(\boldsymbol{r}') - \nabla p^-(\boldsymbol{r}') q^-(\boldsymbol{r}')\right) \nabla \mathcal{G}(\boldsymbol{r} - \boldsymbol{r}')\right] \,, \end{aligned} \tag{3.99}$$

$$\frac{\partial}{\partial t} q^- = D_I \nabla^2 q^- + \frac{D_I}{k_B T}(ze)\nabla \cdot (q^- \nabla \varphi) - 2D \nabla \cdot (q^- \nabla p^-) \,, \tag{3.100}$$

$$\begin{aligned} \frac{\partial}{\partial t} p^- = & -D_I \nabla^2 p^- - D_I |\nabla p^-|^2 \\ & + \frac{D_I}{k_B T}(ze)\left[\nabla p^- \cdot \nabla \varphi + ze \int \mathrm{d}\boldsymbol{r}' \left(\nabla p^-(\boldsymbol{r}') q^-(\boldsymbol{r}') - \nabla p^+(\boldsymbol{r}') q^+(\boldsymbol{r}')\right) \nabla \mathcal{G}(\boldsymbol{r} - \boldsymbol{r}')\right] \,, \end{aligned} \tag{3.101}$$

where $\mathcal{G}$ is the Green function of the Poisson equation 3.66. We expand all functions q^+, q^-, p^+, p^- and φ in a series expansion of power of λ. Assuming an homogeneous state for the order 0 ($q_0^+ = q_0^- = C_I$ and $p_0^+ = p_0^- = 0$), the equations at order 1 are

$$\frac{\partial}{\partial t} q_1^+ = D_I \nabla^2 q_1^+ - \frac{D_I}{k_B T}(ze) C_I \nabla^2 \varphi_1 - 2 D_I C_I \nabla^2 p_1^+ \,, \tag{3.102}$$

$$\frac{\partial}{\partial t} p_1^+ = -D_I \nabla^2 p_1^+ + \frac{D_I}{k_B T} C_I (ze)^2 \int \mathrm{d}\boldsymbol{r}' \nabla \left(p_1^+(\boldsymbol{r}') - p_1^-(\boldsymbol{r}')\right) \nabla \mathcal{G}(\boldsymbol{r} - \boldsymbol{r}') - \lambda^+ \,, \tag{3.103}$$

$$\frac{\partial}{\partial t} q_1^- = D_I \nabla^2 q_1^- + \frac{D_I}{k_B T}(ze) C_I \nabla^2 \varphi_1 - 2 D C_I \nabla^2 p_1^- \,, \tag{3.104}$$

$$\frac{\partial}{\partial t} p_1^- = -D_I \nabla^2 p_1^- + \frac{D_I}{k_B T} C_I (ze)^2 \int \mathrm{d}\boldsymbol{r}' \nabla \left(p_1^-(\boldsymbol{r}') - p_1^+(\boldsymbol{r}')\right) \nabla \mathcal{G}(\boldsymbol{r} - \boldsymbol{r}') - \lambda^- \,. \tag{3.105}$$

Inserting explicitly the Poisson equation 3.66 at order 1 ($\nabla^2 \varphi_1 = -(q_1^+ - q_1^-)/(\varepsilon_0 \varepsilon_w)$ and the definition of the corresponding Green function ($\nabla^2 \mathcal{G} = -\delta(\boldsymbol{r})/(\varepsilon_0 \varepsilon_w)$, one formulates the equations as

$$\frac{\partial}{\partial t}q_1^+ - D_I\nabla^2 q_1^+ + D_I\frac{\kappa_{\rm imp}^2}{2}\left(q_1^+ - q_1^-\right) + 2D_I C_I\nabla^2 p_1^+ = 0\ , \tag{3.106}$$

$$\frac{\partial}{\partial t}p_1^+ + D_I\nabla^2 p_1^+ - D_I\frac{\kappa_{\rm imp}^2}{2}\left(p_1^+ - p_1^-\right) = -\lambda^+\ , \tag{3.107}$$

$$\frac{\partial}{\partial t}q_1^- - D_I\nabla^2 q_1^- - D_I\frac{\kappa_{\rm imp}^2}{2}\left(q_1^+ - q_1^-\right) + 2D_I C_I\nabla^2 p_1^- = 0\ , \tag{3.108}$$

$$\frac{\partial}{\partial t}p_1^- - D_I\nabla^2 p_1^- + D_I\frac{\kappa_{\rm imp}^2}{2}\left(p_1^+ - p_1^-\right) = -\lambda^-\ . \tag{3.109}$$

Using the variables $q_1^I = q_1^+ - q_1^-$, $q_1^N = q_1^+ + q_1^-$ (and likewise for $p^\pm$ and $\lambda^\pm$), we obtain two uncoupled sets of equations for the pair (q_1^I, p_1^I) and for the pair (q_1^N, p_1^N):

$$\frac{\partial}{\partial t}q_1^I - D_I\nabla^2 q_1^I + D_I\kappa_{\rm imp}^2 q_1^I + 2D_I C_I\nabla^2 p_1^I = 0\ , \tag{3.110}$$

$$\frac{\partial}{\partial t}p_1^I + D_I\nabla^2 p_1^I - D_I\kappa_{\rm imp}^2 p_1^I = -\lambda^I\ , \tag{3.111}$$

$$\frac{\partial}{\partial t}q_1^N - D_I\nabla^2 q_1^N + 2DC_I\nabla^2 p_1^N = 0\ , \tag{3.112}$$

$$\frac{\partial}{\partial t}p_1^N + D_I\nabla^2 p_1^N - = \lambda^N\ . \tag{3.113}$$

The equation for p_I^1 can be solved directly with space and time Fourier transforms, $\tilde{p}_1^I = \tilde{\lambda}^I/(\mathrm{i}\omega + D_I k^2 + D_I\kappa_{\rm imp}^2)$. The resolution of the equations for q_1^I gives $\tilde{q}_1^I = 2D_I C_I k^2\tilde{p}_1^I/(-\mathrm{i}\omega + D_I k^2 + D_I\kappa_{\rm imp}^2)$. After inserting the results for $\tilde{p}_1^I$ and do the derivative over λ, we obtain the same 2-point correlation functions as in equation 3.87. Finally, I write below the mean-field equations at order 2:

$$\frac{\partial}{\partial t}q_2^+ - D_I\nabla^2 q_2^+ - D_I\frac{\kappa_{\rm imp}^2}{2}\left(q_2^+ - q_2^-\right) + 2D_I C_I\nabla^2 p_2^+ = -\frac{D_I}{k_BT}(ze)\nabla\cdot(q_1^+\nabla\varphi_1) - 2D\nabla\cdot(q_1^+\nabla p_1^+)\,, \tag{3.114}$$

$$\frac{\partial}{\partial t}p_2^+ + D_I\nabla^2 p_2^+ - D_I\frac{\kappa_{\rm imp}^2}{2}\left(p_2^+ - p_2^-\right) = -D_I|\nabla p_1^+|^2 + \frac{D_I}{k_BT}(ze)\Bigg[\nabla p_1^+\cdot\nabla\varphi_1 + ze\int \mathrm{d}\boldsymbol{r}'\big(\nabla p_1^+(\boldsymbol{r}')q_1^+(\boldsymbol{r}') - \nabla p_1^-(\boldsymbol{r}')q_1^-(\boldsymbol{r}')\big)\nabla\mathcal{G}(\boldsymbol{r}-\boldsymbol{r}')\Bigg]\,, \tag{3.115}$$

$$\frac{\partial}{\partial t}q_2^- - D_I\nabla^2 q_2^- + D_I\frac{\kappa_{\rm imp}^2}{2}\left(q_2^+ - q_2^-\right) + 2D_I C_I\nabla^2 p_2^- = -\frac{D_I}{k_BT}(ze)\nabla\cdot(q_1^-\nabla\varphi_1) - 2D\nabla\cdot(q_1^-\nabla p_1^-)\,, \tag{3.116}$$

$$\frac{\partial}{\partial t}p_2^- - D_I\nabla^2 p_2^- + D_I\frac{\kappa_{\rm imp}^2}{2}\left(p_2^+ - p_2^-\right) = -D_I|\nabla p_1^-|^2 + \frac{D_I}{k_BT}(ze)\Bigg[\nabla p_1^-\cdot\nabla\varphi_1 + ze\int \mathrm{d}\boldsymbol{r}'\big(\nabla p_1^-(\boldsymbol{r}')q_1^-(\boldsymbol{r}') - \nabla p_1^+(\boldsymbol{r}')q_1^+(\boldsymbol{r}')\big)\nabla\mathcal{G}(\boldsymbol{r}-\boldsymbol{r}')\Bigg]\,. \tag{3.117}$$

As these are new results, I stopped short of calculating the 3-point correlation functions. We can notice a similar structure as for the case of identical particles (equations 3.56 and 3.57), with the same linear operator (put in the left-hand side) at order 1 and order 2 and non-linear source terms appearing at order 2. The main question for me is the justification of the mean-field limit for that system, where the pair interaction is independent of the average densities of ions. Nevertheless, it is interesting to see we can easily extend the path integral formulation to a binary system. Let us now review SDFT for a dipolar solvent.

IV SDFT for electrolytes in dipolar solvent

I will now present a brief summary of our recent work [AC22]. Our aim is to derive SDFT equations for an electrolyte with an explicit dipolar solvent, which is described by both translational and rotational degrees of freedom. I will first review the Dean-Kawasaki equations for this system, and then present the results of their linearisation. In the final subsection, I will relate this explicit description of the solvent to the implicit description discussed in section III.

IV.A Dean-Kawasaki equations

We consider a symmetric binary electrolyte consisting of N_I cations, N_I anions and N_S solvent molecules. The cations and the anions have a charge $\pm ze$ and overall densities $C_I = N_I/V$, where V is the volume of the system, while the solvent molecules bear a point charge dipoles $\mathbf{p}$ and have a concentration $C_S = N_S/V$. We assume that the ionic diffusion

coefficients are equal, $D^+ = D^-$ and we denote D_S and D_S^r the translational and rotational diffusion coefficients of the solvent. The ion dynamics is described the set of $2N$ overdamped Langevin equations obeyed by their positions $\boldsymbol{r}_i^{\pm}$ and the solvent dynamics are described by the set of $2N$ overdamped Langevin equations, which are obeyed by their positions $\boldsymbol{r}_j^S$ and their orientations $\hat{\boldsymbol{u}}_j$. These $4N$ equations read

$$\frac{\mathrm{d}\boldsymbol{r}_i^{\pm}}{\mathrm{d}t} = \pm\frac{D_I}{k_BT}ze\nabla\left[-\varphi(\boldsymbol{r}_i^{\pm})\right] + \sqrt{2D_I}\boldsymbol{\eta}_i^{\pm}(t)\ , \tag{3.118}$$

$$\frac{\mathrm{d}\boldsymbol{r}_j^S}{\mathrm{d}t} = \frac{D_S}{k_BT}(p\hat{\boldsymbol{u}}_j\cdot\nabla)\nabla\left[-\varphi(\boldsymbol{r}_j^S)\right] + \sqrt{2D_S}\boldsymbol{\eta}_j^S(t)\ , \tag{3.119}$$

$$\frac{\mathrm{d}\hat{\boldsymbol{u}}_j}{\mathrm{d}t} = \left[\frac{D_S^r}{k_BT}p\hat{\boldsymbol{u}}_j\times\nabla[-\varphi(\boldsymbol{r}_j^S)] + \sqrt{2D_S^r}\boldsymbol{\eta}_j^{S,r}(t)\right]\times\hat{\boldsymbol{u}}_j\ , \tag{3.120}$$

where the noises $\boldsymbol{\eta}_i^{\alpha}(t)$ are uncorrelated Gaussian white noises of zero average, unit variance, and correlations:

$$\langle\eta_i^{\alpha a}(t)\rangle = 0, \tag{3.121}$$

$$\langle\eta_i^{\alpha a}(t)\eta_j^{\beta b}(t')\rangle = \delta_{ij}\delta_{\alpha\beta}\delta_{ab}\delta(t-t'), \tag{3.122}$$

where α or β are the Cartesian components of the vectors and a, b denote the nature of the noises ($\pm$, S or S, r). We assumed that the ions only interact through electrostatic interactions, and that short-range repulsive interactions are neglected. The electrostatic potential is the solution of the Poisson equation

$$-\nabla^2\varphi(\boldsymbol{r},t) = \frac{1}{\varepsilon_0}\left(ze\rho^+(\boldsymbol{r},t) - ze\rho^-(\boldsymbol{r},t) + +\rho_S^c(\boldsymbol{r},t)\right) \tag{3.123}$$

where we define the charge density of the solvent as

$$\rho_S^c(\boldsymbol{r},t) = -\int\mathrm{d}\hat{\boldsymbol{u}}p\hat{\boldsymbol{u}}\cdot\nabla\rho_S(\boldsymbol{r},\hat{\boldsymbol{u}},t)\ , \tag{3.124}$$

with the molecular density of the solvent

$$\rho_S(\boldsymbol{r},\hat{\boldsymbol{u}},t) = \sum_{j=1}^{N_S}\delta\left(\boldsymbol{r}-\boldsymbol{r}_j^S(t)\right)\delta\left(\hat{\boldsymbol{u}}-\hat{\boldsymbol{u}}_j\right)\ , \tag{3.125}$$

which depends both on $\boldsymbol{r}$ and $\hat{\boldsymbol{u}}$, the translational and rotational degree of freedom respectively.

Following Dean's strategy for ions, [Dean, 1996] we obtain the Dean-Kawasaki equations for the cationic and anionic densities

$$\frac{\partial}{\partial t}\rho^+ = D_I\nabla^2\rho^+ + \frac{D_I}{k_BT}ze\nabla\cdot(\rho^+\nabla\varphi) + \nabla\cdot(\sqrt{2D_I\rho^+}\boldsymbol{\xi}^+(\boldsymbol{r},t)) \;, \tag{3.126}$$

$$\frac{\partial}{\partial t}\rho^- = D_I\nabla^2\rho^- - \frac{D_I}{k_BT}ze\nabla\cdot(\rho^-\nabla\varphi) + \nabla\cdot(\sqrt{2D_I\rho^-}\boldsymbol{\xi}^-(\boldsymbol{r},t)) \;, \tag{3.127}$$

where $\xi^\pm$ are two uncorrelated unit Gaussian white noise vector fields with statistics,

$$\left\langle \xi^{\alpha\pm}(\boldsymbol{r},t)\right\rangle = 0, \tag{3.128}$$

$$\left\langle \xi^{\alpha\pm}(\boldsymbol{r},t)\xi^{\beta\pm}(\boldsymbol{r}',t')\right\rangle = \delta_{\alpha\beta}\delta(t-t')\delta(\boldsymbol{r}-\boldsymbol{r}')\delta_\pm \;. \tag{3.129}$$

We have presented the derivation of the Dean-Kawasaki equations for the solvent density $\rho_S(\boldsymbol{r},\hat{\boldsymbol{u}},t)$ in the paper [AC22], which is more complicated by the presence of the orientational degree of freedom $\hat{\boldsymbol{u}}$. It reads:

$$\begin{aligned}\partial_t n_S(\boldsymbol{r},\hat{\boldsymbol{u}},t) = {}& D_S\nabla^2_{\boldsymbol{r}}n_S + D^r_S\boldsymbol{\mathcal{R}}^2_{\hat{\boldsymbol{u}}}n_S \\ &+ \frac{D_S}{k_BT}\nabla_{\boldsymbol{r}}\cdot[n_Sp(\hat{\boldsymbol{u}}\cdot\nabla)\nabla\varphi(\boldsymbol{r})] + \frac{D^r_S}{k_BT}\boldsymbol{\mathcal{R}}_{\hat{\boldsymbol{u}}}\cdot[n_Sp\hat{\boldsymbol{u}}\times\nabla\varphi(\boldsymbol{r})] \\ &+ \nabla_{\boldsymbol{r}}\cdot(\sqrt{2D_Sn_S}\boldsymbol{\xi}_S(\boldsymbol{r},t)) + \boldsymbol{\mathcal{R}}_{\hat{\boldsymbol{u}}}\cdot(\sqrt{2D^r_Sn_S}\boldsymbol{\xi}_{S,r}(\boldsymbol{r},t)) \;,\end{aligned} \tag{3.130}$$

where $\boldsymbol{\mathcal{R}}_{\hat{\boldsymbol{u}}} = \hat{\boldsymbol{u}}\times\nabla_{\hat{\boldsymbol{u}}}$ is the rotational gradient operator. The three Dean-Kawasaki equations 3.126, 3.127 and 3.130 form a closed set of nonlinear equations, which reformulate exactly the overdamped Langevin equations. As we have already discussed in section II.A, we cannot solve these equations. The proper approach would be to write down the path integral formulation and try to solve the mean-field equations order by order, as done in section III.C. This should be addressed for a future work.

IV.B Linearisation

For now we will simply consider a linearisation around the uniform state. For the ions, we write $n_\pm = C_I + \delta n_\pm$ and obtain

$$\frac{\partial}{\partial t}\rho^+ = D_I\nabla^2\rho^+ + \frac{D_I}{k_BT}zeC_I\nabla^2\varphi + \nabla\cdot(\sqrt{2D_IC_I}\boldsymbol{\xi}^+(\boldsymbol{r},t)) \;, \tag{3.131}$$

$$\frac{\partial}{\partial t}\rho^- = D_I\nabla^2\rho^- - \frac{D_I}{k_BT}zeC_I\nabla^2\varphi + \nabla\cdot(\sqrt{2D_IC_I}\boldsymbol{\xi}^-(\boldsymbol{r},t)) \;. \tag{3.132}$$

For the solvent, we write $n_S = C_S/4\pi$ where the $1/4\pi$ factor accounts for the uniform density of orientations. This gives us the linearised equation for the solvent charge density,

$$\frac{\partial}{\partial t}\rho^c_S = D_S\nabla^2\rho^c_S - 2D^r_S\rho^c_S + \frac{1}{3k_BT}p^2C_S\nabla^2(D_S\nabla^2\varphi - 2D^r_S\varphi) + \Xi_S(\boldsymbol{r},t) \;. \tag{3.133}$$

The correlations of the noises Ξ_S are given by

$$\langle \Xi_S(\boldsymbol{r},t)\rangle = 0 \ , \tag{3.134}$$
$$\langle \Xi_S(\boldsymbol{r},t)\Xi_S(\boldsymbol{r}',t')\rangle = 2D_S k_B T\varepsilon_0(\varepsilon_w-1)\nabla^2\left(-\nabla^2+2a^{-2}\right)\delta(\boldsymbol{r}-\boldsymbol{r}')\delta(t-t') \ . \tag{3.135}$$

Inserting the Poisson equation 3.123 and introducing the ionic charge density $\rho_I = (ze)\left(\rho^+-\rho^-\right)$ and the ionic number density $c=\rho^++\rho^-$, we obtain two uncoupled sets of equations. The first set of equations couples the ionic and solvent charge densities,

$$\frac{\partial}{\partial t}\rho_I = D_I\nabla^2\rho_I - D_I\kappa_I^2\left(\rho_I+\rho_S^c\right)+\Xi_I(\boldsymbol{r},t) \ , \tag{3.136}$$
$$\frac{\partial}{\partial t}\rho_S^c = D_S\left[\varepsilon_w\left(\nabla^2\rho_S^c-2a^{-2}\rho_S^c\right)+(\varepsilon_w-1)\left(\nabla^2\rho_I-2a^{-2}\rho_I\right)\right] \ ,+\Xi_S(\boldsymbol{r},t) \tag{3.137}$$

where we denoted the vacuum Debye length κ_I^{-1} through $\kappa_I^2 = 2C_I(ze)^2/(\varepsilon_0 k_B T)$ and the relative permittivity of the dipolar solvent $\varepsilon_b = 1+p^2C_S/(3k_BT\varepsilon_0)$. We showed in the reference [AC22] that ε_b corresponds indeed to the zero-frequency permittivity of this dipolar fluid. The second set is the equation for the number ionic density,

$$\frac{\partial}{\partial t}c = D_I\nabla^2 c+\sqrt{4D_IC_I}\xi_c(\boldsymbol{r},t)) \ . \tag{3.138}$$

Based on the translational invariance, we apply a spatial Fourier transform to equations 3.136 and 3.137 and obtain the following matrix equation

$$\partial_t\begin{pmatrix}\tilde{\rho}_I(\boldsymbol{k},t)\\ \tilde{\rho}_S^c(\boldsymbol{k},t)\end{pmatrix} = -\begin{pmatrix}D_I(k^2+\kappa_I^2) & D_I\kappa_I^2\\ D_S(\varepsilon_b-1)\left(k^2+2a^{-2}\right) & D_S\varepsilon_b\left(k^2+2a^{-2}\right)\end{pmatrix}\begin{pmatrix}\tilde{\rho}_I(\boldsymbol{k},t)\\ \tilde{\rho}_S^c(\boldsymbol{k},t)\end{pmatrix}+\begin{pmatrix}\tilde{\Xi}_I(\boldsymbol{k},t)\\ \tilde{\Xi}_S(\boldsymbol{k},t)\end{pmatrix}, \tag{3.139}$$

where the correlations of the noises are

$$\left\langle\begin{pmatrix}\tilde{\Xi}_I(\boldsymbol{k},t)\tilde{\Xi}_I(\boldsymbol{k}',t') & \tilde{\Xi}_I(\boldsymbol{k},t)\tilde{\Xi}_S(\boldsymbol{k}',t')\\ \tilde{\Xi}_S(\boldsymbol{k},t)\tilde{\Xi}_I(\boldsymbol{k}',t') & \tilde{\Xi}_S(\boldsymbol{k},t)\tilde{\Xi}_S(\boldsymbol{k}',t')\end{pmatrix}\right\rangle =$$
$$2(2\pi)^3k_BTk^2\varepsilon_0\begin{pmatrix}D_I\kappa_I^2 & \\ & D_S(\varepsilon_b-1)(k^2+2a^{-2})\end{pmatrix}\delta(\boldsymbol{k}+\boldsymbol{k}')\delta(t-t') \ . \tag{3.140}$$

IV.C Link with the implicit solvent model

I want to finish this section by presenting the relation between the explicit solvent model and the implicit solvent model discussed in section III. The implicit solvent model corresponds to a solvent that relaxes faster than the ion dynamics — at least within a certain range of k. This can be expressed as $\partial_t\tilde{\rho}_S^c = 0$. When this is applied to equation 3.137, the result is

$$\tilde{\rho}_S^c = -\frac{\varepsilon_b-1}{\varepsilon_b}\tilde{\rho}_I+\frac{\tilde{\Xi}_S(\boldsymbol{k},t)}{D_S\varepsilon_b(k^2+2a^{-2})} \ . \tag{3.141}$$

We insert this result into equation 3.136 for $\tilde{\rho}_I$ and obtain

$$\begin{aligned}\partial_t\tilde{\rho}_I &= -D_I(k^2+\frac{\kappa_I^2}{\varepsilon_b})\tilde{\rho}_I - D_I\kappa_I^2\frac{\tilde{\Xi}_S(\boldsymbol{k},t)}{D_S\varepsilon_b(k^2+2a^{-2})} + \tilde{\Xi}_I(\boldsymbol{k},t)\\ &= -D_I(k^2+\kappa_{\text{imp}}^2)\tilde{\rho}_I + \tilde{\Xi}_I'(\boldsymbol{k},t)\ ,\end{aligned} \tag{3.142}$$

where we retrieve the implicit Debye length $\kappa_{\text{imp}}^2 = \kappa_I^2/\varepsilon_b$. The result is similar to the linearised Dean-Kawasaki equation 3.81 of the implicit model, but with a coloured noise $\tilde{\Xi}_I'(\boldsymbol{k},t)$ of variance,

$$\left\langle\tilde{\Xi}_I'(\boldsymbol{k},t)\right\rangle = 0\ , \tag{3.143}$$

$$\left\langle\tilde{\Xi}_I'(\boldsymbol{k},t)\tilde{\Xi}_I'(\boldsymbol{k}',t')\right\rangle = 2(2\pi)^3k_BT\varepsilon_0D_I\kappa_{\text{imp}}^2k^2\left(\varepsilon_b+\frac{D_I\kappa_{\text{imp}}^2(\varepsilon_b-1)}{D_S(k^2+2a^{-2})}\right)\delta(\boldsymbol{k}+\boldsymbol{k}')\delta(t-t')\ . \tag{3.144}$$

In particular, we can solved the Dean-Kawasaki linearised equation 3.142 as in subsection III.B. After performing a time Fourier transform, the ionic density reads

$$\tilde{\rho}_I(\boldsymbol{k},\omega) = \frac{\tilde{\Xi}_I'(\boldsymbol{k},\omega)}{-i\omega+D_Ik^2+D_I\kappa_{\text{imp}}^2}\ , \tag{3.145}$$

and the 2-point correlation function reads in frequency domain,

$$\langle\rho_I(\boldsymbol{k},\omega)\rho_I(\boldsymbol{k}',\omega')\rangle = \frac{2(2\pi)^4D_I\varepsilon_0\varepsilon_bk_BT\kappa_{\text{imp}}^2k^2}{\omega^2+D_I^2\left(k^2+\kappa_{\text{imp}}^2\right)^2}\left(1+\frac{D_I\kappa_{\text{imp}}^2(\varepsilon_b-1)}{D_S\varepsilon_b(k^2+2a^{-2})}\right)\delta(\boldsymbol{k}+\boldsymbol{k}')\delta(\omega+\omega')\ , \tag{3.146}$$

and in time domain,

$$\begin{aligned}\langle\rho_I(\boldsymbol{k},t)\rho_I(\boldsymbol{k}',t')\rangle &= \frac{2(2\pi)^3\varepsilon_0\varepsilon_bk_BT\kappa_{\text{imp}}^2k^2}{k^2+\kappa_{\text{imp}}^2}\left(1+\frac{D_I\kappa_{\text{imp}}^2(\varepsilon_b-1)}{D_S\varepsilon_b(k^2+2a^{-2})}\right)\\ &\quad\times\exp\left(-D_I\left(k^2+\kappa_{\text{imp}}^2\right)|t-t'|\right)\delta(\boldsymbol{k}+\boldsymbol{k}')\ ,\end{aligned} \tag{3.147}$$

$$\approx \frac{2(2\pi)^3\varepsilon_0\varepsilon_bk_BT\kappa_{\text{imp}}^2k^2}{k^2+\kappa_{\text{imp}}^2}\exp\left(-D_I\left(k^2+\kappa_{\text{imp}}^2\right)|t-t'|\right)\delta(\boldsymbol{k}+\boldsymbol{k}')\ . \tag{3.148}$$

We see that we retrieve the implicit solvent correlation (equation 3.90) in the limit of the fast solvent relaxation, $D_Sa^{-2} \gg D_I\kappa_{\text{imp}}^2(\varepsilon_b-1)/(2\varepsilon_b)$.

Having reviewed SDFT for electrolytes with implicit and dipolar solvents, I will now discuss my current work on including particle size in the SDFT framework.

V Project : SDFT for finite-size particles

In the study of solvation dynamics, the size of the solute —*i.e.*, the steric repulsion from its core— affects deeply the solvent density fluctuations. For instance, Chandler and his collaborators have demonstrated that the presence of a hard-core solute is sufficient to generate new timescales in the solvent fluctuations. [Song and Chandler, 1998, Song et al., 1996] Furthermore, the translational invariance of these fluctuations is broken in the solute frame, leading to correlations between their different modes.

In the following, I will propose two approaches to explicitly incorporate the solute radius into SDFT for an electrolyte with an implicit solvent. The aim is to calculate the 2-point correlation function in the presence of the solute, which can then be used to determine the time correlation of an observable A. To conclude this section, I will suggest a path integral formulation to include the solute size, as well as a a strategy to develop a SDFT consisting of finite-size particles (solute and solvent).

V.A Cut-off approach

The first strategy to take into account the size of the tracer ion is to "cut-off" the integral 3.6. If A depends only of the ionic density, this reads

$$A(t) = \int_\sigma^\infty \mathrm{d}r a^{lm}(r)\rho_I^{lm}(r,t)\theta(r-\sigma) \tag{3.149}$$

$$= \int_\sigma^\infty \mathrm{d}r a_\sigma^{lm}(r)\rho_I^{lm}(r,t) \tag{3.150}$$

$$= \int \mathrm{d}k \tilde{a}_\sigma^{lm}(k)\tilde{\rho_I}^{lm}(k,t)\ , \tag{3.151}$$

where I introduced an effective local contribution $a_\sigma^{lm}(r) = a^{lm}(r)\theta(r-\sigma)$ and its Hankel transform $\tilde{a}_\sigma^{lm}(k)$. The autocorrelation of A reads

$$C_A(t) = \int_\sigma^\infty \mathrm{d}r \int_\sigma^\infty \mathrm{d}r' r^2 r'^2 a_\sigma^{lm}(r) a_\sigma^{lm}(r') C_I^{lm}(r,r',t) \tag{3.152}$$

$$= \int \mathrm{d}k \int \mathrm{d}k' \tilde{a}_\sigma^{lm}(k) k^2 k'^2 \tilde{a}_\sigma^{lm}(k') \tilde{C}_I^{lm}(k,k',t)\ , \tag{3.153}$$

where

$$C_I^{lm}(r,r',t) = \left\langle \rho_I^{lm}(r,t)\rho_I^{lm}(r',0)\right\rangle_1\ , \tag{3.154}$$

$$\tilde{C}_I^{lm}(k,k',t) = \left\langle \tilde{\rho}_I^{lm}(k,t)\tilde{\rho}_I^{lm}(k',0)\right\rangle_1\ . \tag{3.155}$$

I will now propose 3 approximations for the solvent density correlations C_I^{lm}.

V.A.1 Uniform approximation

Often used in the literature, [Perng and Ladanyi, 1998] the uniform approximation assumes that

$$\tilde{C}_I(\boldsymbol{k}, t, \boldsymbol{k}', t') \approx \tilde{C}_{u,I}(\boldsymbol{k}, t, \boldsymbol{k}', t') \ , \tag{3.156}$$

i.e., that the solvent fluctuations around the tracer ion are identical to the bulk one $\tilde{C}_{u,I}$. For instance, we could use the result of the linearised SDFT for electrolytes in an implicit solvent (equation 3.90) and write the autocorrelation of A as

$$C_A(t) = \boxed{2(2\pi)^3 C_I(ze)^2 \int \mathrm{d}k |\tilde{a}_\sigma^{lm}(k)|^2 \frac{k^4}{k^2 + \kappa_{\mathrm{imp}}^2} \exp\left(-D_I \left(k^2 + \kappa_{\mathrm{imp}}^2\right) t\right)} \ . \tag{3.157}$$

For a given observable A, the calculation could be performed if we know the so-called effective vertex function $|\tilde{a}_\sigma^{lm}(k)|^2$. Of course, the uniform approximation is very crude, as it assumes the translational invariance of the correlations, which decouples the different k-mode.

V.A.2 Linearised SDFT

Instead of approximating the density correlation with its bulk value, we can calculate it using SDFT. In presence of the tracer ion, the Dean-Kawasaki equations for the electrolytes are equivalent as before,

$$\frac{\partial}{\partial t}\rho^+ = D_I \nabla^2 \rho^+ + \frac{D_I}{k_B T} ze \nabla \cdot (\rho^+ \nabla \varphi) + \nabla \cdot (\sqrt{2 D_I \rho^+} \boldsymbol{\xi}^+(\boldsymbol{r}, t)) \ , \tag{3.158}$$

$$\frac{\partial}{\partial t}\rho^- = D_I \nabla^2 \rho^- - \frac{D_I}{k_B T} ze \nabla \cdot (\rho^- \nabla \varphi) + \nabla \cdot (\sqrt{2 D_I \rho^-} \boldsymbol{\xi}^-(\boldsymbol{r}, t)) \ , \tag{3.159}$$

where the noises $\boldsymbol{\xi}^+$ and $\boldsymbol{\xi}^-$ are Gaussian white noise vector fields. The cation density are now defined with one cation left out,

$$\rho^+(\boldsymbol{r}, t) = \sum_{\alpha=2}^{N} \delta(\boldsymbol{r} - \boldsymbol{r}_\alpha^+(t)) \ . \tag{3.160}$$

The Poisson equation now reads

$$\varphi(\boldsymbol{r}, t) = \int \mathrm{d}\boldsymbol{r}' \ \mathcal{G}(\boldsymbol{r} - \boldsymbol{r}') ze \left[\rho^+(\boldsymbol{r}, t) - \rho^-(\boldsymbol{r}, t) + Q\delta(\boldsymbol{r})\right] , \tag{3.161}$$

where Q is the size of the tracer ion, which are assumed to stay immobile at the origin, $\boldsymbol{R}(t) = 0$. We then linearise the Dean-Kawasaki equations and write them for the variable $\rho_I = (ze)(\rho^+ - \rho^-)$ and $\mathcal{C} = \rho^+ + \rho^-$,

$$\frac{\partial}{\partial t}\rho_I(\boldsymbol{r},t) = D_I\nabla^2\rho_I - D_I\kappa_{\text{imp}}^2\left(\rho_I + Q\delta(\boldsymbol{r})\right) + (ze)\sqrt{4D_IC_I}\Xi_{\rho_I}(\boldsymbol{r},t), \tag{3.162}$$

$$\frac{\partial}{\partial t}c(\boldsymbol{r},t) = D_I\nabla^2 c + \sqrt{4D_IC_I}\Xi_c(\boldsymbol{r},t), \tag{3.163}$$

where the noises Ξ_{ρ_I} and Ξ_c have a statistics given by equation 3.83. Taking the spatial Fourier transform gives for ρ_I:

$$\frac{\partial}{\partial t}\tilde{\rho}_I(\boldsymbol{k},t) = -D_Ik^2\rho_I - D_I\kappa_{\text{imp}}^2\left(\tilde{\rho}_I + Q\right) + (ze)\sqrt{4D_IC_I}\tilde{\Xi}_{\rho_I}(\boldsymbol{k},t)\ . \tag{3.164}$$

where $\left\langle\tilde{\Xi}_{\rho_I}(\boldsymbol{k},t)\tilde{\Xi}_{\rho_I}(\boldsymbol{k}',t')\right\rangle = (2\pi)^3k^2\delta(\boldsymbol{k}+\boldsymbol{k}')\delta(t-t')$. After projecting onto the 'lm' spherical harmonic, we get

$$\frac{\partial}{\partial t}\tilde{\rho}_I^{lm}(k,t) = -D_I(k^2+\kappa_{\text{imp}}^2)\tilde{\rho}_I^{lm}(k,t) + ze\sqrt{4D_IC_I}\underbrace{\int_0^{\pi}\mathrm{d}\theta\ \sin\theta\int_0^{2\pi}\mathrm{d}\varphi\ Y_{lm}(\theta,\varphi)\tilde{\Xi}_{\rho_I}(\boldsymbol{k},t)}_{\equiv\tilde{\Xi}_I^{lm}(k,t)}\ , \tag{3.165}$$

where the correlation of $\tilde{\Xi}_I^{lm}(k,t)$ is derived in annex I.B and reads:

$$\langle\tilde{\Xi}_I^{lm}(k,t)\tilde{\Xi}_I^{lm}(k',t')\rangle = (2\pi)^3\delta(t-t')\delta(k-k'). \tag{3.166}$$

Solving equation 3.165 in frequency domain yields

$$\tilde{\rho}_I^{lm}(k,\omega) = ze\sqrt{4D_IC_I}\frac{\tilde{\Xi}_I^{lm}(k,\omega)}{-\mathrm{i}\omega + D_I\left(k^2+\kappa_{\text{imp}}^2\right)}\ . \tag{3.167}$$

where $\langle\tilde{\Xi}_I^{lm}(k,\omega)\tilde{\Xi}_I^{lm}(k',\omega')\rangle = (2\pi)^4\delta(\omega+\omega')\delta(k-k')$ The density-density correlations are deduced straightforwardly

$$C_I^{lm}(k,k',\omega,\omega') = \frac{(2\pi)^4(ze)^2 4D_IC_I}{\omega^2 + D_I^2\left(k^2+\kappa_{\text{imp}}^2\right)^2}\delta(k-k')\delta(\omega+\omega')\ , \tag{3.168}$$

and in time domain,

$$C_I^{lm}(k,k',t,t') = \frac{2(2\pi)^3C_I(ze)^2}{k^2+\kappa_{\text{imp}}^2}\mathrm{e}^{-D_I(k^2+\kappa_{\text{imp}}^2)|t-t'|}\delta(k-k')\ . \tag{3.169}$$

Finally, the autocorrelation function of A reads

$$C_A(t) = \boxed{2(2\pi)^3C_I(ze)^2\int\mathrm{d}k|\tilde{a}_\sigma^{lm}(k)|^2\frac{k^4}{k^2+\kappa_{\text{imp}}^2}\exp\left(-D_I\left(k^2+\kappa_{\text{imp}}^2\right)t\right)}\ . \tag{3.170}$$

We obtain the same result as the uniform approximation (equation 3.157)! This probably stems from the linearised approximation of the Dean-Kawasaki equations which removes the interaction between the electrolyte and the tracer ion. Moreover, both approaches include the size of the tracer in an *ad-hoc* manner through the effective vertex function $|\tilde{a}_\sigma^{lm}(k)|^2$, which neglects the actual coupling between the solvent modes induced by the exclusion core of the solute. As a consequence of these approximations, we see that only the timescale of the bulk, $1/(D_I(k^2+\kappa_{\text{imp}}^2))$, appears in the expression of the autocorrelation of A. I will now present a more rigorous derivation, based on the boundary conditions at the interface between the solute and the electrolyte.

V.B Boundary conditions approach

The second strategy is to solve the dynamical equations with a "no-flow" boundary condition, which prevents the density to flow into the vicinity of the tracer ion. As the density remains null inside the core of the tracer ion along the dynamics, we do need to explicitly include its radius in the formulation of A and of the time autocorrelation function. However, the no-flow boundary condition will impose the use of a specific Green operator.

V.B.1 Dean-Kawasaki equations and the boundary conditions

The Dean-Kawasaki equations are given by equations 3.158 and 3.159, but are completed by the following boundary conditions,

$$\lim_{r\to\infty}\rho^+(\boldsymbol{r},t)=\lim_{r\to\infty}\rho^-(\boldsymbol{r},t)=C_I\;, \tag{3.171}$$

$$J_+^r(r=\sigma)=\left(D_I\nabla\rho^+ + \beta D_I(ze)\rho^+\nabla\varphi\right)\cdot\hat{\boldsymbol{e}}_r|_{r=\sigma}=0\;, \tag{3.172}$$

$$J_-^r(r=\sigma)=\left(D_I\nabla\rho^- - \beta D_I(ze)\rho^-\nabla\varphi\right)\cdot\hat{\boldsymbol{e}}_r|_{r=\sigma}=0\;, \tag{3.173}$$

where the radial flux for the cations J_r^+ and for the anions J_r^- are both null at the interface with the tracer ion.

V.B.2 Linearisation

We then determine the linearised Dean-Kawasaki equations with the boundary conditions. As in subsection III.B, we define $\rho^\pm = C_I \pm \delta\rho^\pm$ and get for the boundary conditions

$$\lim_{r\to\infty}\delta\rho^+(\boldsymbol{r},t)=\lim_{r\to\infty}\delta\rho^-(\boldsymbol{r},t)=0\;, \tag{3.174}$$

$$\left(\nabla\delta\rho^+ + \beta ze\rho^-\nabla\varphi\right)\cdot\hat{\boldsymbol{e}}_r|_{r=\sigma}=0\;, \tag{3.175}$$

$$\left(\nabla\delta\rho^- - \beta ze\rho^-\nabla\varphi\right)\cdot\hat{\boldsymbol{e}}_r|_{r=\sigma}=0\;. \tag{3.176}$$

Assuming that the electrostatic potential is of order 1, $\varphi=\mathcal{O}(\delta\rho^\pm)$, one gets

$$\lim_{r\to\infty}\delta\rho^+(\boldsymbol{r},t)=\lim_{r\to\infty}\delta\rho^-(\boldsymbol{r},t)=0\;, \tag{3.177}$$

$$\partial_r(\delta\rho^+ + \beta ze\rho^+\varphi)|_{r=\sigma}=0\;, \tag{3.178}$$

$$\partial_r(\delta\rho^- - \beta ze\rho^-\varphi)|_{r=\sigma}=0\;. \tag{3.179}$$

$$\tag{3.180}$$

With the variable, $\rho_I = (ze)(\rho^+ - \rho^-) = (ze)(\delta\rho^+ - \delta\rho^-)$ and $c = \delta\rho^+ + \delta\rho^-$, we obtain

$$\lim_{r\to\infty} c(\boldsymbol{r},t) = \lim_{r\to\infty} \rho_I(\boldsymbol{r},t) = 0 \ , \tag{3.181}$$

$$\partial_r(\rho_I + 2\beta C_I(ze)\varphi)|_{r=\sigma} = 0 \ , \tag{3.182}$$

$$\partial_r c|_{r=\sigma} = 0 \ . \tag{3.183}$$

Finally, because of the application of the Gauss theorem at the interface of the tracer ion ($r = \sigma$),

$$\oint_{r=\sigma} \mathbf{E}(\sigma)\cdot \mathrm{d}\mathbf{S} = \int_{S^2} E_r(\sigma)\mathrm{d}\Omega = Q \ , \tag{3.184}$$

which means $E_r^{lm}(\sigma) = 0$ for $lm \neq 00$. This gives $\partial_r\varphi|_{r=\sigma} = 0$ and the boundary conditions for ρ_I read

$$\partial_r\rho_I|_{r=\sigma} = 0 \ . \tag{3.185}$$

V.B.3 Formal expression with the Green function

The ionic density can be formally obtain as

$$\rho_I(\boldsymbol{r},t) = \sqrt{4D_IC_I}(ze)\int \mathrm{d}\boldsymbol{r}' \int_0^T \mathrm{d}t' G_{\rho_I}(\boldsymbol{r},\boldsymbol{r}',t,t')\Xi_{\rho_I}(\boldsymbol{r}',t') \ , \tag{3.186}$$

where the Green operator G satisfies the following equation and boundary conditions,

$$\frac{\partial}{\partial t}G_{\rho_I} - D_I\nabla^2 G_{\rho_I} + D_I\kappa_{\mathrm{imp}}^2 G_{\rho_I} = \delta(\boldsymbol{r}-\boldsymbol{r}')\delta(t-t') \ , \tag{3.187}$$

$$\partial_r G_{\rho_I}|_{r=\sigma} = 0 \ . \tag{3.188}$$

We are in particular interested in the lm projection of the density, which is related to the Green operator *via*

$$\rho_I^{lm}(r,t) = \sqrt{4D_IC_I}(ze)\int_\sigma^\infty \mathrm{d}r' \int \mathrm{d}t' r'^2 G_{\rho_I}^l(r,r',t-t')\Xi_{\rho_I}^{lm}(r',t') \ , \tag{3.189}$$

where $G_{\rho_I}^l$ and $\Xi_{\rho_I}^{lm}$ are the components of the spherical harmonics expansions,

$$G_{\rho_I}(\boldsymbol{r},\boldsymbol{r}',t-t') = \sum_{lm} \tilde{G}_{\rho_I}^l(r,r',t-t')Y_{lm}(\Omega)Y_{lm}(\Omega') \ , \tag{3.190}$$

$$\Xi_{\rho_I}(\boldsymbol{r},t)) = \sum_{lm} \Xi_{\rho_I}^{lm}(r,t)Y_{lm}(\Omega) \ , \tag{3.191}$$

respectively. The correlation of the noises are

$$\left\langle \Xi_{\rho_I}^{lm}(r,t)\Xi_{\rho_I}^{l'm'}(r',t')\right\rangle = l(l+1)\delta_{ll'}\delta_{mm'}\delta(t-t')\frac{\delta(r-r')}{r^4}\ , \tag{3.192}$$

which leads to the formal expression of the density correlations in terms of the Green function.

$$\tilde{C}_I^{lm}(r,t,r',t') = 4D_I C_I(ze)^2 l(l+1)\int_\sigma^\infty \mathrm{d}r''\int \mathrm{d}t''\tilde{G}_{\rho_I}^l(r,r'',t-t'')\tilde{G}_{\rho_I}^l(r'',r',t''-t')\ . \tag{3.193}$$

V.B.4 Solution at $\omega = 0$

We present in the annex II.B the resolution of the Green equation at frequency $\omega = 0$. The Green operator reads

$$\begin{aligned}\tilde{G}_{\rho_I}^l(r,r',\omega=0) &= \tilde{G}_{\rho_I}^{l<}(r,r',\omega=0)\\ &= \frac{2\kappa_{\mathrm{imp}}}{\pi D_I}\left(i_l(\kappa_{\mathrm{imp}}r) - \frac{i_l'(\kappa_{\mathrm{imp}}\sigma)}{k_l'(\kappa_{\mathrm{imp}}\sigma)}k_l(\kappa_{\mathrm{imp}}r)\right)k_l(\kappa_{\mathrm{imp}}r') \text{ for } \sigma \le r < r' \end{aligned} \tag{3.194}$$

$$\begin{aligned}&= \tilde{G}_{\rho_I}^{l>}(r,r',\omega=0)\\ &= \frac{2\kappa_{\mathrm{imp}}}{\pi D_I}\left(i_l(\kappa_{\mathrm{imp}}r') - \frac{i_l'(\kappa_{\mathrm{imp}}\sigma)}{k_l'(\kappa_{\mathrm{imp}}\sigma)}k_l(\kappa_{\mathrm{imp}}r')\right)k_l(\kappa_{\mathrm{imp}}r) \text{ for } r' < r\ . \end{aligned} \tag{3.195}$$

We will denote $G_{\rho_I}^l(r,r',\omega=0) = \frac{2\kappa_{\mathrm{imp}}}{\pi D_I}f^l(\kappa_{\mathrm{imp}}r,\kappa_{\mathrm{imp}}r',\kappa_{\mathrm{imp}}\sigma)$ and express the density correlation function as

$$\begin{aligned}\tilde{C}_I^{lm}(r,r',\omega=0) = 4D_I C_I(ze)^2 l(l+1)\frac{4\kappa_{\mathrm{imp}}^2}{\pi^2 D_I^2}\times\\ \int_\sigma^\infty \mathrm{d}r'' f^l(\kappa_{\mathrm{imp}}r,\kappa_{\mathrm{imp}}r'',\kappa_{\mathrm{imp}}\sigma)f^l(\kappa_{\mathrm{imp}}r'',\kappa_{\mathrm{imp}}r',\kappa_{\mathrm{imp}}\sigma)\ ,\end{aligned} \tag{3.196}$$

and the autocorrelation at zero-frequency as

$$\begin{aligned}\tilde{C}_A(\omega=0) = \frac{8\kappa_{\mathrm{imp}}^4 k_B T\varepsilon_0\varepsilon_w}{D_I\pi^2}\times\\ \int_\sigma^\infty \mathrm{d}r\int_\sigma^\infty \mathrm{d}r'\int_\sigma^\infty \mathrm{d}r'' f^l(\kappa_{\mathrm{imp}}r,\kappa_{\mathrm{imp}}r'',\kappa_{\mathrm{imp}}\sigma)f^l(\kappa_{\mathrm{imp}}r'',\kappa_{\mathrm{imp}}r',\kappa_{\mathrm{imp}}\sigma)a^{lm}(r)a^{lm}(r')\ .\end{aligned} \tag{3.197}$$

The next steps of the calculation depend on the local contribution a. I will propose in section VI an application where A is the EFG experienced by the tracer ion.

V.C Path integral approach

The size of the particles could also be taken into account in the path integral formalism presented in subsection II.B. It is clear that the solvent densities cannot have a non-zero value inside the core of the solute,

$$\mathcal{P}\left[\rho\right] = 0 \text{ if } \exists\, r < \sigma, \rho(\boldsymbol{r}) \neq 0 \ . \tag{3.198}$$

Of course, this constraint is exactly fulfilled if we consider the exact path integral presented in equation 3.37. In practice, the path integration is performed using approximations, such as the mean-field approach II.C or the Gaussian approximation. [Chandler, 1993, Song et al., 1996, Song and Chandler, 1998] Twenty years ago, Chandler and his collaborators proposed performing the path integration by explicitly excluding the solvent densities present in the core of the solute. They only considered a Gaussian field model, but demonstrated that the 2-point correlation function in the presence of the solute differs from that in the bulk (as assumed in the uniform approximation). More recently, Speck applied this theory to the velocity field around a solute particle and showed that it reproduces the overdamped Langevin equation. [Speck, 2013] In what follows, I will first recall the results of Chandler *et al.* in my notation, before exploring how to combine their ideas with the mean-field SDFT.

V.C.1 Gaussian field model

Chandler and his collaborators assumed that the probability to observe a given solvent density is given by

$$\mathcal{P}\left[\rho\right] = \exp\left(-\mathcal{S}_g\left[\rho\right]\right) \ , \tag{3.199}$$

where the action is quadratic in the density,

$$\mathcal{S}_g\left[\rho\right] = \int_0^T \mathrm{d}t \int \mathrm{d}\boldsymbol{r} \int_0^T \mathrm{d}t' \int \mathrm{d}\boldsymbol{r}' \rho_I(\boldsymbol{r},t) C_b^{-1}(\boldsymbol{r},t,\boldsymbol{r}',t') \rho(\boldsymbol{r}',t') + \beta \int \mathrm{d}\boldsymbol{r} v_{\mathrm{ext}}(\boldsymbol{r}) \rho(\boldsymbol{r},t) \ , \tag{3.200}$$

and where v_{ext} is the interaction potential between the solute and the solvent, while the tensor $C_b^{-1}(\boldsymbol{r},t,\boldsymbol{r}',t')$ denotes the inverse of the bulk correlation functions,

$$\int_0^T \mathrm{d}t'' \int \mathrm{d}\boldsymbol{r}'' C_b^{-1}(\boldsymbol{r},\boldsymbol{r}'',t,t'') C_b(\boldsymbol{r}'',\boldsymbol{r}',t'',t) = \delta(\boldsymbol{r}-\boldsymbol{r}')\delta(t-t') \ . \tag{3.201}$$

The generative cumulant function read in our notation

$$\mu\left[\lambda\right] = \ln \frac{\int \mathcal{D}\rho_I \delta_\sigma\left[\rho\right] \exp\left(-\mathcal{S}_g\left[\rho\right]\right) + \int_0^T \mathrm{d}t \int \mathrm{d}\boldsymbol{r} \lambda(\boldsymbol{r},t)\rho(\boldsymbol{r},t)}{\int \mathcal{D}\rho \delta_\sigma\left[\rho\right] \exp\left(-\mathcal{S}_g\left[\rho\right]\right)} \ , \tag{3.202}$$

where the Dirac functional $\delta_\sigma[\rho_I]$ if $\rho_I(\boldsymbol{r}) \neq 0$ for $r < \sigma$. After inserting the Fourier-like expression of the Dirac functional 3.29 and performing the Gaussian path integral, they found the correlation

$$C(\boldsymbol{r},\boldsymbol{r}',t-t') = C_b(\boldsymbol{r},\boldsymbol{r}',t) - \int_0^T \mathrm{d}t'' \int \mathrm{d}\boldsymbol{r}'' \int_0^T \mathrm{d}t''' \int \mathrm{d}\boldsymbol{r}''' C_b(\boldsymbol{r},\boldsymbol{r}'',t-t'') C_{\mathrm{in}}^{-1}(\boldsymbol{r}'',\boldsymbol{r}''',t''-t''') C_b(\boldsymbol{r}''',\boldsymbol{r}',t'''-t') \,, \tag{3.203}$$

where C_{in}^{-1} denotes the functional inverse of

$$\begin{aligned} C_{\mathrm{in}}(\boldsymbol{r},\boldsymbol{r}',t) &= C_b(\boldsymbol{r},\boldsymbol{r}',t) \text{ for } r, r' < \sigma \text{ and} \\ &= 0 \text{ otherwise.} \end{aligned} \tag{3.204}$$

The 2-point correlation function, C (equation 3.203), is thus different from the bulk function, $C_b(\boldsymbol{r},\boldsymbol{r}',t)$, and is directly affected by the presence of the solute. In particular, C will not exhibit the translational invariance of C_b, and the rotational invariance will depend on the solute structure. We note however that the solute/solvent interaction v_{ext} does not contribute to C, as would be expected in a Gaussian field model with a quadratic action 3.200. Determining C through equation 3.203 is complicated as it involves taking the functional inverse of C_{in}. Next, I will outline the initial steps to derive C with the complete Dean-Kawasaki action, but in the mean-field limit.

V.C.2 Mean field for solvation

Instead of the Gaussian action 3.200, we could use the exact Dean-Kawasaki action 3.38 (or equation 3.94 for the electrolyte) and try to determine the 2-point correlation function of the solvent in presence of the solute. Assuming that the solute is a hard sphere with a radius σ, its only effect is to exclude the solvent density from its core. We will express the cumulant generative function 3.39, but restrict the path integral to the solvent densities with no values inside the solute core. It reads

$$\mu[\lambda] = \ln\left(\frac{\int \mathcal{D}\rho \int \mathcal{D}\hat{\rho}\delta_\sigma[\rho]\exp\left(-\mathcal{S}_\lambda[\rho,\hat{\rho}]\right)}{\int \mathcal{D}\rho \int \mathcal{D}\hat{\rho}\delta_\sigma[\rho]\exp\left(-\mathcal{S}[\rho,\hat{\rho}]\right)}\right) \,, \tag{3.205}$$

$$= \ln\left(\frac{\int \mathcal{D}\rho \int \mathcal{D}\hat{\rho} \int \mathcal{D}\psi \exp\left(-\mathcal{S}_\lambda[\rho,\hat{\rho}] - \int_0^T \mathrm{d}t \int_{r<\sigma} \mathrm{d}\boldsymbol{r}\psi(\boldsymbol{r})\rho(\boldsymbol{r},t)\right)}{\int \mathcal{D}\rho \int \mathcal{D}\hat{\rho} \int \mathcal{D}\psi \exp\left(-\mathcal{S}[\rho,\hat{\rho}] - \int_0^T \mathrm{d}t \int_{r<\sigma} \mathrm{d}\boldsymbol{r}\psi(\boldsymbol{r})\rho(\boldsymbol{r},t)\right)}\right) \,, \tag{3.206}$$

where we used the tilted action 3.42 and the the Fourier-like expression of the Dirac functional 3.29. In the mean-field limit, we should find the path (q,p,x) that minimises the action $\mathcal{S}'_\lambda[\rho,\hat{\rho},\psi] = \mathcal{S}_\lambda[\rho,\hat{\rho}] + \int_0^T \mathrm{d}t \int_{r<\sigma} \mathrm{d}\boldsymbol{r}\psi(\boldsymbol{r})\rho(\boldsymbol{r},t)$. We study the small variations around this path

$$\rho(\boldsymbol{r},t) = q(\boldsymbol{r},t) + \delta\rho(\boldsymbol{r},t) \ , \tag{3.207}$$
$$\hat{\rho}(\boldsymbol{r},t) = p(\boldsymbol{r},t) + \delta\hat{\rho}(\boldsymbol{r},t) \ , \tag{3.208}$$
$$\psi(\boldsymbol{r},t) = x(\boldsymbol{r},t) + \delta\psi(\boldsymbol{r},t) \ . \tag{3.209}$$

Defining $\delta\mathcal{S} \equiv \mathcal{S}_\lambda(\rho,\hat{\rho}) - \mathcal{S}_\lambda(q,p)$, we look for the conditions $\delta\mathcal{S} = 0$ at leading order in $(\delta\rho, \delta\hat{\rho}, \delta\psi)$. We find that the path (q,p,x) should satisfy

$$\frac{\partial}{\partial t}q = \frac{D}{k_BT}\nabla\cdot\left[q(\boldsymbol{r},t)\nabla\frac{\delta F[q]}{\delta q(\boldsymbol{r},t)}\right] - 2D\nabla\cdot(q\nabla p) \ , \tag{3.210}$$
$$\frac{\partial}{\partial t}p = -\frac{D}{k_BT}\frac{\delta}{\delta q}\nabla\cdot\left[q(\boldsymbol{r},t)\nabla\frac{\delta F'[q]}{\delta q(\boldsymbol{r},t)}\right] - \lambda + x \ , \tag{3.211}$$
$$q(\boldsymbol{r},t) = 0 \text{ for } r < \sigma \ . \tag{3.212}$$

After performing the λ-expansion, the mean-field equation at order 0 is

$$\frac{\partial}{\partial t}q_0 = D\nabla^2 q_0 - 2D\nabla\cdot(q_0\nabla p_0) + \frac{D}{k_BT}\nabla\cdot\left(q_0\left(\int \mathrm{d}\boldsymbol{r}' q_0(\boldsymbol{r}')\nabla v(\boldsymbol{r}-\boldsymbol{r}')\right)\right) \ , \tag{3.213}$$
$$\frac{\partial}{\partial t}p_0 = -D\nabla^2 p_0 - D|\nabla p_0|^2 + \frac{D}{k_BT}(\nabla p_0)\cdot\left(\int \mathrm{d}\boldsymbol{r}' q_0(\boldsymbol{r}')\nabla v(\boldsymbol{r}-\boldsymbol{r}')\right) - \frac{D}{k_BT}\left(\int \mathrm{d}\boldsymbol{r}' q_0(\boldsymbol{r}')\nabla p_0(\boldsymbol{r}')\cdot\nabla v(\boldsymbol{r}-\boldsymbol{r}')\right) + x_0 \ , \tag{3.214}$$
$$q_0(\boldsymbol{r},t) = 0 \text{ for } r < \sigma \ . \tag{3.215}$$

Unlike to subsection II.C, the presence of the hard-sphere solute prevents fluctuations from being considered around the uniform state ($q_0 = \rho_0$). I should therefore solve the equation at order 0 before to obtain the order 1 (which will give me the 2-point correlation). The following steps would probably involve assuming a perfect gas ($v = 0$) and performing the Cole-Hopf transformation (($P_0 \equiv \mathrm{e}^{p_0}$; $Q_0 \equiv q_0\mathrm{e}^{-p_0}$). In this case, the equations at order 0 are

$$\frac{\partial}{\partial t}Q_0 = D\nabla^2 Q_0 - x_0 Q_0 \ , \tag{3.216}$$
$$\frac{\partial}{\partial t}P_0 = -D\nabla^2 P_0 + x_0 P_0 \tag{3.217}$$
$$Q_0(\boldsymbol{r},t) = 0 \text{ for } r < \sigma \ ., \tag{3.218}$$

which seem soluble. The next step would be to insert the results at order 0 into the equations at order 1 to determine the 2-point correlation function.

V.C.3 Mean field for pairs of particles

Finally, I want to sketch another idea to explicitly incorporating the size of all the particles into the SDFT framework (not only the solute). This idea is still based on Chandler's

approach, [Chandler, 1993] but is now applied to all pairs of particles. In the path integral expression of the cumulant generative function, equation 3.39, only density fields without particles overlapping should contribute. These "correct" density fields must satisfy the conditions,

$$\rho(\boldsymbol{r}_i(t)+\boldsymbol{r},t)=\delta(\boldsymbol{r}) \text{ for all } \boldsymbol{r}\in V_{\mathrm{HC}}, \text{ for all } i\in\{1,\dots,N\} \text{ and for all } t\in[0,T]\ . \quad (3.219)$$

Using the relation $\rho(\boldsymbol{r}_i(t)+\boldsymbol{r},t)=\int \mathrm{d}\boldsymbol{r}'\delta(\boldsymbol{r}'-\boldsymbol{r}_i(t))\rho(\boldsymbol{r}'+\boldsymbol{r},t)$ and summing over all the particles, we obtain the following functional constraint on the density: $\Gamma[\rho]=0$, where

$$\Gamma[\rho]=\int \mathrm{d}\boldsymbol{r}'\rho(\boldsymbol{r}',t)\rho(\boldsymbol{r}'+\boldsymbol{r},t)-N\delta(\boldsymbol{r}) \text{ for all } \boldsymbol{r}\in V_{\mathrm{HC}}\ . \quad (3.220)$$

We can explicitly incorporate this constraint into equation 3.39 and transform it using the Dirac functional Fourier-like formulation 3.29,

$$\mu[\lambda]=\ln\left(\frac{\int\mathcal{D}\rho\int\mathcal{D}\hat{\rho}\delta[\Gamma]\exp\left(-\mathcal{S}_\lambda[\rho,\hat{\rho}]\right)}{\int\mathcal{D}\rho\int\mathcal{D}\hat{\rho}\delta[\Gamma]\exp\left(-\mathcal{S}[\rho,\hat{\rho}]\right)}\right)\ , \quad (3.221)$$

$$=\ln\left(\frac{\int\mathcal{D}\rho\int\mathcal{D}\hat{\rho}\int\mathcal{D}\psi\exp\left(-\mathcal{S}'_\lambda[\rho,\hat{\rho}]\right)}{\int\mathcal{D}\rho\int\mathcal{D}\hat{\rho}\int\mathcal{D}\psi\exp\left(-\mathcal{S}'[\rho,\hat{\rho}]\right)}\right)\ , \quad (3.222)$$

with the following tilted action:

$$\mathcal{S}'_\lambda[\rho,\hat{\rho},\psi]=\mathcal{S}_\lambda[\rho,\hat{\rho}]+\int_0^T\mathrm{d}t\int_{\boldsymbol{r}\in V_{\mathrm{HC}}}\mathrm{d}\boldsymbol{r}\ \psi(\boldsymbol{r},t)\left[\int\mathrm{d}\boldsymbol{r}'\rho(\boldsymbol{r}',t)\rho(\boldsymbol{r}'+\boldsymbol{r},t)-N\delta(\boldsymbol{r})\right]\ . \quad (3.223)$$

Following the same mean-field strategy as in subsection II.C and subsection V.C.2, we now postulate that the integral over ρ, $\hat{\rho}$ and ψ is dominated by the path that minimises the action 3.223. We denote this path as (q,p,x), and study small variations around it:

$$\rho(\boldsymbol{r},t)=q(\boldsymbol{r},t)+\delta\rho(\boldsymbol{r},t)\ , \quad (3.224)$$

$$\hat{\rho}(\boldsymbol{r},t)=p(\boldsymbol{r},t)+\delta\hat{\rho}(\boldsymbol{r},t)\ , \quad (3.225)$$

$$\psi(\boldsymbol{r},t)=x(\boldsymbol{r},t)+\delta\psi(\boldsymbol{r},t)\ . \quad (3.226)$$

Defining $\delta\mathcal{S}\equiv\mathcal{S}(\rho,\hat{\rho})-\mathcal{S}(q,p)$, we find, at leading order in $\delta\rho$, $\delta\hat{\rho}$ and $\delta\psi$:

$$\begin{aligned}\delta\mathcal{S}'=\delta\mathcal{S}&+\int_0^T\mathrm{d}t\int_{\boldsymbol{r}\in V_{\mathrm{HC}}}\mathrm{d}\boldsymbol{r}\ \delta\psi(\boldsymbol{r},t)\left[\int\mathrm{d}\boldsymbol{r}'q(\boldsymbol{r}',t)q(\boldsymbol{r}'+\boldsymbol{r},t)-N\delta(\boldsymbol{r})\right]\\&+\int_0^T\mathrm{d}t\int_{\boldsymbol{r}\in V_{\mathrm{HC}}}\mathrm{d}\boldsymbol{r}\ x(\boldsymbol{r},t)\int\mathrm{d}\boldsymbol{r}'q(\boldsymbol{r}',t)\delta\rho(\boldsymbol{r}'+\boldsymbol{r},t)\\&+\int_0^T\mathrm{d}t\int_{\boldsymbol{r}\in V_{\mathrm{HC}}}\mathrm{d}\boldsymbol{r}\ x(\boldsymbol{r},t)\int\mathrm{d}\boldsymbol{r}'\delta\rho(\boldsymbol{r}',t)q(\boldsymbol{r}'+\boldsymbol{r},t)\ . \quad (3.227)\end{aligned}$$

The condition $\delta\mathcal{S}' = 0$ gives the differential equations that follow the path of least action,

$$\frac{\partial}{\partial t}q = D\nabla^2 q - 2D\nabla\cdot(q\nabla p) + \frac{D}{k_BT}\nabla\cdot\left(q\left(\int \mathrm{d}\boldsymbol{r}' q(\boldsymbol{r}')\nabla v(\boldsymbol{r}-\boldsymbol{r}')\right)\right) , \tag{3.228}$$

$$\begin{aligned}\frac{\partial}{\partial t}p = &-D\nabla^2 p - D|\nabla p|^2 + \frac{D}{k_BT}(\nabla p)\cdot\left(\int \mathrm{d}\boldsymbol{r}' q(\boldsymbol{r}')\nabla v(\boldsymbol{r}-\boldsymbol{r}')\right)\\ &- \frac{D}{k_BT}\int \mathrm{d}\boldsymbol{r}'(q(\boldsymbol{r}')\nabla p(\boldsymbol{r}')\nabla v'\boldsymbol{r}-\boldsymbol{r}')\\ &+ \int_{\boldsymbol{r}'\in V_{\mathrm{HC}}} \mathrm{d}\boldsymbol{r}'\; x(\boldsymbol{r}',t)\left[q(\boldsymbol{r}-\boldsymbol{r}',t)+q(\boldsymbol{r}'+\boldsymbol{r},t)\right] ,\end{aligned} \tag{3.229}$$

$$0 = \int_{\boldsymbol{r}'\in V_{\mathrm{HC}}} \mathrm{d}\boldsymbol{r}' q(\boldsymbol{r}',t)q(\boldsymbol{r}'+\boldsymbol{r},t) - N\delta(\boldsymbol{r}) . \tag{3.230}$$

In comparison with the mean-field approach described in subsection II.C, we see that the equation for q is identical to equation 3.48, while the equation for q contains an additional term compared to equation 3.49. As in subsection II.C, we expand q, p and x in powers of λ, where λ is the source term in equation 3.39. We find at order 0,

$$\frac{\partial}{\partial t}q_0 = D\nabla^2 q_0 - 2D\nabla\cdot(q_0\nabla p_0) , \tag{3.231}$$

$$\begin{aligned}\frac{\partial}{\partial t}p_0 = &-D|\nabla p_0|^2 - D\nabla^2 p_0\\ &+ \int_{\boldsymbol{r}'\in V_{\mathrm{HC}}} \mathrm{d}\boldsymbol{r}'\; q_0(\boldsymbol{r}'+\boldsymbol{r},t)\left[x_0(-\boldsymbol{r}',t)+x_0(\boldsymbol{r}',t)\right] ,\end{aligned} \tag{3.232}$$

$$0 = \int_{\boldsymbol{r}'\in V_{\mathrm{HC}}} \mathrm{d}\boldsymbol{r}' q_0(\boldsymbol{r}',t)q_0(\boldsymbol{r}'+\boldsymbol{r},t) - N\delta(\boldsymbol{r}) . \tag{3.233}$$

We obtain 3 equations for 3 unknown functions x_0, q_0 and p_0. We have not yet succeeded in solving these equations, but I would like to mention two ideas: (i) The Cole-Hopf transformation ($P_0 \equiv \mathrm{e}^{p_0}$; $Q_0 \equiv q_0\mathrm{e}^{-p_0}$) may help to remove the nonlinearities. This transformation yields

$$\begin{aligned}\frac{\partial}{\partial t}Q_0 = &\; D\nabla^2 Q_0\\ &- Q_0(\boldsymbol{r})\int_{\boldsymbol{r}'\in V_{\mathrm{HC}}} \mathrm{d}\boldsymbol{r}'\; Q_0(\boldsymbol{r}'+\boldsymbol{r},t)P_0(\boldsymbol{r}'+\boldsymbol{r},t)\left[x_0(-\boldsymbol{r}',t)+x_0(\boldsymbol{r}',t)\right] ,\end{aligned} \tag{3.234}$$

$$\begin{aligned}\frac{\partial}{\partial t}P_0 = &-D\nabla^2 P_0\\ &+ P_0(\boldsymbol{r})\int_{\boldsymbol{r}'\in V_{\mathrm{HC}}} \mathrm{d}\boldsymbol{r}'\; Q_0(\boldsymbol{r}'+\boldsymbol{r},t)P_0(\boldsymbol{r}'+\boldsymbol{r},t)\left[x_0(-\boldsymbol{r}',t)+x_0(\boldsymbol{r}',t)\right] ,\end{aligned} \tag{3.235}$$

$$0 = \int \mathrm{d}\boldsymbol{r}' Q_0(\boldsymbol{r}',t)P_0(\boldsymbol{r}',t)Q_0(\boldsymbol{r}'+\boldsymbol{r},t)P_0(\boldsymbol{r}'+\boldsymbol{r},t) - N\delta(\boldsymbol{r}) . \tag{3.236}$$

which could be solved for Q_0, then for P_0 as a function of x_0, the latter of which could be obtained from the third equation. (ii) The system is still translation-invariant, so a description using spatial Fourier modes would probably be helpful.

VI Application to NMR relaxation rate for quadrupolar atomic ions in liquids

The original aim in developing a molecular SDFT was to identify the molecular motions that drive the NMR relaxation of quadrupolar atomic ions in electrolytes. In these systems, the NMR relaxation rate $1/T_1$ depends on the time correlation of the electric field gradient (EFG), which itself is related to the density fluctuations of the electrolytes.

In this section, I will first recall the expression of the NMR relaxation rate for a quadrupolar atomic ion and review the latest experimental results. I will then apply SDFT for two situations: (i) explaining how the rate changes at different concentrations and (ii) modelling the rate in the presence of a dipolar solvent at infinite dilution.

VI.A Formal expression

For most of the quadrupolar nuclei ($I > 1/2$), the dominant relaxation channel is the energy exchange $\mathcal{H}_Q = QV_{zz}$ between the quadrupole moment Q of the nucleus and the electric field gradient (EFG) V_{zz} it experiences. [Abragam, 1983] In the case of quadrupolar nucleus of an atomic ion, the EFG is primarily induced by the distortions of the electronic cloud of the ion, which in turn originate from the instantaneous structure of the surrounding solvent. In my previous work, [AC3][AC16] we showed the validity of the Sternheimer approximation, [Sternheimer, 1950] which assumes a linear relationship between the total EFG experienced by the nucleus and the EFG induced by the charge distribution of the solvent, $V_{zz}^{\mathrm{tot}} = (1+\gamma_\infty)V_{zz}$, where γ_∞ is the so-called Sternheimer factor. [Foley et al., 1954, Sternheimer, 1966] Finally, since the solvent EFG V_{zz} fluctuates on a much faster timescale (1 ps) than the Larmor frequency (10 ns), we can apply the extreme-narrowing approximation and find that the NMR relaxation rate reads [Roberts and Schnitker, 1993]

$$\frac{1}{T_1} = \frac{3}{16}\frac{2I+2}{I^2(2I-1)}\left(1+\gamma_\infty\right)^2\left(\frac{eQ}{\hbar}\right)^2 \tilde{C}_{\mathrm{EFG}}(\omega=0) \;, \tag{3.237}$$

where V_{zz} is the zz component of the electric field gradient (EFG) tensor. We introduced the Fourier transform $\tilde{C}_{\mathrm{EFG}}(\omega)$ of the EFG correlation function $C_{\mathrm{EFG}}(t)$, defined by

$$C_{\mathrm{EFG}}(t) = \langle V_{zz}(0)V_{zz}(t)\rangle \;. \tag{3.238}$$

The EFG V_{zz} for an ion at the position $\boldsymbol{R}(t)$ depends on the solvent charge density ρ_{c},

$$V_{zz}(t) = \int \mathrm{d}\boldsymbol{r}\rho_{\mathrm{c}}(\boldsymbol{r}-\boldsymbol{R}(t),t)v_{zz}(\boldsymbol{r}) \;, \tag{3.239}$$

where we used the EFG density

$$v_{zz}(\boldsymbol{r}) = \frac{1}{\varepsilon_0\sqrt{5\pi}}\frac{1}{r^3}Y_{20}(\theta) + \frac{1}{4\pi\varepsilon_0}\delta(\boldsymbol{r}) \;, \tag{3.240}$$

and the charge density,

$$\rho_{\mathrm{c}}(\boldsymbol{r},t) = \sum_{S}^{N_{\mathrm{atoms}}} q_S \delta(\boldsymbol{r}_S(t) - \boldsymbol{r}) \ . \tag{3.241}$$

The sum runs over all the atoms with position $\boldsymbol{r}_S(t)$ and charge q_S. The expressions 3.239 and 3.238 are similar to the expressions 3.1 and 3.2, respectively. The charge density can also be expressed as linear sum of the molecular densities $\rho_i(\boldsymbol{r},\boldsymbol{\omega},t)$ of the solvent species (*e.g.*, water and ions). Modelling the NMR relaxation rate means modelling the coupled dynamics of the molecular densities $\rho_i(\boldsymbol{r},\boldsymbol{\omega},t)$ and of the position of the tracer ion $\boldsymbol{R}(t)$, as in equation 3.4. In the following, I will assume that the tracer ion remains fixed, $\boldsymbol{R}(t) = 0$. In the frame of the central ion, the EFG also reads

$$V_{zz}(t) = \frac{1}{(2\pi)^3} \int \mathrm{d}\boldsymbol{k}\ \tilde{\rho}_c(\boldsymbol{k},t)\tilde{v}_{zz}(\boldsymbol{k}) \tag{3.242}$$

where we introduced the Fourier transform of the charge density

$$\tilde{\rho}_c(\boldsymbol{k},t) = \exp(-\mathrm{i}\boldsymbol{R}\cdot\boldsymbol{k})\tilde{\rho}_c(\boldsymbol{k},t) = \sum_{S}^{N_{\mathrm{atoms}}} q_S \exp\left(-\mathrm{i}(\,\boldsymbol{r}_S(t) - \boldsymbol{R}(t)\,)\cdot\boldsymbol{k}\right) \ , \tag{3.243}$$

and of the EFG density

$$\tilde{v}_{zz}(\boldsymbol{k}) \ = \ -\frac{1}{\varepsilon_0}\frac{4}{3}\sqrt{\frac{\pi}{5}}Y_{20}(\theta_k,\phi_k) + \frac{1}{\varepsilon_0} \ . \tag{3.244}$$

Note that the final constant term originates from the Poisson equation and does not contribute to the EFG experienced by the central ion. In Fourier space, the EFG correlation is given by

$$C^{\mathrm{EFG}}(t) \ = \ \frac{1}{(2\pi)^6} \int \mathrm{d}\boldsymbol{k} \int \mathrm{d}\boldsymbol{k}' \tilde{C}_c(\boldsymbol{k},\boldsymbol{k}',t)\tilde{v}_{zz}(\boldsymbol{k})\tilde{v}_{zz}(\boldsymbol{k}') \ , \tag{3.245}$$

where we introduced the charge density correlation functions,

$$\tilde{C}_c(\boldsymbol{k},\boldsymbol{k}',t) \ = \ \langle\tilde{\rho}_c(\boldsymbol{k},0)\tilde{\rho}_c(\boldsymbol{k}',t)\rangle_1 \ . \tag{3.246}$$

The EFG tensor (excluding the Poisson term) is related to the second-order spherical harmonic Y_{20}. We therefore expand the ion-frame charge density $\rho_c(\boldsymbol{r})$ into spherical harmonics,

$$\rho_c(\boldsymbol{r},t) = \sum_{l=1}^{\infty}\sum_{m=-l}^{l} \rho^{c,lm}(r,t)Y_{lm}(\theta,\phi) \ . \tag{3.247}$$

By inserting the expansion into equation 3.239 and using the orthogonality of the spherical harmonics, we can demonstrate that the EFG depends solely on the quadrupolar component of the ion-frame charge density $\rho_c^{20}(r,t)$. It reads

$$V_{zz}(t) = -\frac{1}{\varepsilon_0\sqrt{5\pi}}\int_0^\infty \mathrm{d}r r^2 \rho^{20}(r,t)\frac{1}{r^3}\ . \tag{3.248}$$

When we insert this result into the EFG correlation functions, we obtain

$$C^{\mathrm{EFG}}(t) = \frac{1}{5\pi\varepsilon_0^2}\int_0^\infty \mathrm{d}r \int_0^\infty \mathrm{d}r' C_c^{20}(r,r',t)\frac{1}{rr'}\ , \text{with} \tag{3.249}$$

$$C_c^{20}(r,r',t) = \left\langle \rho_c^{20}(r,t)\rho_c^{20}(r',0)\right\rangle_1\ . \tag{3.250}$$

which is equivalent to equation 3.9. Finally, we can combine the Fourier formulation and the spherical harmonics expansion. The EFG density, the EFG and the EFG correlation function are given by the following expressions, respectively,

$$\tilde{v}_{zz}^{20}(\boldsymbol{k}) = -\frac{1}{\varepsilon_0}\frac{4}{3}\sqrt{\frac{\pi}{5}}\ , \tag{3.251}$$

$$V_{zz}(t) = -\frac{1}{\varepsilon_0}\frac{4}{3}\sqrt{\frac{\pi}{5}}\frac{1}{(2\pi)^3}\int_0^\infty \mathrm{d}k\ k^2\tilde{\rho}_c^{20}(k,t) \text{ and} \tag{3.252}$$

$$C^{\mathrm{EFG}}(t) = \frac{1}{180\pi^5\varepsilon_0^2}\int_0^\infty \mathrm{d}k \int_0^\infty \mathrm{d}k' C_c^{20}(k,k',t)k^2k'^2 \text{ with} \tag{3.253}$$

$$\tilde{C}_c^{20}(k,k',t) = \left\langle \tilde{\rho}_c^{20}(k,0)\tilde{\rho}_c^{20}(k',t)\right\rangle_1\ . \tag{3.254}$$

Overall, modelling the NMR quadrupole relaxation requires calculating the charge correlation function of the solvent in the frame of the tracer ion, which acts as an external potential. While it is difficult to determine such a complex correlation using standard dynamic DFT, it can be achieved using a fluctuation-based theory, such as SDFT.

VI.B Experimental results

In a recent work, Jershow and his collaborators have determined the $^{23}Na^+$ NMR relaxation rate in aqueous NaCl solutions at different concentrations (ranging from 0 to 5 mol.kg^{-1}) and different temperatures (ranging from 25 to 50° C). [Chubak et al., 2023] They showed that the relaxation rates increase with respect to the concentration and decrease with respect to the temperature. In collaboration with the team of B. Rotenberg, they have also assessed the validity of the Stokes-Einstein-Debye model, which is often used to explain the relaxation data. [Eisenstadt and Friedman, 1966, Price et al., 1990, Mitchell, 2016, D'Agostino et al., 2021] This model assumes that the relaxation is induced by the Brownian rotation of the solvation shell around the ion. It predicts that the NMR relaxation time is

$$\tau_{\mathrm{EFG}} = \frac{\tilde{C}^{\mathrm{EFG}}(\omega=0)}{C^{\mathrm{EFG}}(t=0)}\ , \tag{3.255}$$

is given by $\tau_{\mathrm{EFG}} = 4\pi\eta r_0^3/(3k_BT)$, where η is the viscosity and r_0 the radius of the solvation shell. By combining experimental and theoretical results, they found that τ_{EFG} evolves as $4\pi\eta r_0^3/(3k_BT) + \tau^0_{\mathrm{EFG}}$, but with a radius of $r_0 = 0.69$ Å, much smaller than the radius of the solvation shell (the first peak of the radial distribution function is about 2.5 Å). The offset τ^0_{EFG} is approximately 0.11 ps. The Stokes-Einstein-Debye model therefore fails to explain the relaxation mechanism. However, the strong correlation between the NMR relaxation time and the ratio η/k_BT triggered our interest, leading us to try to rationalise the relaxation mechanism using a more elaborate theory than Brownian rotation.

VI.C Relaxation at finite concentration

We first apply SDFT for electrolytes in implicit solvent to evaluate the effect of the ionic concentration for the NMR relaxation rate. Since the EFG density diverges as $r \to 0$ (see equation 3.240), we must explicitly account for the size of the tracer ion. We will test the different strategies discussed in section V.

Cut-off approach The effective EFG density with zero-contribution within a shell of radius σ reads

$$v^{\sigma}_{zz}(\boldsymbol{r}) = v_{zz}(\boldsymbol{r})\theta(r-\sigma) \ , \tag{3.256}$$

and the EFG induced by the ionic density is

$$\begin{aligned} V_{zz}(t) &= \int \mathrm{d}\boldsymbol{r}\rho_I(\boldsymbol{r},t)v^{\sigma}_{zz}(\boldsymbol{r}) = \int_0^\infty \mathrm{d}r r^2 \rho_I^{20}(r,t)v^{\sigma\,20}_{zz}(r) && (3.257)\\ &= \int_0^\infty \mathrm{d}k k^2 \tilde{\rho}_I^{20}(k,t)\tilde{v^{\sigma}}^{20}_{zz}(k) \ . && (3.258) \end{aligned}$$

The term $\tilde{v^{\sigma}}^{20}_{zz}(k)$ can be obtained *via* an Hankel-transform,

$$\tilde{v^{\sigma}}^{20}_{zz}(k) = 4\sqrt{\frac{\pi}{5}}\frac{1}{\varepsilon_0\varepsilon_w}\frac{\sin k\sigma - k\sigma\cos k\sigma}{(k\sigma)^3} \ , \tag{3.259}$$

and the EFG correlation is given by

$$C^{\mathrm{EFG}}(t) = \frac{1}{(2\pi)^6}\int_0^\infty \mathrm{d}k \int_0^\infty \mathrm{d}k' k^2 k'^2 \tilde{v^{\sigma}}^{20}_{zz}(k)\tilde{v^{\sigma}}^{20}_{zz}(k')C_I^{20}(k,k',t) \ , \tag{3.260}$$

with the charge correlation functions

$$C_I^{20}(k,k',t) = \left\langle \rho_I^{20}(k,t)\rho_I^{20}(k',0)\right\rangle_1 \ . \tag{3.261}$$

Combining the results for the charge correlation in the cut-off approach (equation 3.169) and the vertex function for the EFG density 3.259, we obtain

$$C^{\mathrm{EFG}}(t) = \frac{4}{5\pi^2}\frac{C_I(ze)^2}{\varepsilon_w^2\varepsilon_0^2}\int_0^\infty \mathrm{d}k\; k^4 \frac{\mathrm{e}^{-D_I(k^2+\kappa_{\mathrm{imp}}^2)t}}{k^2+\kappa_{\mathrm{imp}}^2}\left[\frac{\sin k\sigma - k\sigma\cos k\sigma}{(k\sigma)^3}\right]^2 . \tag{3.262}$$

This integral does not seem to be computable explicitly, except at zero frequency where it reads

$$\tilde{C}^{\mathrm{EFG}}(\omega=0) = \int_{-\infty}^{\infty}\mathrm{d}t\; C^{\mathrm{EFG}}(|t|) = \frac{8}{5\pi^2}\frac{C_I(ze)^2}{\varepsilon_w^2\varepsilon_0^2 D_I}\int_0^\infty \mathrm{d}k\; k^4 \frac{1}{(k^2+\kappa_{\mathrm{imp}}^2)^2}\left[\frac{\sin k\sigma - k\sigma\cos k\sigma}{(k\sigma)^3}\right]^2 \tag{3.263}$$

$$= \boxed{\frac{k_BT\kappa_{\mathrm{imp}}^3}{5\pi D_I\varepsilon_0\varepsilon_w}\frac{1}{x^6}\left[\frac{x^2}{2}-\frac{3}{2}+\frac{1}{2}(1+x)(2x^2+3x+3)\mathrm{e}^{-2x}\right]}, \tag{3.264}$$

where $x = \kappa_{\mathrm{imp}}\sigma$. Let us now calculate the results with the other method, the no-flow boundary conditions detailed in subsection V.B.

Boundary conditions approach The EFG correlation is given in equation 3.249, where the charge correlations can be expressed in function of the Green operator as in equation 3.193,

$$\tilde{C}_I^{20}(r,r',\omega) = 12D_IC_I(ze)^2\int_\sigma^\infty \mathrm{d}r''\tilde{G}_{\rho_I}^{(2)}(r,r'',\omega)\tilde{G}_{\rho_I}^{(2)}(r'',r',\omega)\ . \tag{3.265}$$

The Green operator is shown at $\omega = 0$ in equations 3.194 and 3.195. If we write $G_{\rho_I}^{(2)}(r,r',\omega = 0) = \frac{2\kappa_{\mathrm{imp}}}{\pi D_I} f^{(2)}(\kappa_{\mathrm{imp}}r, \kappa_{\mathrm{imp}}r', \kappa_{\mathrm{imp}}\sigma)$, we can expressed the EFG correlation as

$$\tilde{C}^{\mathrm{EFG}}(\omega=0) = \frac{12D_IC_I(ze)^2}{5\pi\varepsilon_0^2\varepsilon_w^2}\int_\sigma^\infty \mathrm{d}r\int_\sigma^\infty \mathrm{d}r'\int_\sigma^\infty \mathrm{d}r''\tilde{G}_{\rho_I}^{(2)}(r,r'',0)\tilde{G}_{\rho_I}^{(2)}(r'',r',0)\frac{1}{rr'} \tag{3.266}$$

$$= \boxed{\frac{24}{5\pi^3}\frac{\kappa_{\mathrm{imp}}^3k_BT}{D_I\varepsilon_0\varepsilon_w}\int_{\kappa_{\mathrm{imp}}\sigma}^\infty \mathrm{d}x\int_{\kappa_{\mathrm{imp}}\sigma}^\infty \mathrm{d}x'\int_{\kappa_{\mathrm{imp}}\sigma}^\infty \mathrm{d}x'' f(x,x'',\kappa_{\mathrm{imp}}\sigma)f(x'',x',\kappa_{\mathrm{imp}}\sigma)\frac{1}{xx'}}\ . \tag{3.267}$$

We observe that both the prefactors of equations 3.264 and 3.267 are proportional to $k_BT\kappa_{\mathrm{imp}}^3/(D_I\varepsilon_0\varepsilon_w)$. Although equation 3.267 does not appear to be analytically computable, it can be integrated numerically.

Comparison with the experiments and the simulations We then compare the relaxation rate obtained through equations 3.264 and 3.267 with the experimental and numerical results of Chubak *et al.* [Chubak et al., 2023] The chosen parameters for the solvent and ion properties are gathered in table 3.1. As both equations 3.264 and 3.267 were obtained for an implicit solvent, we aim to calculate only the ionic contribution, $\Delta T_1^{-1}(C_I) = T_1^{-1}(C_I) - T_1^{-1}(C_I)$, where C_I

Table 3.1 – Numerical parameters for the calculation of the NMR relaxation rates for $^{23}Na^{+}$ at different concentrations and at $T = 298\ K$.

D_I	σ	γ_∞	ε_w	I	Q
1.3×10^{-9} ($m^2.s^{-1}$)	1 Å	12.1	80	3/2	104×10^{-31} (m^2)

is the ionic concentration and the NMR relaxation rate within the Sternheimer approximation is given in equation 3.237.

Figure 3.1 shows the $\Delta T_1^{-1}(C_I)$ as obtained using the different methods (experiments, simulations and the two SDFT approaches). SDFT results are ten times smaller than the experimental results. This discrepancy could be explained by the oversimplification of the SDFT models. These models do not take into account the dependence of the diffusion coefficient D_I and of the relative permittivity ε_w with respect to the ionic contribution. The self-diffusion of the tracer ion was also neglected. These aspects are currently under study, but I do not expect a major difference with the present results: the changes in the concentration of D_I and ε_w are limited and will counteract each other. Similarly, the timescale of the self-diffusion is larger than that of the EFG fluctuations, meaning that the motion of the tracer ion will not have significantly impact on the NMR relaxation rate.

On the other hand, the prediction of a small ionic contribution to the NMR relaxation rate could be a physical outcome. At the highest concentration, the average distance between the ions is around 10 Å, at which point the EFG contribution becomes negligible. If the ions impact the NMR relaxation rate, it is more likely to be through their effect on the water dynamics. In the next subsection, I will attempt to use the dipolar SDFT to calculate the full NMR relaxation rate induced by the water.

VI.D Relaxation at infinite dilution

The ultimate goal would be to predict the NMR rate using the dipolar SDFT developed in section IV. However, we first considered the case of the infinite dilution ($C_I = 0$), which was challenging enough. I will first discuss the charge and EFG correlations using a dipolar SDFT and a cut-off approximation. I will then present the theory of Hynes and Wolynes (HW), which is the most accurate model in the literature. [Hynes and Wolynes, 1981] Finally, I will compare SDFT with the HW theory, as well as with simulations and experiments.

Cut-off approach In the infinite dilution limit ($C_I = 0$), the linearised Dean-Kawasaki equation for a dipolar fluid in presence of the fixed tracer ion read

$$\frac{\partial}{\partial t}\rho_S^c = D_S\varepsilon_w\left(\nabla^2\rho_S^c - 2a^{-2}\rho_S^c\right) - (\varepsilon_w - 1)(k^2 + 2a^{-2})Q\delta(\boldsymbol{r}) + \Xi_S(\boldsymbol{r}, t)\ , \tag{3.268}$$

where the statistics of the noise Ξ_S are given by equation 3.135 and where we assumed that $\varepsilon_b = \varepsilon_w$. After performing a spatial Fourier transform and a spherical harmonics expansion, we obtain the following charge correlation function,

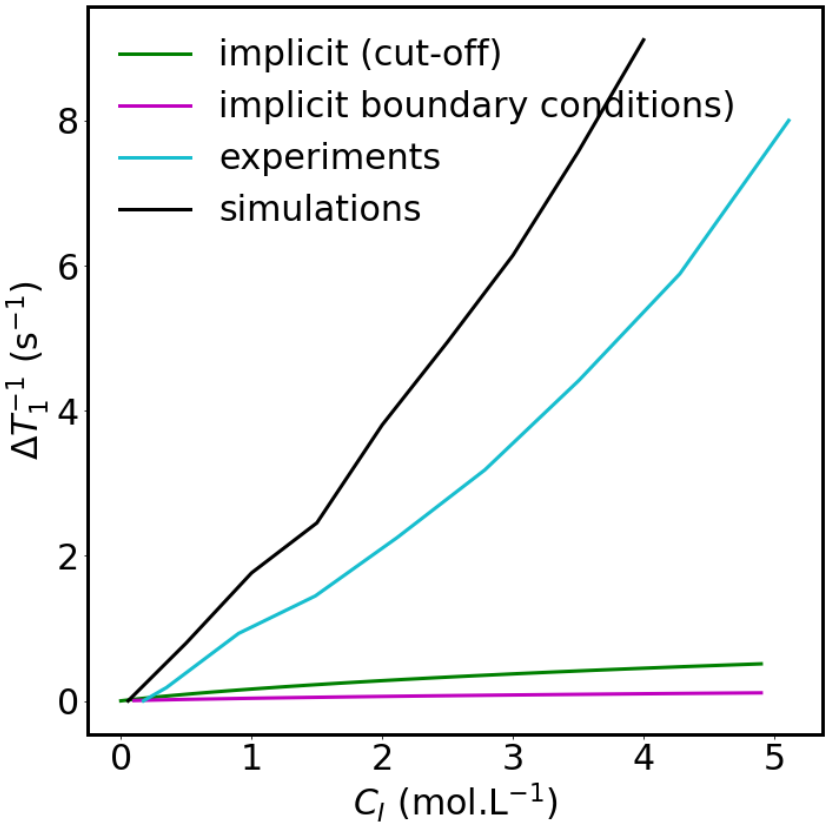

Figure 3.1 – Comparison between the ionic contribution to the NMR relaxation rate $\Delta T_1^{-1}(C_1)$ obtained *via* the implicit cut-off model (green, equation 3.264), the implicit boundary-condition model (magenta, equation3.267), the experiences (cyan), and the simulations (black). Experimental and simulation data are taken from the reference [Chubak et al., 2023].

$$C_c^{20}(k,k',t) = \left\langle \tilde{\rho}_S^{c,20}(k,t)\rho_S^{c,20}(k',0)\right\rangle_1 \tag{3.269}$$

$$= \frac{2(2\pi)^3 k_B T\varepsilon_0(\varepsilon_w-1)}{\varepsilon_w}\mathrm{e}^{-D_S(2a^{-2}+k^2)\varepsilon_w t}\delta(k-k') \ . \tag{3.270}$$

We insert this result into the EFG correlation with a cut-off, equation 3.260, and obtain

$$C^{\mathrm{EFG}}(t) = \frac{4}{5\pi^2}\frac{k_B T(\varepsilon_w-1)}{\varepsilon_0\varepsilon_w}\int_0^\infty \mathrm{d}k\ k^4\mathrm{e}^{-D_S(2a^{-2}+k^2)\varepsilon_w t}\left[\frac{\sin k\sigma - k\sigma\cos k\sigma}{(k\sigma)^3}\right]^2 \ . \tag{3.271}$$

The zero-frequency value is given by

$$\tilde{C}^{\mathrm{EFG}}(\omega=0) = \frac{8}{5\pi^2}\frac{k_B T(\varepsilon_w-1)}{D_S\varepsilon_0\varepsilon_w^2}\int_0^\infty \mathrm{d}k\ k^4\frac{1}{2a^{-2}+k^2}\left[\frac{\sin k\sigma - k\sigma\cos k\sigma}{(k\sigma)^3}\right]^2 \tag{3.272}$$

$$= \boxed{\frac{k_B T(\varepsilon_w-1)}{5\pi D_S\varepsilon_0\varepsilon_w^2 a^3}\frac{1}{2y^6}\left[\sqrt{2}\left(1+\sqrt{2}y\right)^2\mathrm{e}^{-2\sqrt{2}y} - \sqrt{2}\left(1-2y^2\right)\right]} \ , \tag{3.273}$$

where $y = \sigma/a$.

Boundary conditions approach On the other hand, the linearised Dean-Kawasaki equation with the no-flow boundary condition at the surface of the tracer ion is given by

$$\partial_t \rho_S^c(\boldsymbol{r},t) = D_S \varepsilon_w \left(\nabla^2 \rho_S^c - a^{-2}\rho_S^c\right) + \Xi_S(\boldsymbol{r},t) \;, \tag{3.274}$$

$$\partial_r \rho_S^c|_{r=\sigma} = 0 \;. \tag{3.275}$$

These equations are similar to the ones for the ionic density in presence of an implicit solvent, with the mapping $\kappa_{\mathrm{imp}}^2 \to 2a^{-2}$. We can therefore obtain the Green operator at $\omega = 0$ following the steps presented in the appendix II.B. The EFG correlation function reads

$$\begin{aligned}\tilde{C}^{\mathrm{EFG}}(\omega=0) &= \frac{24 D_S k_B T(\varepsilon_w - 1)}{5\pi\varepsilon_0} \times \\ &\int_\sigma^\infty \mathrm{d}r \int_\sigma^\infty \mathrm{d}r' \int \mathrm{d}r'' G^{(2)}_{\rho_S^c}(r,r'',0) G^{(2)}_{\rho_S^c}(r'',r',0) \left(3r^{-2} - a^{-2}\right) \frac{1}{rr'} \\ &= \frac{384}{5\pi^3} \frac{k_B T(\varepsilon_w - 1)}{D_S \varepsilon_0 \varepsilon_w^2 a^3} \times \\ &\int_{\sigma/a}^\infty \mathrm{d}x \int_{\sigma/a}^\infty \mathrm{d}x' \int_{\sigma/a}^\infty \mathrm{d}x'' f(x,x'',\sigma/a) f(x'',x',\sigma/a) \left(3x^{-2} - 1\right) \frac{1}{xx'} \;. \end{aligned} \tag{3.276}$$

Hynes and Wolynes result In the early 1980s, Hynes and Wolynes derived an expression for the correlation function $C^{\mathrm{EFG}}(t)$ in the infinite dilution case. [Hynes and Wolynes, 1981] They assumed that the solvent (*e.g.*, water) is a continuum described by a frequency-dependent permittivity $\varepsilon_w(\omega)$. This takes the following Debye-like form:

$$\varepsilon_w(\omega) = \varepsilon_\infty + \frac{\varepsilon_w - \varepsilon_\infty}{1 - \mathrm{i}\omega\tau_D} \;, \tag{3.277}$$

where τ_D is the Debye time, $\varepsilon_w = \varepsilon_w(\omega = 0)$ is the static permittivity and ε_∞ is the ultrafast response of the solvent accounting for the electronic degrees of freedom. They calculate the EFG correlation functions using the (inverse) linear response theory, employing the same strategy as one used to determine the dipolar friction. [Nee and Zwanzig, 1970, Titulaer and Deutch, 1974] In practice, they consider the solvent response to a rotating quadrupole of a fixed ion with radius σ. They used standard electrostatic calculations, which explicitly consider the boundary conditions at the solvent/ion interface. [Böttcher et al., 1973] This leads them to the following zero-frequency component of the EFG correlation

$$\tilde{C}^{\mathrm{EFG}}(\omega=0) = \frac{5 k_B T}{2\pi\varepsilon_0 \sigma^5} \frac{(\varepsilon_w - \varepsilon_\infty)}{(2 + 3\varepsilon_w)^2} \tau_D \;, \tag{3.278}$$

They obtained semi-quantitative equivalence in comparison with the experimental results. [Hynes and Wolynes, 1981]

Comparison between the different methods Our idea was to assess how the dipolar SDFT performs in the simple case of an electrolyte at infinite dilution ($C_I = 0$). In figure 3.2, we

plot the zero-frequency component of the EFG correlation, $\tilde{C}^{\mathrm{EFG}}(\omega = 0)$, with respect to the radius σ of the ion. We compare the results obtained from the recent simulations of Chubak *et al.* (reference [AC16]), from the experiments (where we combined the experimental T_1 with the numerical evaluation of the Sternheimer factor [AC16]), from the HW theory 3.278 and from SDFT 3.273. However, we did not for now implement the SDFT result with the boundary condition approach (equation 3.276). The parameters for the Debye-like permittivity in equation 3.277 are the same as is in the paper of Hynes and Wolynes ($\varepsilon_w = 78.6, \varepsilon_\infty = 1.85$ and $\tau_D = 8.2$ ps). [Hynes and Wolynes, 1981] The parameters or the SDFT solvent are the same as in the reference [AC22]) : $\varepsilon_w = 80$, $a = 2.14$ Å, and $D_S = 2.3 \times 10^{-9}$ ($\mathrm{m}^2.\mathrm{s}^{-1}$).

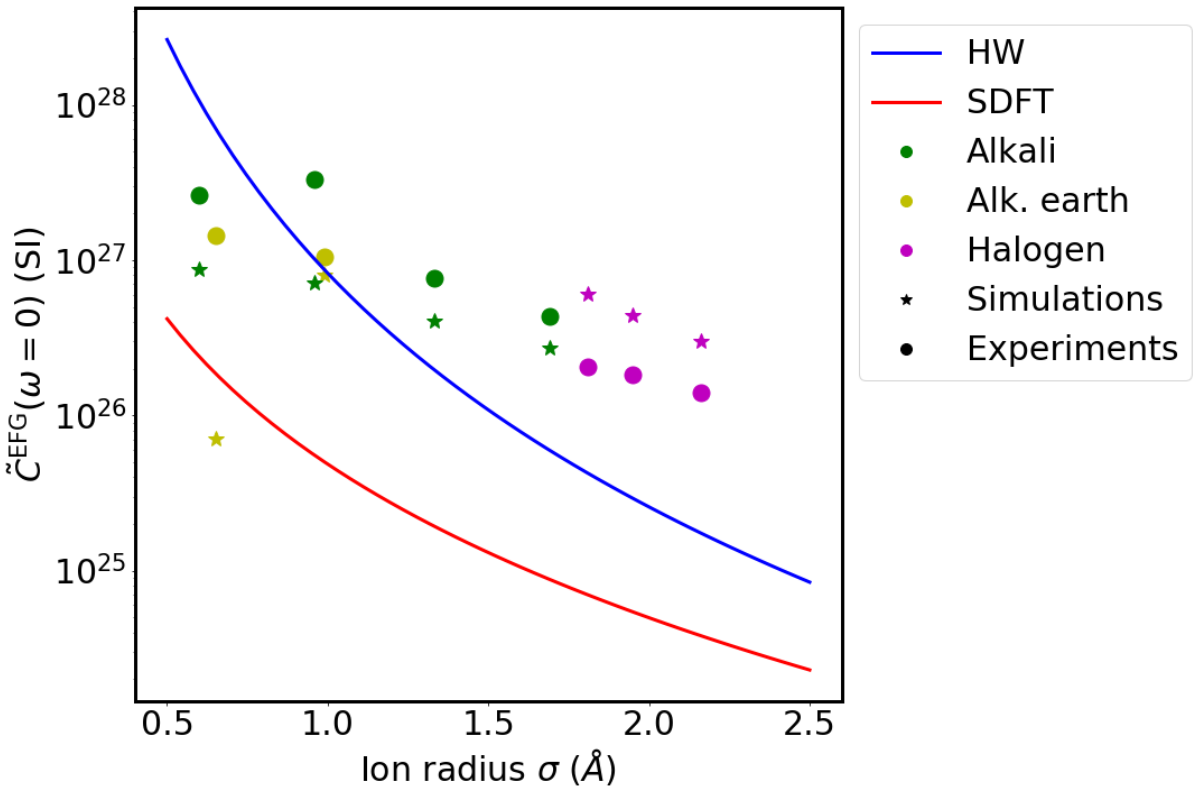

Figure 3.2 – Comparison of the NMR correlations at zero-frequency, $\tilde{C}^{EFG}(\omega = 0)$ between the experiments (circle symbol), the simulations (star symbol), the linearised SDFT with the cut-off approach (red line, equation 3.273), and the Hynes-Wolynes theory (blue line, equation 3.278). Experimental and simulation data are taken from the reference [Chubak et al., 2023].

Figure 3.2 shows that SDFT captures the correct trend decreasing with respect to the size of the tracer, but completely fails to obtain the correct order of magnitude. On the contrary, the simpler HW theory seems to reproduce the zero-frequency correlation of the EFG more accurately. To explain the failure of SDFT, it is instructive to compare the structure of equations 3.278 and 3.273. Assuming that the Debye time is related to the rotational self-diffusion coefficient as $\tau_D \sim 1/D_S^r = a^2/D_S$, the zero-frequency correlations are proportional to

$$\tilde{C}^{\mathrm{EFG}}(\omega = 0) \sim \frac{k_B T(\varepsilon_w - \varepsilon_\infty)}{D_S \varepsilon_0 (2 + 3\varepsilon_w)^2} \text{ (HW)} \tag{3.279}$$

$$\tilde{C}^{\mathrm{EFG}}(\omega = 0) \sim \frac{k_B T(\varepsilon_w - 1)}{D_S \varepsilon_0 \varepsilon_w^2} \text{ (SDFT)} \tag{3.280}$$

where we put aside the numerical and size-related prefactors here. Note that both the cut-off approach (equation 3.271) and the boundary conditions approach (equation 3.276) show the same prefactor. The ultrafast permittivity is close to one, $\varepsilon_\infty \approx 1$, which means that the main difference resides in the denominator, $(2 + 3\varepsilon_w)^2$ for HW and ε_w^2 for SDFT. For $\varepsilon_w \approx 80$, the ratio $(2 + 3\varepsilon_w)^2/\varepsilon_w^2 \approx 9$, which could partly explain the failure of SDFT. The term $(2 + 3\varepsilon_w)$ stems from the electrostatic boundary conditions between a sphere of radius σ and a dielectric solvent. It appears that both the cut-off approach and the no-flow boundary conditions approach combined with the linearised SDFT failed to properly capture the electrostatic boundary conditions correctly. A proper treatment may require overcoming the linearisation and adopting the mean-field limit presented in subsection II.C. In subsections V.C, I discussed different strategies to include the size of the solute (here the tracer ion) in the mean-field limit of SDFT.

VII Conclusion

In this chapter, I present my current and future works on the study of the solvation dynamics in fluids. The solvation dynamics determine various properties of interest, such as the spectroscopic data, the transport coefficients, and the reactivity. At the microscopic scale, the solvation dynamics are controlled by the solvent density fluctuations, which are affected by the interactions with a dynamical solute. Describing these density fluctuations is therefore challenging because it requires the modelling of the coupling between the solute and solvent dynamics correctly, as well as the impact of the solute on the solvent. Even when approximating a fixed solute, the solvent density fluctuations must be described by taking the solute/solvent interaction potential into account. The steric repulsion of the latter is sufficient to couple the solvent modes.

In the literature, most of the theories were however based on the uniform approximation, which assumes that the solvent density fluctuations are similar in the bulk and in the vicinity of the solute. I therefore propose developing a new approach that correctly takes into account the impact of the solute. I have chosen to use the stochastic density functional theory (SDFT), a powerful framework powerful framework capable of properly describing the effects of fluctuations and the presence of an external field.

After reviewing the standard SDFT, SDFT for electrolytes with an implicit solvent, and SDFT for electrolytes with a dipolar solvent, I presented my present works on explicitly incorporating solute size into the SDFT framework. I concluded the chapter by demonstrating how these developments could be applied to the NMR relaxation rate. While these applications fail to capture the experimental results, they provide valuable guidance for future research.

CHAPTER 4

Conclusion and perspectives

To wrap up this manuscript, I will first review three other projects on which I am not the principal investigator (PI), or which are less significant. I will then present the long-term direction I wish to explore in terms of both systems and methods, before drawing a final conclusion.

I Secondary projects

Micro-solvation and solvation under confinement (PI: F. Ingrosso) Since joining the LPCT, I have also participated in F. Ingrosso's project on modelling micro-solvation and spectroscopy experiments. I accompanied the various members of the team on this project: a PhD student (**V.K. Porwal**) and two postdoctoral researchers (**K. Anand** and **A. Semmeq**). I helped to write the analysis codes and interpret the simulation data.

The first task was to compare and develop three solvation models: the continuous solvent model, the MM solvent model, and the QM/MM model. We first studied the micro-solvation of carboxylates. [AC19] Then, using an innovative method of force-field fitting on quantum calculations, [Giannini et al., 2025] we developed an intramolecular force field for a bicyclic diol species and its tautomers. This methodological development allowed us to study the micro-solvation of these species in water, to demonstrate their relative stability, and explain for the first time the absorption spectrum of these species. [AC20]

In parallel, we were interested in solvation in complex environments, such as confined media. In collaboration with experimentalists from LCPME (Nancy), we studied the properties of layered double hydroxides (LDH). These materials are of interest in the context of decontamination applications and are considered favourable environments for the formation of the peptide bond (which is related to the origin of life). [Grégoire et al., 2016] We were first able to precisely describe the interactions between three anions (aspartate, glutamate, and succinate) and the LDH lamellae for different hydration rates. These results are presented in the article [AC21].

We also studied LDH intercalated with small inorganic ions (chloride, chlorate, nitrate, iodide, carbonate). We characterised the structural differences between LDH with these different ions at various hydration levels and demonstrated that the carbonate ion exhibits different behaviour in LDH. [AC24]

This work permitted me to collaborate with experimentalists and to study rich solvation phenomena in complex environments. While this research has so far been carried out using standard simulation methods (MD, QM/MM), I intend to apply density-based theories (MDFT, SDFT) to them in the future. For instance, I have started discussing with D. Cornu (LCPME, Nancy) how to explain the difference in diffusion mechanisms between monovalent and divalent cations in the interlamellar space of the LDH.

Long-range correlations in electrolytes (Collaboration: F. Ingrosso, D. Lesnicki) The existence of long-range structural correlations in electrolytes is an active field of research from both the experimental and numerical perspectives. Current questions include: what is the shape of the long-range decay of the ion-ion correlations (monotonic or oscillatory)? [Kjellander, 2018] How do the correlation lengths change with the ionic concentration? [Coupette et al., 2018, Kjellander, 2020a, Elliott et al., 2024] Recent data from force apparatus experiments has shown that the correlations may exhibit an underscreening at high concentrations [Smith et al., 2016]— a phenomenon that remains unexplained by the current simulations and existing liquid-state theories. [Pluhařová et al., 2017, Belloni et al., 2018, Rotenberg et al., 2018, Coles et al., 2020]

The team in Nancy (F. Ingrosso, D. Lesnicki, and myself) were contacted one year ago by J. Duboisset, an experimental specialist in second order harmonic scattering (Institut Fresnel, Marseille, France). He had developed a powerful experiments to measure the long-range orientational correlations between water molecules. [Duboisset et al., 2020, Rondepierre et al., 2025] His previous collaboration with theorists had helped to rationalise the experiments, at least for a small ionic concentrations. [Borgis et al., 2018]

Within the project Harmonix (ANR grant), we are starting a collaboration with J. Duboisset and his collaborators. Our objectives is to combine MD simulations and liquid-state theories [Belloni, 2017] to accurately calculate the long-range correlations in two systems: (i) pure water at different pressures and temperatures (and up to the critical region), and (ii) various electrolytes at different concentrations. A postdoctoral researcher will join us in November 2025 to begin working on this interesting project. From my perspective, this project nicely aligns between the development of the MDFT for supercritical CO_2 (which requires long-range correlations) and the investigation of the electrolyte dynamics using the SDFT.

Dynamic properties of supercritical fluids In addition to my work on the solvation in supercritical CO_2 using the classical DFT, I have also been interested in dynamics near the critical point. In particular, recent experiments and simulations have revealed the presence of two distinct behaviours in the supercritical region: a rigid domain, with a liquid-like diffusive mechanism, and a non-rigid domain, with a gas-like diffusive mechanism. [Brazhkin et al., 2013, Bolmatov et al., 2015, Bryk et al., 2017, Skarmoutsos et al., 2022, Ranieri et al., 2024] These domains are separated by the so-called Frenkel line, one of the lines that divides the supercritical region into liquid- and gas-like domains (such as the Widom lines). [Simeoni et al.,

2010,Banuti et al., 2017,Fomin et al., 2015,Li and Jin, 2024] While these lines do not represent a thermodynamic transition, they still affect the solvation properties and the operating conditions of supercritical CO_2-based processes. [Yang et al., 2015, Pipich and Schwahn, 2018, Mouahid et al., 2022] I proposed exploring these aspects to several M1 interns (**M. Rieff**, **Q. Greffe**, **J. Klein**, **G. Szczepan**, and **A. Tarif Almodares**) as well as to M. Houssein Mohamed during his M2 internship. I would be interested to find out if a density-based theory (dynamical DFT, as in the references [Egorov et al., 2002, Egorov, 2003] or stochastic DFT) could capture the rigid/non-rigid transition.

II Long-term projects

In the longer term, I would like to generalise this work in order to examine a broader range of "green" solvents, such as ionic liquids and deep eutectic solvents (DES). These fluids are used in various industrial technologies, including batteries, synthesis processes, or CO_2 capture technologies [Anastas and Eghbali, 2010, Hansen et al., 2021]. Their vast chemical diversity offers immense potential for optimising industrial processes [Alizadeh et al., 2020]. Molecular density theories would enable these fluids to be modelled efficiently and chemical space to be explored rapidly. However, these are complex fluids, with all the features that I discussed in the introduction : electrostatic moments, nonspherical shapes, associativity, flexibility, and even reactivity. I present below some of the theoretical work required for the development of molecular density theory for these complex fluids.

Solvent mixtures The first challenge will be to develop an MDFT for a mixture of solvents. The functional will need to be adapted to include terms specific to each fluid, as well as interaction terms between them. This approach will initially be applied to the case of supercritical CO_2: the latter is indeed generally used with a cosolvent to enhance its solvating power or to exploit its anti-solvent properties. In parallel, a natural extension of the SDFT previously developed for an electrolyte with a dipolar solvent will be extended to include several solvents. This development is essential for studying the DES, which are mixtures of solvents. [Hansen et al., 2021]

Non-Markovian dynamics As discussed in the subsection II.D, the dynamics at the molecular scale comprise complicated mechanisms operating at different timescales. For instance, the rotation of water molecules occurs with jumps, [Laage and Hynes, 2006] the translation motion of the small solutes alternates between short-time cage rattling and diffusion *via* a cage-hopping mechanism, [Polimeno and Moro, 1994, Bier et al., 2008, Acharya et al., 2015, Dokko et al., 2018] and the ions form long-lived pairs which impacts the macroscopic conductivity. [Kirchner et al., 2015, van der Vegt et al., 2016, Brünig et al., 2022] One of my objectives is to develop a dynamic/stochastic DFT that incorporates these mechanisms, through the presence of a memory kernel, as well as some complex interaction potentials between the particles.

Associativity and network Molecules that interact directionally can form strong associations, creating dimers, trimers, and ultimately forming a network at high density. The hydrogen bond network of water is well known, [Kühne and Khaliullin, 2014] but networks also form in high-concentration electrolytes, [Roget et al., 2023, Goloviznina et al., 2024, Liang et al., 2025], ionic liquids, [Salanne et al., 2006], deep eutectic solvents, [Stettler et al., 2025], and even nonpolar fluids [Moog et al., 2021, Hosokawa et al., 2024] Network formation can impact the

phase transitions in fluids , [Simeski and Ihme, 2023, Neophytou et al., 2024], spectroscopic properties, [Miguel et al., 2014] and transport properties. [Imai et al., 2020, Becher et al., 2022, Gao et al., 2024] In terms of molecular modelling, I propose combining the multiple-scale DFT framework developed by Bui and Cox, [Bui and Cox, 2024, Lum et al., 1999] in combination with a coarse-grained density theory based on the patchy particle model. [Simon and Oettel, 2024, Simon et al., 2025] Extending this approach to dynamics would also present a fascinating challenge.

Molecular flexibility So far, I have only considered solvents composed of rigid molecules. While this approximation is relevant for small molecules (CO_2, water, atomic ions), it is too strong for molecules that form a DES (for example, glycerol-choline chloride [Hinz et al., 2023]) or those that form molecular ionic liquids (such as those based on imidazolium chains, $[C_nIm]^+$ [Groves and Perkin, 2024], or other molecular cations like $[TEA]^+$ or $[C_5Py]^+$ [Dziubinska-Kühn et al., 2025]). It is therefore important to explicitly include the flexibility of these molecules in order to correctly describe the dynamic or thermodynamic properties of these fluids. In terms of strategy, I propose adding the internal degrees of freedom to the molecular density, $n(\boldsymbol{r}, \omega, \alpha)$, and determining new functionals that depend on these internal degrees. Some of these degrees are quantised (their energy is greater than thermal energy), which will allow them to be modelled simply. The main challenge will be to develop a formalism for conformational degrees of freedom. From a dynamic point of view, it will be particularly interesting to model the couplings between translation and conformational dynamics.

III Conclusion

In this manuscript, I have presented my past, present and future research projects. My work focuses on the theoretical study of the molecular fluids, particularly the structure, the thermodynamics and the dynamics of solvation. My aim is to develop density-based theories that could:(i) reproduce quantitively and efficiently the experimental data, and (ii) establish a relationship between the chaotic molecular modes (rotation, collision and collective motions) and the macroscopic properties. This could facilitate the design of more powerful solvents and industrial fluids, *e.g.* for the development of ecological technologies.

APPENDIX A

List of papers and communications

I Publications in peer-reviewed international journals

[AC25] Non-Gaussian density fluctuations in the Dean-Kawasaki equation
L. Le Bon, A. Carof and P. Illien
Phys. Rev. E, **112**, 3, 034127 (2025).
DOI: https://doi.org/10.1103/5mjd-m46h
Preprint: https://arxiv.org/abs/2501.16206

[AC24] On the Local Structure of Water Surrounding Inorganic Anions Within Layered Double Hydroxides
A. Semmeq, K. Anand, A. Carof, A. Bastida and F. Ingrosso
Molecules, **30**, 8, 1678 (2025).
DOI: https://doi.org/10.3390/molecules30081678

[AC23] Molecular integral equations theory in the near critical region of CO_2
M. Houssein Mohamed, L. Belloni, D. Borgis, F. Ingrosso and A. Carof
J. Mol. Liq., **418**, 126623 (2025).
DOI: https://doi.org/10.1016/j.molliq.2024.126623
Preprint: arXiv:2310.14667
Dataset: https://doi.org/10.57745/GI6LLZ

[AC22] Stochastic density functional theory for ions in a polar solvent
P. Illien, A. Carof and B. Rotenberg
Phys. Rev. Lett., **133**, 268002 (2024).
DOI: https://doi.org/10.1103/PhysRevLett.133.268002
Preprint: arXiv:2407.17232
Dataset: https://doi.org/10.57745/T0UQ4A

[AC21] Structural and Vibrational Properties of Carboxylates Intercalated into Layered Double Hydroxides: A Joint Computational and Experimental Study
V.K. Porwal, E. André, A. Carof, A. Bastida, C. Carteret and F. Ingrosso
Molecules, **29**, 8, 1853 (2024).
DOI: https://doi.org/10.3390/molecules29081853

[AC20] Tautomeric contributions to the absorption spectrum of [2,2'-bipyridyl]-3,3'-diol in water unveiled by molecular dynamics with accurate quantum mechanically derived force-fields
G. Prampolini, V.K. Porwal and F. Ingrosso
J. Mol. Liq., **396**, 123898 (2024).
DOI: https://doi.org/10.1016/j.molliq.2023.123898

[AC19] Hydration effects on the vibrational properties of carboxylates: From continuum models to QM/MM simulations
V.K. Porwal, A. Carof and F. Ingrosso
J. Comp. Chem., **44**, 23, 1-14 (2023).
DOI: https://doi.org/10.1002/jcc.27171

[AC18] Study of Speciation and Transport Properties for Different Compositions of Carbonates in Li_2CO_3-Na_2CO_3 and Li_2CO_3-K_2CO_3 Binary Systems at High Temperature in Molten State
A. Zhadan, A. Carof, V. Sarou-Kanian, L. del Campo, L. Cosson, R. Vuilleumier, M. Malki and C. Bessada
J. Phys. Chem. C., **127**, 23, 11186-11194 (2023).
DOI: https://doi.org/10.1021/acs.jpcc.3c01226

[AC17] Exciton transport in molecular organic semiconductors boosted by transient quantum delocalization
S. Giannini, W.T. Peng, L. Cupellini, D. Padula, A. Carof and J. Blumberger
Nature comm. **13**, 1, 2755 (2022).
DOI: https://doi.org/10.1038/s41467-022-30308-5
Correction: https://www.nature.com/articles/s41467-024-47500-4

[AC16] NMR Relaxation Rates of Quadrupolar Aqueous Ions from Classical Molecular Dynamics Using Force-Field Specific Sternheimer Factors
I. Chubak, L. Scalfi, A. Carof and B. Rotenberg
J. Chem. Theory Comput. **17**, 10, 6006-6017 (2021).
DOI: https://doi.org/10.1021/acs.jctc.1c00690
Preprint: arXiv:2107.04355

[AC15] Carbon species solvated in molten carbonate electrolyser cell from first-principles simulations
A. Carof, F.X. Coudert, D. Corradini, D. Lesnicki, E. Desmaele and R. Vuilleumier
Int. J. Hydrog. Energy **46**, 28, 15008-15023 (2021).
DOI: https://doi.org/10.1016/j.ijhydene.2020.10.022

[AC14] Flickering Polarons Extending over Ten Nanometres Mediate Charge Transport in High-Mobility Organic Crystals
S. Giannini, Z. Orestis, A. Carof, M. Ellis and J. Blumberger
Adv. Theory Simul. **3**, 9, 2000093 (2020).
DOI: https://doi.org/10.1002/adts.202000093

[AC13] Ultrafast light-driven electron transfer in Ru(II) tris(bipyridine)-labeled multiheme cytochrome
J.H. van Wonderen, C.R. Hall, X. Jiang, K. Adamczyk, A. Carof, I. Heisler, S.E.H. Piper, T.A. Clarke, N.J. Watmough, I.V. Sazanovich, M. Towrie, S.R. Meech, J. Blumberger et J.N. Butt
JACS **141**, 38, 15190-15200 (2019).
DOI: https://doi.org/10.1021/jacs.9b06858

[AC12] Quantum localization and delocalization of charge carriers in organic semiconducting crystals
S. Giannini, A. Carof, M. Ellis, H. Yang, O.G. Ziogos, S. Ghosh and J. Blumberger,
Nature comm. **10**, 1, 1-12 (2019).
DOI: https://doi.org/10.1038/s41467-019-11775-9

[AC11] How to calculate charge mobility in molecular materials from surface hopping non-adiabatic molecular dynamics-beyond the hopping/band paradigm
A. Carof, S. Giannini and J. Blumberger,
Phys. Chem. Chem. Phys. **21**, 48, 26368-26386 (2019).
DOI: https://doi.org/10.1039/C9CP04770K

[AC10] Crossover from Hopping to Band-Like Charge Transport in Organic Semiconductor Model: Atomistic Nonadiabatic Molecular Dynamics
S. Giannini, A. Carof and J. Blumberger,
J. Phys. Chem. Lett. **9**, 11, 3116-3123 (2018).
DOI: https://doi.org/10.1021/acs.jpclett.8b01112

[AC9] Detailed balance, internal consistency, and energy conservation in fragment orbital-based surface hopping
A. Carof, S. Giannini and J. Blumberger,
J. Chem. Phys. **147**, 21, 214113 (2017). **Editor's choice**
DOI: https://doi.org/10.1063/1.5003820

[AC8] Cysteine linkages accelerate electron flow through tetra-heme protein STC
X. Jiang, Z. Futera, E. Ali, F. Gajdos, G. von Rudorff, A. Carof, M. Breuer and J. Blumberger,
JACS Communication **139**, 48, 17237-17240 (2017).
DOI: https://doi.org/10.1021/jacs.7b08831
Correction: https://doi.org/10.1021/jacs.2c02709

[AC7] Confronting surface hopping molecular dynamics with Marcus theory for a molecular donor-acceptor system
J. Spencer, L. Scalfi, A. Carof and J. Blumberger,
Faraday Discuss. **195**, 215-236 (2016).
DOI: https://doi.org/10.1039/C6FD00107F

[AC6] Collective water dynamics in the first solvation shell drive the NMR relaxation of aqueous quadrupolar ion
A. Carof, M. Salanne, T. Charpentier and B. Rotenberg,
J. Chem. Phys. **145**, 124508 (2016).
DOI: https://doi.org/10.1063/1.4963682

[AC5] Molecular hydrodynamics from memory kernels
D. Lesnicki, A. Carof, R. Vuilleumier and B. Rotenberg,
Phys. Rev. Lett. **116**, 147804 (2016).
DOI: https://doi.org/10.1103/PhysRevLett.116.147804
Preprint: arXiv:1605.03075

[AC4] On the microscopic fluctuations driving the NMR relaxation of quadrupolar ions in waters
A. Carof, M. Salanne, T. Charpentier and B. Rotenberg,
J. Chem. Phys. **143**, 194504 (2015).
DOI: https://doi.org/10.1063/1.4935496

[AC3] Accurate Quadrupolar NMR Relaxation Rates of Aqueous Cations from Classical Molecular Dynamics
A. Carof, M. Salanne, T. Charpentier and B. Rotenberg,
J. Phys. Chem. B **18**, 13252 (2014).
DOI: https://doi.org/10.1021/jp5105054

[AC2] Two algorithms to compute projected correlation functions in molecular dynamics simulations
A. Carof, R. Vuilleumier and B. Rotenberg,
J. Chem. Phys. **140**, 124103 (2014).
DOI: https://doi.org/10.1063/1.4868653

[AC1] Coarse-graining the dynamics of nano-confined solutes: The case of ions in clays
A. Carof, V. Marry, M. Salanne, J.-P. Hansen, P. Turq and B. Rotenberg,
Mol. Simul. **40**, 237 (2013).
DOI: https://doi.org/10.1080/08927022.2013.840894

II Chapters of books

[1] Chapter 6. From Atomic Orbitals to Nano-scale Charge Transport with Mixed Quantum/Classical Non-adiabatic Dynamics: Method, Implementation and Application.
S. Giannini, A. Carof, M. Ellis, O.G. Ziogos and J. Blumberger,
Theoretical and Computational Chemistry Series (eds. Salahub, D. R. and Wei, D.) 172-202 (Royal Society of Chemistry, 2021).

III Oral communication at conferences

Nov. 2024	**SolvATE24**, Dijon, France Fast calculation of solvation structure and thermodynamics in supercritical CO_2
Juin 2024	**RCTF**, Rouen, France Fast calculation of solvation structure and thermodynamics in supercritical CO_2
Sept. 2023	**EMLG-JMLG**, Bordeaux, France Ultrafast calculation of solvation in supercritical CO_2 with cDFT
Sept. 2023	**DFTDays**, Tübingen, Germany Ultrafast calculation of solvation in supercritical CO_2 with cDFT
Juin 2023	**SCF2023**, Nantes, France Ultrafast calculation of solvation in supercritical CO_2 with cDFT
Oct. 2022	**JTMS22**, Rennes, France Ultrafast calculation of solvation in supercritical CO_2 with cDFT
Sept. 2022	**DFTDays**, Tübingen, Germany Ultrafast calculation of solvation in supercritical CO_2 with cDFT
Juin 2021	**IWOM**, online (invited conference) How to calculate charge mobility in molecular materials from surface hopping
Juill. 2019	**IUPAC**, Paris, France Structure and solvation in molten carbonates with ab-initio simulation
Mai 2019	**MS11**, Orléans, France Structure and solvation in molten carbonates with ab-initio simulation
Mai 2018	**JTMS18**, Paris, France Modeling charge transfer in organic crystals : Fragment Orbital-Based Surface Hopping
Sept. 2017	**ECPC17**, Borgo, France Ultrafast calculation of solvation in supercritical CO_2 with cDFT
Juill. 2017	**CCP2017**, Paris, France Charge transfer in Organic Materials : Development of Fragment Orbital-Based Surface Hopping
Juin 2017	**CECAM: Seeking synergy between dynamics and statistics for non-equilibrium quantum processes**, Paris, France Detailed balance and detection of trivial crossing in FOB-SH
Avril 2017	**Faraday Joint Interest Group Conference**, Warwick, UK Electron Transfer in Organic and Biological Materials
Oct. 2016	**CPC16**, Nancy, France Electron Transfer in Biological Materials
Juin 2016	**CECAM Workshop: Different Routes to Quantum Molecular Dynamics**, Lausanne, Switzerland Electron Transfer in Organic and Biological Materials
Août 2015	**ICSC**, Prague, Czech Republic Water dynamics around alkaline cations: Molecular Dynamics simulation of NMR relaxation time
Août 2014	**CMD 25 - JMC 14**, Paris, France Water dynamics around alkaline cations: Molecular Dynamics simulation of NMR relaxation time

IV Poster communications at conferences

June 2025	*WATOC*, Oslo, Norway
June 2022	*JPH*, Paris, France
June 2019	*JTMS*, Paris, France
Oct. 2018	*CECAM Workshop: Dynamic Coarse-Graining and Memory Effects in Soft Matter System*, Mainz, Germany
Oct. 2018	*RCTF*, Toulouse, France
Oct. 2017	*CECAM CCDYN*, Bremen, Germany
August 2019	*WATOC2017*, Munich, Germany, **Best poster prize**
March 2017	*CMS*, Warwick, UK
Sept. 2016	*Faraday Discussion: Reaction Rate Theory*, Oxford, UK
Sept. 2016	*Future of Chemical Physics*, Cambridge, UK
July. 2014	*Gordon Research Seminar and Conference: Water & Aqueous Solutions*, Holderness, USA
June 2014	*WaterEurope* Zaragoza, Spain

V Invited seminars

Feb. 2019	*LPCT*, Nancy, France
Sept. 2018	*LPTMC*, Paris, France
Oct. 2016	*Paris en résonance*, Paris, France
Oct. 2016	*Invited seminar, CEMHTI*, Orléans, France
Feb. 2016	*Invited seminar, Grey Group*, Cambridge, UK
Feb. 2016	*CP2K UK User Meeting* , London, UK
Sept. 2014	*Journées Modélisation* , Paris, France
Oct. 2013	*Journée relaxométrie*, Paris, France
Oct. 2013	*JFJPC*, Frejus, France

VI Communications by researchers under supervision

Nov. 2023	**SolvATE2023**, Nancy, France M. Houssein Mohamed, poster communication
Sept. 2023	**DFT Days**, Tübingen, Germany M. Houssein Mohamed, poster communication
Juil. 2023	**SFP**, Paris, France M. Houssein Mohamed, oral presentation
Mai 2023	**RCTGE**, Reims, France M. Houssein Mohamed, oral presentation
Juil. 2022	**RCTF**, Nancy, France M. Houssein Mohamed, poster communication

VII Details of Scientific Supervisions

Thesis of M. Houssein Mohamed (10/2021-09/2024). Topic: Development of an ultra-efficient method for calculating solvation in supercritical CO_2.

I had the opportunity to be the co-director (50% supervision) of M. Houssein Mohamed with F. Ingrosso (director, 50% supervision). I defended the thesis project to the CPM department council in March 2021 and obtained my authorization to co-direct a thesis in September 2022. Table A.1 summarizes the achievements obtained during this thesis.

Table A.1 – Achievements obtained by M. Houssein Mohamed during his thesis.

Publication	Molecular integral equations theory in the near critical region of CO_2, M. Houssein Mohamed, L. Belloni, D. Borgis, F. Ingrosso et A. Carof, *J. Mol. Liq.*, **418**, 126623 (2025). [AC23]
Oral presentations at conferences	2022, Master of Physics Day, Nancy 2023, RCTF-Grand Est, Reims 2023, Congress of the Société Française de Physique (SFP), Paris
Poster presentations at conferences	2023, RCTF, Bordeaux 2023, DFT Days, Tübingen (Germany) 2023, SolvATE, Nancy
Future of the Doctor	Post-doctorate at the PHENIX laboratory (Sorbonne Université)

Since my arrival at the University of Lorraine, I have also been heavily involved in supervising M1 and M2 internships at the Faculty of Science and Technology (FST). Table A.2 lists all the internships I have supervised or co-supervised since 2021.

Table A.2 – List of M1 or M2 interns supervised or co-supervised since my recruitment at LPCT in 2019.

Date	Level	Student(s)	Topic	Co-supervision
02/25—07/25	M2 Physics	C. Cao	Statistical field theory to study CO_2 in confinement	
01/24—03/24	M1 Physics	C. Wenger and N. Couval	Confined fluid: Simulation by classical density functional theory	Co-supervisor: D. Lesnicki
02/23—07/23	M2 Physics	G. Szczepan	Density functional theory near the critical point	
02/23—07/23	M2 Chemistry	R. Martin	Simulation of chiral liquids in the presence of an electric field	Main supervisor: C. Millot
01/23—03/23	M1 Physics	A. Tarif Almodares	Statistical physics of fluids	
02/22—07/22	M2 Chemistry	M. Msaad	Rotation/translation coupling in water	Main supervisor: C. Millot
01/22—03/22	M1 Physics	J. Klein and G. Szczepan	Dynamic transition in supercritical fluids, what impact on thermodynamics?	Co-supervisor: F. Ingrosso
02/21—07/21	M2 Physics	M. Houssein Mohamed	Rigid/non-rigid transitions of supercritical fluids. What impact on solubility?	Co-supervisor: F. Ingrosso
01/21—03/21	M1 Physics	M. Rieff and Q. Greffe	Modeling the solubility of hard spheres in supercritical fluids	Co-supervisor: F. Ingrosso

VIII Funding

Table A.3 summarizes all the funding obtained since my recruitment at the University of Lorraine. I am in particular the leader of an ANR JCJC selected in July 2024. It started in January 2025 and will allow me to recruit a PhD student starting in October 2025.

Table A.3 – List of funding and research contracts obtained following calls for projects since my recruitment at LPCT in 2019.

Contract Type	Year	Title	Role	Total Amount	Laboratory Share
Agence Nationale de la Recherche, JCJC	2025	Bridging the gap for CO_2 fluid modeling: a new multi-scale molecular liquid state theory (BAC2MOL)	Leader	168 k€	100%
UL International Research Partnerships	2024	Green Chemistry Strategies Driven by Molecular Modeling (GreenMoMod)	Partner (Leader: F. Ingrosso)	152 k€	100%
Thesis from the Doctoral School C2MP	2021	Développement d'une méthode ultra-efficace pour le calcul de la solvatation dans le CO_2 supercritique	Leader	100 k€	100%
CPM Call for Projects	2020		Leader	15 k€	100%

IX Dissemination and Outreach

Thesis Jury outside the institution Examiner of the thesis of J.-X. Bardaud (06/12/2024), Université de Saclay. Topic: Édifices moléculaires isolés sondés par spectroscopie laser : formation par vaporisation assistée par CO_2 supercritique et dissociation ionique contrôlée par microhydratation. [Bardaud, 2024]

Comité de suivi individuel I participate in individual monitoring committees of PhD students:

- Méthodes de modélisation innovantes pour décrire les propriétés des fluides, H.R. Asmuni (start 2023)
- Modèles de Richardson-Gaudin et systèmes quantiques ouverts, R. Burgun (start 2023)
- Description thermodynamique des machines quantique autonomes, Y. Jha (start 2023)
- Étude de la diffusion en présence de défauts topologiques et application aux tissues biologiques, A. Manapany (2020-2024)

Activities in Scientific Societies Since June 2024, I have been an elected member of the board of the Modeling and Simulation (ModSim) subdivision of the Physical Chemistry Division (DCP) of the Société Chimique de France (SCF). ModSim animates the scientific community around theory and modelling in physical chemistry: it nominates members for various national awards, co-awards the Gaston Berthier Prize with the ThéMoSiA GDR which distinguishes an exceptional thesis in theoretical chemistry, it also supports congresses and organizes the "Theory, Modelling, Simulation" days.

Conference Organization 2021: Co-organization of the CECAM conference in Dijon "Recent progress in the statistical mechanics of solutions through Kirkwood-Buff integrals and related approaches." (Main organizer: J.-M. Simon). This conference allowed me to meet part of the European and French community working on liquid theory, and in particular to strengthen my ties with L. Belloni and D. Borgis.

2023: Co-organization of the SolvATE2023 conference in Nancy (main organizer: F. Ingrosso). This conference brought together members of the SolvATE GDR (GDR 2035) in Nancy.

2025: Organization of the DFT Days conference. This conference brings together the community of classical DFT developers (static and dynamic). It was organized in Tübingen for 10 years. In collaboration with P. Illien, D. Lesnicki, G. Jeanmairet, we will organize it in Nancy in September 2025.

APPENDIX B

Teaching and Administrative Duties

I Synthesis of Teaching Activity

I.A Synthetic Presentation of Teaching Activity

Since my recruitment in 2019, I have been teaching computer science and digital technology in healthcare within the computer science department of the Faculté de Pharmacie de Nancy. My teachings are for all diploma programs at the faculty.: Diplôme de Formation Générale en Sciences Pharmaceutiques (DFG-SP2 and DFG-SP3, equivalent to L2/L3), Diplôme de Formation Approfondie en Sciences Pharmaceutiques (DFA-SP1 and DFA-SP2, equivalent to M1/M2), and the sixth year of the Diplôme d'État de Docteur en Sciences Pharmaceutiques (DE-SP). These courses are conducted in person and are part of initial training. My teaching load is approximately 210 hours (equivalent to TD hours) per year, primarily in the form of practical work (TP), but also lectures (CM), tutorials (TD), and student monitoring activities. The courses in which I participate are:

- TIC: Information and Communication Technologies (DFG-SP2, course leader, 102 TD hours, 100 students)
- DOC: Critical Analysis of Documents (DFG-SP3, 57.5 TD hours, 100 students)
- ODS: Health Data Tools (DFA-SP1, 9 TD hours, 100 students)
- MOD: Health Modelling (course leader, elective course, DFG-SP3, 33 TD hours, 20 students)
- TDS: Health Data Processing (course leader, elective course, DFA-SP2, industry track, 13.5 TD hours, 5 students)
- SCD: Future of Connected Health (DE-SP, pharmacy track, 11.5 TD hours, 80 students)

I.B Pedagogical Evolution and Transformation of Teaching

Since my arrival in 2019, I have actively participated in the reflection and evolution of teaching within the computer science section of the college of Pharmacy. Indeed, digital health is a rapidly changing field that is transforming the professions of pharmacists, whether in pharmacies (digitization of the care circuit, digital prescriptions, Mon Espace Santé, in the industrial world (connected objects, new data-based production methods), or in research. To respond to these transformations, the French government implemented a strategy in 2021 to accelerate digital health, which includes a deepening of digital skills in the initial training of health studies. This deepening is codified in a national competency framework through a specific decree. [Ministère de la Santé et de la Prévention, 2022] We therefore conducted an analysis of our courses during the 2021-2022 academic year to propose evolutions in our teaching and respond to this new framework. Following this reflection, I created two elective courses in 2022 for pharmacy students interested in data professions in the pharmaceutical world. I also participated in establishing a convention between the college of Pharmacy and the TELECOM Nancy engineering school to allow pharmacy students to integrate TELECOM Nancy and obtain a double diploma in pharmacy and engineering. I also helped reorganize the ODS course in 2024, at the heart of the teaching on digital health.

In addition to these developments, I took responsibility for the TIC course (2nd year) in 2021, reorganizing the course to allow students to take the PIX certification and introduce them to new computer tools offered by the University of Lorraine. I also created new practical work on health databases, infographics, and information monitoring. I also implemented and shared with my colleagues new teaching methods (based on the interactive software Wooclap, in particular).

I.C Detailed Presentation of Courses

Table B.1 presents all my courses at the college of Pharmacy of Nancy, with a brief description of the content given below (UEB: Basic Course, UEO: Mandatory Course, UEL: Elective Course).

UEB Information and Communication Technology (TIC). This 2nd-year course aims to provide students with the necessary computer skills for their studies: word processing, computer-assisted presentations, spreadsheets, tools for communication and collaboration. This course also allows them to take the PIX certification, thus validating their computer skills.

UEB Critical Document Analysis (DOC). This course provides students with the tools for documentary research: online information search, use of bibliographic software, information search in specific databases (medication databases, open data digital databases), critical reading of articles.

UEB Distribution-Dispensing-Traceability of Medicines (DIS). I participated in this 3rd-year course for three years during the practical work on the discovery and use of dispensing assistance software.

UEB Health Data and Tools (ODS). This 4th-year course presents to students the essential developments in their future professions as pharmacists with regard to digital health. It covers

most of the points of the national digital competency framework. [Ministère de la Santé et de la Prévention, 2022] I have been involved since 2021 to present a course on artificial intelligence and algorithms in health, as well as a tutorial on information monitoring for pharmacists.

UEO Future of Connected Health (SCD). This 6th-year course, pharmacy track, allows students to reflect on the impacts of digital technology on the profession of community pharmacist. I help students prepare their report and then summarize the latest developments in the pharmaceutical world regarding artificial intelligence and algorithms in health.

Legislation/Management. As part of the reform of pharmacy technician studies (beginning in 2024/2025), the computer science department was responsible for presenting digital health to them. I intervene in the field of cybersecurity.

UEL Health Modelling (MOD). I created this elective course in 2022, with the aim of familiarizing students with the modelling of processes in the health world. It introduces students to mathematical notions (probability, statistics, regression), algorithms, and the description of databases. Students must then carry out a modelling or database analysis project.

UEL Health Data Processing (TDS). In the 5th year, industry track, the UEL TDS focuses on the processing of health data in the industrial world. It details the industrial approach to be implemented (governance, new professions), offers to discover the codes used to process data (Python, SQL), to visit the Lorraine datacenter, and to participate in a half-day dedicated to AI in health (drug design, pharmaceutical decision support, optimization of production processes).

I.D Other Pedagogical Activities at the University of Lorraine

In addition to my teaching, I participate in other supervision and tutoring activities at the College of Pharmacy and the University of Lorraine. The detailed list of these activities and the associated framework is presented in Table B.2.

Student Monitoring. The courses for monitoring students for their professional orientation were set up in 2019 and 2020 (UEB POP1 and POP2). As part of these courses, I am a tutor for 4 students per year, with whom I hold 2 or 3 individual meetings to discuss their career choices, their feelings about pharmacy studies, and to advise them on their track choice (industry, pharmacy, or hospital tracks, the choice being made in the 4th year).

PharmD Thesis. I participate in the supervision of doctor of pharmacy (PharmD) theses (2 defended, 4 ongoing) and in the juries (2 participations). These theses mainly concern artificial intelligence and digital health. In detail, I was co-director of two PharmD theses defended in 2024:

— Processing of health affairs in the media, impact on health perception and role of the community pharmacist, C. Sakfa, 2024,

— Optimizing the care of patients with ocular diseases through algorithms, M.-A. J. Hobekkaya, 2024.

I am currently director or co-director of 4 PharmD theses:

Table B.1 – Detailed list of fundamental and optional courses conducted at the College of Pharmacy of Nancy. The hours of lectures (CM), tutorials (TD), practical work (TP), and the number of students are given as an indication and reflect the workload provided since 2020.

Type	Course name	Period	hCM	hTD	hTP	Level	Number of Students
Fundamental Courses	Information and Communication Technology (TIC)	2020-...	1.5		100	DFG-SP2 (L2)	Group of 25, class of 100
	Critical Document Analysis (DOC)	2020-...		7.5	50	DFG-SP3 (L3)	Group of 25, class of 100
	Distribution-Dispensing-Traceability of Medicines (DIS)	2020-2023			6	DFA-SP1 (M1)	Group of 25, class of 100
	Health Data and Tools (ODS)	2021-...	1	7.5		DFA-SP1 (M1)	Group of 25, class of 100
	Future of Connected Health (SCD)	2020-...	1		10	DE-SP, pharmacy track	Group of 30, class of 80
	Legislation / Management	2024-...	1			DEUST2 Pharmacy Technician	Class of 150
Optional Courses	Health Modeling (MOD)	2022-...		3	30	DFG-SP3 (L3)	Group of 20 students
	Health Data Processing (TDS)	2022-...		1.5	12	DFA-SP2, industry track (M2)	Group of 5

— What are the key success factors for an effective integration of generative AI in the work experience of pharmaceutical laboratory employees in France?, A. Weber,
— Pharmacy in the era of intelligent systems: between expectations and concerns, H. Bolettieri,
— The use of artificial intelligence in the industry: a catalyst for the revolution of the pharmaceutical supply chain, V. Baesjou,
— The influence of social networks on dietary supplements, from their beneficial effects to their deleterious effects, D. Joly.

Internship Monitoring. I regularly monitor hospital internships and application internships of students in the industry track, and I have also been a reference teacher for a student in the 6th year of the industry track.

Hack'in Pharma. Since January 2024, I have been one of the three teachers accompanying the Hack'in Pharma team of the College of Pharmacy of Nancy. Hack'in Pharma is a competition between teams from different faculties of pharmacy. After 33 hours of continuous work, each team presents a start-up project to a jury composed of industrialists and patient associations. The winning teams will be helped to launch their start-up. I help the students during their preparation before the event and I participate with them in the two days of Hack'in Pharma in Saclay. The Nancy team won the jury prize in March 2025.

Open Days. I participate every year in the Open Days of the College of Pharmacy, particularly to present the computer platform and its equipment (serious games, teleconsultation terminal, connected health objects).

Internship Supervision. I have also had the opportunity to supervise various research internships at the laboratory (LPCT): 5 M1 interns and 4 M2 interns from the College of Science and Technology (University of Lorraine). These internships are detailed in Section VII on scientific supervision.

I.E Dissemination and Scientific Outreach Activities

I have been participating for several years in the organization of the International Chemistry Olympiads (IChO). In 2019, I participated in the creation of the competition subjects during the international events in Paris. Since 2019, I have been involved in the preparation of students in preparatory classes (Poincaré high school, Nancy) for the preselection test. I present 3 or 4 hours of classes per year (equivalent to tutorials) to about ten students. These classes allow me to teach on a theme different from my position at the College of Pharmacy. I also regularly participate in the Science Festival organized by the College of Science and Technology, at the stand of the laboratory dedicated to modelling in chemistry. We present different visualizations of molecular concepts to classes of students (from primary to high school) using various tools (virtual reality, origami, molecular simulation videos, candies).

Table B.2 – List of teaching duties carried out at the University of Lorraine. The number of students is given as an indication and reflects the workload provided since 2020.

Type	Course name	Period	Hours equivalence	Level	Number of students
Internship Monitoring and Tutoring	Professional Orientation Project 1 (POP1)	2020-...	1/student	DFG-SP2 (L2)	1 to 3 students per year
	Professional Orientation Project 2 (POP2)	2021-...	1/student	DFG-SP3 (L3)	1 to 3 students per year
	Monitoring of hospital and industrial internships	2022-...	4/student	DFA-SP2, industry track (M2)	1 to 3 students per year
	Supervision of PharmD theses	2024-...	2/student	Doctoral	1 to 3 students per year
	Monitoring of master's internships	2021-...	1/student in M1, 3/student in M2	M1 and M2 Physics	1 to 3 students per year

II Administrative and collective activities

Member of the Unit Council. (2023-...) Since June 2023, I have been a member of the unit council of the LPCT laboratory. I joined the council during a special renewal to prepare for the new contractualisation, following the recommendations of the Hcéres (the independent public authority responsible for evaluating all higher education and research structures). During this transitional phase, we were able to consider the opinions of all laboratory members and proposed a new governance model, rebalancing the roles of the management, the unit council, and the general assembly. During the elections for the new laboratory contract (2024-2029), I was re-elected to the council (college of category B executives). The council meets about ten times a year to discuss topics essential to the life of the laboratory: budget, scientific activities, selection of theses supported for applications to the doctoral school or the region, decisions on the computing cluster.

Ecological Transition Correspondent. (2022-...) Interested in the issues of ecological and energy transition, I spontaneously applied to the laboratory management to become the ecological transition correspondent for the laboratory. I have set up waste sorting bins and initiated a reflection on the laboratory's carbon emissions. I lead a working group within the laboratory to implement the carbon assessment, with the goal of proposing a first assessment in 2025. I also participate in the network of sustainable correspondents of the University, through which I regularly train on climate issues and participate in discussions on the evolution of the campus.

Member of the Computer Science Commission. (2019-...) The commission advises the unit council and the laboratory management on the management of the computer equipment, both for users (office automation) and for computing machines (storage, computing power, and long-term perspectives). It meets about six times a year. I joined it in 2019 upon my arrival at

the laboratory as a user of the computing cluster. The commission has had to make important decisions on the management of the cluster, outsourcing to an external company, the purchase of computing and storage machines, or the positioning of the cluster in relation to the University's data centre and the regional computing mesocentre (eXplor).

Open Science Ambassador. (2023-...) The LPCT is both a major producer of data and a developer of codes and software, but this data and these codes are not always fully utilized. Interested in new tools to promote the opening of data, codes, and publications, I joined the network of data ambassadors of the University of Lorraine in 2023 (which became the network of Open Science ambassadors in 2025). This network allowed me to train on issues related to the opening and reuse of data, the creation of data management plans, and bibliographic tools. I was then able to raise awareness among laboratory members on these issues during general assemblies or during the half-day for new entrants (four times a year).

APPENDIX C

Mathematical Details for the Chapter 3

I Correlation of the noises in Fourier space and using spherical harmonics expansion

I.A Space and time Fourier transforms

In the chapter 3, we are dealing with noise correlation of the form

$$\langle \Xi(\boldsymbol{r},t)\Xi(\boldsymbol{r}',t')\rangle = -\nabla^2\delta(\boldsymbol{r}-\boldsymbol{r}')\delta(t-t') \tag{C.1}$$

We perform a Fourier transform, $\tilde{\Xi}(\boldsymbol{k},t) = \int \mathrm{d}\boldsymbol{r}\exp(\mathrm{i}\boldsymbol{r}\cdot\boldsymbol{k})\Xi(\boldsymbol{r},t)$ and obtain

$$\langle \tilde{\Xi}(\boldsymbol{k},t)\tilde{\Xi}(\boldsymbol{k}',t')\rangle = \int \mathrm{d}\boldsymbol{r}\int \mathrm{d}\boldsymbol{r}'\,\langle \Xi(\boldsymbol{r},t)\Xi(\boldsymbol{r}',t')\rangle \exp(\mathrm{i}\boldsymbol{r}\cdot\boldsymbol{k}+\mathrm{i}\boldsymbol{r}'\cdot\boldsymbol{k}') \tag{C.2}$$

$$= -\int \mathrm{d}\boldsymbol{r}\int \mathrm{d}\boldsymbol{r}'\nabla^2\delta(\boldsymbol{r}-\boldsymbol{r}')\delta(t-t')\exp(\mathrm{i}\boldsymbol{r}\cdot\boldsymbol{k}+\mathrm{i}\boldsymbol{r}'\cdot\boldsymbol{k}') \tag{C.3}$$

After performing a double integration by parts, we get

$$\langle \tilde{\Xi}(\boldsymbol{k},t)\tilde{\Xi}(\boldsymbol{k}',t')\rangle = \int \mathrm{d}\boldsymbol{r}\int \mathrm{d}\boldsymbol{r}'\,\langle \Xi(\boldsymbol{r},t)\Xi(\boldsymbol{r}',t')\rangle \exp(\mathrm{i}\boldsymbol{r}\cdot\boldsymbol{k}+\mathrm{i}\boldsymbol{r}'\cdot\boldsymbol{k}') \tag{C.4}$$

$$= k^2\int \mathrm{d}\boldsymbol{r}\int \mathrm{d}\boldsymbol{r}'\delta(\boldsymbol{r}-\boldsymbol{r}')\exp(\mathrm{i}\boldsymbol{r}\cdot\boldsymbol{k}+\mathrm{i}\boldsymbol{r}'\cdot\boldsymbol{k}')\delta(t-t') \tag{C.5}$$

$$= k^2\int \mathrm{d}\boldsymbol{r}\exp(\mathrm{i}\boldsymbol{r}\cdot(\boldsymbol{k}+\boldsymbol{k}'))\delta(t-t') \tag{C.6}$$

$$= (2\pi)^3k^2\delta(\boldsymbol{k}+\boldsymbol{k}')\delta(t-t') \tag{C.7}$$

The time Fourier transform reads

$$\langle\tilde{\Xi}(\boldsymbol{k},\omega)\tilde{\Xi}(\boldsymbol{k}',\omega')\rangle = \int \mathrm{d}t \int \mathrm{d}t' \left\langle \tilde{\Xi}(\boldsymbol{k},t)\tilde{\Xi}(\boldsymbol{k}',t')\right\rangle \exp(\mathrm{i}\omega t + \mathrm{i}\omega' t') \tag{C.8}$$

$$= (2\pi)^3 k^2 \int \mathrm{d}t \int \mathrm{d}t' \delta(\boldsymbol{k}+\boldsymbol{k}')\delta(t-t')\exp(\mathrm{i}\omega t + \mathrm{i}\omega' t') \tag{C.9}$$

$$= (2\pi)^3 k^2 \delta(\boldsymbol{k}+\boldsymbol{k}') \int \mathrm{d}t \exp(\mathrm{i}\omega t + \mathrm{i}\omega' t) \tag{C.10}$$

$$= (2\pi)^4 k^2 \delta(\boldsymbol{k}+\boldsymbol{k}')\delta(\omega+\omega') \tag{C.11}$$

$$\tag{C.12}$$

I.B Spherical harmonics expansion

We expand the noise as

$$\Xi(\boldsymbol{r},t) = \sum_{l=0}^{\infty}\sum_{m=-l}^{l} \Xi^{lm}(r,t)Y_{lm}(\Omega)\ , \tag{C.13}$$

where the spherical harmonics coefficients are defined by

$$\Xi^{lm}(r,t) = \int \mathrm{d}\Omega\, \Xi(\boldsymbol{r},t)Y_{lm}(\Omega)\ . \tag{C.14}$$

The correlations of the spherical harmonics coefficient read

$$\left\langle \Xi^{lm}(r,t)\Xi^{l'm'}(r',t')\right\rangle = \int \mathrm{d}\Omega \int \mathrm{d}\Omega' \langle \Xi(\boldsymbol{r},t)\Xi(\boldsymbol{r}',t')\rangle Y_{lm}(\Omega)Y_{lm}(\Omega') \tag{C.15}$$

$$= -\int \mathrm{d}\Omega \int \mathrm{d}\Omega' \nabla^2 \delta(\boldsymbol{r}-\boldsymbol{r}')\delta(t-t')Y_{lm}(\Omega)Y_{lm}(\Omega') \tag{C.16}$$

After performing a double integration by parts, we get

$$\left\langle \Xi^{lm}(r,t)\Xi^{l'm'}(r',t')\right\rangle = l(l+1)\int \mathrm{d}\Omega \int \mathrm{d}\Omega' \frac{1}{r^2}\delta(\boldsymbol{r}-\boldsymbol{r}')Y_{lm}(\Omega)Y_{lm}(\Omega')\delta(t-t') \tag{C.17}$$

$$= l(l+1)\int \mathrm{d}\Omega \int \mathrm{d}\Omega' \frac{\delta(r-r')}{r^4}$$

$$\times \sum_{l''m''} Y_{l''m''}(\Omega)Y_{l''m''}(\Omega')Y_{lm}(\Omega)Y_{l'm'}(\Omega')\delta(t-t') \tag{C.18}$$

$$= l(l+1)\frac{\delta(r-r')}{r^4}\int \mathrm{d}\Omega Y_{l'm'}(\Omega)Y_{lm}(\Omega)\delta(t-t') \tag{C.19}$$

$$= l(l+1)\frac{\delta(r-r')}{r^4}\delta_{ll'}\delta_{mm'}\delta(t-t') \tag{C.20}$$

Similarly, if we consider the noises in Fourier space,

$$\Xi(\boldsymbol{k},t)=\sum_{l=0}^{\infty}\sum_{m=-l}^{l}\Xi^{lm}(k,t)Y_{lm}(\Omega_k)\ , \tag{C.21}$$

where the spherical harmonics coefficients are defined by

$$\Xi^{lm}(k,t)=\int \mathrm{d}\Omega_k\ \Xi(\boldsymbol{k},t)Y_{lm}(\Omega_k)\ . \tag{C.22}$$

The correlations of the spherical harmonics coefficient read

$$\left\langle\tilde{\Xi}^{lm}(k,t)\tilde{\Xi}^{l'm'}(k',t')\right\rangle=\int \mathrm{d}\Omega_k\int \mathrm{d}\Omega'_k\langle\tilde{\Xi}(\boldsymbol{k},t)\tilde{\Xi}(\boldsymbol{k}',t')\rangle Y_{lm}(\Omega_k)Y_{lm}(\Omega'_k) \tag{C.23}$$

$$=(2\pi)^3k^2\int \mathrm{d}\Omega_k\int \mathrm{d}\Omega'_k\delta(\boldsymbol{k}+\boldsymbol{k}')\delta(t-t')Y_{lm}(\Omega_k)Y_{lm}(\Omega'_k) \tag{C.24}$$

$$=(2\pi)^3k^2\int \mathrm{d}\Omega_k\int \mathrm{d}\Omega'_k\frac{\delta(k-k')}{k^2}$$

$$\times\sum_{l''m''}Y_{l''m''}(\Omega_k)Y_{l''m''}(\Omega'_k)Y_{lm}(\Omega_k)Y_{lm}(\Omega'_k)\delta(t-t') \tag{C.25}$$

$$=(2\pi)^3\delta(k-k')\delta(t-t')\delta_{ll'}\delta_{mm'} \tag{C.26}$$

And after a time Fourier transform, we get

$$\left\langle\tilde{\Xi}^{lm}(k,\omega)\tilde{\Xi}^{l'm'}(k',\omega')\right\rangle=(2\pi)^4\delta(k-k')\delta(\omega+\omega')\delta_{ll'}\delta_{mm'} \tag{C.27}$$

II Green operator for SDFT with boundary conditions

II.A General solution

In time-Fourier space, the Green equation reads

$$\left(\mathrm{i}\omega+D_I\kappa_{\mathrm{imp}}^2\right)\tilde{G}_{\rho_I}-D_I\nabla^2\tilde{G}_{\rho_I}=\delta(\boldsymbol{r}-\boldsymbol{r}') \tag{C.28}$$

$$\partial_r\tilde{G}_{\rho_I}|_{r=\sigma}=0 \tag{C.29}$$

which amounts to an inhomogeneous Helmholtz equation with a Neumann boundary condition. We expand the Dirac function in spherical harmonics,

$$\delta(\boldsymbol{r}-\boldsymbol{r}')=\frac{1}{r^2}\delta(r-r')\sum_{lm}Y_{lm}(\Omega)Y^*_{lm}(\Omega') \tag{C.30}$$

which leads to

$$\left(\mathrm{i}\omega + D_I\kappa_{\mathrm{imp}}^2\right)\tilde{G}^l_{\rho_I}(r,r') - D_I\Delta^l_r\tilde{G}^l_{\rho_I}(r,r') = \frac{1}{r^2}\delta(r-r') \tag{C.31}$$

$$\partial_r\tilde{G}^l_{\rho_I}(r,r')|_{r=\sigma} = 0 \tag{C.32}$$

We re-write the Helmholtz equation in the usual form,

$$\left(\frac{\mathrm{d}^2}{\mathrm{d}^2 r} + \frac{2}{r}\frac{\mathrm{d}}{\mathrm{d}r} + \lambda^2 - \frac{l(l+1)}{r^2}\right)\tilde{G}^l_{\rho_I}(r,r') = -\frac{\delta(r-r')}{D_I r r'} \tag{C.33}$$

$$\lambda^2 = -\frac{\mathrm{i}\omega}{D_I} - \kappa_{\mathrm{imp}}^2 \tag{C.34}$$

We solve this equation interval by interval. For $\sigma < r'$

$$\sigma \le r < r' : \tilde{G}^{l<}_{\rho_I}(r,r') = a(r')j_l(\lambda r) + b(r')y_l(\lambda r) \tag{C.35}$$

$$r' < r : \tilde{G}^{l>}_{\rho_I}(r,r') = c(r')j_l(\lambda r) + d(r')y_l(\lambda r) \tag{C.36}$$

The boundary condition at $r = \sigma$ implies

$$a(r')j_l'(\lambda\sigma) + b(r')y_l'(\lambda\sigma) = 0 \tag{C.37}$$

or

$$\frac{a(r')}{b(r')} = -\frac{y_l'(\lambda\sigma)}{j_l'(\lambda\sigma)} \tag{C.38}$$

and

$$\sigma \le r < r' : \tilde{G}^{l<}_{\rho_I}(r,r') = A(r')\left(y_l'(\lambda\sigma)j_l(\lambda r) - j_l'(\lambda\sigma)y_l(\lambda r)\right) \tag{C.39}$$

II.B Results at $\omega = 0$

In the following, we will restrict to $\omega = 0$, which gives $\lambda = \mathrm{i}\kappa_{\mathrm{imp}}$. We will use the modified Bessel function, $i_l(x) = j_l(\mathrm{i}x)$ and $k_l(x) = y_l(\mathrm{i}x)$. For $\sigma \le r'$, we obtain

$$\sigma \le r < r' : \tilde{G}^{l<}_{\rho_I}(r,r') = B(r')\left(k_l'(\kappa_{\mathrm{imp}}\sigma)i_l(\kappa_{\mathrm{imp}}r) - i_l'(\kappa_{\mathrm{imp}}\sigma)k_l(\kappa_{\mathrm{imp}}r)\right) \tag{C.40}$$

with $B = -iA$. The divergence of i_l for $x \to \infty$ imposes that $c(r') = 0$. The continuity conditions at $r = r'$ imposes

$$B(r')\left(k_l'(\kappa_{\text{imp}}\sigma)i_l(\kappa_{\text{imp}}r') - i_l'(\kappa_{\text{imp}}\sigma)k_l(\kappa_{\text{imp}}r')\right) = d(r')k_l(\kappa_{\text{imp}}r') \tag{C.41}$$

And,

$$\lim_{\varepsilon\to 0}\left[\frac{\mathrm{d}}{\mathrm{d}r}\tilde{G}^l_{\rho_I}(r,r')\right]_{r=r'-\varepsilon}^{r=r'+\varepsilon} = -\frac{1}{D_I r'^2} \tag{C.42}$$

which leads to

$$\kappa_{\text{imp}}d(r')k_l'(\kappa_{\text{imp}}r') - \kappa_{\text{imp}}B(r')\left(k_l'(\kappa_{\text{imp}}\sigma)i_l'(\kappa_{\text{imp}}r') - i_l'(\kappa_{\text{imp}}\sigma)k_l'(\kappa_{\text{imp}}r')\right) = -\frac{1}{D_I r^2} \tag{C.43}$$

Here we solve the linear system with two equations and two unknowns:

$$\kappa_{\text{imp}}d(r')k_l'(\kappa_{\text{imp}}r') - \kappa_{\text{imp}}B(r')\left(k_l'(\kappa_{\text{imp}}\sigma)i_l'(\kappa_{\text{imp}}r') - i_l'(\kappa_{\text{imp}}\sigma)k_l'(\kappa_{\text{imp}}r')\right) = -\frac{1}{D_I r^2} \tag{C.44}$$

$$d(r')k_l(\kappa_{\text{imp}}r') - B(r')\left(k_l'(\kappa_{\text{imp}}\sigma)i_l(\kappa_{\text{imp}}r') - i_l'(\kappa_{\text{imp}}\sigma)k_l(\kappa_{\text{imp}}r')\right) = 0 \tag{C.45}$$

$$\kappa_{\text{imp}}d(r')k_l'(\kappa_{\text{imp}}r')k_l(\kappa_{\text{imp}}r') - \kappa_{\text{imp}}k_l(\kappa_{\text{imp}}r')B(r')\left(k_l'(\kappa_{\text{imp}}\sigma)i_l'(\kappa_{\text{imp}}r') - i_l'(\kappa_{\text{imp}}\sigma)k_l'(\kappa_{\text{imp}}r')\right) = -\frac{k_l(\kappa_{\text{imp}}r')}{D_I r^2} \tag{C.46}$$

$$\kappa_{\text{imp}}d(r')k_l(\kappa_{\text{imp}}r')k_l'(\kappa_{\text{imp}}r') - \kappa_{\text{imp}}k_l'(\kappa_{\text{imp}}r')B(r')\left(k_l'(\kappa_{\text{imp}}\sigma)i_l(\kappa_{\text{imp}}r') - i_l'(\kappa_{\text{imp}}\sigma)k_l(\kappa_{\text{imp}}r')\right) = 0 \tag{C.47}$$

It gives

$$B(r')\Big[-\kappa_{\text{imp}}k_l(\kappa_{\text{imp}}r')\left(k_l'(\kappa_{\text{imp}}\sigma)i_l'(\kappa_{\text{imp}}r') - i_l'(\kappa_{\text{imp}}\sigma)k_l'(\kappa_{\text{imp}}r')\right) \tag{C.48}$$

$$+\kappa_{\text{imp}}k_l'(\kappa_{\text{imp}}r')\left(k_l'(\kappa_{\text{imp}}\sigma)i_l(\kappa_{\text{imp}}r') - i_l'(\kappa_{\text{imp}}\sigma)k_l(\kappa_{\text{imp}}r')\right)\Big] = -\frac{k_l(\kappa_{\text{imp}}r')}{D_I r^2} \tag{C.49}$$

$$B(r') = -\frac{k_l(\kappa_{\text{imp}}r')}{\kappa_{\text{imp}}k_l'(\kappa_{\text{imp}}\sigma)D_I r^2\left[-k_l(\kappa_{\text{imp}}r')i_l'(\kappa_{\text{imp}}r') + k_l'(\kappa_{\text{imp}}r')i_l(\kappa_{\text{imp}}r')\right]} \tag{C.50}$$

Knowing that,

$$-k_l(x)i_l'(x) + k_l'(x)i_l(x) = -\frac{\pi}{2x^2} \tag{C.51}$$

we obtain,

$$B(r') = \frac{2\kappa_{\text{imp}} k_l(\kappa_{\text{imp}} r')}{\pi D_I k_l'(\kappa_{\text{imp}}\sigma)} \tag{C.52}$$

And

$$d(r') = \frac{2\kappa_{\text{imp}}}{\pi D_I k_l'(\kappa_{\text{imp}}\sigma)} \left(k_l'(\kappa_{\text{imp}}\sigma) i_l(\kappa_{\text{imp}} r') - i_l'(\kappa_{\text{imp}}\sigma) k_l(\kappa_{\text{imp}} r')\right) \tag{C.53}$$

$$= \frac{2\kappa_{\text{imp}}}{\pi D_I} \left(i_l(\kappa_{\text{imp}} r') - \frac{i_l'(\kappa_{\text{imp}}\sigma)}{k_l'(\kappa_{\text{imp}}\sigma)} k_l(\kappa_{\text{imp}} r')\right) \tag{C.54}$$

Bibliography

[Abragam, 1983] Abragam, A. (1983). The principles of nuclear magnetism. Clarendon Press ; Oxford University Press, Oxford [Oxfordshire]; New York.

[Acharya et al., 2015] Acharya, S., Nandi, M. K., Mandal, A., Sarkar, S., and Bhattacharyya, S. M. (2015). Diffusion of Small Solute Particles in Viscous Liquids: Cage Diffusion, a Result of Decoupling of Solute–Solvent Dynamics, Leads to Amplification of Solute Diffusion. J. Phys. Chem. B, page 150717062906004.

[Adar et al., 2018] Adar, R. M., Markovich, T., Levy, A., Orland, H., and Andelman, D. (2018). Dielectric constant of ionic solutions: Combined effects of correlations and excluded volume. J. Chem. Phys., 149(5):054504.

[Agency, 2022] Agency, I. E. (2022). CO2 storage resources and their development.

[Alizadeh et al., 2020] Alizadeh, V., Malberg, F., Pádua, A. A. H., and Kirchner, B. (2020). Are There Magic Compositions in Deep Eutectic Solvents? Effects of Composition and Water Content in Choline Chloride/Ethylene Glycol from Ab Initio Molecular Dynamics. J. Phys. Chem. B, 124(34):7433–7443.

[Altarsha et al., 2012a] Altarsha, M., Ingrosso, F., and Ruiz-Lopez, M. F. (2012a). A New Glimpse into the CO $_2$ -Philicity of Carbonyl Compounds. ChemPhysChem, 13(14):3397–3403.

[Altarsha et al., 2012b] Altarsha, M., Ingrosso, F., and Ruiz-López, M. F. (2012b). Cavity Closure Dynamics of Peracetylated β-Cyclodextrins in Supercritical Carbon Dioxide. J. Phys. Chem. B, 116(13):3982–3990.

[Anastas and Eghbali, 2010] Anastas, P. and Eghbali, N. (2010). Green Chemistry: Principles and Practice. Chem. Soc. Rev., 39(1):301–312.

[Anta et al., 1995] Anta, J., Lomba, E., Martín, C., Lombardero, M., and Lado, F. (1995). A fast method of solving the hypernetted-chain equation for molecular Lennard-Jones fluids. Mol. Phys., 84(4):743–755.

[Archer, 2009] Archer, A. J. (2009). Dynamical density functional theory for molecular and colloidal fluids: A microscopic approach to fluid mechanics. J. Chem. Phys., 130(1):014509.

[Archer et al., 2017] Archer, A. J., Chacko, B., and Evans, R. (2017). The standard mean-field treatment of inter-particle attraction in classical DFT is better than one might expect. J. Chem. Phys., 147(3).

[Avni et al., 2022a] Avni, Y., Adar, R. M., Andelman, D., and Orland, H. (2022a). Conductivity of Concentrated Electrolytes. Phys. Rev. Lett., 128(9):098002.

[Avni et al., 2022b] Avni, Y., Andelman, D., and Orland, H. (2022b). Conductance of concentrated electrolytes: Multivalency and the Wien effect. J. Chem. Phys., 157(15):154502.

[Azofra et al., 2013] Azofra, L. M., Altarsha, M., Ruiz-López, M. F., and Ingrosso, F. (2013). A theoretical investigation of the CO2-philicity of amides and carbamides. Theor. Chem. Acc., 132(4):1–9.

[Bagchi, 1989] Bagchi, B. (1989). Dynamics of Solvation and Charge Transfer Reactions in Dipolar Liquids. Annu. Rev. Phys. Chem., 40(1):115–141.

[Bagchi, 1998] Bagchi, B. (1998). Microscopic derivation of the Hubbard–Onsager–Zwanzig expression of limiting ionic conductivity. J. Chem. Phys., 109(10):3989–3993.

[Bagchi, 2001] Bagchi, B. (2001). Relation between orientational correlation time and the self-diffusion coefficient of tagged probes in viscous liquids: A density functional theory analysis. J. Chem. Phys., 115(5):2207–2211.

[Bagchi and Biswas, 1998] Bagchi, B. and Biswas, R. (1998). Ionic Mobility and Ultrafast Solvation: Control of a Slow Phenomenon by Fast Dynamics. Acc. Chem. Res., 31(4):181–187.

[Bagchi and Chandra, 1988] Bagchi, B. and Chandra, A. (1988). Dynamics of polar solvation: Route to single exponential relaxation via translational diffusion. Proc. Indian Acad. Sci. (Chem. Sci.), 100(4):353–357.

[Bagchi and Chandra, 1992] Bagchi, B. and Chandra, A. (1992). Ultrafast solvation dynamics: Molecular explanation of computer simulation results in a simple dipolar solvent. J. Chem. Phys., 97(7):5126–5131.

[Bagchi and Jana, 2010] Bagchi, B. and Jana, B. (2010). Solvation dynamics in dipolar liquids. Chem. Soc. Rev., 39(6):1936–1954.

[Banerjee and Bagchi, 2019] Banerjee, P. and Bagchi, B. (2019). Ions' motion in water. J. Chem. Phys., 150(19):190901.

[Banuti et al., 2017] Banuti, D. T., Raju, M., and Ihme, M. (2017). Similarity law for Widom lines and coexistence lines. Phys. Rev. E, 95(5):052120.

[Bardaud, 2024] Bardaud, J.-X. (2024). Édifices moléculaires isolés sondés par spectroscopie laser : formation par vaporisation assistée par CO2 supercritique et dissociation ionique contrôlée par microhydratation. Thèse de doctorat, Université Paris-Saclay.

[Bartle et al., 1991] Bartle, K. D., Clifford, A. A., Jafar, S. A., and Shilstone, G. F. (1991). Solubilities of Solids and Liquids of Low Volatility in Supercritical Carbon Dioxide. J. Phys. Chem. Ref. Data, 20(4):713–756.

[Becher et al., 2022] Becher, M., Horstmann, R., Kloth, S., Rössler, E. A., and Vogel, M. (2022). A Relation between the Formation of a Hydrogen-Bond Network and a Time-Scale Separation of Translation and Rotation in Molecular Liquids. J. Phys. Chem. Lett., 13(20):4556–4562.

[Becker et al., 2025] Becker, M. R., Netz, R. R., Loche, P., Bonthuis, D. J., Mouhanna, D., and Berthoumieux, H. (2025). Dielectric Properties of Aqueous Electrolytes at the Nanoscale. Phys. Rev. Lett., 134(15):158001.

[Belloni, 1993] Belloni, L. (1993). Inability of the hypernetted chain integral equation to exhibit a spinodal line. J. Chem. Phys., 98(10):8080–8095.

[Belloni, 2017] Belloni, L. (2017). Exact molecular direct, cavity, and bridge functions in water system. J. Chem. Phys., 147(16):164121.

[Belloni et al., 2018] Belloni, L., Borgis, D., and Levesque, M. (2018). Screened Coulombic Orientational Correlations in Dilute Aqueous Electrolytes. J. Phys. Chem. Lett., 9(8):1985–1989.

[Belloni and Chikina, 2014] Belloni, L. and Chikina, I. (2014). Efficient full Newton–Raphson technique for the solution of molecular integral equations – example of the SPC/E water-like system. Mol. Phys., 112(9-10):1246–1256.

[Berendsen et al., 1987] Berendsen, H. J. C., Grigera, J. R., and Straatsma, T. P. (1987). The missing term in effective pair potentials. J. Phys. Chem., 91(24):6269–6271.

[Bernard et al., 2023] Bernard, O., Jardat, M., Rotenberg, B., and Illien, P. (2023). On analytical theories for conductivity and self-diffusion in concentrated electrolytes. J. Chem. Phys., 159(16):164105.

[Bernet et al., 2020] Bernet, T., Piñeiro, M. M., Plantier, F., and Miqueu, C. (2020). A 3D non-local density functional theory for any pore geometry. Mol. Phys., 118(9-10):e1767308.

[Berthoumieux, 2018] Berthoumieux, H. (2018). Gaussian field model for polar fluids as a function of density and polarization: Toward a model for water. J. Chem. Phys., 148(10):104504.

[Berthoumieux et al., 2024] Berthoumieux, H., Démery, V., and Maggs, A. C. (2024). Non-monotonic conductivity of aqueous electrolytes: beyond the first Wien effect. arXiv:2405.05882 [cond-mat].

[Berthoumieux and Maggs, 2015] Berthoumieux, H. and Maggs, A. C. (2015). Fluctuation-induced forces governed by the dielectric properties of water—A contribution to the hydrophobic interaction. J. Chem. Phys., 143(10):104501.

[Berthoumieux and Paillusson, 2019] Berthoumieux, H. and Paillusson, F. (2019). Dielectric response in the vicinity of an ion: A nonlocal and nonlinear model of the dielectric properties of water. J. Chem. Phys., 150(9):094507.

[Bier et al., 2008] Bier, M., van Roij, R., Dijkstra, M., and van der Schoot, P. (2008). Self-Diffusion of Particles in Complex Fluids: Temporary Cages and Permanent Barriers. Phys. Rev. Lett., 101(21):215901.

[Biswas and Bagchi, 1997] Biswas, R. and Bagchi, B. (1997). Limiting Ionic Conductance of Symmetrical, Rigid Ions in Aqueous Solutions: Temperature Dependence and Solvent Isotope Effects. J. Am. Chem. Soc., 119(25):5946–5953.

[Blum, 1972] Blum, L. (1972). Invariant Expansion. II. The Ornstein-Zernike Equation for Nonspherical Molecules and an Extended Solution to the Mean Spherical Model. J. Chem. Phys., 57(5):1862–1869.

[Blum and Torruella, 1972] Blum, L. and Torruella, A. J. (1972). Invariant Expansion for Two-Body Correlations: Thermodynamic Functions, Scattering, and the Ornstein—Zernike Equation. J. Chem. Phys., 56(1):303–310.

[Blumberger, 2015] Blumberger, J. (2015). Recent Advances in the Theory and Molecular Simulation of Biological Electron Transfer Reactions. Chem. Rev., 115(20):11191–11238.

[Bolmatov et al., 2015] Bolmatov, D., Zhernenkov, M., Zav'yalov, D., Tkachev, S. N., Cunsolo, A., and Cai, Y. Q. (2015). The Frenkel Line: a direct experimental evidence for the new thermodynamic boundary. Sci. Rep., 5(1):15850.

[Bonneau et al., 2024] Bonneau, H., Avni, Y., Andelman, D., and Orland, H. (2024). Frequency-dependent conductivity of concentrated electrolytes: A stochastic density functional theory. J. Chem. Phys., 161(24):244501.

[Bonneau et al., 2023] Bonneau, H., Démery, V., and Raphaël, É. (2023). Temporal response of the conductivity of electrolytes. J. Stat. Mech., 2023(7):073205.

[Bonneau et al., 2025] Bonneau, H., Démery, V., and Raphaël, E. (2025). Stationary and transient correlations in driven electrolytes. J. Stat. Mech.: Theory Exp., 2025(3):033201.

[Borgis et al., 2018] Borgis, D., Belloni, L., and Levesque, M. (2018). What Does Second-Harmonic Scattering Measure in Diluted Electrolytes? J. Phys. Chem. Lett., 9(13):3698–3702.

[Borgis et al., 2020] Borgis, D., Luukkonen, S., Belloni, L., and Jeanmairet, G. (2020). Simple Parameter-Free Bridge Functionals for Molecular Density Functional Theory. Application to Hydrophobic Solvation. J. Phys. Chem. B, 124(31):6885–6893.

[Borgis et al., 2021] Borgis, D., Luukkonen, S., Belloni, L., and Jeanmairet, G. (2021). Accurate prediction of hydration free energies and solvation structures using molecular density functional theory with a simple bridge functional. J. Chem. Phys., 155(2):024117.

[Brazhkin et al., 2013] Brazhkin, V. V., Fomin, Y. D., Lyapin, A. G., Ryzhov, V. N., Tsiok, E. N., and Trachenko, K. (2013). "Liquid-Gas" Transition in the Supercritical Region: Fundamental Changes in the Particle Dynamics. Phys. Rev. Lett., 111(14):145901.

[Bryk et al., 2017] Bryk, T., Gorelli, F. A., Mryglod, I., Ruocco, G., Santoro, M., and Scopigno, T. (2017). Behavior of Supercritical Fluids across the "Frenkel Line". J. Phys. Chem. Lett., 8(20):4995–5001.

[Brünig et al., 2022] Brünig, F. N., Daldrop, J. O., and Netz, R. R. (2022). Pair-Reaction Dynamics in Water: Competition of Memory, Potential Shape, and Inertial Effects. J. Phys. Chem. B, 126(49):10295–10304.

[Budkov, 2020] Budkov, Y. A. (2020). Statistical field theory of ion–molecular solutions. Phys. Chem. Chem. Phys., 22(26):14756–14772.

[Bui and Cox, 2024] Bui, A. T. and Cox, S. J. (2024). A classical density functional theory for solvation across length scales. J. Chem. Phys., 161(10):104103.

[Bui and Cox, 2025] Bui, A. T. and Cox, S. J. (2025). Learning Classical Density Functionals for Ionic Fluids. Phys. Rev. Lett., 134(14):148001.

[Bymaster et al., 2008] Bymaster, A., Emborsky, C., Dominik, A., and Chapman, W. G. (2008). Renormalization-Group Corrections to a Perturbed-Chain Statistical Associating Fluid Theory for Pure Fluids Near to and Far from the Critical Region. Ind. Eng. Chem. Res., 47(16):6264–6274.

[Böttcher et al., 1973] Böttcher, C. J. F., Belle, O. C. v., Bordewijk, P., and Rip, A. (1973). Theory of electric polarization. Elsevier Scientific Pub. Co, Amsterdam New York, 2d ed. completely rev, by O.C. Van Belle, P. Bordewijk , and A. Rip edition.

[Bültmann and Härtel, 2022] Bültmann, M. and Härtel, A. (2022). The primitive model in classical density functional theory: beyond the standard mean-field approximation. J. Phys.: Condens. Matter, 34(23):235101.

[Cerezo et al., 2023] Cerezo, J., Gao, S., Armaroli, N., Ingrosso, F., Prampolini, G., Santoro, F., Ventura, B., and Pastore, M. (2023). Non-Phenomenological Description of the Time-Resolved Emission in Solution with Quantum–Classical Vibronic Approaches—Application to Coumarin C153 in Methanol. Molecules, 28(9):3910.

[Champeau et al., 2016] Champeau, M., Thomassin, J.-M., Jérôme, C., and Tassaing, T. (2016). Solubility and Speciation of Ketoprofen and Aspirin in Supercritical CO $_2$ by Infrared Spectroscopy. J. Chem. Eng. Data, 61(2):968–978.

[Chandler, 1993] Chandler, D. (1993). Gaussian field model of fluids with an application to polymeric fluids. Phys. Rev. E, 48(4):2898.

[Chandra and Bagchi, 1988] Chandra, A. and Bagchi, B. (1988). The role of translational diffusion in the polarization relaxation in dense polar liquids. Chem. Phys. Lett., 151(1):47–53.

[Chandra and Bagchi, 1989a] Chandra, A. and Bagchi, B. (1989a). A molecular theory of collective orientational relaxation in pure and binary dipolar liquids. J. Chem. Phys., 91(3):1829–1842.

[Chandra and Bagchi, 1989b] Chandra, A. and Bagchi, B. (1989b). Molecular theory of solvation and solvation dynamics of a classical ion in a dipolar liquid. J. Phys. Chem., 93(19):6996–7003.

[Chandra and Bagchi, 1990] Chandra, A. and Bagchi, B. (1990). Collective orientational relaxation in a dense liquid of ellipsoidal molecules. Physica A: Statistical Mechanics and its Applications, 169(2):246–262.

[Chandra and Bagchi, 2000] Chandra, A. and Bagchi, B. (2000). Frequency dependence of ionic conductivity of electrolyte solutions. J. Chem. Phys., 112(4):1876–1886.

[Chapman et al., 1989] Chapman, W. G., Gubbins, K. E., Jackson, G., and Radosz, M. (1989). SAFT: Equation-of-state solution model for associating fluids. Fluid Phase Equilibr., 52:31–38.

[Cheng et al., 2003] Cheng, J.-S., Tang, M., and Chen, Y.-P. (2003). Calculation of Solid Solubility of Complex Molecules in Supercritical Carbon Dioxide using a Solution Model Approach. Mol. Simulat., 29(12):749–754.

[Chery, 2015] Chery, D. (2015). Approche prévisionnelle de la valorisation électrochimique du CO2 dans les carbonates fondus. Thèse de doctorat, UPMC.

[Chery et al., 2016] Chery, D., Albin, V., Meléndez-Ceballos, A., Lair, V., and Cassir, M. (2016). Mechanistic approach of the electrochemical reduction of CO2 into CO at a gold electrode in molten carbonates by cyclic voltammetry. Int. J. Hydrog. Energy, 41(41):18706–18712.

[Chong and Hirata, 1998a] Chong, S.-H. and Hirata, F. (1998a). Dynamics of solvated ion in polar liquids: An interaction-site-model description. J. Chem. Phys., 108(17):7339–7349.

[Chong and Hirata, 1998b] Chong, S.-H. and Hirata, F. (1998b). Interaction-site-model description of collective excitations in classical molecular fluids. Phys. Rev. E, 57(2):1691.

[Chong and Hirata, 1998c] Chong, S.-H. and Hirata, F. (1998c). Time-correlation functions in molecular liquids studied by the mode-coupling theory based on the interaction-site model. Phys. Rev. E, 58(6):7296.

[Chong and Hirata, 1999] Chong, S.-H. and Hirata, F. (1999). Dynamics of ions in liquid water: An interaction-site-model description. J. Chem. Phys., 111(8):3654–3667.

[Chrastil, 1982] Chrastil, J. (1982). Solubility of solids and liquids in supercritical gases. J. Phys. Chem., 86(15):3016–3021.

[Chubak et al., 2023] Chubak, I., Alon, L., Silletta, E. V., Madelin, G., Jerschow, A., and Rotenberg, B. (2023). Quadrupolar 23Na+ NMR relaxation as a probe of subpicosecond collective dynamics in aqueous electrolyte solutions. Nat. Commun., 14(1):84.

[Chubak et al., 2021] Chubak, I., Scalfi, L., Carof, A., and Rotenberg, B. (2021). NMR Relaxation Rates of Quadrupolar Aqueous Ions from Classical Molecular Dynamics Using Force-Field Specific Sternheimer Factors. J. Chem. Theory Comput., 17(10):6006–6017.

[Clemens et al., 2015] Clemens, J. B., Kibar, O., and Chachisvilis, M. (2015). A molecular propeller effect for chiral separation and analysis. Nat. Commun., 6(1):7868.

[Coles et al., 2020] Coles, S. W., Park, C., Nikam, R., Kanduč, M., Dzubiella, J., and Rotenberg, B. (2020). Correlation Length in Concentrated Electrolytes: Insights from All-Atom Molecular Dynamics Simulations. J. Phys. Chem. B, 124(9):1778–1786.

[Colussi et al., 2006] Colussi, S., Elvassore, N., and Kikic, I. (2006). A comparison between semi-empirical and molecular-based equations of state for describing the thermodynamic of supercritical micronization processes. J. Supercritical Fluids, 39:118–126.

[Coropceanu et al., 2007] Coropceanu, V., Cornil, J., da Silva Filho, D. A., Olivier, Y., Silbey, R., and Brédas, J.-L. (2007). Charge Transport in Organic Semiconductors. Chem. Rev., 107(4):926–952.

[Coupette et al., 2018] Coupette, F., Lee, A. A., and Härtel, A. (2018). Screening Lengths in Ionic Fluids. Phys. Rev. Lett., 121(7):075501.

[Coutinho et al., 2021] Coutinho, I. T., Maia-Obi, L. P., and Champeau, M. (2021). Aspirin-Loaded Polymeric Films for Drug Delivery Systems: Comparison between Soaking and Supercritical CO2 Impregnation. Pharmaceutics, 13(6):824.

[Crespo-Otero and Barbatti, 2018] Crespo-Otero, R. and Barbatti, M. (2018). Recent Advances and Perspectives on Nonadiabatic Mixed Quantum–Classical Dynamics. Chem. Rev., 118(15):7026–7068.

[Cugliandolo et al., 2015] Cugliandolo, L. F., Déjardin, P.-M., Lozano, G. S., and van Wijland, F. (2015). Stochastic dynamics of collective modes for Brownian dipoles. Phys. Rev. E, 91(3):032139.

[Curtin and Ashcroft, 1985] Curtin, W. A. and Ashcroft, N. W. (1985). Weighted-density-functional theory of inhomogeneous liquids and the freezing transition. Phys. Rev. A, 32(5):2909–2919.

[Cygan et al., 2012] Cygan, R. T., Romanov, V. N., and Myshakin, E. M. (2012). Molecular Simulation of Carbon Dioxide Capture by Montmorillonite Using an Accurate and Flexible Force Field. J. Phys. Chem. C, 116(24):13079–13091.

[da Silva et al., 2018] da Silva, V. M., do Carmo, R. P., Fleming, F. P., Daridon, J.-L., Pauly, J., and Tavares, F. W. (2018). High pressure phase equilibria of carbon dioxide + n-alkanes mixtures: Experimental data and modeling. Fluid Phase Equilibr., 463:114–120.

[Dandekar et al., 2023] Dandekar, R., Krapivsky, P. L., and Mallick, K. (2023). Dynamical fluctuations in the Riesz gas. Phys. Rev. E, 107(4):044129.

[Dandekar et al., 2024] Dandekar, R., Krapivsky, P. L., and Mallick, K. (2024). Current fluctuations in the Dyson gas. Phys. Rev. E, 110(6):064153.

[Dantchev and Dietrich, 2023] Dantchev, D. M. and Dietrich, S. (2023). Critical Casimir effect: Exact results. Phys. Rep., 1005:1–130.

[Dardin et al., 1998] Dardin, A., DeSimone, J. M., and Samulski, E. T. (1998). Fluorocarbons Dissolved in Supercritical Carbon Dioxide. NMR Evidence for Specific Solute-Solvent Interactions. J. Phys. Chem. B, 102(10):1775–1780.

[Das and Yoshimori, 2013] Das, S. P. and Yoshimori, A. (2013). Coarse-grained forms for equations describing the microscopic motion of particles in a fluid. Phys. Rev. E, 88(4):043008.

[Dean, 1996] Dean, D. S. (1996). Langevin equation for the density of a system of interacting Langevin processes. J. Phys. A: Math. Gen., 29(24):L613.

[Dean et al., 2016] Dean, D. S., Lu, B.-S., Maggs, A., and Podgornik, R. (2016). Nonequilibrium Tuning of the Thermal Casimir Effect. Phys. Rev. Lett., 116(24):240602.

[Dean and Podgornik, 2014] Dean, D. S. and Podgornik, R. (2014). Relaxation of the thermal Casimir force between net neutral plates containing Brownian charges. Phys. Rev. E, 89(3):032117.

[Di Caprio et al., 1998] Di Caprio, D., Stafiej, J., and Badiali, J.-P. (1998). A field theory study of the effect of specific interactions in ionic systems: A simple model. J. Chem. Phys., 108(20):8572–8583.

[Dias et al., 2006] Dias, A. M. A., Carrier, H., Daridon, J. L., Pàmies, J. C., Vega, L. F., Coutinho, J. A. P., and Marrucho, I. M. (2006). Vapor-Liquid Equilibrium of Carbon Dioxide-Perfluoroalkane Mixtures: Experimental Data and SAFT Modeling. Ind. Eng. Chem. Res., 45(7):2341–2350.

[Ding et al., 2017] Ding, L., Levesque, M., Borgis, D., and Belloni, L. (2017). Efficient molecular density functional theory using generalized spherical harmonics expansions. J. Chem. Phys., 147(9):094107.

[Dokko et al., 2018] Dokko, K., Watanabe, D., Ugata, Y., Thomas, M. L., Tsuzuki, S., Shinoda, W., Hashimoto, K., Ueno, K., Umebayashi, Y., and Watanabe, M. (2018). Direct Evidence for Li Ion Hopping Conduction in Highly Concentrated Sulfolane-Based Liquid Electrolytes. J. Phys. Chem. B, 122(47):10736–10745.

[Du et al., 2025a] Du, G., Dean, D. S., Miao, B., and Podgornik, R. (2025a). Correlation decoupling of Casimir interaction in an electrolyte driven by external electric fields. arXiv:2404.06028 [cond-mat].

[Du et al., 2025b] Du, G., Dean, D. S., Miao, B., and Podgornik, R. (2025b). Repulsive thermal van der Waals interaction in multispecies asymmetric electrolytes driven by external electric fields. Phys. Rev. E, 111(4):044108.

[Duboisset et al., 2020] Duboisset, J., Rondepierre, F., and Brevet, P.-F. (2020). Long-Range Orientational Organization of Dipolar and Steric Liquids. J. Phys. Chem. Lett., 11(22):9869–9875.

[Dufour-Décieux et al., 2025] Dufour-Décieux, V., Rehner, P., Schilling, J., Moubarak, E., Gross, J., and Bardow, A. (2025). Classical density functional theory as a fast and accurate method for adsorption property prediction of porous materials. AIChE J., page e18779.

[Dufrêche et al., 2002] Dufrêche, J.-F., Bernard, O., Turq, P., Mukherjee, A., and Bagchi, B. (2002). Ionic Self-Diffusion in Concentrated Aqueous Electrolyte Solutions. Phys. Rev. Lett., 88(9):095902.

[Dujarric et al., 2022] Dujarric, K., Coutinho, I. T., Mantuaneli, G. T., Tassaing, T., and Champeau, M. (2022). Solubility of aspirin, ketoprofen and R-(-)-carvone in supercritical CO2 in binary, ternary and quaternary systems: Effect of co-solutes. J. Supercritical Fluids, 189:105697.

[Duque et al., 2004] Duque, D., Pàmies, J. C., and Vega, L. F. (2004). Interfacial properties of Lennard-Jones chains by direct simulation and density gradient theory. J. Chem. Phys., 121(22):11395–11401.

[Durán-Olivencia et al., 2016] Durán-Olivencia, M. A., Goddard, B. D., and Kalliadasis, S. (2016). Dynamical Density Functional Theory for Orientable Colloids Including Inertia and Hydrodynamic Interactions. J. Stat. Phys., 164(4):785–809.

[Dziubinska-Kühn et al., 2025] Dziubinska-Kühn, K., Jolivet, R. B., and Rumble, C. A. (2025). Nuclear Magnetic Resonance and Computational Studies of Sodium Ions in an Ionic Liquid/Water Mixture. J. Phys. Chem. B.

[Démery and Dean, 2016] Démery, V. and Dean, D. S. (2016). The conductivity of strong electrolytes from stochastic density functional theory. J. Stat. Mech., 2016(2):023106.

[D'Agostino et al., 2021] D'Agostino, C., Davis, S. J., and Abbott, A. P. (2021). 23Na NMR T1 relaxation measurements as a probe for diffusion and dynamics of sodium ions in salt–glycerol mixtures. J. Chem. Phys., 154(22):224501.

[Egorov, 2003] Egorov, S. A. (2003). A mode-coupling theory of diffusion in supercritical fluids. J. Chem. Phys., 119(9):4798–4810.

[Egorov et al., 2002] Egorov, S. A., Denny, R. A., and Reichman, D. R. (2002). On the multiple time scales in solvation dynamics: A mode-coupling theory approach. J. Chem. Phys., 116(12):5080.

[Eisenstadt and Friedman, 1966] Eisenstadt, M. and Friedman, H. L. (1966). Nuclear Magnetic Relaxation in Ionic Solution. I. Relaxation of 23Na in Aqueous Solutions of NaCl and NaClO4. J. Chem. Phys., 44(4):1407–1415.

[Elliott et al., 2024] Elliott, G. R., Gregory, K. P., Robertson, H., Craig, V. S., Webber, G. B., Wanless, E. J., and Page, A. J. (2024). The known-unknowns of anomalous underscreening in concentrated electrolytes. Chem. Phys. Lett., 843:141190.

[Evans, 1979] Evans, R. (1979). The nature of the liquid-vapour interface and other topics in the statistical mechanics of non-uniform, classical fluids. Adv. Phys., 28(2):143–200.

[Evans et al., 2016] Evans, R., Oettel, M., Roth, R., and Kahl, G. (2016). New developments in classical density functional theory. J. Phys.: Condens. Matter, 28(24):240401.

[Farhadi and Limmer, 2025] Farhadi, J. and Limmer, D. T. (2025). Large deviations of ionic currents in dilute electrolytes. arXiv:2507.18556 [cond-mat].

[Feng et al., 2025] Feng, L., Goldstein, M., Wang, Y., Mohanty, U., and Grimaud, A. (2025). Polarization-Induced Breaching of the Liquid/Liquid Interface Formed with Water-in-Salt Electrolytes. J. Am. Chem. Soc.

[Foley et al., 1954] Foley, H. M., Sternheimer, R. M., and Tycko, D. (1954). Nuclear Quadrupole Coupling in Polar Molecules. Phys. Rev., 93(4):734–742.

[Foltran et al., 2011] Foltran, S., Méreau, R., and Tassaing, T. (2011). On the interaction between supercritical CO2 and epoxides combining infrared absorption spectroscopy and quantum chemistry calculations. Phys. Chem. Chem. Phys., 13(20):9209.

[Fomin et al., 2015] Fomin, Y. D., Ryzhov, V. N., Tsiok, E. N., and Brazhkin, V. V. (2015). Thermodynamic properties of supercritical carbon dioxide: Widom and Frenkel lines. Phys. Rev. E, 91(2):022111.

[Forte et al., 2011] Forte, E., Llovell, F., Vega, L. F., Trusler, J. P. M., and Galindo, A. (2011). Application of a renormalization-group treatment to the statistical associating fluid theory for potentials of variable range (SAFT-VR). J. Chem. Phys., 134(15):154102.

[Frenkel and Smit, 2002] Frenkel, D. and Smit, B. (2002). Understanding molecular simulation from algorithms to applications. Academic Press, San Diego.

[Fries and Cosnard, 1987] Fries, P. H. and Cosnard, M. (1987). Résolution des équations intégrales des fluides à potentiels intermoléculaires anisotropes par l'algorithme Général de Minimisation du RESte. Journal de Physique, 48(5):723–731.

[Fries and Patey, 1985] Fries, P. H. and Patey, G. N. (1985). The solution of the hypernetted-chain approximation for fluids of nonspherical particles. A general method with application to dipolar hard spheres. J. Chem. Phys., 82(1):429–440.

[Fuentes-Azcatl and Domínguez, 2019] Fuentes-Azcatl, R. and Domínguez, H. (2019). Carbon Dioxide Confined between Two Charged Single Layers of Graphene: Molecular Dynamics Studies. J. Phys. Chem. C, 123(38):23705–23710.

[Gao et al., 2023] Gao, A., Remsing, R. C., and Weeks, J. D. (2023). Local Molecular Field Theory for Coulomb Interactions in Aqueous Solutions. J. Phys. Chem. B.

[Gao et al., 2024] Gao, Y., Wu, J., Feng, Y., Han, J., and Fang, H. (2024). Effects of Hydrogen Bond Networks on Viscosity in Aqueous Solutions. J. Phys. Chem. B.

[Garlapati and Madras, 2009] Garlapati, C. and Madras, G. (2009). Temperature independent mixing rules to correlate the solubilities of antibiotics and anti-inflammatory drugs in SCCO2. Thermochim. Acta, 496(1-2):54–58.

[Geissler and Chandler, 2000] Geissler, P. L. and Chandler, D. (2000). Importance sampling and theory of nonequilibrium solvation dynamics in water. J. Chem. Phys., 113(21):9759–9765.

[Giannini et al., 2025] Giannini, S., Martinez, P. M., Semmeq, A., Galvez, J. P., Piras, A., Landi, A., Padula, D., Vilhena, J. G., Cerezo, J., and Prampolini, G. (2025). JOYCE3.0: A General Protocol for the Specific Parametrization of Accurate Intramolecular Quantum Mechanically Derived Force Fields. J. Chem. Theory Comput.

[Gillespie et al., 2002] Gillespie, D., Nonner, W., and Eisenberg, R. S. (2002). Coupling Poisson–Nernst–Planck and density functional theory to calculate ion flux. J. Phys.: Condens. Matter, 14(46):12129.

[Goloviznina et al., 2024] Goloviznina, K., Serva, A., and Salanne, M. (2024). Formation of Polymer-like Nanochains with Short Lithium–Lithium Distances in a Water-in-Salt Electrolyte. J. Am. Chem. Soc.

[Grelet et al., 2008] Grelet, E., Lettinga, M. P., Bier, M., Roij, R. v., and Schoot, P. v. d. (2008). Dynamical and structural insights into the smectic phase of rod-like particles. J. Phys.: Condens. Matter, 20(49):494213.

[Groves and Perkin, 2024] Groves, T. and Perkin, S. (2024). Wave mechanics in an ionic liquid mixture. Faraday Discuss.

[Grégoire et al., 2016] Grégoire, B., Erastova, V., Geatches, D. L., Clark, S. J., Greenwell, H. C., and Fraser, D. G. (2016). Insights into the behaviour of biomolecules on the early Earth: The concentration of aspartate by layered double hydroxide minerals. Geochim. Cosmochim. Acta, 176:239–258.

[Hansen et al., 2021] Hansen, B. B., Spittle, S., Chen, B., Poe, D., Zhang, Y., Klein, J. M., Horton, A., Adhikari, L., Zelovich, T., Doherty, B. W., Gurkan, B., Maginn, E. J., Ragauskas, A., Dadmun, M., Zawodzinski, T. A., Baker, G. A., Tuckerman, M. E., Savinell, R. F., and Sangoro, J. R. (2021). Deep Eutectic Solvents: A Review of Fundamentals and Applications. Chem. Rev., 121(3):1232–1285.

[Hansen and McDonald, 2013] Hansen, J.-P. and McDonald, I. R. (2013). Theory of Simple Liquids: with Applications to Soft Matter. Academic Press, Amstersdam, Édition : 4 edition.

[Hansen-Goos and Mecke, 2009] Hansen-Goos, H. and Mecke, K. (2009). Fundamental Measure Theory for Inhomogeneous Fluids of Nonspherical Hard Particles. Phys. Rev. Lett., 102(1):018302.

[Hansen-Goos and Mecke, 2010] Hansen-Goos, H. and Mecke, K. (2010). Tensorial density functional theory for non-spherical hard-body fluids. J. Phys.: Condens. Matter, 22(36):364107.

[Hansen-Goos and Roth, 2006] Hansen-Goos, H. and Roth, R. (2006). Density functional theory for hard-sphere mixtures: the White Bear version mark II. J. Phys.: Condens. Matter, 18(37):8413–8425.

[Harris and Yung, 1995] Harris, J. G. and Yung, K. H. (1995). Carbon Dioxide's Liquid-Vapor Coexistence Curve And Critical Properties as Predicted by a Simple Molecular Model. J. Phys. Chem., 99(31):12021–12024.

[Hedley et al., 2023] Hedley, J. G., Berthoumieux, H., and Kornyshev, A. A. (2023). The Dramatic Effect of Water Structure on Hydration Forces and the Electrical Double Layer. J. Phys. Chem. C, 127(18):8429–8447.

[Hinz et al., 2023] Hinz, Y., Beerwerth, J., and Böhmer, R. (2023). Anion dynamics and motional decoupling in a glycerol–choline chloride deep eutectic solvent studied by one- and two-dimensional 35Cl NMR. Phys. Chem. Chem. Phys., 25(41):28130–28140.

[Hojjati et al., 2007] Hojjati, M., Yamini, Y., Khajeh, M., and Vatanara, A. (2007). Solubility of some statin drugs in supercritical carbon dioxide and representing the solute solubility data with several density-based correlations. J. Supercritical Fluids, 41(2):187–194.

[Hosokawa et al., 2024] Hosokawa, S., Katayama, Y., Tsutsui, S., and Baron, A. Q. R. (2024). Collective dynamics of liquid sulphur across the polymerisation transition temperature probed by inelastic x-ray scattering. J. Phys.: Condens. Matter, 36(42):425102.

[Houssein Mohamed, 2024] Houssein Mohamed, M. (2024). Développement d'une méthode ultra-efficace pour le calcul de la solvatation du CO_2 supercritique. These de doctorat, Université de Lorraine.

[Houssein Mohamed et al., 2025] Houssein Mohamed, M., Belloni, L., Borgis, D., Ingrosso, F., and Carof, A. (2025). Molecular integral equations theory in the near critical region of CO2. J. Mol. Liq., 418:126623.

[Huang and Chandler, 2000] Huang, D. M. and Chandler, D. (2000). Cavity formation and the drying transition in the Lennard-Jones fluid. Phys. Rev. E, 61(2):1501–1506.

[Huang et al., 1985] Huang, F.-H., Li, M.-H., Lee, L. L., Starling, K. E., and Chung, F. T. H. (1985). An accurate equation of state for carbon dioxide. J. Chem. Eng. Japan, 18(6):490–496.

[Hynes and Wolynes, 1981] Hynes, J. T. and Wolynes, P. G. (1981). A continuum theory for quadrupole relaxation of ions in solution. J. Chem. Phys., 75(1):395–401.

[Härtel, 2025] Härtel, A. (2025). Performance of DFT for charged systems.

[Idrissi et al., 2010] Idrissi, A., Vyalov, I., Damay, P., Kiselev, M., Puhovski, Y., and Jedlovszky, P. (2010). Local structure in sub- and supercritical CO2: A Voronoi polyhedra analysis study. J. Mol. Liq., 153(1):20–24.

[Illien, 2025] Illien, P. (2025). The Dean–Kawasaki equation and stochastic density functional theory. Reports on Progress in Physics, 88(8):086601.

[Imai et al., 2020] Imai, M., Yokota, Y., Tanabe, I., Inagaki, K., Morikawa, Y., and Fukui, K.-i. (2020). Correlation between mobility and the hydrogen bonding network of water at an electrified-graphite electrode using molecular dynamics simulation. Phys. Chem. Chem. Phys., 22(3):1767–1773.

[Ingrosso et al., 2016] Ingrosso, F., Altarsha, M., Dumarçay, F., Kevern, G., Barth, D., Marsura, A., and Ruiz-López, M. F. (2016). Driving Forces Controlling Host-Guest Recognition in Supercritical Carbon Dioxide Solvent. Chem.-Eur. J., 22(9):2972–2979.

[Ingrosso and Ruiz-López, 2017] Ingrosso, F. and Ruiz-López, M. F. (2017). Modeling Solvation in Supercritical CO_2. ChemPhysChem, 18(19):2560–2572.

[Ingrosso and Ruiz-López, 2018] Ingrosso, F. and Ruiz-López, M. F. (2018). Electronic Interactions in Iminophosphorane Superbase Complexes with Carbon Dioxide. J. Phys. Chem. A, 122(6):1764–1770.

[Iwai et al., 1992] Iwai, Y., Koga, Y., Fukuda, T., and Arai, Y. (1992). Correlation of solubilities of high-boiling components in supercritical carbon dioxide using a solution model. J. Chem. Eng. Japan, 25(6):757–760.

[Janssen, 1976] Janssen, H.-K. (1976). On a Lagrangean for classical field dynamics and renormalization group calculations of dynamical critical properties. Zeitschrift für Physik B Condensed Matter, 23(4):377–380.

[Jeanmairet and Giner, 2025] Jeanmairet, G. and Giner, E. (2025). A variational formulation of the free energy of mixed quantum-classical systems: coupling classical and electronic density functional theories. arXiv:2411.11821 [cond-mat].

[Jeanmairet et al., 2013a] Jeanmairet, G., Levesque, M., and Borgis, D. (2013a). Molecular density functional theory of water describing hydrophobicity at short and long length scales. J. Chem. Phys., 139(15):154101–1–154101–9.

[Jeanmairet et al., 2015] Jeanmairet, G., Levesque, M., Sergiievskyi, V., and Borgis, D. (2015). Molecular density functional theory for water with liquid-gas coexistence and correct pressure. J. Chem. Phys., 142(15):154112.

[Jeanmairet et al., 2013b] Jeanmairet, G., Levesque, M., Vuilleumier, R., and Borgis, D. (2013b). Molecular Density Functional Theory of Water. J. Phys. Chem. Lett., 4(4):619–624.

[Jeanmairet et al., 2016] Jeanmairet, G., Levy, N., Levesque, M., and Borgis, D. (2016). Molecular density functional theory of water including density–polarization coupling. J. Phys.-Condens. Mat., 28(24):244005.

[Jeanmairet et al., 2014] Jeanmairet, G., Marry, V., Levesque, M., Rotenberg, B., and Borgis, D. (2014). Hydration of clays at the molecular scale: the promising perspective of classical density functional theory. Mol. Phys., 112(9-10):1320–1329.

[Jeanmairet et al., 2019] Jeanmairet, G., Rotenberg, B., Borgis, D., and Salanne, M. (2019). Study of a water-graphene capacitor with molecular density functional theory. J. Chem. Phys., 151(12):124111.

[Jeanmairet et al., 2022] Jeanmairet, G., Rotenberg, B., and Salanne, M. (2022). Microscopic Simulations of Electrochemical Double-Layer Capacitors. Chem. Rev., 122(12):10860–10898.

[Jimenez et al., 1994] Jimenez, R., Fleming, G. R., Kumar, P. V., and Maroncelli, M. (1994). Femtosecond solvation dynamics of water. Nature, 369(6480):471–473.

[Johnston et al., 1987] Johnston, K. P., Barry, S. E., Read, N. K., and Holcomb, T. R. (1987). Separation of isomers using retrograde crystallization from supercritical fluids. Ind. Eng. Chem. Res., 26(11):2372–2377.

[Jorgensen et al., 1996] Jorgensen, W. L., Maxwell, D. S., and Tirado-Rives, J. (1996). Development and Testing of the OPLS All-Atom Force Field on Conformational Energetics and Properties of Organic Liquids. J. Am. Chem. Soc., 118(45):11225–11236.

[Kahl et al., 1996] Kahl, G., Bildstein, B., and Rosenfeld, Y. (1996). Structure and thermodynamics of binary liquid mixtures: Universality of the bridge functional. Phys. Rev. E, 54(5):5391–5406.

[Kajiya and Saitow, 2013] Kajiya, D. and Saitow, K.-i. (2013). Investigation of attractive and repulsive interactions associated with ketones in supercritical CO $_2$, based on Raman spectroscopy and theoretical calculations. J. Chem. Phys., 139(5):054509.

[Kalikin et al., 2021a] Kalikin, N., Budkov, Y., Kolesnikov, A., Ivlev, D., Krestyaninov, M., and Kiselev, M. (2021a). Computation of drug solvation free energy in supercritical CO 2 : Alternatives to all-atom computer simulations. Fluid Phase Equilibr., 544-545:113096.

[Kalikin et al., 2020] Kalikin, N., Kurskaya, M., Ivlev, D., Krestyaninov, M., Oparin, R., Kolesnikov, A., Budkov, Y., Idrissi, A., and Kiselev, M. (2020). Carbamazepine solubility in supercritical CO2: A comprehensive study. J. Mol. Liq., 311:113104.

[Kalikin et al., 2021b] Kalikin, N., Oparin, R., Kolesnikov, A., Budkov, Y., and Kiselev, M. (2021b). A crossover of the solid substances solubility in supercritical fluids: What is it in fact? J. Mol. Liq., 334:115997.

[Kirchner et al., 2015] Kirchner, B., Malberg, F., Firaha, D. S., and Hollóczki, O. (2015). Ion pairing in ionic liquids. J. Phys.: Condens. Matter, 27(46):463002.

[Kjellander, 2018] Kjellander, R. (2018). Focus Article: Oscillatory and long-range monotonic exponential decays of electrostatic interactions in ionic liquids and other electrolytes: The significance of dielectric permittivity and renormalized charges. J. Chem. Phys., 148(19):193701.

[Kjellander, 2020a] Kjellander, R. (2020a). A multiple decay-length extension of the Debye–Hückel theory: to achieve high accuracy also for concentrated solutions and explain under-screening in dilute symmetric electrolytes. Phys. Chem. Chem. Phys., 22(41):23952–23985.

[Kjellander, 2020b] Kjellander, R. (2020b). Statistical mechanics of liquids and solutions: intermolecular forces, structure and surface interactions. CRC Press, Taylor & Francis Group, Boca Raton, FL.

[Klink and Gross, 2014] Klink, C. and Gross, J. (2014). A Density Functional Theory for Vapor–Liquid Interfaces of Mixtures Using the Perturbed-Chain Polar Statistical Associating Fluid Theory Equation of State. Ind. Eng. Chem. Res., 53(14):6169–6178.

[Klink et al., 2015] Klink, C., Planková, B., and Gross, J. (2015). Density Functional Theory for Liquid–Liquid Interfaces of Mixtures Using the Perturbed-Chain Polar Statistical Associating Fluid Theory Equation of State. Ind. Eng. Chem. Res., 54(16):4633–4642.

[Kobryn et al., 2005] Kobryn, A. E., Yamaguchi, T., and Hirata, F. (2005). Pressure dependence of diffusion coefficient and orientational relaxation time for acetonitrile and methanol in water: RISM/mode-coupling study. J. Mol. Liq., 119(1):7–13.

[Korb, 2018] Korb, J.-P. (2018). Multiscale nuclear magnetic relaxation dispersion of complex liquids in bulk and confinement. Prog. Nucl. Mag. Res. Sp., 104:12–55.

[Krapivsky et al., 2014] Krapivsky, P., Mallick, K., and Sadhu, T. (2014). Large Deviations in Single-File Diffusion. Phys. Rev. Lett., 113(7):078101.

[Krapivsky et al., 2015] Krapivsky, P. L., Mallick, K., and Sadhu, T. (2015). Tagged Particle in Single-File Diffusion. J. Stat. Phys., 160(4):885–925.

[Kumar and Johnston, 1988] Kumar, S. K. and Johnston, K. P. (1988). Modelling the solubility of solids in supercritical fluids with density as the independent variable. J. Supercritical Fluids, 1(1):15–22.

[Kühne and Khaliullin, 2014] Kühne, T. D. and Khaliullin, R. Z. (2014). Nature of the Asymmetry in the Hydrogen-Bond Networks of Hexagonal Ice and Liquid Water. J. Am. Chem. Soc., 136(9):3395–3399.

[Laage et al., 2017] Laage, D., Elsaesser, T., and Hynes, J. T. (2017). Perspective: Structure and ultrafast dynamics of biomolecular hydration shells. Struct. Dynam., 4(4):044018.

[Laage and Hynes, 2006] Laage, D. and Hynes, J. T. (2006). A Molecular Jump Mechanism of Water Reorientation. Science, 311(5762):832–835.

[Lado, 1982] Lado, F. (1982). Integral equations for fluids of linear molecules. Mol. Phys., 47(2):283–298.

[Lado et al., 1983] Lado, F., Foiles, S. M., and Ashcroft, N. W. (1983). Solutions of the reference-hypernetted-chain equation with minimized free energy. Phys. Rev. A, 28(4):2374–2379.

[Lado et al., 1995] Lado, F., Lomba, E., and Lombardero, M. (1995). Integral equation algorithm for fluids of fully anisotropic molecules. J. Chem. Phys., 103(1):481–484.

[Le Guennec et al., 2016] Le Guennec, Y., Privat, R., and Jaubert, J.-N. (2016). Development of the translated-consistent tc-PR and tc-RK cubic equations of state for a safe and accurate

prediction of volumetric, energetic and saturation properties of pure compounds in the sub- and super-critical domains. Fluid Phase Equilibr., 429:301–312.

[Lesellier and West, 2015] Lesellier, E. and West, C. (2015). The many faces of packed column supercritical fluid chromatography – A critical review. J. Chromotogr. A, 1382:2–46.

[Lesnicki et al., 2021] Lesnicki, D., Gao, C. Y., Limmer, D. T., and Rotenberg, B. (2021). On the molecular correlations that result in field-dependent conductivities in electrolyte solutions. J. Chem. Phys., 155(1):014507.

[Lesnicki et al., 2020] Lesnicki, D., Gao, C. Y., Rotenberg, B., and Limmer, D. T. (2020). Field-Dependent Ionic Conductivities from Generalized Fluctuation-Dissipation Relations. Phys. Rev. Lett., 124(20):206001.

[Lesnicki and Vuilleumier, 2017] Lesnicki, D. and Vuilleumier, R. (2017). Microscopic flow around a diffusing particle. J. Chem. Phys., 147(9):094502.

[Levesque et al., 2012] Levesque, M., Marry, V., Rotenberg, B., Jeanmairet, G., Vuilleumier, R., and Borgis, D. (2012). Solvation of complex surfaces via molecular density functional theory. J. Chem. Phys., 137(22):224107–224107–8.

[Levy et al., 2012] Levy, A., Andelman, D., and Orland, H. (2012). Dielectric Constant of Ionic Solutions: A Field-Theory Approach. Phys. Rev. Lett., 108(22):227801.

[Levy, 1979] Levy, M. (1979). Universal variational functionals of electron densities, first-order density matrices, and natural spin-orbitals and solution of the v-representability problem. Proc. Natl. Acad. Sci. U.S.A., 76(12):6062–6065.

[Li et al., 2020] Li, J., Wang, J., Wang, Y., Lu, D., and Wu, J. (2020). A Multiscale Procedure for Predicting the Hydration Free Energies of Polycyclic Aromatic Hydrocarbons. J. Chem. Eng. Data, 65(4):2206–2211.

[Li and Jin, 2024] Li, X. and Jin, Y. (2024). Thermodynamic crossovers in supercritical fluids. Proc. Natl. Acad. Sci. U.S.A., 121(18):e2400313121.

[Liang et al., 2025] Liang, Z., Jiahui, P., Min, Y., Jianing, Y., XiaoBin, F., Miao, S., Hongtao, B., and Yuan, Q. (2025). Concentration-Dependent Structures and Ultrafast Dynamics within Aqueous BeF2: From Ion Complexes to Extended Networks. J. Phys. Chem. B.

[Lieb, 1983] Lieb, E. H. (1983). Density functionals for coulomb systems. Int. J. Quantum Chem., 24(3):243–277.

[Liu et al., 2010] Liu, R., Yu, Y., Yoshida, K., Li, G., Jiang, H., Zhang, M., Zhao, F., Fujita, S.-i., and Arai, M. (2010). Physically and chemically mixed TiO2-supported Pd and Au catalysts: unexpected synergistic effects on selective hydrogenation of citral in supercritical CO2. J. Catal., 269(1):191–200.

[Liu et al., 2013a] Liu, Y., Fu, J., and Wu, J. (2013a). High-Throughput Prediction of the Hydration Free Energies of Small Molecules from a Classical Density Functional Theory. J. Phys. Chem. Lett., 4(21):3687–3691.

[Liu et al., 2013b] Liu, Y., Zhao, S., and Wu, J. (2013b). A Site Density Functional Theory for Water: Application to Solvation of Amino Acid Side Chains. J. Chem. Theory Comput., 9(4):1896–1908.

[Llovell and Vega, 2006] Llovell, F. and Vega, L. F. (2006). Prediction of Thermodynamic Derivative Properties of Pure Fluids through the Soft-SAFT Equation of State. J. Phys. Chem. B, 110(23):11427–11437.

[Llovell and Vega, 2007] Llovell, F. and Vega, L. F. (2007). Phase equilibria, critical behavior and derivative properties of selected n-alkane/n-alkane and n-alkane/1-alkanol mixtures by the crossover soft-SAFT equation of state. J. Supercritical Fluids, 41(2):204–216.

[Llovell and Vega, 2015] Llovell, F. and Vega, L. F. (2015). Accurate modeling of supercritical CO2 for sustainable processes: Water+CO2 and CO2+fatty acid esters mixtures. J. Supercritical Fluids, 96:86–95.

[Lu et al., 2015] Lu, B.-S., Dean, D. S., and Podgornik, R. (2015). Out-of-equilibrium thermal Casimir effect between Brownian conducting plates. EPL, 112(2):20001.

[Lum et al., 1999] Lum, K., Chandler, D., and Weeks, J. D. (1999). Hydrophobicity at Small and Large Length Scales. J. Phys. Chem. B, 103(22):4570–4577.

[Lutsko, 2022] Lutsko, J. F. (2022). Classical density functional theory in the canonical ensemble. Phys. Rev. E, 105(3):034120.

[Luukkonen et al., 2020] Luukkonen, S., Levesque, M., Belloni, L., and Borgis, D. (2020). Hydration free energies and solvation structures with molecular density functional theory in the hypernetted chain approximation. J. Chem. Phys., 152(6):064110.

[Löwen, 2002] Löwen, H. (2002). Density functional theory of inhomogeneous classical fluids: recent developments and new perspectives. J. Phys.: Condens. Matter, 14(46):11897.

[Maggs and Everaers, 2006] Maggs, A. C. and Everaers, R. (2006). Simulating Nanoscale Dielectric Response. Phys. Rev. Lett., 96(23):230603.

[Mahdisoltani and Golestanian, 2021a] Mahdisoltani, S. and Golestanian, R. (2021a). Long-Range Fluctuation-Induced Forces in Driven Electrolytes. Phys. Rev. Lett., 126(15):158002.

[Mahdisoltani and Golestanian, 2021b] Mahdisoltani, S. and Golestanian, R. (2021b). Transient fluctuation-induced forces in driven electrolytes after an electric field quench. New J. Phys., 23(7):073034.

[Malheiro et al., 2014a] Malheiro, C., Mendiboure, B., Míguez, J.-M., Piñeiro, M. M., and Miqueu, C. (2014a). Nonlocal Density Functional Theory and Grand Canonical Monte Carlo Molecular Simulations of Water Adsorption in Confined Media. J. Phys. Chem. C, 118(43):24905–24914.

[Malheiro et al., 2014b] Malheiro, C., Mendiboure, B., Plantier, F., Blas, F. J., and Miqueu, C. (2014b). Density functional theory for the description of spherical non-associating monomers in confined media using the SAFT-VR equation of state and weighted density approximations. J. Chem. Phys., 140(13):134707.

[Mallick et al., 2022] Mallick, K., Moriya, H., and Sasamoto, T. (2022). Exact Solution of the Macroscopic Fluctuation Theory for the Symmetric Exclusion Process. Phys. Rev. Lett., 129(4):040601.

[Marechal et al., 2011] Marechal, M., Goetzke, H. H., Härtel, A., and Löwen, H. (2011). Inhomogeneous fluids of colloidal hard dumbbells: Fundamental measure theory and Monte Carlo simulations. J. Chem. Phys., 135(23):234510.

[Maroncelli and Fleming, 1988] Maroncelli, M. and Fleming, G. R. (1988). Computer simulation of the dynamics of aqueous solvation. J. Chem. Phys., 89(8):5044–5069.

[Martin et al., 1973] Martin, P. C., Siggia, E. D., and Rose, H. A. (1973). Statistical Dynamics of Classical Systems. Phys. Rev. A, 8(1):423–437.

[McQuarrie, 2000] McQuarrie, D. A. (2000). Statistical mechanics. University Science Books, Sausalito, Calif.

[Mendez-Santiago and Teja, 2012] Mendez-Santiago, J. and Teja, A. S. (2012). Solubility of Benzoic Acid in Mixtures of CO $_2$ + Hexane. J. Chem. Eng. Data, 57(12):3438–3442.

[Mermin, 1965] Mermin, N. D. (1965). Thermal Properties of the Inhomogeneous Electron Gas. Phys. Rev., 137(5A):A1441–A1443.

[Messiah, 1962] Messiah, A. (1962). Quantum Mechanics, Volume II. North-Holland Publishing Company, 1 edition.

[Mi et al., 2019] Mi, W., Ramos, P., Maranhao, J., and Pavanello, M. (2019). Ab Initio Structure and Dynamics of CO $_2$ at Supercritical Conditions. J. Phys. Chem. Lett., 10(24):7554–7559.

[Miguel et al., 2014] Miguel, B., Zúñiga, J., Requena, A., and Bastida, A. (2014). Theoretical Study of the Temperature Dependence of the Vibrational Relaxation of the H $_2$ O Bend Fundamental in Liquid Water and the Subsequent Distortion of the Hydrogen Bond Network. J. Phys. Chem. B, 118(31):9427–9437.

[Ministère de la Santé et de la Prévention, 2022] Ministère de la Santé et de la Prévention (2022). Arrêté du 10 novembre 2022 relatif à la formation socle au numérique en santé des étudiants en santé.

[Miqueu and Grégoire, 2020] Miqueu, C. and Grégoire, D. (2020). Estimation of pore pressure and phase transitions of water confined in nanopores with non-local density functional theory. Mol. Phys., 118(9-10):e1742935.

[Mitchell, 2016] Mitchell, J. (2016). Can sodium NMR provide more than a tracer for brine in petrophysics? J. Pet. Sci. Eng., 146:360–368.

[Molineau et al., 2021] Molineau, J., Hideux, M., and West, C. (2021). Chromatographic analysis of biomolecules with pressurized carbon dioxide mobile phases – A review. J. Pharmaceut. Biomed., 193:113736.

[Moog et al., 2021] Moog, M., Pietrucci, F., and Saitta, A. M. (2021). Carbon Dioxide under Earth Mantle Conditions: From a Molecular Liquid through a Reactive Fluid to Polymeric Regimes. J. Phys. Chem. A, 125(27):5863–5869.

[Mouahid et al., 2022] Mouahid, A., Boivin, P., Diaw, S., and Badens, E. (2022). Widom and extrema lines as criteria for optimizing operating conditions in supercritical processes. J. Supercritical Fluids, 186:105587.

[Nakamura and Yoshimori, 2009] Nakamura, T. and Yoshimori, A. (2009). Derivation of the nonlinear fluctuating hydrodynamic equation from the underdamped Langevin equation. J. Phys. A, 42(6):065001.

[Nandi et al., 1995] Nandi, N., Roy, S., and Bagchi, B. (1995). Ultrafast solvation dynamics in water: Isotope effects and comparison with experimental results. J. Chem. Phys., 102(3):1390–1397.

[Nee and Zwanzig, 1970] Nee, T. and Zwanzig, R. (1970). Theory of Dielectric Relaxation in Polar Liquids. J. Chem. Phys., 52(12):6353–6363.

[Neophytou et al., 2024] Neophytou, A., Starr, F. W., Chakrabarti, D., and Sciortino, F. (2024). Hierarchy of topological transitions in a network liquid. Proc. Natl. Acad. Sci. U.S.A., 121(36):e2406890121.

[Nguyen et al., 2025] Nguyen, H. T. D., Lee, S.-C., Lyu, X., Fang, L., Trojanowski, L., Gonzalez, R., Harr, M., Rai, L., Z, Y., and Li, T. (2025). Unique Conductivity Behavior in Water-In-Salt Electrolytes Driven by Ion Clusters. J. Am. Chem. Soc., 147(30):26704–26713.

[Nishiyama et al., 2009] Nishiyama, K., Yamaguchi, T., and Hirata, F. (2009). Solvation Dynamics in Polar Solvents Studied by Means of RISM/Mode-Coupling Theory. J. Phys. Chem. B, 113(9):2800–2804.

[Nordholm et al., 1980] Nordholm, S., Johnson, M., and Freasier, B. (1980). Generalized van der Waals theory. III. The prediction of hard sphere structure. Australian Journal of Chemistry, 33(10):2139–2150.

[Noroozi et al., 2016] Noroozi, J., Ghotbi, C., Sardroodi, J. J., Karimi-Sabet, J., and Robert, M. A. (2016). Solvation free energy and solubility of acetaminophen and ibuprofen in supercritical carbon dioxide: Impact of the solvent model. J. Supercritical Fluids, 109:166–176.

[Noroozi and Paluch, 2017] Noroozi, J. and Paluch, A. S. (2017). Microscopic Structure and Solubility Predictions of Multifunctional Solids in Supercritical Carbon Dioxide: A Molecular Simulation Study. J. Phys. Chem. B, 121(7):1660–1674.

[Oberhofer et al., 2017] Oberhofer, H., Reuter, K., and Blumberger, J. (2017). Charge Transport in Molecular Materials: An Assessment of Computational Methods. Chem. Rev., 117(15):10319–10357.

[Ornstein and Zernike, 1917] Ornstein, L. S. and Zernike, F. (1917). The influence of accidental deviations of density on the equation of state. Procedings of Royal Netherlands Academy of Arts and Sciences, 19(II):5.

[Oulebsir et al., 2018] Oulebsir, F., Vermorel, R., and Galliero, G. (2018). Diffusion of Supercritical Fluids through Single-Layer Nanoporous Solids: Theory and Molecular Simulations. Langmuir, 34(2):561–571.

[Patey, 1977] Patey, G. (1977). An integral equation theory for the dense dipolar hard-sphere fluid. Mol. Phys., 34(2):427–440.

[Perng and Ladanyi, 1998] Perng, B.-C. and Ladanyi, B. M. (1998). A dielectric theory of spin-lattice relaxation for nuclei with electric quadrupole moments. J. Chem. Phys., 109(2):676–684.

[Pipich and Schwahn, 2018] Pipich, V. and Schwahn, D. (2018). Densification of Supercritical Carbon Dioxide Accompanied by Droplet Formation When Passing the Widom Line. Phys. Rev. Lett., 120(14):145701.

[Piron and Blenski, 2019] Piron, R. and Blenski, T. (2019). Simpler free-energy functional of the Debye-Hückel model of fluids and the nonuniqueness of free-energy functionals in the theory of fluids. Phys. Rev. E, 99(5):052134.

[Pluhařová et al., 2017] Pluhařová, E., Laage, D., and Jungwirth, P. (2017). Size and Origins of Long-Range Orientational Water Correlations in Dilute Aqueous Salt Solutions. J. Phys. Chem. Lett., 8(9):2031–2035.

[Polimeno and Moro, 1994] Polimeno, A. and Moro, G. J. (1994). A cage model of liquids supported by molecular dynamics simulations. II. The stochastic model. J. Chem. Phys., 101(1):703–712.

[Poncet et al., 2021] Poncet, A., Bénichou, O., Démery, V., and Nishiguchi, D. (2021). Pair correlation of dilute active Brownian particles: From low-activity dipolar correction to high-activity algebraic depletion wings. Phys. Rev. E, 103(1):012605.

[Potoff and Siepmann, 2001] Potoff, J. J. and Siepmann, J. I. (2001). Vapor–liquid equilibria of mixtures containing alkanes, carbon dioxide, and nitrogen. AIChE J., 47(7):1676–1682.

[Prampolini et al., 2019] Prampolini, G., Ingrosso, F., Segalina, A., Caramori, S., Foggi, P., and Pastore, M. (2019). Dynamical and Environmental Effects on the Optical Properties of an Heteroleptic Ru(II)–Polypyridine Complex: A Multilevel Approach Combining Accurate Ground and Excited State QM-Derived Force Fields, MD and TD-DFT. J. Chem. Theory Comput., 15(1):529–545.

[Price et al., 1990] Price, W. S., Chapman, B. E., and Kuchel, P. W. (1990). Correlation of Viscosity and Conductance with 23Na+ NMR T1 Measurements. Bulletin of the Chemical Society of Japan, 63(10):2961–2965.

[Puibasset and Belloni, 2012] Puibasset, J. and Belloni, L. (2012). Bridge function for the dipolar fluid from simulation. J. Chem. Phys., 136(15):154503.

[Ramirez et al., 2002] Ramirez, R., Gebauer, R., Mareschal, M., and Borgis, D. (2002). Density functional theory of solvation in a polar solvent: Extracting the functional from homogeneous solvent simulations. Phys. Rev. E, 66(3):031206–031206–8.

[Ranieri et al., 2024] Ranieri, U., Formisano, F., Gorelli, F. A., Santoro, M., Koza, M. M., De Francesco, A., and Bove, L. E. (2024). Crossover from gas-like to liquid-like molecular diffusion in a simple supercritical fluid. Nat. Commun., 15(1):4142.

[Rastgar et al., 2023] Rastgar, M., Moradi, K., Burroughs, C., Hemmati, A., Hoek, E., and Sadrzadeh, M. (2023). Harvesting Blue Energy Based on Salinity and Temperature Gradient: Challenges, Solutions, and Opportunities. Chem. Rev., 123(16):10156–10205.

[Reatto and Parola, 1996] Reatto, L. and Parola, A. (1996). Liquid-state theory and the renormalization group reconciled: a theory of phase transitions in fluids. J. Phys.: Condens. Matter, 8(47):9221.

[Reddy and Saharay, 2019] Reddy, V. and Saharay, M. (2019). Solubility of Caffeine in Supercritical CO_2 : A Molecular Dynamics Simulation Study. J. Phys. Chem. B, 123(45):9685–9691.

[Redfield, 1957] Redfield, A. (1957). On the Theory of Relaxation Processes. IBM J.

[Reverchon, 1997] Reverchon, E. (1997). Supercritical fluid extraction and fractionation of essential oils and related products. J. Supercritical Fluids, 10(1):1–37.

[Rex et al., 2007] Rex, M., Wensink, H. H., and Löwen, H. (2007). Dynamical density functional theory for anisotropic colloidal particles. Phys. Rev. E, 76(2):021403.

[Roberts and Schnitker, 1993] Roberts, J. E. and Schnitker, J. (1993). Ionic quadrupolar relaxation in aqueous solution: dynamics of the hydration sphere. J. Phys. Chem., 97(20):5410–5417.

[Robitschko et al., 2025] Robitschko, S., Sammüller, F., Schmidt, M., and Evans, R. (2025). Learning the bulk and interfacial physics of liquid-liquid phase separation with neural density functionals. arXiv:2507.08395 [cond-mat].

[Roget et al., 2023] Roget, S. A., Heck, T. R., Carter-Fenk, K. A., and Fayer, M. D. (2023). Ion/Water Network Structural Dynamics in Highly Concentrated Lithium Chloride and Lithium Bromide Solutions Probed with Ultrafast Infrared Spectroscopy. J. Phys. Chem. B, 127(20):4532–4543.

[Rondepierre et al., 2025] Rondepierre, F., Brevet, P.-F., and Duboisset, J. (2025). Asymptotic Underscreening in Concentrated Electrolytes Measured by Optical Second Harmonic Scattering of Water. J. Phys. Chem. Lett., pages 2690–2694.

[Rosenfeld, 1989] Rosenfeld, Y. (1989). Free-energy model for the inhomogeneous hard-sphere fluid mixture and density-functional theory of freezing. Phys. Rev. Lett., 63(9):980–983.

[Rosenfeld, 1993] Rosenfeld, Y. (1993). Free energy model for inhomogeneous fluid mixtures: Yukawa-charged hard spheres, general interactions, and plasmas. J. Chem. Phys., 98(10):8126–8148.

[Rosenfeld and Ashcroft, 1979] Rosenfeld, Y. and Ashcroft, N. W. (1979). Theory of simple classical fluids: Universality in the short-range structure. Phys. Rev. A, 20(3):1208–1235.

[Rossmann et al., 2012] Rossmann, M., Braeuer, A., Dowy, S., Gallinger, T. G., Leipertz, A., and Schluecker, E. (2012). Solute solubility as criterion for the appearance of amorphous particle precipitation or crystallization in the supercritical antisolvent (SAS) process. J. Supercritical Fluids, 66:350–358.

[Rotenberg et al., 2018] Rotenberg, B., Bernard, O., and Hansen, J.-P. (2018). Underscreening in ionic liquids: a first principles analysis. J. Phys.: Condens. Matter, 30(5):054005.

[Roth, 2010] Roth, R. (2010). Fundamental measure theory for hard-sphere mixtures: a review. J. Phys.: Condens. Matter, 22(6):063102.

[Roth et al., 2002] Roth, R., Evans, R., Lang, A., and Kahl, G. (2002). Fundamental measure theory for hard-sphere mixtures revisited: the White Bear version. J. Phys.: Condens. Matter, 14(46):12063–12078.

[Roth et al., 2012] Roth, R., Mecke, K., and Oettel, M. (2012). Communication: Fundamental measure theory for hard disks: Fluid and solid. J. Chem. Phys., 136(8):081101.

[Roy and Bagchi, 1993] Roy, S. and Bagchi, B. (1993). Ultrafast underdamped solvation: Agreement between computer simulation and various theories of solvation dynamics. J. Chem. Phys., 99(2):1310–1319.

[Roy et al., 2015] Roy, S., Yashonath, S., and Bagchi, B. (2015). Mode coupling theory analysis of electrolyte solutions: Time dependent diffusion, intermediate scattering function, and ion solvation dynamics. J. Chem. Phys., 142(12):124502.

[Rull et al., 1996] Rull, L., Vega, C., and Lago, S. (1996). Absence of criticality in the reference hypernetted chain equation for short ranged potentials. Mol. Phys., 87(5):1235–1242.

[Rébiscoul et al., 2019] Rébiscoul, D., Sananes Israel, S., Tardif, S., Larrey, V., Ayral, A., and Rieutord, F. (2019). Impact of Silica Surface Nanoconfinement on the Microstructure of Alkoxysilane Layers Grafted by Supercritical Carbon Dioxide. J. Phys. Chem. C, 123(19):12305–12312.

[Saharay and Balasubramanian, 2004] Saharay, M. and Balasubramanian, S. (2004). Ab initio molecular-dynamics study of supercritical carbon dioxide. J. Chem. Phys., 120(20):9694–9702.

[Salanne et al., 2006] Salanne, M., Simon, C., Turq, P., Heaton, R. J., and Madden, P. A. (2006). A First-Principles Description of Liquid BeF_2 and Its Mixtures with LiF: 2. Network Formation in LiF-BeF_2. J. Phys. Chem. B, 110(23):11461–11467.

[Sammüller et al., 2023] Sammüller, F., Hermann, S., de las Heras, D., and Schmidt, M. (2023). Neural functional theory for inhomogeneous fluids: Fundamentals and applications. Proc. Natl. Acad. Sci. U.S.A., 120(50):e2312484120.

[Sampaio de Sousa et al., 2007] Sampaio de Sousa, A., Simplício, A. L., de Sousa, H. C., and Duarte, C. M. (2007). Preparation of glyceryl monostearate-based particles by PGSS®—Application to caffeine. J. Supercritical Fluids, 43(1):120–125.

[San-Fabián et al., 2014] San-Fabián, E., Ingrosso, F., Lambert, A., Bernal-Uruchurtu, M. I., and Ruiz-López, M. F. (2014). Theoretical insights on electron donor–acceptor interactions involving carbon dioxide. Chem. Phys. Lett., 601:98–102.

[Schurtenberger and Heuberger, 2012] Schurtenberger, E. and Heuberger, M. (2012). Supercritical Casimir effect in carbon dioxide. J. Supercritical Fluids, 71:120–126.

[Sergiievskyi et al., 2017] Sergiievskyi, Levesque, Rotenberg, and Borgis (2017). Solvation in atomic liquids: connection between Gaussian field theory and density functional theory. Condens. Matter Phys., 20(3):33005.

[Sergiievskyi et al., 2015] Sergiievskyi, V., Jeanmairet, G., Levesque, M., and Borgis, D. (2015). Solvation free-energy pressure corrections in the three dimensional reference interaction site model. J. Chem. Phys., 143(18):184116.

[Sergiievskyi et al., 2014] Sergiievskyi, V. P., Jeanmairet, G., Levesque, M., and Borgis, D. (2014). Fast Computation of Solvation Free Energies with Molecular Density Functional Theory: Thermodynamic-Ensemble Partial Molar Volume Corrections. J. Phys. Chem. Lett., 5(11):1935–1942.

[Shang-Chun and Oettel, 2019] Shang-Chun, L. and Oettel, M. (2019). A classical density functional from machine learning and a convolutional neural network. SciPost Physics, 6(2):025.

[Sheridan et al., 2018] Sheridan, Q. R., Schneider, W. F., and Maginn, E. J. (2018). Role of Molecular Modeling in the Development of CO $_2$ –Reactive Ionic Liquids. Chem. Rev., 118(10):5242–5260.

[Shimoyama et al., 2008] Shimoyama, Y., Sonoda, M., Miyazaki, K., Higashi, H., Iwai, Y., and Arai, Y. (2008). Measurement of solubilities for rhodium complexes and phosphine ligands in supercritical carbon dioxide. J. Supercritical Fluids, 44(3):266–272.

[Shin et al., 2001] Shin, H. Y., Matsumoto, K., Higashi, H., Iwai, Y., and Arai, Y. (2001). Development of a solution model to correlate solubilities of inorganic compounds in water vapor under high temperatures and pressures. J. Supercritical Fluids, 21(2):105–110.

[Simeoni et al., 2010] Simeoni, G. G., Bryk, T., Gorelli, F. A., Krisch, M., Ruocco, G., Santoro, M., and Scopigno, T. (2010). The Widom line as the crossover between liquid-like and gas-like behaviour in supercritical fluids. Nat. Phys., 6(7):503–507.

[Simeski and Ihme, 2023] Simeski, F. and Ihme, M. (2023). Supercritical fluids behave as complex networks. Nat. Commun., 14(1):1996.

[Simon et al., 2025] Simon, A., Belloni, L., Borgis, D., and Oettel, M. (2025). The orientational structure of a model patchy particle fluid: Simulations, integral equations, density functional theory, and machine learning. J. Chem. Phys., 162(3):034503.

[Simon and Oettel, 2024] Simon, A. and Oettel, M. (2024). Machine Learning approaches to classical density functional theory. arXiv:2406.07345 [cond-mat].

[Skarmoutsos et al., 2022] Skarmoutsos, I., Samios, J., and Guardia, E. (2022). Fingerprints of the Crossing of the Frenkel and Melting Line on the Properties of High-Pressure Supercritical Water. J. Phys. Chem. Lett., 13(33):7636–7644.

[Smith et al., 2016] Smith, A. M., Lee, A. A., and Perkin, S. (2016). The Electrostatic Screening Length in Concentrated Electrolytes Increases with Concentration. J. Phys. Chem. Lett., 7(12):2157–2163.

[Song and Chandler, 1998] Song, X. and Chandler, D. (1998). Dielectric solvation dynamics of molecules of arbitrary shape and charge distribution. J. Chem. Phys., 108(6):2594–2600.

[Song et al., 1996] Song, X., Chandler, D., and Marcus, R. A. (1996). Gaussian Field Model of Dielectric Solvation Dynamics. J. Phys. Chem., 100(29):11954–11959.

[Span and Wagner, 1996] Span, R. and Wagner, W. (1996). A New Equation of State for Carbon Dioxide Covering the Fluid Region from the Triple-Point Temperature to 1100 K at Pressures up to 800 MPa. J. Phys. Chem. Ref. Data, 25(6):1509–1596.

[Speck, 2013] Speck, T. (2013). Gaussian field theory for the Brownian motion of a solvated particle. Phys. Rev. E, 88(1):014103.

[Sternheimer, 1950] Sternheimer, R. (1950). On Nuclear Quadrupole Moments. Phys. Rev., 80(1):102–103.

[Sternheimer, 1966] Sternheimer, R. M. (1966). Shielding and Antishielding Effects for Various Ions and Atomic Systems. Phys. Rev., 146(1):140–160.

[Stettler et al., 2025] Stettler, A., Baker, G. A., and Blanchard, G. J. (2025). The Importance of Hydrogen Bonded Networks in the Dynamic Heterogeneity of Deep Eutectic Solvents. J. Phys. Chem. B.

[Stubbs, 2016] Stubbs, J. M. (2016). Molecular simulations of supercritical fluid systems. J. Supercritical Fluids, 108:104–122.

[Stubbs et al., 2005] Stubbs, J. M., Drake-Wilhelm, D. D., and Siepmann, J. I. (2005). Partial Molar Volume and Solvation Structure of Naphthalene in Supercritical Carbon Dioxide: A Monte Carlo Simulation Study. J. Phys. Chem. B, 109(42):19885–19892.

[Su and Maroncelli, 2006] Su, Z. and Maroncelli, M. (2006). Simulations of solvation free energies and solubilities in supercritical solvents. J. Chem. Phys., 124(16):164506.

[Tabernero, 2011] Tabernero, A. (2011). On the use of semiempirical models of (solid+supercritical fluid) systems to determine solid sublimation properties. J. Chem. Thermodyn., 43:711–718.

[Tai et al., 2000] Tai, C. Y., You, G.-S., and Wang, D.-C. (2000). Modified Retrograde Crystallization Process for Separation of Binary Solid Mixtures Exploiting the Crossover Region of Supercritical Carbon Dioxide. Ind. Eng. Chem. Res., 39(11):4357–4364.

[Tang and Gross, 2010] Tang, X. and Gross, J. (2010). Modeling the phase equilibria of hydrogen sulfide and carbon dioxide in mixture with hydrocarbons and water using the PCP-SAFT equation of state. Fluid Phase Equilibr., 293(1):11–21.

[Tarazona, 1985a] Tarazona, P. (1985a). Erratum: Free-energy density functional for hard spheres. Phys. Rev. A, 32(5):3148–3148.

[Tarazona, 1985b] Tarazona, P. (1985b). Free-energy density functional for hard spheres. Phys. Rev. A, 31(4):2672–2679.

[te Vrugt et al., 2020] te Vrugt, M., Löwen, H., and Wittkowski, R. (2020). Classical dynamical density functional theory: from fundamentals to applications. Adv. Phys., 69(2):121–247.

[Ten Wolde and Chandler, 2002] Ten Wolde, P. R. and Chandler, D. (2002). Drying-induced hydrophobic polymer collapse. Proc. Natl. Acad. Sci. U.S.A., 99(10):6539–6543.

[Titulaer and Deutch, 1974] Titulaer, U. M. and Deutch, J. M. (1974). Analysis of conflicting theories of dielectric relaxation. J. Chem. Phys., 60(4):1502–1513.

[Troisi, 2011] Troisi, A. (2011). Charge transport in high mobility molecular semiconductors: classical models and new theories. Chem. Soc. Rev., 40(5):2347.

[Tschopp et al., 2020] Tschopp, S. M., Vuijk, H. D., Sharma, A., and Brader, J. M. (2020). Mean-field theory of inhomogeneous fluids. Phys. Rev. E, 102(4):042140.

[Tully, 2012] Tully, J. C. (2012). Perspective: Nonadiabatic dynamics theory. J. Chem. Phys., 137(22):22A301.

[Türk, 2009] Türk, M. (2009). Manufacture of submicron drug particles with enhanced dissolution behaviour by rapid expansion processes. J. Supercritical Fluids, 47(3):537–545.

[van der Vegt et al., 2016] van der Vegt, N. F. A., Haldrup, K., Roke, S., Zheng, J., Lund, M., and Bakker, H. J. (2016). Water-Mediated Ion Pairing: Occurrence and Relevance. Chem. Rev., 116(13):7626–7641.

[Vatin et al., 2021] Vatin, M., Porro, A., Sator, N., Dufrêche, J.-F., and Berthoumieux, H. (2021). Electrostatic interactions in water: a nonlocal electrostatic approach. Mol. Phys., 119(5):e1825849.

[Vega, 2018] Vega, L. F. (2018). Perspectives on molecular modeling of supercritical fluids: From equations of state to molecular simulations. Recent advances, remaining challenges and opportunities. J. Supercritical Fluids, 134:41–50.

[Vijayadamodar et al., 1989] Vijayadamodar, G., Chandra, A., and Bagchi, B. (1989). Effects of translational diffusion on dielectric friction in a dipolar liquid. Chem. Phys. Lett., 161(4–5):413–419.

[Wang et al., 2025] Wang, Y., Wang, Y., Zhao, Y., Fu, J., and Liu, Z. (2025). Ionic Liquids Promoted Transformation of Carbon Dioxide. Chem. Rev.

[Weinstein et al., 2010] Weinstein, R. D., Muske, K. R., Martin, S.-A., and Schaeber, D. D. (2010). Liquid and Supercritical Carbon Dioxide-Assisted Implantation of Ketoprofen into Biodegradable Sutures. Ind. Eng. Chem. Res., 49(16):7281–7286.

[Wertheim, 1984] Wertheim, M. S. (1984). Fluids with highly directional attractive forces. II. Thermodynamic perturbation theory and integral equations. J. Stat. Phys., 35(1):35–47.

[White, 1992] White, J. A. (1992). Contribution of fluctuations to thermal properties of fluids with attractive forces of limited range: theory compared with PρT and Cv data for argon. Fluid Phase Equilibr., 75:53–64.

[White and Zhang, 1993] White, J. A. and Zhang, S. (1993). Renormalization group theory for fluids. J. Chem. Phys., 99(3):2012–2019.

[White and Zhang, 1995] White, J. A. and Zhang, S. (1995). Renormalization theory of nonuniversal thermal properties of fluids. J. Chem. Phys., 103(5):1922–1928.

[Widom, 1963] Widom, B. (1963). Some Topics in the Theory of Fluids. J. Chem. Phys., 39(11):2808–2812.

[Wilson, 1971] Wilson, K. G. (1971). Renormalization Group and Critical Phenomena. I. Renormalization Group and the Kadanoff Scaling Picture. Phys. Rev. B, 4(9):3174–3183.

[Wittkowski and Löwen, 2011] Wittkowski, R. and Löwen, H. (2011). Dynamical density functional theory for colloidal particles with arbitrary shape. Mol. Phys., 109(23-24):2935–2943.

[Wittmann et al., 2015] Wittmann, R., Marechal, M., and Mecke, K. (2015). Fundamental mixed measure theory for non-spherical colloids. EPL, 109(2):26003.

[Wittmann et al., 2016] Wittmann, R., Marechal, M., and Mecke, K. (2016). Fundamental measure theory for non-spherical hard particles: predicting liquid crystal properties from the particle shape. J. Phys.: Condens. Matter, 28(24):244003.

[Wittmann et al., 2017] Wittmann, R., Sitta, C. E., Smallenburg, F., and Löwen, H. (2017). Phase diagram of two-dimensional hard rods from fundamental mixed measure density functional theory. J. Chem. Phys., 147(13):134908.

[Wolde and Frenkel, 1997] Wolde, P. R. t. and Frenkel, D. (1997). Enhancement of Protein Crystal Nucleation by Critical Density Fluctuations. Science, 277(5334):1975–1978.

[Wolf et al., 2025] Wolf, M., Chubak, I., and Rotenberg, B. (2025). Quadrupolar NMR relaxation as a local probe of collective dynamics in aqueous alkaline and alkaline-earth chloride solutions. J. Chem. Phys., 162(17):174504.

[Wu, 2006] Wu, J. (2006). Density functional theory for chemical engineering: From capillarity to soft materials. AIChE J., 52(3):1169–1193.

[Wu and Gu, 2023] Wu, J. and Gu, M. (2023). Perfecting Liquid-State Theories with Machine Intelligence. J. Phys. Chem. Lett., 14(47):10545–10552.

[Yamaguchi et al., 2002] Yamaguchi, T., Chong, S.-H., and Hirata, F. (2002). Translational diffusion and reorientational relaxation of water analyzed by site–site generalized Langevin theory. J. Chem. Phys., 116(6):2502–2507.

[Yamaguchi et al., 2003] Yamaguchi, T., Chong, S.-H., and Hirata, F. (2003). Dielectric relaxation spectrum of water studied by the site—site generalized Langevin/modified mode-coupling theory. Mol. Phys., 101(8):1211–1220.

[Yamaguchi et al., 2004] Yamaguchi, T., Chong, S.-H., and Hirata, F. (2004). Mode-coupling analysis of the translational and rotational diffusion of polar liquids; acetonitrile and water. J. Mol. Liq., 112(3):117–124.

[Yamaguchi and Hirata, 2002] Yamaguchi, T. and Hirata, F. (2002). Interaction-site model description of the reorientational relaxation of molecular liquids: Incorporation of the interaxial coupling into the site–site generalized Langevin/mode-coupling theory. J. Chem. Phys., 117(5):2216–2224.

[Yang et al., 2015] Yang, C., Brazhkin, V. V., Dove, M. T., and Trachenko, K. (2015). Frenkel line and solubility maximum in supercritical fluids. Phys. Rev. E, 91(1):012112.

[Yang et al., 2025] Yang, J., Pan, R., Sun, J., and Wu, J. (2025). High-Dimensional Operator Learning for Molecular Density Functional Theory. J. Chem. Theory Comput., 21(12):5905–5915.

[Yoon et al., 2017] Yoon, T. J., Ha, M. Y., Lee, W. B., and Lee, Y.-W. (2017). Molecular dynamics simulation on the local density distribution and solvation structure of supercritical CO 2 around naphthalene. J. Supercritical Fluids, 130:364–372.

[Zhang and Duan, 2005] Zhang, Z. and Duan, Z. (2005). An optimized molecular potential for carbon dioxide. J. Chem. Phys., 122(21):214507.

[Zhao et al., 2017] Zhao, Q., Mecheri, M., Neveux, T., Privat, R., and Jaubert, J.-N. (2017). Selection of a Proper Equation of State for the Modeling of a Supercritical CO $_2$ Brayton Cycle: Consequences on the Process Design. Ind. Eng. Chem. Res., 56(23):6841–6853.

[Zhao et al., 2011a] Zhao, S., Jin, Z., and Wu, J. (2011a). Correction to New Theoretical Method for Rapid Prediction of Solvation Free Energy in Water. J. Phys. Chem. B, 115(51):15445–15445.

[Zhao et al., 2011b] Zhao, S., Jin, Z., and Wu, J. (2011b). New Theoretical Method for Rapid Prediction of Solvation Free Energy in Water. J. Phys. Chem. B, 115(21):6971–6975.

[Zhao et al., 2011c] Zhao, S., Ramirez, R., Vuilleumier, R., and Borgis, D. (2011c). Molecular density functional theory of solvation: From polar solvents to water. J. Chem. Phys., 134(19):194102.

[Zosel, 1978] Zosel, K. (1978). Separation with Supercritical Gases: Practical Applications. Angew. Chem. Int. Ed. Engl., 17(10):702–709.

[Zwanzig, 2001] Zwanzig, R. (2001). Nonequilibrium statistical mechanics. Oxford University Press, Oxford; New York.

Antoine Carof - Habilitation à diriger des recherches - 2025

Titre : Thermodynamique et dynamique des fluides moléculaires par la théorie de la fonctionnelle de la densité classique.

Résumé : Les propriétés des fluides à l'échelle moléculaire sont centrales dans de nombreux processus physico-chimiques. Leur modélisation est donc nécessaire pour le développement de technologies innovantes, notamment pour la transition écologique. Mes projets de recherche proposent de développer de nouvelles approches théoriques pour étudier les propriétés de ces fluides, en se basant sur la densité moléculaire. En combinant des résolutions analytiques et numériques, ces théories donneront accès aux propriétés structurales, thermodynamiques et dynamiques des fluides à l'échelle moléculaire. Grâce à cette approche basée sur la densité moléculaire, ces théories permettent d'obtenir ces résultats bien plus efficacement que les simulations standard à cette échelle. Dans la continuité de mes travaux précédents, j'appliquerai ces méthodes pour étudier : (1) la solvatation dans le CO_2 supercritique, un solvant prometteur pour la chimie verte, et (2) la dynamique dans les électrolytes, des fluides essentiels pour le stockage et la production d'énergie décarbonnée. À plus long terme, j'étendrai ces méthodes basées sur la densité moléculaire à des fluides plus complexes comme les liquides ioniques ou les solvants eutectiques profonds et et à des environnements plus variés (confinement, interfaces).

Title: Thermodynamics and Dynamics of Molecular Fluids with Classical Density Functional Theory.

Abstract: The properties of fluids at the molecular scale are fundamental to many physico-chemical processes. Modelling these properties is therefore necessary for developing innovative technologies, particularly for the ecological transition. My research projects aim to develop new theoretical approaches based on molecular density to study the properties of these fluids. By combining analytical and numerical resolutions, these theories will enable us access to the structural, thermodynamic and dynamic properties of fluids at the molecular scale. This molecular density-based approach will make it possible to obtain these results much more efficiently than standard simulations at this scale. Building on my previous work, I will apply these methods to study: (1) solvation in supercritical CO_2, a promising solvent for green chemistry, and (2) dynamics in electrolytes, which are essential for carbon-free energy storage and production. In the longer term, I intend to extend these molecular density-based methods to more complex fluids such as ionic liquids and deep eutectic solvents and to more varied environments (confinement, interfaces).